

Contract # DTPH56-06-T-000006

Prepared for: U.S. DOT/PHMSA

**LONG-TERM MONITORING OF CASED PIPELINES USING  
LONGRANGE  
GUIDED-WAVE TECHNIQUE**

**Final Report**

**NYSEARCH/Northeast Gas Association**

1515 Broadway, 43<sup>rd</sup> Floor

New York, NY 10036

(212) 354 4790 Ext. 211

George Janega

Program Manager, NYSEARCH

[www.northeastgas.org](http://www.northeastgas.org)

May 19, 2009

# Table of Contents

	Page
Executive Summary.....	2
General Background.....	5
Technical Background.....	7
Procedures & Results.....	9 thru 43
Task 1   Refine & Validate Simulation Model.....	9
Task 2   Develop Algorithm.....	12
Task 3   Improve Data Analysis Software for Pipeline Inspection...	15
Task 4   Evaluate Alternate Adhesives.....	16
Task 5   Test on NYSEARCH/NGA Test Bed.....	17
Task 6   Conduct Field Evaluation.....	22
Additional Task   Investigation of Guided Wave Attenuation Change with Coated Pipe Temperature and General Corrosion.....	35
Task 7   Project Review Meetings.....	42
Conclusions, Recommendations and Next Steps.....	44
Appendix   Southwest Research Institute Final Report.....	46

## Executive Summary

Integrity management programs for *gas transmission pipelines* are required by The Office of Pipeline Safety (OPS)/DOT. Direct Assessment (DA) and 'Other Technologies' have become the focus of assessment options for pipeline integrity on cased crossings. Long Range Guided Ultrasonics (LRUT) may qualify as an 'Other Technology'.

The Magnetostrictive Sensor (MsS) technology is a unique type of remote inspection tool in the field of LRUT also known as guided wave. The MsS technology from Southwest Research Institute<sup>®</sup> (SwRI) incorporates cobalt alloy strips that are semi-permanently attached to a pipe and wrapped with a simple coil of wire. MsS uses materials and an approach that is cost effective to install on a permanent basis. This can allow defect monitoring over time after an initial excavation has been restored. There has also been reason to believe that through the use of software, MsS could indicate defect type, size, and shape.

The objective of this project was to develop the defect characterization & sizing capabilities, develop the long-term structural health monitoring (SHM) of cased sections, and evaluate field performance. The project work was focused on defects whose circumferential cross-sectional area (CSA) is up to 10% of the total pipe wall cross-section for which the application of SHM would be valuable. In addition to MsS technology, these project results are highly related to the challenges in using LRUT. They strictly highlight the effect that coatings and temperature have on the effectiveness of LRUT and should be used in the context of the Guided Wave UT Checklist guidance by DOT/OPS.

In order to develop algorithms to characterize defects (axial length, shape, and CSA) a defect signal simulation model was refined and validated experimentally. The simulation model facilitated the development of defect characterization algorithms. The algorithms determine the cross sectional area at a given axial position, but cannot separately determine defect depth and circumferential width. Multiple or single defects within the same axial pipe position are represented as a single defect in terms of % CSA wall loss.

The performance of the MsS technology for defect detection, characterization, and long-term SHM was evaluated on cased pipes in the NYSEARCH/NGA test bed facility which contains various machined defects in buried cased pipe. The performance was further field tested at an RG&E facility on coated mock-up cased pipes which were subjected to accelerated corrosion using a 'reversed' cathodic protection system. Attenuation caused by general corrosion and certain coatings was observed.

Remaining funding in the project budget allowed for two additional investigations via project extensions as follows. The temperature dependence of wave attenuation was investigated on three different coating types (popular vintage

style coal tar (TGF-3), coal tar epoxy (CTE), and polyethylene) at various frequencies. Secondly, the attenuation caused by general corrosion was investigated by subjecting bare pipe samples to 82 days of accelerated corrosion treatment.

Results and findings of the performance evaluation are summarized as follows:

- (1) MsS can detect corrosion activity and its locations in the cased sections of pipelines. This is accomplished by using permanently installed sensors combined with periodic measurements and comparing the periodic data. Further work pertaining to non-weld calibration, attenuation from temperature influenced coatings, and attenuation from general corrosion may allow MsS to exceed traditional LRUT and facilitate its reliability for DA inspections.
- (2) MsS is durable for long-term field use on cased pipe applications.
- (3) Changes in the pipe wall CSA can be detected (as small as 1 to 2% in bare pipe and 2 to 4% in coal-tar-TGF-3-coated pipe). Further development of data processing techniques on coal tar TGF-3 coated pipes is needed to correct for the effects of wave attenuation on the defect signal.
- (4) Defect characterization within 1 to 2 inches in axial length and 2 to 4% in CSA is achievable.
- (5) It was proven that wave attenuation in TGF-3 coal tar or PE coated pipes increases significantly with increasing temperature. For example, as the temperature of the coating increased from 70 to 100 degrees F in TGF-3 coated pipe, the attenuation at 10 kHz increased from about 0.03 to 0.17 dB/ft; the attenuation at 50 kHz increased from about 1.1 dB/ft to 2.2 dB/ft.

Because of the large increase in attenuation with temperature, results of guided-wave inspection of TGF-3 or PE coated pipelines become increasingly poorer with increasing temperature. Temperature effects in the TFG-3 coated pipe were about twice as much as that in the PE coated pipe. Thus, the consideration of temperature is even more so important for guided-wave inspection of Coal Tar (TGF-3) coated pipelines which are predominantly used by the industry in cased applications. It should also be noted that TGF-3 coated pipelines are usually of such a vintage that they are higher priority due to age. If a guided wave inspection would be performed during warmer conditions, and again during cooler conditions, it would appear as if the severity of the defect increased. However, the attenuation would simply decrease and reflect a greater signal; leading to the appearance of a worsening defect and false calls.

- (6) Wave attenuation significantly increases with general corrosion as corrosion products adhere to the pipe surface (from approximately 0.13 dB/ft at 10 kHz to 0.23 dB/ft at 50 kHz for a 0.004 inch depth wall loss). Therefore, wave attenuation is a good indicator of the degree of general corrosion on bare pipe even in early its stages. As a result, the monitoring of corrosion is possible on highly attenuative polyethylene or coal tar TGF-3 coated pipelines using low frequency waves (such as 10 kHz). However, it is unlikely that general corrosion would exist on the outside of a coated pipe. Attenuation from localized patches may be insignificant. Therefore, this claim is most feasible for detecting general corrosion on the inner surface of a coated pipe.

#### General Recommendations:

- (1) Improve the detection accuracy of CSA change in coated pipelines by developing signal processing methods for correcting attenuation effects on waveforms. The focus would be to solve attenuation issues resulting from popular coating materials and their behavior to temperature.
- (2) Develop an improved calibration methodology. The current calibration method is based on weld signals. If a corrosion defect develops at a weld area, it can lead to significant errors in data analysis and may fail to detect the defect in the weld area.
- (3) Determine the magnitude of attenuation increase that would be caused by the natural corrosion process under realistic conditions. Corrosion effects on wave attenuation should be investigated at a low corrosion rate over a long duration of time (such as 1 year or more).
- (4) Take steps for technology transfer that include: develop a GUI program for data analysis intended for use by inspectors, prepare training material, and establish industry-accepted procedures for probe installation and testing.
- (5) Guided wave inspection of Coal Tar (TGF-3) or PE coated pipelines should be conducted at the lowest temperatures possible. Subsequent tests on the same pipe should be performed at relatively consistent temperatures.

## General Background

The Office of Pipeline Safety (OPS) ruled for the requirement of an integrity management program for *gas transmission pipelines*, as defined by 49 CFR Part 192 (December 2003). Assessment options identified in the rule are:

- 1) In-Line Inspection
- 2) Pressure Testing
- 3) Direct Assessment (DA): ECDA (External Corrosion Direct Assessment)  
ICDA (Internal Corrosion Direct Assessment)  
SCCDA (Stress Corrosion Cracking Direct Assessment)
- 4) Other Technology: An operator demonstrated technique providing an equivalent understanding of pipe condition.

Options 3 & 4 have become the focus for assessment methods of unpiggable pipelines due to cost and service disruptions involved with the remaining options. As a result, the 2004 NYSEARCH/NGA RFP identified new technologies addressing difficult or special applications of DA. These technologies aim to address cased crossings such as those under roads, train tracks, rivers, etc. An RFP review team (composed of DA representatives) decided to pursue the Magnetostrictive Sensor (MsS) technology from Southwest Research Institute® (SwRI).

The MsS technology is a unique type of remote inspection tool in the field of Long Range Guided Ultrasonics (LRUT) also known as guided wave. Generally, LRUT has been marketed by some inspection service companies as a screening tool to detect internal / external corrosion and coating defects in gas pipes up to 60" diameter. Traditional LRUT technologies use piezoelectric transducer materials within costly belts installed at the time of an inspection. The MsS technology is unique in that it incorporates magnetostrictive sensing strips that are semi-permanently attached to the pipe and wrapped with a simple coil of wire. MsS provides the same general signal energy as traditional LRUT yet uses materials and an approach that is cost effective to install on a permanent basis. This can allow defect monitoring over time after an initial excavation has been restored. There has been reason to believe that through the use of software, MsS could indicate defect type, size, and shape.

In October 2004, several NYSEARCH companies approved a project to determine the feasibility of using the MsS as a longer term monitoring device. The study investigated the effects of varying pipeline pressure on the sensor, sensor bonding stability, effects of varying cathodic protection, and the ability of the sensor to measure change in a defect's cross sectional area over time. It was proven that the MsS generally worked under varying conditions and was able to see small-sized defects (1% cross sectional area).

In September 2005, NYSEARCH companies approved the second (current) phase of the project with DOT/PHMSA cofunding. The phase II objective is to develop the defect characterization & sizing capabilities, develop the long-term structural health monitoring (SHM) of cased sections, and evaluate field performance. The project work was focused on defects whose circumferential cross-sectional area (CSA) is up to 10% of the total pipe wall cross-section.

## Technical Background

The MsS is composed of a thin strip of magnetostrictive material bonded around the pipe circumference with epoxy adhesive (Figure 1). The strip material used is a heat treated iron-cobalt alloy approximately 0.006 inch thick and 1 inch wide. Once the adhesive has cured the strip is manually magnetized (Figure 2) and a coil is wound around it (Figure 3). After electrical connections are installed, the assembly may be coated with a wax or similar coating prior to burial (Figure 4).



Figure 1. Alloy strips bonded to pipe with epoxy



Figure 2. Manual magnetization of the alloy strips



Figure 3. Coil installed around strips



Figure 4. Wax coating applied over MsS assembly

The MsS probe assembly generates and detects guided waves electromagnetically. A transmitter applies pulses of electric current to the coil. Magnetic fields produced by the coil generate pulses of mechanical torsion to the magnetized strip via magnetostrictive effects. These torsion pulses are propagated to the pipe via adhesive. The torsional pulses propagating along the pipe are referred to as guided waves. After arriving at a feature (defect, weld, etc.), some guided waves reflect back to the MsS probe assembly. Detection is achieved when the reflected guided wave at the magnetized strip produces an

electrical voltage in the coil via induction. This occurs according to Faraday effects which the receiver detects in terms of amplitude. Percent reflection is the value derived from these reflected signals and is synonymous with the percent Cross Sectional Area (% CSA) of pipe wall lost.

Because the defect signal is a function of multiple parameters, the signal amplitude alone used as the defect detection criterion cannot provide defect characteristics other than a rough estimate of CSA of the defect. Detailed knowledge on how the signal varies with defect characteristics and wave frequency is needed to characterize a defect from these guided-wave signals. A knowledge base may be established that is useful for developing defect characterization algorithms from measured guided-wave signal features. Collecting a large number of defect signals experimentally is impractical because of the high cost involved in machining a large collection of pipe samples. Therefore, to create a database, a simulation model was employed in this project. The database was utilized to identify key signal features that are useful for relating to defect characteristics. Algorithms for defect characterization were developed using these key signal features.

The advantages of this model are in its simplicity and short computation time. Shortcomings of the model are that it cannot treat mode conversions when guided waves interact with a defect. (This issue is similar to a wave scattering resulting from an effect akin to optical diffraction.) For defect characterization algorithm development, the pipeline model requires refinement and validation in the lab with a small collection of machined defects in actual pipe (a task within this project).

# Task Procedures and Results

## Task #1 Refine and Validate Simulation Model

### *Pipeline Model Refinement*

From previous experimental investigations, it was observed that, when the guided wave interacts with an abrupt change in pipe wall cross-section, the reflection coefficient differed depending on the direction of the incident wave. This difference (termed 'geometric shadow effects') increased with the wave frequency and the magnitude of the abrupt change. The initial transmission line model could not produce the observed geometric effects and, thus, required a modification by introducing appropriate correction factors for the effects.

The refinement efforts in this project therefore were focused on finding and incorporating proper correction factors for the geometric effects in the simulation model. To determine the proper correction factors as a function of defect depth and torsional wave frequency, a series of experimental measurements of the front and rear end signals from a 360-degree notch was made. The MsS was placed on one end of the pipe sample, and the measurements were made at 32-, 64-, and 128-kHz frequencies while varying the notch depth from 10- to 100-percent wall at 10-percent increments.

The differences between theoretical values and the experimental values are due to the geometric effects, which increase with increasing frequency. The magnitude of the geometric effects and their dependence on the notch depth/CSA and wave frequency were measured from the experimental data and were subsequently incorporated into the defect signal simulation model.

In addition to the geometric effects discussed above, the phase shift between the front and rear reflected signals was found to be proportional to the wave frequency and measured to be approximately 36° at 128 kHz. This phase shift was also incorporated into the simulation model.

After the geometric effects had been incorporated into the model, it became apparent that the acoustic impedance used takes a different form, depending on the guided wave mode. For up to 10-percent defect CSA in schedule 40 pipes, the model's error is negligible but should be discussed for revision at some point to achieve greater accuracy.

A GUI (graphical user interface) version of the simulation software was developed for this project. The software can handle defects inside or on the outside of the pipe wall. The defects could be either rounded or trapezoidal

shapes with various axial length, width (in circumferential direction of pipe), and depth. The software now has a feature that allows random noise to be mixed with the simulated defect signals to reflect real-world situations.

A series of experimental measurements of simulated defect signals was performed on bare pipe samples to validate the results from the simulation model. The 6 inch pipe was 20 feet in length with a 0.28-inch-wall thickness. Defect signals were measured at three frequencies (32, 64, and 128 kHz) using the MsS system. The notch defects were machined in the sample as defect signals were collected. Ellipsoidal defects were manually placed in the sample with a grinder.

Within the test range investigated (32 to 128 kHz and up to 10% CSA defects) and experimental measurement error ( $\pm 0.5\%$  in reflection coefficient), the simulation software was accurate and reliable in simulating defect waveforms. Since the simulation software is based on a one-dimensional model, it cannot handle the mode conversions and beam spreading that occur when guided waves interact with a localized defect. Also, the software is limited to simulating the signal from a single defect. It could be extended to handle multiple defects.

#### *Wave Attenuation Coefficients in Bare Pipe*

To determine the reflection coefficient from a defect placed in the test pipe, the attenuation effects on the signal amplitude must be corrected for. The attenuation in the coal tar (TGF-3) coated pipe is much higher than in bare or FBE-coated pipe. In low frequencies (up to approximately 40 kHz), the attenuation coefficients are similar in both bare and FBE-coated pipes. The difference between the two becomes significant in frequencies higher than 40 kHz.

#### *Behavior of Notch Rear-end Signal with Notch Length*

Notch signal waveforms obtained at various axial notch lengths were studied. It was observed that as the axial length of a given notch increased from 1 to 4 inches, the signal relating to the front of the notch gradually separated from the signal associated with the rear of the notch. The amplitude from the rear notch signal was expected to remain constant over length. The large decrease in its amplitude was therefore unexpected and indicated the presence of a significant energy-loss mechanism in the notched region. Presently, SwRI does not understand how this energy loss occurs. The simulation model cannot account for this phenomenon.

#### *Trailing Signals*

In addition to the signals normally expected from a notch, SwRI observed other signals appearing after the notch signal. These trailing signals were more noticeable for the 80% depth notches than for the 50% depth notches. The level of trailing signals was higher at lower frequency. The occurrence of the trailing signals and their level varied with the axial length of the notch in no predictable manner. SwRI does not have a clear picture of why this happens. There may be

a possible relationship with the guided wave's mode conversion and beam spreading. It is important to be aware that these trailing signals will increase the background noise level and could also be mistaken as defect signals. The simulation model cannot account for these trailing signals.

#### *Variations in Transmitted Signals*

From the detailed analysis of the experimental data, we also have recognized that the transmitted signal waveform varied from sensor to sensor. This is speculated to be related to minor inconsistencies associated with sensor installation. The degree of variation was greater with increasing wave frequency. Fortunately, the variations at 32 kHz (typically used for long-range pipe inspection) appeared to be small. However, since the defect waveform is directly related to the transmitted signal waveform, any variations in the transmitted signal waveform will affect the defect signal waveform and, thus, contribute to the error in defect characterization.

# Task Procedures and Results

## Task #2                      Develop Algorithm

### *Feature Signal Analyses for Relevance to Defect Characteristics*

The first step toward developing defect characterization algorithms is identifying the features of defect signals that are most useful to correlate to defect size (depth, width, and length) and shape. To identify the most relevant features, a total of 37 feature parameters were defined and their correlation to any of the defect characteristics was evaluated.

For the feature evaluation, a total of 19,809 defect signals were simulated, including both elliptical and trapezoidal-shaped defects with various lengths, widths, depths, and slopes and for different transmitter signal waveforms. The wave frequency was fixed at 32 kHz and the range of defect size was limited to:

Length - Up to 8 inches (equivalent to  $2\lambda$  at 32 kHz)

CSA - Up to 8% of the total pipe wall cross-sectional area

From the linear correlation analyses, the following six feature parameters were the most relevant for defect characterization:

- Base of Envelope – (correlates to defect length)
- Center of Envelope – (correlates to defect length)
- Center of Spectrum – (correlates to defect length)
- Spectral Peak Amplitude – (correlates to defect CSA)
- Peak Amplitude of Envelope – (correlates to defect CSA)
- Max-Fall-Slope of Envelope– (correlates to defect CSA & length)

The six parameters characterize each defect parameter together in groups, therefore each is equally important.

In the absence of noise, a good linear correlation existed between Base of Envelope and the simulation's defect length. Since general noise occurs with any analog signal's detection, it was important to add simulated noise during the observation of the parameters. The addition of noise to the defect signals removed the good linear correlation. A wavelet-based de-noising algorithm was applied to improve the signal to noise ratio. To improve the length determination, the combination of the three feature parameters (base of envelope, center of envelope, and center of spectrum) was used in the defect characterization (or classification) algorithms. It was observed that the signal to noise ratio (SNR) for most of the simulations using the three parameters was above the 6 dB SNR criterion (minimum level of a valid signal in general industry). Signal to noise ratios less than 6dB would be undetectable.

For a known defect length, there is an excellent linear relationship between the spectral peak amplitude and CSA or volume even in the presence of noise. Similarly, the peak amplitude of envelope also has an excellent linear relationship with CSA or volume. If the defect length is unknown, the correlation is not good. Therefore, to get an accurate measure of defect CSA, accurate determination of the defect length is prerequisite.

No feature parameters were found to correlate well with either defect depth or defect width. Therefore, although CSA of the defect could be determined from the guided-wave feature parameters, a separate determination of both depth and width is not feasible. This was expected because the guided wave examines the entire cross-section of the pipe and the reflection coefficient of a defect is dependent on the defect CSA and is insensitive to the individual width or depth.

For distinguishing defect type (namely ellipsoidal or trapezoidal), the center of spectrum and the spectral peak amplitude were most useful.

#### *Development of the Defect Characterization Algorithm*

Using the six feature parameters, classification algorithms (i.e., classifiers) were developed to estimate defect length, shape, and CSA. Figure 1 illustrates the flow diagram of the defect classification algorithm. The defect signals containing noise were de-noised by a wavelet-based filter. Then from the defect signal, the six feature parameters were extracted and normalized (to the corresponding features extracted from the transmit signal to minimize the effect of probe variations). The normalized values of the six feature parameters are then input to the classifier, which outputs the classification of defect length, shape, and max-cross-section area. The classification of max-cross-section area requires the determination of the defect length and shape.

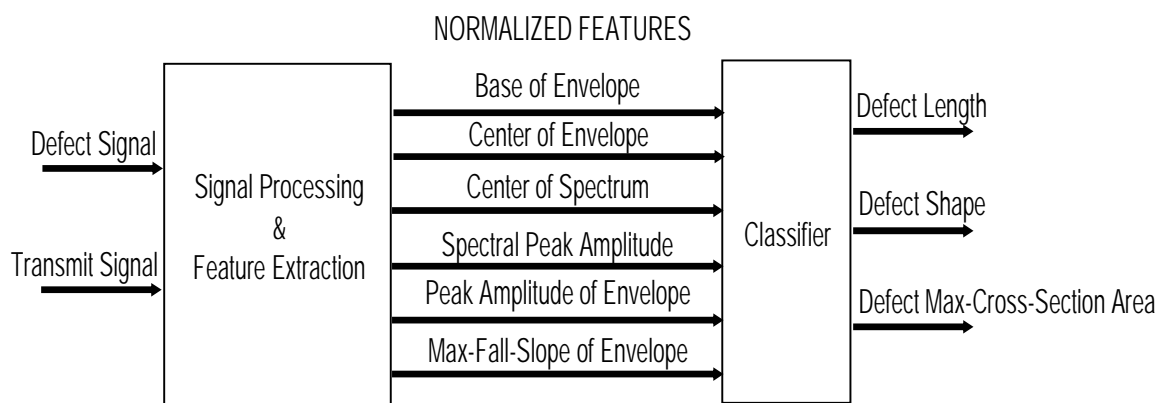


**Figure 1. Flow diagram of the defect classification algorithm**

- The defect length output from the classifier is an integer between 1 and 8, indicating a defect length between 0–1, 1–2, 2–3, 3–4, 4–5, 5–6, 6–7, and 7–8 inches, respectively.

- The defect shape output from the classifier is 0 or 1, indicating ellipsoid and trapezoid shapes, respectively.
- The defect CSA output from the classifier is an integer between 1 and 5, indicating a CSA between 0–2, 2–4, 4–6, and 6–8 percent of the pipe cross-section area.

The classifier was developed by training a total of 18,809 sets of simulation data at 32 kHz that have been generated from different defect shapes, lengths, widths, and depths. All the data sets have a signal to noise ratio of greater than 6 dB (the minimum industrial standard for a credible signal). Results have shown that the use of the *k*-nearest-neighbor classifier with all six features yielded the highest percentage of correct classifications.

On average, the classifier was able to correctly determine the defect length class for approximately 75% of the training data, the defect shape class for approximately 85% of the data, and the defect max-cross-section-area for approximately 84% of the data. The performance of the classifier improved with the increase of SNR, an expected behavior. The results also suggest that 95% of the time, the classifier can determine the defect length within  $\pm 4.8$  inches and the defect max-cross-section area within approximately  $\pm 3\%$  at the minimum signal to noise ratio of 6 dB.

The probability of correctly determining the defect shape (either ellipsoidal or trapezoidal) was approximately 50%, which means that the defect shape could not be determined with any accuracy using the classifier. This is because the difference in the shape of an elliptical defect and a trapezoidal defect of given length and CSA lies only in whether the defect surface is curved or planar, which is a minor variation for low-frequency guided-waves (such as 32-kHz considered here). The algorithm assumes that the transmitted signal waveform does not change with feature to sensor distance. This assumption is satisfactory in low-attenuation pipelines. In high-attenuation pipelines (such as coal-tar-coated or polyethylene-coated lines), however, this assumption is no longer valid. Therefore, proper correction of the attenuation effects on the signal (waveform, amplitude, and spectral content) is necessary to apply the algorithm.

## Task Procedures and Results

### Task #3                    Improve Data Analysis Software for Pipeline Inspection

#### *Improvement of Data Analysis Software*

Various data analysis functions were added to the existing software used at SwRI for pipeline inspection and monitoring to improve its performance. Added functions included:

- (1) Correlating data from both ends of cased section of carrier line for cross-confirmation.
- (2) Adjusting wave properties along the pipeline to properly align known signals (such as weld signals) so that changes occurring over time could be determined accurately. Periodic data from the signals of known features do not line up exactly; primarily due to variations in line temperature between the periodic measurements. (The wave velocity varies.)
- (3) Variable detection threshold and attenuation correction on the signal amplitude.
- (4) Defect characterization that involves gating defect signals, normalizing the gated signal (with respect to the transmitted signal and wave frequency), extracting feature parameters, and applying the defect classifier.

## Task Procedures and Results

### Task #4 Evaluate Alternate Adhesives

#### *Adhesive Bonding Material Testing*

In previous work conducted for NYSEARCH/NGA, it was found that the cured epoxy layer (3M's Scotch-Weld epoxy DP 125, Gray) is rigid and transmits stress changes in pipe to the MsS strip, which in turn affects the MsS sensitivity.

To minimize the effects of line pressure change on the MsS sensitivity, it was desirable to find alternate adhesive materials that are (1) able to transmit the guided waves from the MsS strips to the pipe and vice versa, (2) flexible enough to create a discontinuity in static stress across the adhesive layer so that the stress caused by line pressure changes would not be transmitted to the strip, and (3) suitable for long-term use in pipeline environments.

Various materials were evaluated for their suitability on the 12-inch-OD pressure test sample used in a previous project. Materials evaluated included several construction sealant materials (such as silicone, rubberized asphaltic compound, polyurethane, and rubber cement) and adhesives based on polyurethane. Among the materials tested, Hysol U-10FL, a polyurethane-based adhesive, was found to be suitable for bonding MsS strips and to exhibit the least pressure effects with a small degree of signal degradation.

When the sensor is degraded, it can be restored by manually reconditioning the strips with a magnet in a manner identical to the initial sensor installation. Until recently, reconditioning required access to the installed sensors. Thus, if buried, the line needed to be excavated for reconditioning. SwRI has developed a solution outside of this work scope to address the pressure fluctuation concern for their non-cased pipe monitoring products. It involves the low cost solution of attaching a band of permanent magnets around the coil. This band together with the coil and magnetostrictive strips may be coated and buried as well.

Therefore, 3M's Scotch-Weld epoxy DP 125(Gray) used with the permanent magnetic band eliminates the need for alternate adhesives.

## Task Procedures and Results

### Task #5 Test on NYSEARCH/NGA Test Bed

The NYSEARCH/NGA test bed facility is located in Johnson City, NY. The facility has three, approximately 80 foot long cased test pipes:

- (1) Aboveground, 20 inch bare steel pipe within a 24 inch casing
- (2) Aboveground, 16 inch steel pipe with 0.154 inch thick coal tar TGF-3 coating within a 20 inch casing
- (3) Underground, 12 inch OD steel pipe with 20 mil thick coal tar epoxy (CTE) coating within a 16 inch casing

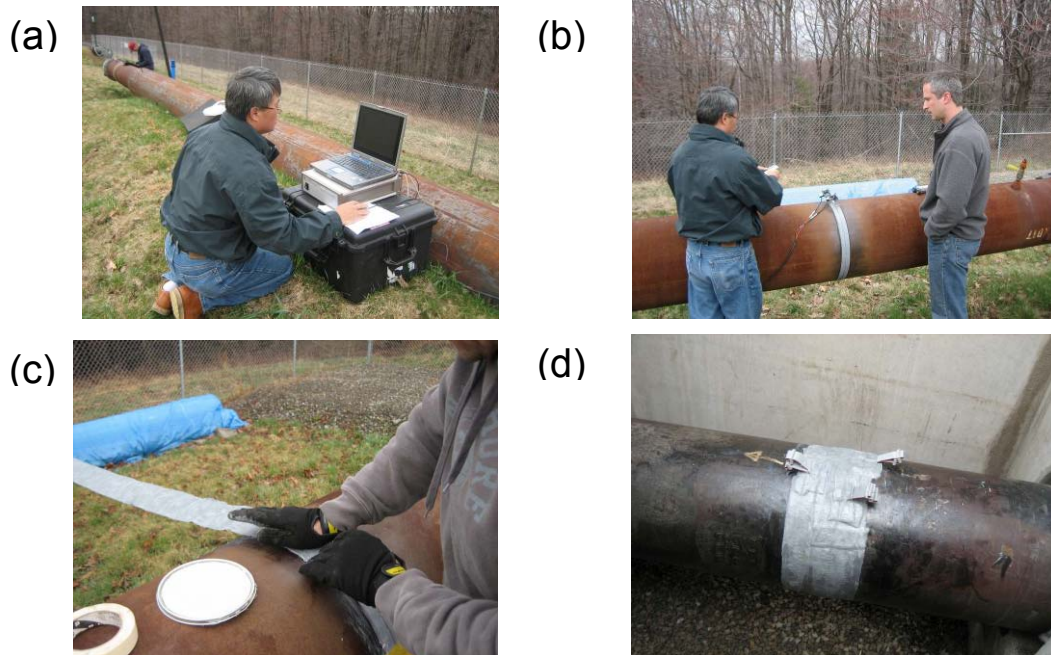
All test pipes are seam-welded and have a 0.375 inch in wall thickness. All test pipes contain machined defects circumferentially and axially along the pipe. The 16 inch pipe also contains simulated natural corrosion defects having smooth contours. Casing spacers are placed along the pipe and the edge of the casing is sealed with a link seals shown in Figure 1. The underground test pipe is accessible for guided-wave testing from the two vaulted excavations shown in the Figure 1.



Figure 1. Link seal at the edge of casing (left) and vaulted access to the buried test pipe (right)

### *Sensor Installation*

MsS installation and baseline testing of the three cased test pipes was conducted during the week of April 23<sup>rd</sup>, 2007. MsS coils were semi permanently installed for long-term condition monitoring (SHM). Photos taken during the testing are shown in Figure 2.



**Figure 2. MsS testing at the NYSEARCH/NGA test bed facility: (a) MsS system during data acquisition from the 20-inch-OD bare steel pipeline, (b) MsS ribbon coils placed over the magnetostrictive strips for testing, (c) wax tape applied over the MsS ribbon coils for protection from environment for long-term monitoring, and (d) MsS ribbon coils installed with protective wax tape on the 12-inch-OD CTE steel pipeline.**

### *Baseline Results*

Details of the baseline test data and results are given in Appendix A of the SwRI final report. The results of defect characterization algorithm (axial length, defect shape, and circumferential cross-sectional area (CSA)) are listed in Tables 1, 2 and 3.

The results in the tables are from the lower-frequency data (i.e., 32 kHz for bare pipe sample and 16 kHz for the coated pipe samples). The results from the higher-frequency data (particularly the data acquired from the coated pipe samples) were unreliable due to the uncertainty in compensating for the attenuation effects on the waveform. For comparison, the % Reflection determined based on the signal amplitude and the actual CSA are also listed in the tables. The CSA determined using the classifier was about the same as the % Reflection determined based on the signal amplitude. This supports the validity of the classifier and the signal analysis for calculating CSA.

**Table 1 Defect characterization results for defects found on the 20 inch bare pipe**

Defect No.	Axial Length	Shape	CSA (%)	% Reflection	Actual CSA (%)
D2	0 ~ 1"	Trapezoid	0 ~ 2	2.2	$2 < x < 3$
D3	0 ~ 1"	Trapezoid	0 ~ 2	3.0	$2 < x < 3$
D4	5 ~ 6"	Trapezoid	0 ~ 2	1.7	$1 < x < 2$

**Table 2 Defect characterization results for defects found on the 16 inch TGF-3 coal tar coated pipe**

Defect No.	Axial Length	Shape	CSA (%)	% Reflection	Actual CSA (%)
D2	0 ~ 1"	Trapezoid	0 ~ 2	2.4	$1 < x < 2$
D3	0 ~ 1"	Ellipsoid	2 ~ 4	3.1	$3 < x < 4$
D4	2 ~ 3"	Trapezoid	2 ~ 4	2.4	$3 < x < 4$
D5	4 ~ 5"	Trapezoid	6 ~ 8	4.4	$4 < x < 5$
D6	5 ~ 6"	Trapezoid	4 ~ 6	3.7	$3 < x < 4$

**Table 3 Defect characterization results for defects found on the 12 inch CTE coated pipe**

Defect No.	Axial Length	Shape	CSA (%)	% Reflection	Actual CSA (%)
D2	6 ~ 7"	Ellipsoid	4 ~ 6	6.4	$6 < x < 7$
D3	0 ~ 1"	Ellipsoid	2 ~ 4	2.3	$x < 1$
D4	3 ~ 4"	Trapezoid	2 ~ 4	3.0	$1 < x < 2$
D5	0 ~ 1"	Trapezoid	4 ~ 6	4.0	$1 < x < 2$
D6	0 ~ 1"	Trapezoid	4 ~ 6	10.1	$3 < x < 4$
D7	2 ~ 3"	Trapezoid	2 ~ 4	2.6	$1 < x < 2$
D8	5 ~ 6"	Ellipsoid	4 ~ 6	3.8	$1 < x < 2$

The baseline test results given in Appendix A of the SwRI final report were evaluated by NGA/NYSEARCH and the overall findings are as follows:

- (1) Welds – All welds in the three test pipes were detected and correctly identified.
- (2) Casing Spacers
  - a. Casing spacers on bare pipe did not produce detectable signals and thus were not detected.
  - b. Casing spacers (and link seal) on TGF-3 and CTE-coated pipe produced detectable signals. Out of a total 17 spacers (9 on the aboveground 16-inch and 8 on the underground 12-inch pipes), 16 (9 on the aboveground 16-inch and 7 on the underground 12-inch pipes) were detected and correctly identified.
- (3) Defects
  - a. In 20-inch aboveground bare pipe
    - i. Detected – 4 ea ( $1\% \leq 3ea \leq 2\%$ ,  $2\% \leq 1ea \leq 3\%$  CSA)
    - ii. Missed – None
  - b. In 16-inch aboveground pipe with 0.154-inch TGF-3 coating
    - i. Detected – 6 ea ( $3ea \leq 2\%$ ,  $3\% \leq 3ea \leq 5\%$  CSA)
    - ii. Missed – 12 ea ( $11ea \leq 2\%$ ,  $2\% \leq 1ea \leq 3.5\%$ )
  - c. In 12-inch underground pipe with 20-mil CTE coating
    - i. Detected – 8 ea ( $1ea \leq 1\%$ ,  $1\% \leq 5ea \leq 2\%$ ,  $1ea \approx 4\%$ ,  $1ea \approx 6\%$  CSA)
    - ii. Missed – 13 ea ( $7ea \leq 1\%$ ,  $1\% \leq 3ea \leq 2\%$ ,  $3\% \leq 3ea \leq 5\%$ )

There were no false calls.

Other observations include:

- (1) Locations were within 12 inches of the actual features (welds, casing spacers, and defects) 92% of the time.
- (2) Shapes of defect were correctly predicted 87% of the time.
- (3) Axial lengths of defect were correctly predicted less than 30% of the time. Noise renders the measurements of axial length of small defects a challenge.

### *Long Term Monitoring Results*

Two monitoring tests were conducted:

- **1<sup>st</sup> Test:** November 6, 2007, Air temperature in the low 40s °F
- **2<sup>nd</sup> Test:** February 20, 2008, Air temperature ranged from 15 to 25 °F

Details of the SHM test data and the comparison results with the baseline data are given in Appendix B and C within the SwRI final report.

Overall Findings from the SHM Measurements:

- (1) All MsS probes installed on the test pipes performed well over a ten month duration, indicating suitability for long-term SHM applications.

- (2) Data from the bare pipe were reproducible within 0.2% reflection, indicating that a 0.4% CSA change could be reliably detected from SHM measurements.
- (3) In the TGF-3 and CTE-coated test pipes, existing signals from actual features on the pipe were reproducible within approximately 1 to 2% reflection – about 5 to 10 times worse than the reproducibility in the bare pipe. This means that the growth of the existing defects or formation of new defects at weld or spacer locations would not be detectable until the changes exceed 2 to 4% reflection level. The primary cause of the poor reproducibility is believed to be variations in temperature affecting: coating properties and spacer to pipe mechanical coupling.
- (4) When excluding existing feature signals in the TGF-3 and CTE coated test pipes, the SHM data were reproducible within 0.5% reflection. This implies that the formation of new defects with 1% CSA would be reliably detected from SHM measurements.

To achieve the detection sensitivity of 1% CSA changes in defect size in coated pipes, the effect of attenuation change with temperature on signal waveforms should be minimized by developing suitable data processing techniques for correcting the attenuation effects. It should be noted that live field installations are typically buried more than 3 feet; resulting in more stabilized temperatures of the materials.

During the removal of the installed sensors, the iron-cobalt strips were found to be in good condition, indicating that the wax tape protected them well over the 10-month period. In some sensor installation locations, water was found at the bottom of the pipe along with corrosion discoloration of the iron-cobalt strips. This indicates that the wax tape did not completely repel the water, perhaps due to imperfect placement of the wax tape during the installation.

## Task Procedures and Results

### Task #6 Conduct Field Evaluation

*ConEd Astoria Tunnel, New York, NY*

Testing was conducted with ConEd during the week of May 28<sup>th</sup>, 2007 at the Astoria Tunnel in Queens, NY. The tunnel is beneath the East River and spans a distance of approximately 1 mile. The gas pipeline is a 26 inch steel pipe coated with wax tape wrap. The MsS probes were installed at two short sections where the wax tape wrap was removed. Generalized corrosion around the pipe circumference was evident at the two areas where the probes were installed. The surface of the pipe had extensive pitting. The length of the test section between the probes was approximately 74 feet.



MsS installed on 26" gas pipeline in the Astoria Tunnel



General corrosion located on much of the pipe

Baseline data were acquired using the installed sensors. The combination of the wax tape coating and general corrosion developed a high attenuation (about 0.5 dB/ft at 16 kHz and 1.0 dB/ft at 32 kHz). The achievable test range at 16 kHz was approximately 40 to 45 ft. The baseline data suggested four defect indications estimated at 10 to 15% CSA. ConEd staff removed the wax tape coating at the four defect indication locations and visually inspected the locations. Generalized corrosion around the circumference was found to be similar to the condition at the sensor installation locations. ConEd reported the severity of wall loss to be benign; however, % CSA was not determined.

SwRI claims that if extensive depth measurements were performed, their predicted CSA could be realized as suggested by the baseline data. It is believed that the corrosion has not been active for many years. Therefore it was decided to not pursue long term monitoring at the Astoria Tunnel for this study. Detailed test data and results are documented in Appendix D of the SwRI final report.

### *RG&E Cased-Line Mockups, Rochester, NY*

In order to fulfill the need of long term monitoring of an actual field location with active corrosion, RG&E identified a cased section scheduled for decommissioning. The intent was to reverse the current in its cathodic protection system to provide a carrier pipe where long term monitoring could be performed at an accelerated pace. It was realized that such reverse cathodic protection could compromise the integrity of its replacement pipe in close proximity. RG&E volunteered to construct a field mockup exclusively for testing under this project in kind. The cased pipe would be aboveground with reversed cathodic protection installed to facilitate the accelerated corrosion. Two mockup cased sections were ultimately constructed by RG&E. The accelerated corrosion on the first cased pipe was overly aggressive and resulted in premature perforation of the pipe wall; therefore a second mockup was constructed.

#### *First RG&E Mockup*

The first mockup was a 4 inch carrier pipe approximately 66 feet long with a 0.237 inch wall thickness. It was inside a 43 foot long, 6 inch steel casing pipe. The carrier pipe was constructed from two 33 foot pipe joints; the first joint had a PRITEC<sup>®</sup> coating, the other joint had a field-applied coal tar tape wrap (Tapecoat<sup>®</sup> 20).

The MsS probes were installed on both sides of the casing and baseline data were measured on September 20, 2007. Figure 1 shows photos of the testing and the installed probes at one end (the probes were wrapped with a protective tape).

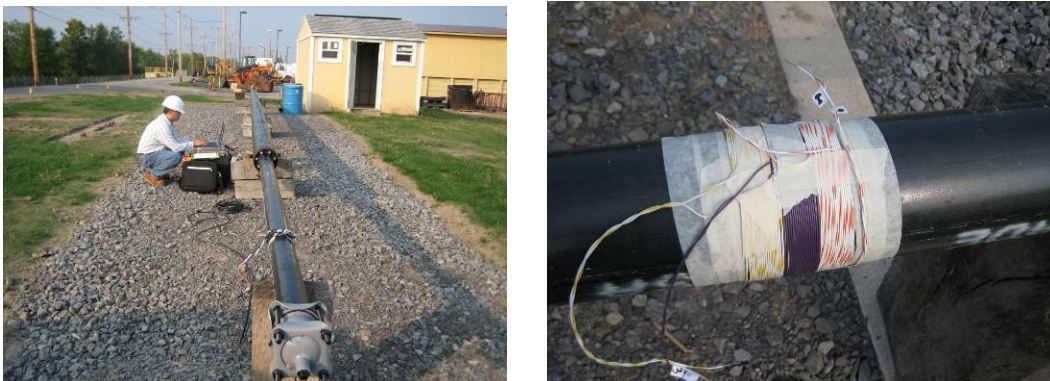


Figure 1. MsS testing on the 1st RG&E cased pipe mockup with installed probes

After recording baseline measurements, the annular space was filled with salt a water solution and reverse cathodic protection current was applied to the test pipe. Accelerated corrosion defects developed at four known locations along the pipe. These known defects were prepared to occur in specific areas by RG&E and kept confidential from SwRI. After several weeks of accelerated corrosion treatments, SHM measurements were conducted on November 6, 2007. The graphs in Figure 1 show the data acquired at 16 and 25 kHz.

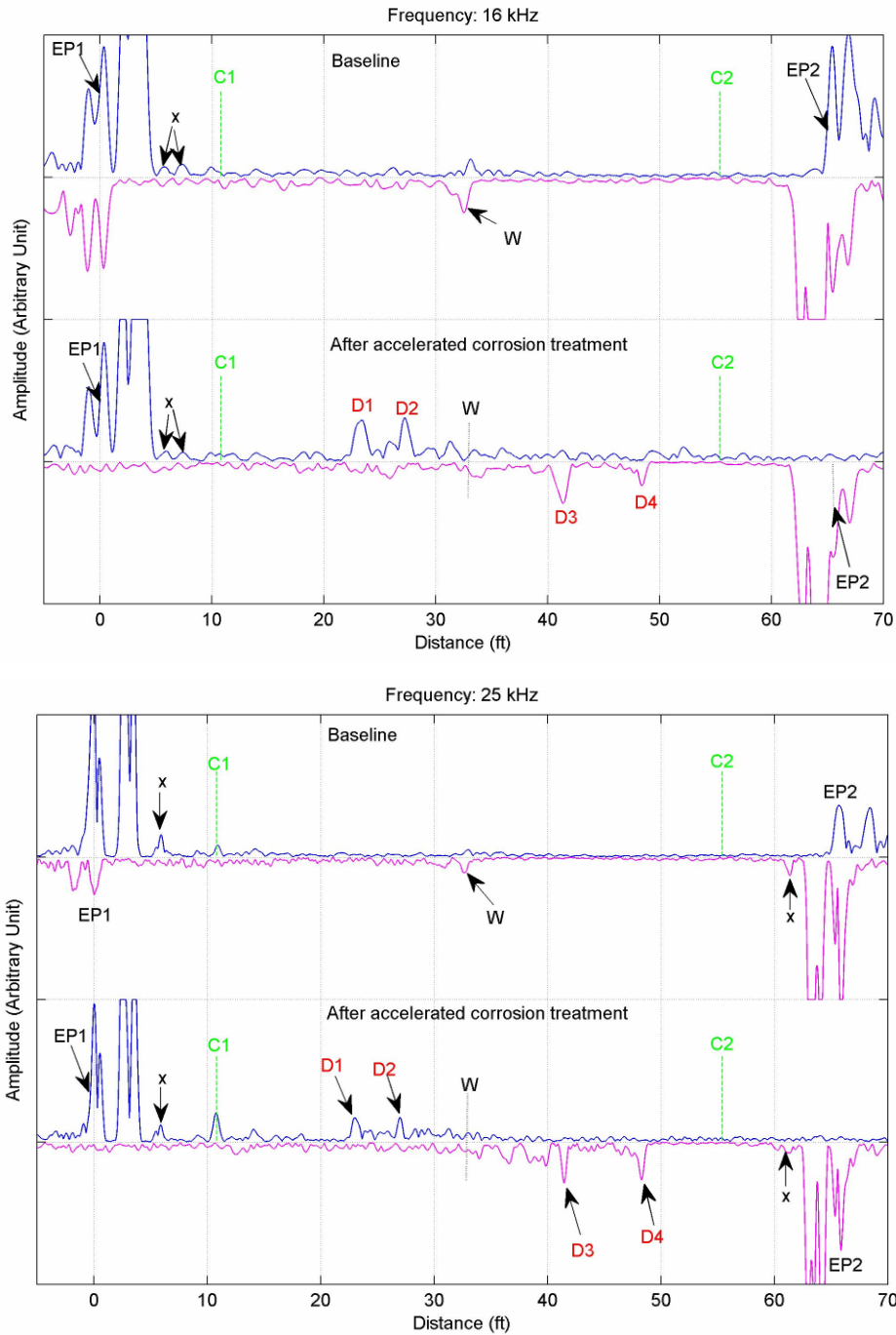


Figure 1. Data at 16-kHz and 25-kHz from the 1<sup>st</sup> RG&E mockup: top half = baseline data, bottom half = data taken after the accelerated corrosion. Blue lines correspond to data taken from the east end of the pipe (EP1). Pink lines correspond to data taken from the west end of the pipe (EP2). C1 and C2 are the casing ends. W is the weld. D1 to D4 are the corrosion defects.

Attenuation was measured to be about 0.2dB/ft at 16 kHz and 0.36 dB/ft at 25 kHz. The signal from the weld was detectable in the baseline data; however its signal-to-noise ratio was low (about 2 to 3). This was due to background noise caused by non-uniform field applied wrap coating.

The SHM data taken after the accelerated corrosion were significantly different from the baseline data. The wave attenuation was much higher than before. As a result, neither the pipe end nor the weld signals were detectable, indicating that severe general corrosion had occurred along the pipe (several local corrosion pits would not lead to the loss of signal from the far end). Additionally, large new defect indications (D1 through D4) were apparent that were originally absent in the baseline data. Judging from the defect signal amplitudes and the lack of weld signal, SwRI assumed all defects to be greater than 10 to 20% CSA. Because of the large defect size and difficulty in determining wave attenuation, no attempts were made to characterize the defects.

While SwRI analyzed the MsS signals in their Texas headquarters, RG&E removed the casing and measured the actual defects for comparison with the SHM results. The four defects were large through-holes about 3 to 6 inches in axial length. The actual % CSA ranged from 21 to 42% of the total cross-section of the pipe. The large defects are shown in Figure 2 including a photo of the 2.8% CSA defect induced at the weld location. The latter defect was not clearly detectable from the SHM data because of the poor S/N ratio.



Figure 2. 1<sup>st</sup> RG&E Test Pipe Defects: Large defects (left two) and 2.8% CSA defect at the weld location (right)

Overall findings from the First RG&E Mockup:

- (1) The large defects induced in the pipe were easily detectable. The defects were too large to continue testing the SHM capability (reason for 2<sup>nd</sup> mockup testing).
- (2) The wave attenuation in the PRITEC<sup>®</sup> coating and the field applied coal tar tape coating was similar to the wave attenuation caused by TGF-3 coated pipe at the NYSEARCH/NGA test bed facility.
- (3) The field-wrapped coal tar coating is uneven and produces relatively large background noise (about 2% reflection level).
- (4) General corrosion increases wave attenuation significantly. Therefore, attenuation measurements can be used to determine the degree of general corrosion (rather than localized corrosion areas).

### Second RG&E Mockup:

The second mockup was also a 4 inch carrier pipe approximately 62 feet long with a 0.237 inch wall thickness. It was inside a 44.5 foot long, 6 inch steel casing pipe. The carrier pipe was constructed from two 44 foot pipe joints; both joints had a FBE (fusion bonded epoxy) coating.

The MsS probes were installed on both sides of the carrier and baseline data were measured on January 8, 2008. After the data was collected, the test pipe was subjected to accelerated corrosion. The 1<sup>st</sup> SHM measurements were made on February 5, 2008, followed by additional accelerated corrosion treatments. The 2<sup>nd</sup> SHM measurements were performed on February 19, 2008.

### Baseline Test Results

Figures 3 and 4 show the baseline data acquired at 32 and 16 kHz. The wave attenuation was low (approximately 0.09 dB/ft at 32 kHz and 0.07 dB/ft at 16 kHz). The data had low background noise (equivalent to approximately 0.4% reflection). The attenuation and background noise level were low due to the FBE coating. There were seven (7) defect indications found with the 32-kHz data, (d1 through d7) their distances from the east end of the pipe were respectively 11.3, 14.4, 20.4, 27.4, 32.2, 37, and 40 ft. The defect indications represented approximately 0.8% CSA. Signals labeled as X in the figures are those caused by imperfections in direction control or multiple reflections. For comparison, the actual defect locations are indicated as bold red dots in the figures.

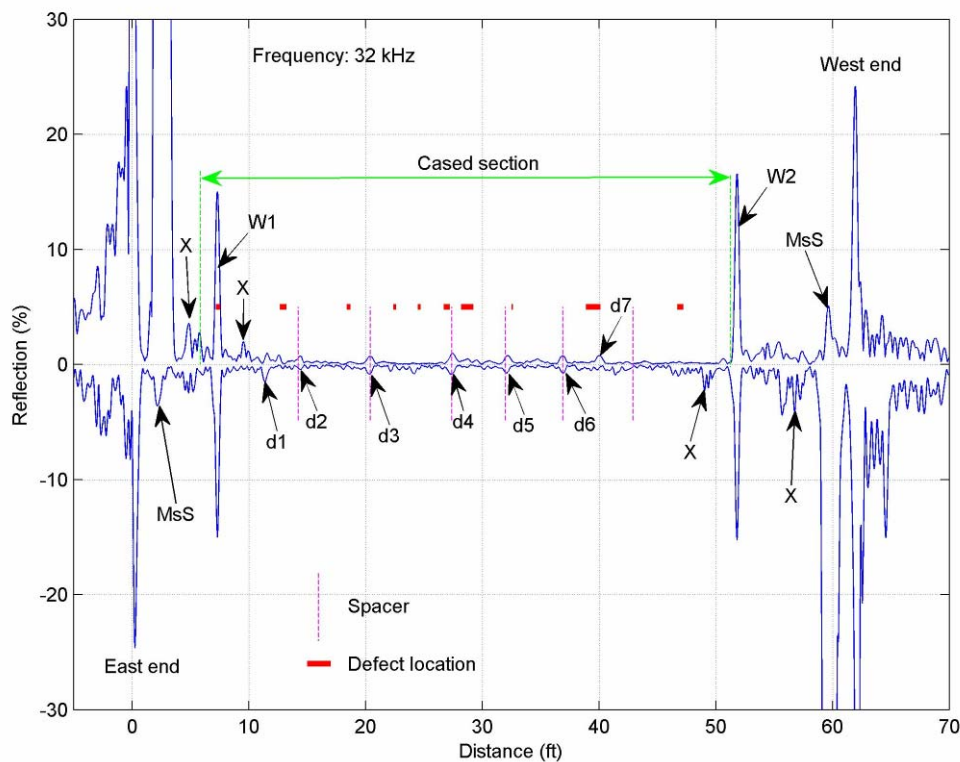


Figure 3. 32 kHz baseline data from the 2<sup>nd</sup> RG&E test pipe

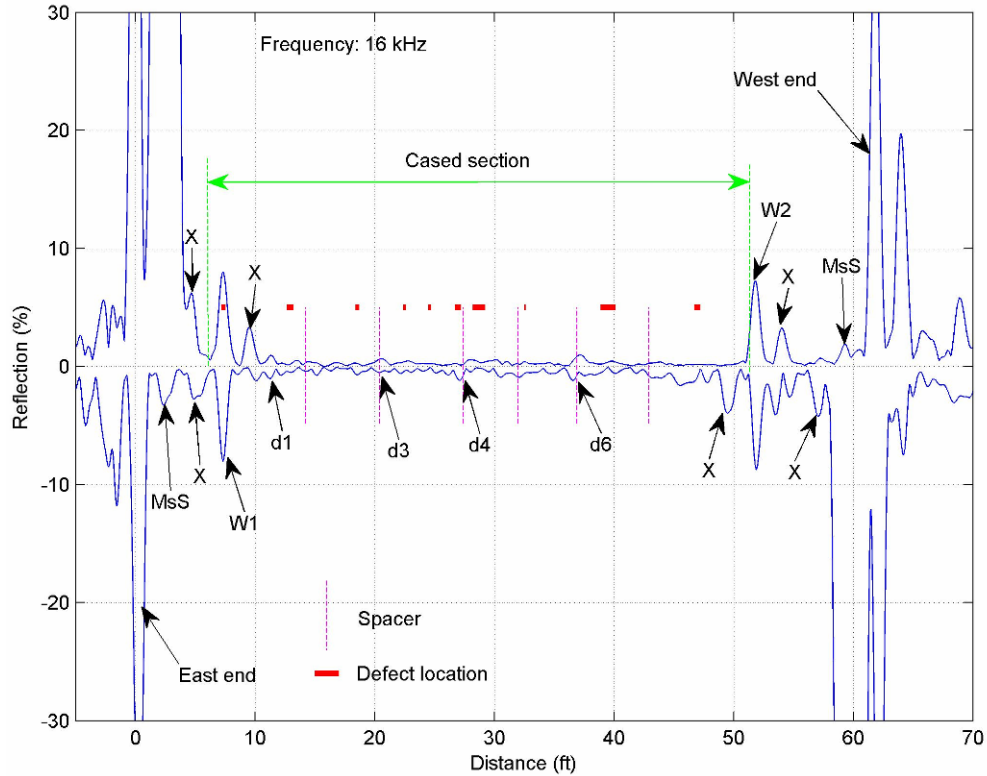


Figure 4. 16 kHz baseline data from the 2<sup>nd</sup> RG&E test pipe

Casing spacers are several inches wide. Therefore, if they produce detectable signals, the signals at 32 kHz are usually double-peaked due to the separation of the signals reflected from the front and rear ends of the spacer. All indications found in the 32-kHz data were single-peaked and thus were thought to be from locations where the coating was removed to produce corrosion defects. In actuality, 5 out of 7 indications turned out to be from casing spacers. It was noted that all the spacers, except the one closest to the west end, produced detectable signals. The coating removal areas did not produce detectable signals, except perhaps at d4 and d7 locations and between d1 and d2. It is unclear what caused the d1 signal.

### 1<sup>st</sup> SHM Test Results

Figures 5 and 6 show the 1<sup>st</sup> SHM data acquired from the mockup at 32 and 16 kHz, respectively. The wave attenuation was higher than before resulting from the general corrosion induced on the carrier pipe. Using the two weld signals as reference, it was determined that the attenuation increased from the baseline values to about 0.24 dB/ft at 32 kHz and to about 0.19 dB/ft at 16 kHz. 8 defect signals were detected. The majority of the 32-kHz defect signals were double-peaked, indicating that the defect length was long enough to separate the signals reflected from the front and the rear of the defect. For comparison, the actual defect locations are indicated as bold red dots in the figures.

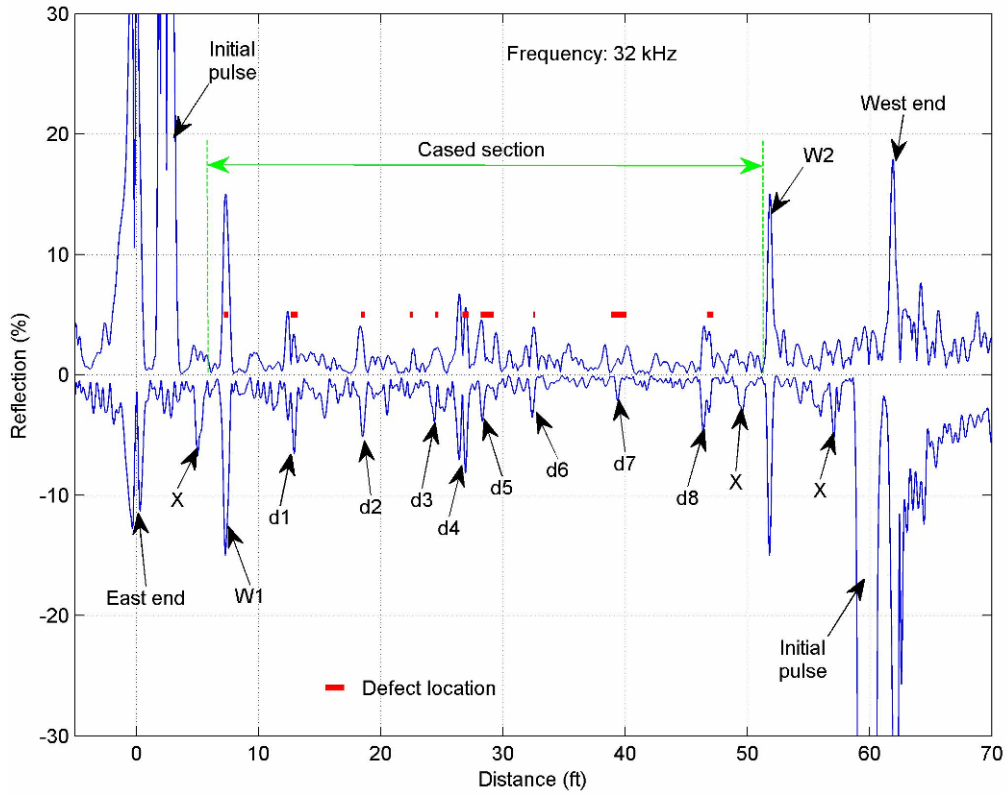


Figure 5. 1<sup>st</sup> SHM data at 32 kHz from the 2<sup>nd</sup> RG&E test pipe

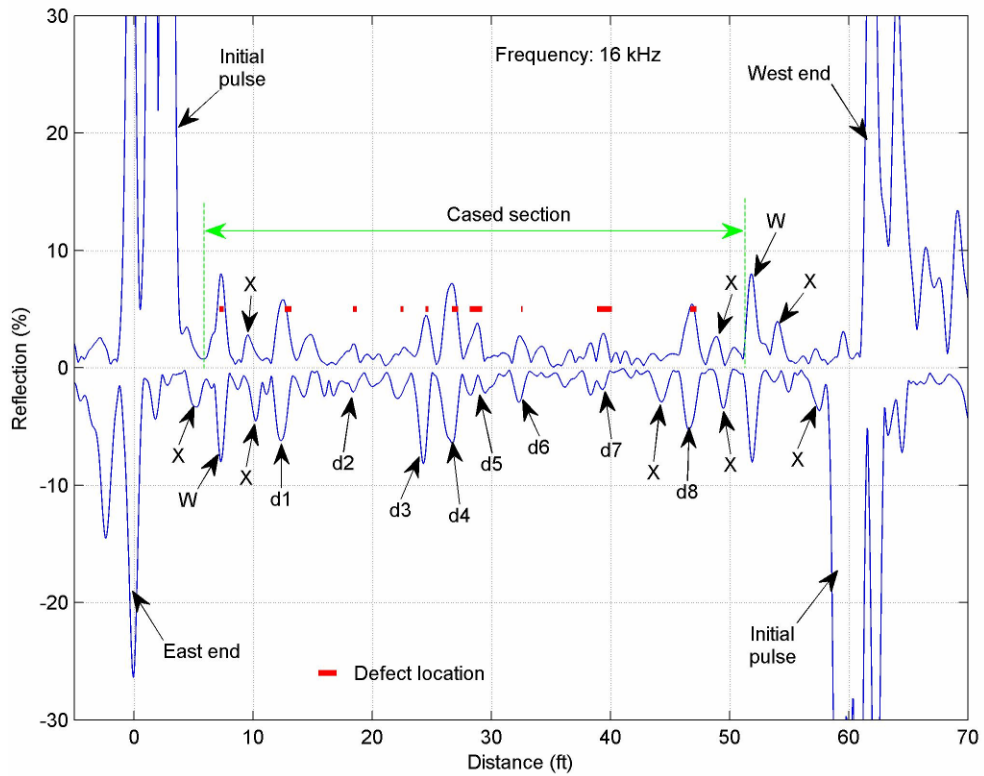


Figure 6. 1<sup>st</sup> SHM data at 16 kHz from the 2<sup>nd</sup> RG&E test pipe

There were substantial weld and end signal differences between the baseline data and the 1<sup>st</sup> SHM data. Reasons why the weld and end signals changed include:

- 1) Waveform change due to attenuation increase
- 2) Energy loss at the defects
- 3) Interference from multiple reflected signals and end caps.

As a result, it was difficult to positively determine whether a defect was formed at or near the weld. In the remaining data analyses, the welds were assumed to be defect-free and their signals were used as the calibration reference.

Table 7 lists the defect axial locations, axial length, shape, and CSA determined from the 1<sup>st</sup> SHM data. The east side weld (W1) in actually contained a large defect (approximately 31% CSA). Therefore, the assumption employed in the analysis underestimates the defect CSA.

**Table 7. Axial Locations and Characteristics of Defects Detected from the 1<sup>st</sup> SHM Data**

Defect		d1	d2	d3	d4	d5	d6	d7	d8
Location* (ft)		12.6	18.5	25.5	26.6	28.5	32.4	39.1	46.6
Length (inch)	A	7	N/A	7	6	13	7	12.5	5
	B	8-10	2-3	4-6	6-8	6-8	4-6	12-14	4-6
Shape	B	Trap.							
CSA (%)	C	6	4.5	4.5	7	3.5	3	2	4
	B	6-8	4-6	6-8	6-8	4-6	2-4	4-6	6-8

\* – Measured from the east end of the test pipe to the center of the defect  
A – Determined from the separation between the two peaks in the 32-kHz signal  
B – Results of defect classifier algorithms (primarily based on the 16-kHz signal)  
C – Based on the average signal % reflection

---

## 2<sup>nd</sup> SHM Test Results

The 2<sup>nd</sup> SHM test exhibited two different properties when compared to the 1<sup>st</sup> SHM test. The first difference was that the overall wave attenuation was significantly higher, evidenced by the fact that the far-end signal was not detectable at 32 kHz and barely noticeable at 16 kHz. The high attenuation indicated that the degree of general corrosion induced in the test pipe was substantially higher than at the time of the 1<sup>st</sup> SHM measurements. The second difference was that the test range of the east-side MsS was about 4 times shorter than that of the west-side MsS, indicating that the section of the pipe between the locations of d1 and d4 was more heavily corroded (and thus more attenuative) than the other sections of the pipe.

The knowledge of attenuation values relating to corrosion product and metal loss is lacking, therefore assumptions and linear corrections were made regarding attenuation dependencies. SwRI claims that without the 1<sup>st</sup> SHM data, the interpretation of the 2<sup>nd</sup> SHM data would have been very difficult and, thus,

subject to a much greater error. The data from the 2<sup>nd</sup> RG&E mockup shows the advantages of SHM over one-time inspection. Therefore, MsS technology is not ideal for one time inspection.

The corrected 2<sup>nd</sup> SHM data (blue) are plotted along with the 1<sup>st</sup> SHM data (red) in Figure 8 for 32 kHz and in Figure 9 for 16 kHz. Defect 2 was not detectable in the 2<sup>nd</sup> SHM data. In general, the CSA of all other defects appeared to be doubled since the 1<sup>st</sup> SHM measurements. The defect characteristics determined from the 2<sup>nd</sup> SHM measurements are listed in Table 10. In the analyses, the weld signals were again used as calibration references. Since the W1 area contained a large defect (at this time, approximately 51% CSA), the CSA of d1 was significantly underestimated.

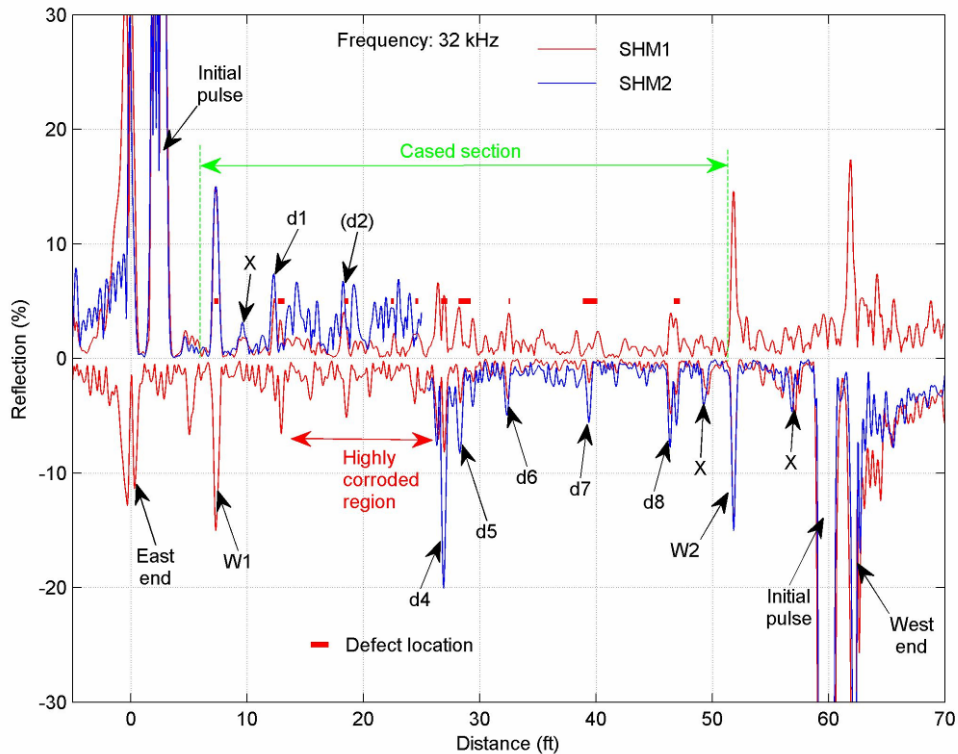


Figure 8. Comparison between the 1<sup>st</sup> and 2<sup>nd</sup> SHM data at 32 kHz

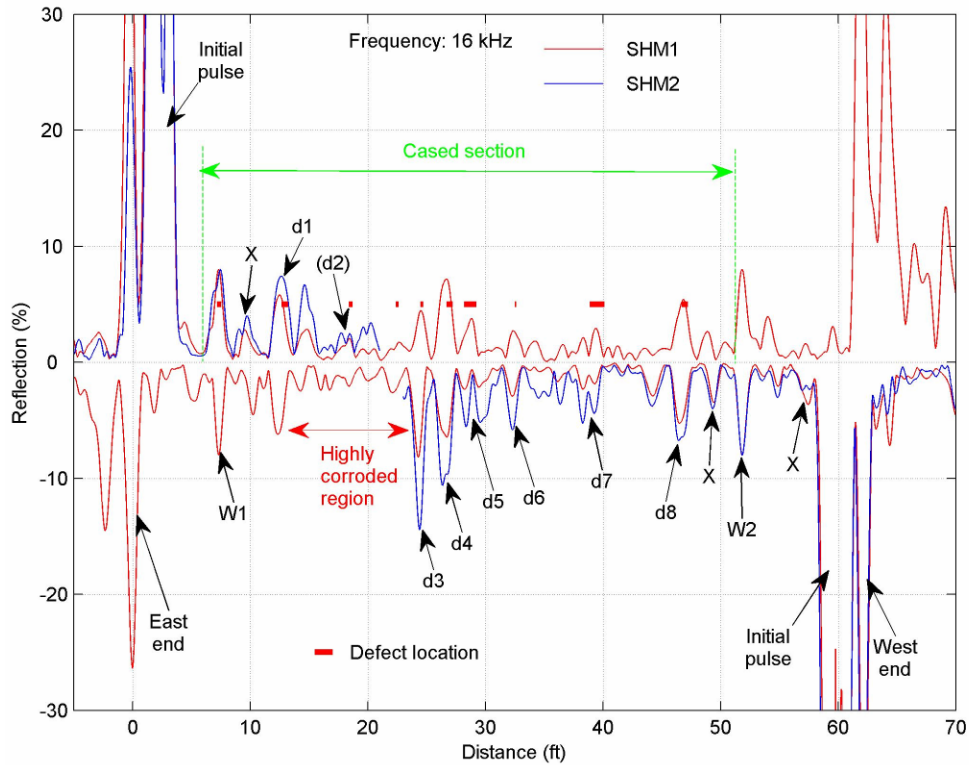


Figure 9. Comparison between the 1<sup>st</sup> and 2<sup>nd</sup> SHM data at 16 kHz

Table 10. Characteristics of Defects Detected from the 2<sup>nd</sup> SHM Data

Defect		d1	d2	d3	d4	d5	d6	d7	d8
Location* (ft)		12.5	N/A	24.4	26.6	28.5	32.3	39.1	46.4
Length (inch)	A	N/A	N/A	N/A	8	N/A	N/A	N/A	8
	B	8-10	N/A	6-8	6-8	6-8	6-8	14-16	6-8
Shape	B	Trap.	N/A	Trap.	Trap.	Trap.	Trap.	Trap.	Trap.
CSA (%)	C	8	N/A	15	15	6.5	6	5	7.5
	B	6-8	N/A	O/R	O/R	6-8	6-8	6-8	6-8

\* – Measured from the east end of the test pipe to the center of the defect

A – Determined from the separation between the two peaks in the 32-kHz signal

B – Results of defect classifier algorithms (primarily based on the 16-kHz signal); O/R –over the range of the classifier algorithm (this means CSA ≥ 10%)

C – Based on the average signal % reflection

Note – The W1 (east-side weld) signal at 16 kHz showed a change, suggesting a possible defect in the vicinity.

### Comparison with Actual Defects

Actual locations and sizes of defects in the mockup are listed in Table 11. Except for the full-circumferential defect in the east-side weld (W1) area (RG&E defect ID No.1), all other defects were square or rectangular in shape. An example of a defect that was taken after the 2<sup>nd</sup> SHM test is shown in Figure 12.

**Table 11. Actual Locations and Sizes of Defects Induced in the Test Pipe**

SHM Defect No.	RG&E Defect ID No.	Axial Location (a)	Clock Position (b)	Circ. Width	Axial Length	At the Time of 1 <sup>st</sup> SHM Test		At the Time of 2 <sup>nd</sup> SHM Test	
						Depth	CSA	Depth	CSA
N.C (c)	1	7.3 ft	—	14" (full)	4"	0.071"	31.3%	0.116"	51.2%
d1	12	12.7	9:00	6	6	0.080	15.1	0.134	25.4
d2	11	18.4	6:00	3	3	0.087	8.2	0.177	16.7
N.C (c)	10	22.4	6:00	1	1	0.101	3.2	0.213	6.7
	13	22.6	9:00	2	2	0.108	6.8	0.176	11.1
d3	14	24.5	9:00	2	2	0.117	7.3	0.170	10.7
d4	5	26.7	3:00	6	6	0.083	15.7	0.101	19.1
d5	6	28.3	3:00	1	1	0.126	4.0	0.186	5.9
	15	28.9	9:00	1	12	0.090	2.8	0.151	4.8
d6	7	32.5	3:00	1	1	0.093	2.9	0.166	5.2
d7	3	38.9	12:00	1	12	0.065	2.0	0.102	3.2
	9	38.9	6:00	1	12	0.074	2.3	0.127	4.0
d8	2	46.7	12:00	1	6	0.049	1.6	0.094	3.0
	8	46.7	3:00	1	6	0.098	3.1	0.098	3.1
	16	46.7	9:00	1	6	0.098	3.1	0.144	4.5

- (a) Measured from the east end of the test pipe to the center of the defect
- (b) Position around the pipe circumference
- (c) Not called during the data analyses



**Figure 12. Typical defect induced in the 2nd RG&E mockup: RG&E Defect ID 11**

A total of (15) defects were created in the test pipe. In guided-wave testing, multiple defects at approximately the same axial location produce one signal. Therefore, defects at approximately the same axial location are grouped together in Table 11 (example: the d5 signal in the SHM data was produced by RG&E

defects 6 and 15; the d8 signal by RG&E defects 2, 8 and 16). This made a total of (10) defects along the length of the cased section of the test pipe.

Out of (10) defects, (8) were positively identified from the SHM data. Indications for the two other defects (RG&E defect 1 in the east-side weld area and RG&E defects 10 and 13 at approximately 22.5-ft location) were present in the SHM data; but because of the uncertainty, they were not called during the data analyses. There were no false calls made from the data analyses.

Table 12 shows a comparison between the actual defect length and CSA and those determined from the SHM data.

**Table 12. Comparison Between Actual Defect Length and CSA and Those Determined from SHM Data**

SHM defect No.	At the time of 1 <sup>st</sup> SHM Test						At the time of 2 <sup>nd</sup> SHM Test					
	Axial Length (inch)			CSA(%)			Axial Length (inch)			CSA (%)		
	Act. <sup>(a)</sup>	A	B	Act. <sup>(b)</sup>	C	B	Act. <sup>(a)</sup>	A	B	Act. <sup>(b)</sup>	C	B
d1	6	7	8-10	15.1	6	6-8	6	--	8-10	25.4	8	6-8
d2	3	--	2-3	8.2	4.5	4-6	3	--	--	16.7	--	--
d3	2	7	4-6	7.3	4.5	6-8	2	--	6-8	10.7	15	≥10
d4	6	6	6-8	15.7	7	6-8	6	8	6-8	19.1	15	≥10
d5	12	13	6-8	6.8	3.5	4-6	12	--	6-8	10.7	6.5	6-8
d6	1	7	4-6	2.9	3	2-4	1	--	6-8	5.2	6	6-8
d7	12	12.5	12-14	4.3	2	4-6	12	--	14-16	7.2	5	6-8
d8	6	5	4-6	7.8	4	6-8	6	8	6-8	10.6	7.5	6-8

- (a) For multiple defects in the same location, it represents the longest length
- (b) For multiple defects in the same location, it represents the sum of all defects
- A Determined from the separation between the two peaks in the 32-kHz signal
- B Results of defect classifier algorithms (primarily based on the 16-kHz signal)
- C Based on the average signal % reflection

As mentioned earlier W1 and W2 signals in the data were used as calibration reference for data analyses. Since a large defect (RG&E defect 1 in Table 11) was present in the W1 area, the above data analysis procedure led to an underestimation of defect CSA – particularly for the defect closest to W1 (namely, d1) and for the defects that were detected from the east side MsS. Otherwise, defect CSAs determined using the classifier algorithm (column B in table 12) was in fair agreement with the actual CSAs. The cause for the short test range of the east side MsS in the 2<sup>nd</sup> SHM data was the presence of the large defect in the W1 area (51% CSA) and d1 (25% CSA) and not the high corrosion area between d1 and d4 (a misinterpretation of the data that resulted from the use of the W1 signal as a reference).

The values of the axial lengths of defects determined using the classifier algorithm (column B in table 12) was in good agreement with the actual lengths except for the short defects (d3 and d6). The axial length of a short defect is harder to determine because the base of the envelope, the primary parameter

related to the defect length, changes little until the length becomes comparable to the wavelength (8 inches at 16 kHz).

Overall Findings:

- (1) The accelerated corrosion defects were readily detectable from the 1<sup>st</sup> SHM data, indicating that the defect growth could be accurately tracked using the SHM approach during the early stages of degradation (for defects up to 10% CSA and until the attenuation caused by the general corrosion limits the detection accuracy).
- (2) Within the known limitations, the classifier algorithms worked well.
- (3) The test results further confirmed the existence of a good correlation between the wave attenuation and the degree of general corrosion. Establishing quantitative correlation between the two would be very useful for DA applications. To relate the attenuation with the degree of corrosion in coated lines, the portion of attenuation that was caused by the coating itself should be separately accounted for. Therefore, collecting attenuation data on various types of coated pipe and their dependence on temperature is needed.
- (4) Since the weld signals are used as references in the data analyses, the presence of a large defect in the weld area led to substantial error in data interpretation. To minimize the error and to be able to positively detect a defect formation and growth in the weld area, more reliable calibration methods and procedures are necessary.
- (5) The MsS probes performed well throughout the whole testing process (which involved mechanical handling) and the winter weather at Rochester. This indicates the probe's long-term durability and reliability in field conditions.

## Task Procedures and Results

### **Additional Task Investigation of Guided Wave Attenuation Changes with Coated Pipe Temperature and General Corrosion**

Long term monitoring during field testing provided the comparison of multiple sets of data with initial baseline results. It became apparent that other variables may have had an affect on the data. SwRI proposed additional tasks of interest in a white paper for a new phase to the current study. Coincidentally, funding was not fully expended near the close of the project. Two tasks in the white paper exhibited high value, and were therefore chosen to answer important questions concerning the data in this project and guided wave in general.

#### *Temperature Dependence of Attenuation in Coated Pipes*

The following three coating type were selected – coal tar (specifically TGF-3), coal tar epoxy (CTE), and polyethylene (PE) (specifically PRITEC®). The basis of selection of these coatings was to maintain consistency with field tests at the NYSEARCH/NGA Test Bed and RG&E performed during this study. These coatings are widely used in cased applications in the gas utility industry. Three 10 foot lengths of 6 inch pipe having a 0.28-inch wall thickness were used for each coating type. MsS probes were installed near one end of each pipe sample. All three samples were then placed within a large environmental chamber where the temperature was raised from 0 to 120° F. MsS data was acquired at 10° F increments using six different frequencies (10 to 60 kHz at 10 kHz increments).

#### Coal Tar Epoxy (CTE) Coating

The attenuation in the CTE coated pipe was low, only slightly higher than in a bare pipe and almost identical to the attenuation in painted pipelines. Apparently the thin CTE coating, acts like a paint coating on pipes. Further at a given frequency, the effect of temperature also produced a very small (<0.05 dB/ft) attenuation change.

The low attenuation values and slight temperature effects indicates that pipelines with CTE coating would be benign to long range guided wave inspection and easiest to detect corrosion state from attenuation measurements.

#### PRITEC® Polyethylene (PE)

The experimental results from the PE (PRITEC®) coated pipe samples are plotted in Figure 1. The plot shows the temperature dependence of attenuation at discrete frequencies (10 to 50 kHz). Unlike the CTE coating, there were limited measurements for the high frequency and high temperature cases as a result of

the attenuation. The absolute attenuation values are shown for this region as “dashed” lines to imply a lower degree of confidence. The PE coated pipe also showed the typical behavior of attenuation; namely increase with increasing frequency and temperature. The attenuation values at 70°F ranged from 0.024 dB/ft at 10-kHz to 0.749 dB/ft at 50-kHz. This is significantly higher than the values in the CTE coated pipe.

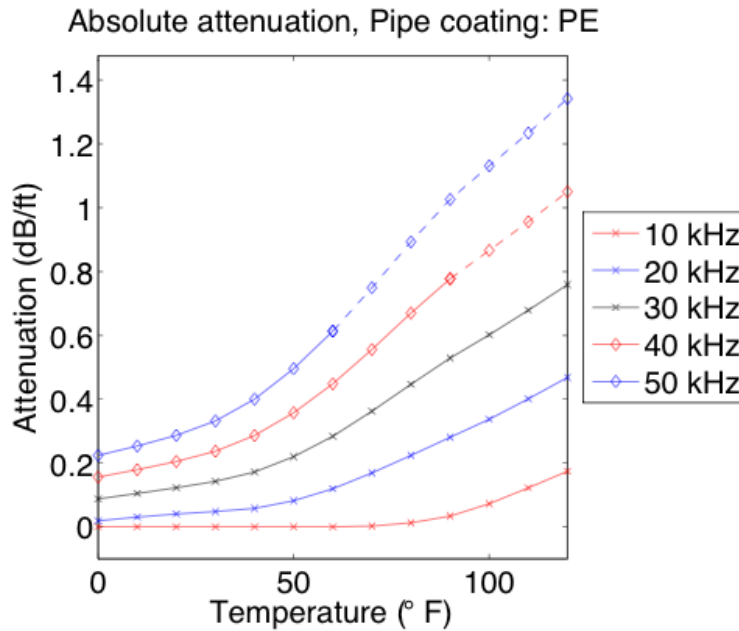


Figure 1. Experimental results from the PE coated pipe illustrating the temperature dependence of attenuation at discrete frequencies. Dashed lines represent extrapolated approximations.

Because of the large increase in attenuation with temperature, results of guided-wave inspection of PE coated pipelines would become increasingly poorer with increasing temperature.

### Coal Tar (TGF-3) Coating

The experimental results from the TGF-3 coated pipe samples are plotted in Figure 2. The plot illustrates the temperature dependence of attenuation at discrete frequencies (10 to 50 kHz). As with the polyethylene coated pipe, there was limited information for the high frequency / high temperature combinations. The interpolations are represented by the “dashed” lines. The attenuation in the TGF-3 coated pipe also increased with increasing frequency and temperature. Of the three coating types investigated in this project, the TGF-3 Coal Tar coating was the most attenuative. Similarly to the PE coated pipe, temperature has a large influence on the attenuation and the temperature effects were greater at higher frequencies. Because of the large increase in attenuation with temperature, results of guided-wave inspection of TGF-3 coated pipelines would become increasingly poorer with increasing temperature. The temperature effects in the TFG-3 coated pipe were about twice as much as that in the PE

coated pipe. Thus, the consideration of temperature is even more so important for guided-wave inspection of Coal Tar (TGF-3) coated pipelines.

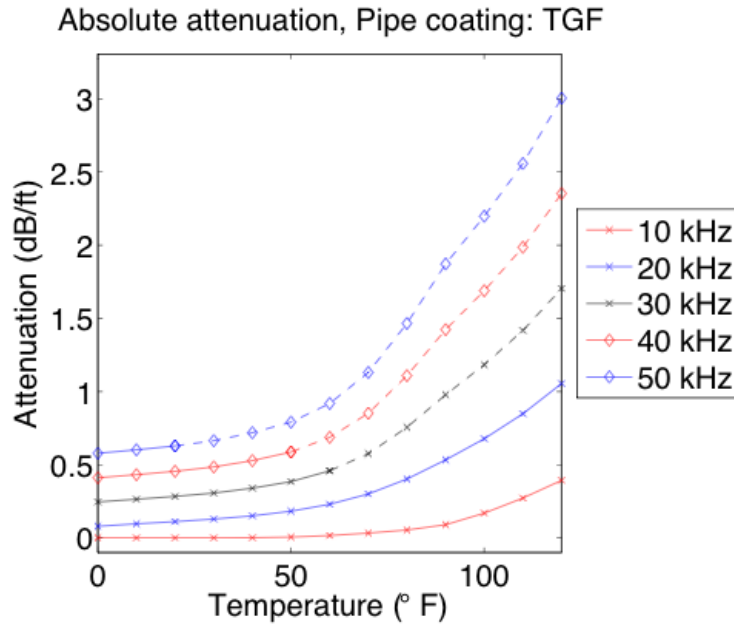


Figure 2. Experimental results from the TGF-3 coal tar coated pipe illustrating the temperature dependence of attenuation at discrete frequencies. Dashed lines represent extrapolated approximations.

If a guided wave inspection would be performed during warmer conditions, and again during cooler conditions, it would appear as if the severity of the defect increased. However, the attenuation would simply decrease and reflect a greater signal; creating the appearance of a worsening defect. Therefore, if practical, a guided wave inspection of PE coated pipelines should be conducted at the lowest temperatures possible and with relatively consistent temperatures.

### *Effects of General Corrosion on Attenuation*

Two 10 foot lengths of 6 inch bare carbon steel (CS) pipe each having a 0.28 inch wall thickness were acquired for the investigation. Each pipe was placed in a 10.5-inch OD PVP pipe with a 4 inch section of one end exposed for MsS as shown in Figure 3.



Figure 3. Experimental setup for investigation of corrosion effects on guided-wave attenuation.



Figure 4. PVC pipe filled with salt water solution (left), power supply used to impress the electric current (middle), and fiberglass mesh wrapped around pipe sample (right)

General corrosion was implemented using salt water solution with impressed electric current to accelerate corrosion as shown in Figure 4. Baseline MsS measurements (made on November 17, 2008), confirmed that the water surrounding the pipe sample has no effects on the wave attenuation. While subjecting the pipe samples to impressed electric current, MsS data were acquired periodically (from 10- to 140-kHz at 10-kHz intervals). Final periodic measurements were made on February 9, 2009.

Over a span of 82 days, a total of 15 periodic MsS measurements were conducted. To determine the corrosion wall loss level during the corrosion treatment, ultrasonic wall thickness measurements were performed periodically together with MsS measurements. Because of large error in ultrasonic thickness measurements (approx.  $\pm 0.003$  inches), the wall loss induced in the pipe samples could not be determined reliably. Instead, the corrosion was estimated from the impressed current level at first, then the overall estimated corrosion at the end of treatment was calibrated using the actual wall thickness measured. Figure 5 shows the pipe surface and a section of corrosion product. Except for

the top ¼ of the pipe circumference, the pipe surface was covered with a thick layer of corrosion product loosely attached to the pipe.



Figure 5. Corrosion products on the pipe surface

After observing the corrosion scales induced on pipe surfaces, both samples were cut into three sections and the remaining wall thickness was measured around the circumference using a caliper at both cuts. Figure 6 shows plots of remaining wall (red line) and its distribution around the pipe. The original wall thickness (black line) was measured at the sensor end of the pipe. As can be seen, the wall loss was not uniform around the pipe. On average, the final wall loss was approximately 0.023 inch for pipe sample A and 0.021 inch for pipe sample B.

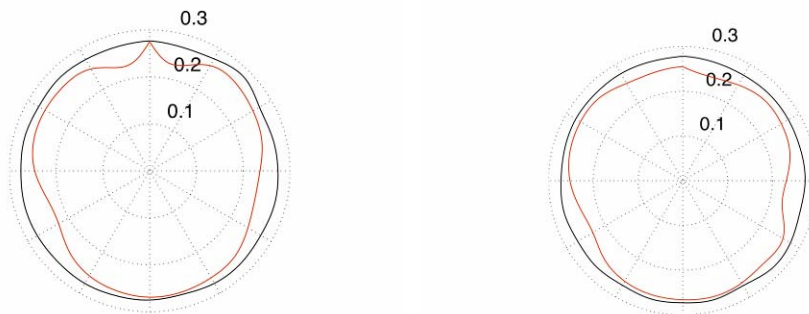


Figure 6. Remaining wall thickness around the circumference of both pipe “A” (left) and pipe “B” (right). The black line represents the original wall thickness and the red line represents the remaining wall at the end of the accelerated corrosion.

Figure 7 shows the theoretical wall loss level over the duration of the corrosion treatment. The three different slopes represent the different impressed current levels. The plateau during days 74-79 in the plot reflects an accidental shut down of the impressed current. The total wall loss level at the end of the corrosion treatment was calculated to be approximately 0.025-inch and was in good agreement the final average wall loss level measured.

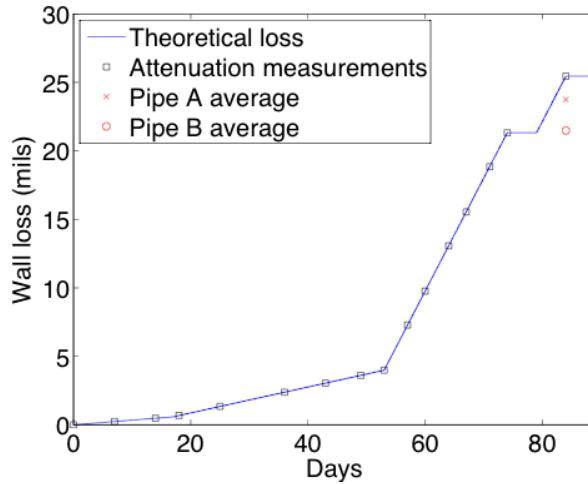


Figure 7. Theoretically calculated wall loss level over the duration of the corrosion treatment. The “squares” indicate the days in which periodic attenuation measurements were made. The final average wall loss measured from both pipes is also shown.

Since the final average wall loss levels measured experimentally were in good agreement with the theoretically calculated values, the theoretical wall loss levels at the time of MsS measurements were used to correlate with the attenuation measurement data.

The attenuation values at discrete frequencies (10, 20, etc.) are plotted in Figure 8.

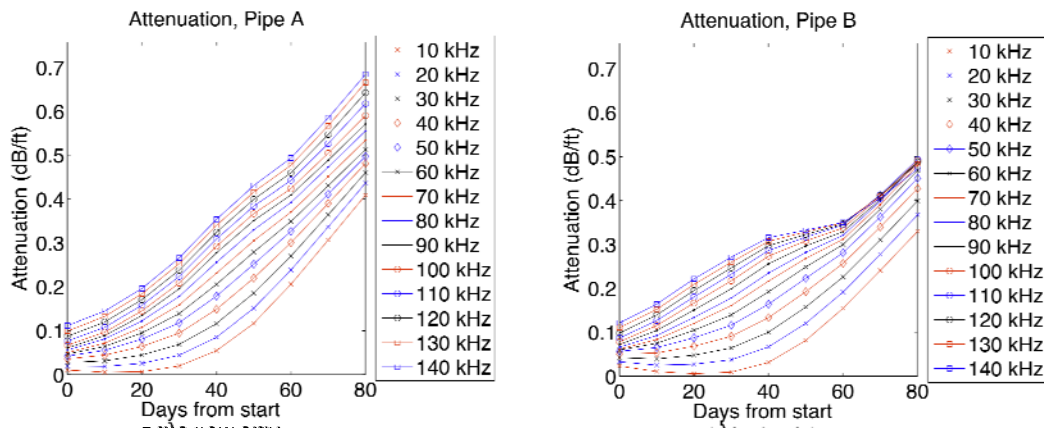


Figure 8. Attenuation as a function of days of corrosion treatment at various frequencies

The attenuation increased continuously with the days of corrosion treatment as expected. The magnitude of corrosion caused attenuation ranged from approximately 0.13 dB/ft at 10 kHz to 0.23 dB/ft at 50 kHz for 0.004 inch wall loss. The attenuation change was greater for pipe sample A than sample B. Corrosion products on sample B were detached during that period of time which

is assumed stunted the attenuation increase. At a given impressed current level, the attenuation for a given frequency increased linearly with the wall loss level. It was observed that, each time the impressed current increased, it lowered the rate of attenuation increase. It appears that the sudden increase of the impressed current level alters surface conditions that diminish the corrosion effects (possibly through the generation of hydrogen gas bubbles).

The corrosion products were found to be loosely attached to the surface of pipe samples (because the samples were kept in aqueous solution). The effects of naturally occurring corrosion on the wave attenuation may differ from what is described in this report. The experimental results show that, once a layer of corrosion product is beyond a certain thickness, adding more corrosion product to the pipe surface has the same effects on all frequencies.

#### *The Capability of Assessing Corrosion State from Attenuation*

The magnitude of corrosion caused attenuation on the bare pipe ranged from approximately 0.13 dB/ft at 10 kHz to 0.23 dB/ft at 50 kHz for 0.004 inch wall loss. The ability to assess corrosion state from attenuation measurements depends on the relative magnitude of corrosion caused attenuation to coating caused attenuation. Localized patches of corrosion on a coated pipe may or may not limit this ability.

In pipelines with a low attenuative coating (such as CTE), corrosion has a high impact on the apparent attenuation. For example, at 10 kHz, the attenuation in pipes with 0.004 inch wall loss would be more than 20 times greater than its initial value with no corrosion. Therefore it is possible to distinguish corrosion caused attenuation from coating caused attenuation. Corrosive wall loss may be determined from attenuation measurements even with patched corrosion. This is also possible for pipelines with a highly attenuative coating (such as PE or coal tar TGF-3) but at low frequencies only (such as 10 kHz).

## **Task Procedures and Results**

### **Task 7**

### **Project Review Meetings**

*Final Project Review Meeting – February 27, 2008*

Daphne D’Zurko, George Janega (NYSEARCH), Robert Smith (PHMSA), and Hegeon Kwun (SwRI) participated in the meeting at the NYSEARCH office in New York, NY. Hegeon provided an overview regarding the results of the project task by task. SwRI’s general technical position was concerning calibrations based on weld locations and the implications that defects on or near a weld have for a guided wave. The second concern was regarding attenuation stemming from coatings and corrosion. PHMSA expressed interest in possibly exploring additional work relating to these concerns. PHMSA emphasized that industry training should be provided by SwRI as part of future phases if they are considered. NYSEARCH requested a white paper from SwRI outlining the tasks for consideration with associated costs.

NYSEARCH and PHMSA discussed the industry concerns with the results of the field tests. The concerns related to the need for a more focused approach to simulated field testing as performed by RG&E but on a larger scale. NYSEARCH staff recommended that further testing should involve a selection of predetermined variables such as defect parameters, coatings, temperature, etc. Staff recommended that the testing should be performed within SwRI labs for the sake of close monitoring and control of variables.

After the review of the white paper (submitted several weeks later) the project was extended to expend unused project funding toward select tasks of the white paper. It was agreed to amend the draft final report with the new information at the time it would become available.

*Additional Project Review Meeting - March 26, 2009*

George Janega (NYSEARCH), Robert Smith (PHMSA), and Hegeon Kwun (SwRI) participated in the meeting at the NYSEARCH office in New York, NY. Hegeon presented the procedures and results of the additional tasks. The influence of weld calibrations on data accuracy and attenuation from general corrosion and coatings was explained. SwRI emphasized the need to develop a new method for calibrating so that defects at welds are not missed. SwRI also stated the need to modify the current algorithms to address the issues regarding attenuation. Furthering MsS research in these areas would enable more accurate data; providing an operator assessment information at the time of sensor installation. SwRI supported the use of long term monitoring as a key asset of the MsS technology.

PHMSA, NYSEARCH and SwRI concurred that long term monitoring and additional research of the MsS technology will not support casing inspection goals to be met by 2012.

## **Conclusions, Recommendations & Next Steps**

### **Conclusions**

The Magnetostrictive Sensor technology is a unique guided wave technology suitable for long term outdoor monitoring of cased pipe sections. MsS can characterize the axial length of a defect within 1 to 2 inches. Defect wall loss changes as small as 1 to 2% cross sectional area (CSA) are detectable in bare pipe. Changes as small as 2 to 4% CSA are detectable in coal tar (TGF-3) coated pipe.

Wave attenuation in the TGF-3 or PE coated pipes increases significantly with increasing temperature. Therefore, a guided wave inspection of TGF-3 or PE coated pipelines should be conducted at the lowest temperatures possible and at consistent temperatures. The wave attenuation in the coal tar epoxy coated pipes is low with very small temperature effects.

Wave attenuation significantly increases with general corrosion as corrosion products build on the pipe surface (from 0.13 dB/ft at 10 kHz to 0.23 dB/ft at 50 kHz for a 0.004 inch depth wall loss). Wave attenuation is a good indicator of the degree of general corrosion on bare pipe even in early its stages. It should be noted that SwRI has independently developed a simple, low cost solution which enables a sensor to retain the magnetic properties in the event of gross depressurization in extreme applications.

### **Recommendations**

Guided wave inspection of Coal Tar (TGF-3) or PE coated pipelines should be conducted at the lowest temperatures possible and with relatively consistent temperatures.

2012 is the date mandated by DoT by which all U.S. cased pipe installations must be assessed. The MsS technology requires further improvements to address shortcomings which prevent it from functioning as a credible and independent solution for DA inspection. Therefore, at this time there are other approaches which have priority for development into short term solutions.

Tasks have been identified to address if continued interest exists for developing the MsS technology as a commercial solution for DA inspection. MsS is a guided wave technology similar to current commercial guided wave technologies; differing mostly in sensor equipment. Therefore, the first recommendation addressed here for improvement applies, in theory, to other mechanical guided wave technologies as well. The following tasks are presented in their order of priority.

- (1) Improve the detection accuracy of CSA change in coated pipelines by developing signal processing methods for correcting attenuation effects on waveforms; especially investigations of the attenuation characteristics of different coating materials/types and temperature effects.
- (2) Develop an improved signal calibration method to the current method which is based on weld signals.
- (3) Determine the magnitude of attenuation increase that would be caused by the natural corrosion process under realistic conditions. Corrosion effects on wave attenuation should be investigated at a low corrosion rate over a long duration of time (such as 1 year or more).
- (4) Take steps for technology transfer that include: develop a GUI program for data analysis intended for use by inspectors, prepare training material, and establish industry-accepted procedures for probe installation and testing.
- (5) Guided wave inspection of Coal Tar (TGF-3) or PE coated pipelines should be conducted at the lowest temperatures possible and with relatively consistent temperatures.

### **Next Steps**

The submission of this final report to funding members and the April 2009 NYSEARCH meeting will allow the industry to express feedback pertaining to a proactive approach, if any, for developing the future commercial readiness of MsS.

During 2009, SwRI will publish a public white paper summarizing the findings from this study relating especially to the additional attenuation task. This will function as a referable and credible body of knowledge aimed at generating awareness of the areas of guided wave that should be addressed.

**Appendix**  
**Southwest Research Institute**  
**Final Report**

# **LONG-TERM MONITORING OF CASED PIPELINES USING LONG-RANGE GUIDED-WAVE TECHNIQUE**

**FINAL REPORT  
SwRI Project 18.12266**

*Prepared for*

**NYSEARCH/Northeast Gas Association  
1515 Broadway, 43rd Floor  
New York, NY 10036-5701**

*Prepared by*

**Sensor Systems and NDE Technology Department  
Mechanical and Materials Engineering Division**

**March 2009**



**SOUTHWEST RESEARCH INSTITUTE®**

**San Antonio  
Detroit**

**Houston  
Washington, DC**

# **LONG-TERM MONITORING OF CASED PIPELINES USING LONG-RANGE GUIDED-WAVE TECHNIQUE**

**FINAL REPORT  
SwRI Project 18.12266**

*Prepared for*

**NYSEARCH/Northeast Gas Association  
1515 Broadway, 43rd Floor  
New York, NY 10036-5701**

*Prepared by*

**Sensor Systems and NDE Technology Department  
Mechanical and Materials Engineering Division**

**March 2009**

*Written by*

**Hegeon Kwun, Ph.D.  
Staff Scientist**

*Approved by*

**Glenn M. Light, Ph.D.  
Director**

## **EXECUTIVE SUMMARY**

The Office of Pipeline Safety (OPS) ruling on 49 CFR Part 192, Pipeline Safety: Gas Pipeline Integrity Management in High Consequence Areas (HCAs), requires all operators of gas transmission lines to develop and implement an Integrity Management Program (IMP) to ensure the safety and integrity of the pipelines. To meet the requirements in HCAs of unpiggable pipelines, direct assessment (DA) methods are used that rely on various cathodic protection (CP) survey tools. Because of the electromagnetic interference from the casing, CP survey tools are not applicable for “cased” sections of pipelines at road crossings. Accessing cased sections for direct examination or retrofitting the lines for pigging is prohibitively expensive. Therefore, a serious need exists to develop technologies that can expand the applicability of the DA method to the cased sections economically.

The long-range guided-wave inspection technique can inspect the inaccessible cased sections of pipeline from an accessible location near the casing ends and detect and locate corrosion damage areas in the line. Particularly if the guided-wave probe is permanently installed and left on the pipeline after the baseline testing, it can be used to monitor and track condition changes any time on demand without costly preparation (excavation for testing and site restoration after testing). With a capability to monitor the corrosion damage over time and determine defect size, the technology would allow accurate tracking of the line conditions with time and could, therefore, provide operators a cost-effective DA tool for cased sections by eliminating unnecessary excavation of the cased section for direct examination.

The objectives of this project were to develop the capability of defect characterization and sizing from guided-wave signals, develop the capability of long-term structural health monitoring (SHM) of cased sections, and evaluate and validate the capabilities in the field. The guided-wave technique employed in this project was based on magnetostrictive sensor (MsS) technology, developed at Southwest Research Institute<sup>®</sup>, which uses a probe consisting of thin magnetostrictive strip bonded around the pipe circumference and coils wrapped over the strip. MsS is inexpensive and rugged and has been in use for long-term SHM in processing plants. The project work was focused on defects whose circumferential cross-sectional area (CSA) is up to 10% of the total pipewall cross-section for which the application of SHM would be valuable. Defects greater than 10% CSA would be considered serious and would require immediate corrective measures.

Algorithms for characterizing defects (axial length, shape, and CSA) using feature parameters determined from defect signals were developed. For the development, the transmission line defect signal simulation model was refined and validated experimentally. Utilizing over 18,000 simulated defect signals and over 30 feature parameters defined from the defect signal amplitude and shape (in both time and frequency domains), the relevance of each parameter to defect characterization was evaluated. Algorithms were then developed based on the relationships of six feature parameters with defect characteristics. The accuracy of the defect sizing is dependent on the signal-to-noise (S/N) ratio of the defect signal (the higher the S/N ratio, the more accurate the sizing results). The algorithms can determine the defect’s CSA, but cannot separately

determine its depth and circumferential width, and its applicability is limited to a single isolated defect.

Additionally usefulness of the attenuation measurements for assessing general corrosion level in coated pipelines was evaluated. To this end, the temperature dependence of wave attenuation was investigated on three different coating types (coal tar TGF-3, coal tar epoxy, and polyethylene) at various frequencies. Also the attenuation caused by general corrosion was investigated by subjecting bare pipe samples to accelerated corrosion treatment to approximately 0.025 inch wall loss.

The performance of the MsS technology for defect detection, characterization, and long-term SHM was then evaluated on mock-up cased pipes in the NYSEARCH/NGA test bed facility that contained various machined defects and on mock-up cased pipes in an RG&E facility that were subjected to accelerated corrosion treatments.

Results and findings of the performance evaluation include the following:

- (1) The long-term guided-wave SHM approach, which involves periodic measurements with permanently installed guided-wave probes and comparison of measurement data, can detect the presence (or lack) of corrosion activity and its locations in the cased sections of pipelines and, therefore, is suitable for DA purposes.
- (2) The MsS is applicable in the field for long-term guided-wave SHM of cased sections .
- (3) Small CSA changes (1 to 2% in bare pipe and 2 to 4% in coal-tar-TGF-3-coated pipe) in the pipewall cross-sectional area could be detectable. To improve detection sensitivity in coal tar TGF-3 coated pipes, further development of data processing techniques is needed to correct for the effects of wave attenuation on the defect signal waveform.
- (4) Defect characterization (within 1 to 2 inches in axial length and 2 to 4% in CSA) is achievable.
- (5) The wave attenuation significantly increases with general corrosion wall loss level as the corrosion products adhere to the pipe surface (from approximately 0.13 dB/ft at 10 kHz to 0.23 dB/ft at 50 kHz for 0.004 inch wall loss). The wave attenuation is therefore a good indicator of the degree of general corrosion and is particularly useful for assessing the early stages of corrosion. Because of the large corrosion effects on wave attenuation, the assessment of corrosion state from attenuation measurements is achievable even in highly attenuative polyethylene or coal tar TGF-3 coated pipelines using low frequency waves (such as 10 kHz).

Recommendations for follow-on work include:

- (1) Implement the guided-wave survey and long-term SHM approach in the field.
- (2) In parallel with the field implantation, further improve the detection accuracy of CSA change in coated pipelines by developing signal processing methods for correcting attenuation effects on waveforms (including investigations of the attenuation characteristics of different coating materials/types and the temperature effects).

- (3) Investigate the corrosion effects on wave attenuation under a low corrosion rate over a long duration of time (such as 1 year or more). Because the attenuation values were measured under a high rate of corrosion over a short duration (less than 3 months), the magnitude of the corrosion-caused-attenuation reported here was significantly undervalued. To utilize the attenuation measurements for corrosion assessment in the fields, the magnitude of attenuation increase that would be caused by natural corrosion process needs to be determined accurately under realistic conditions.
- (4) Develop an improved calibration methodology. If a defect is formed and grows in a weld area, the current method which is based on the weld signals can lead to a significant error in data analysis and may fail to detect the defect in the weld area.
- (5) Develop a method and device for maintaining the MsS sensitivity under large (1,000 psi or greater) line pressure changes.
- (6) Take steps for technology transfer that include the development of a GUI (graphical user interface) program for data analysis that can be used by inspectors, for preparing training material, and for establishing industry-accepted procedures for probe installation and testing.

# Table of Contents

	PAGE
EXECUTIVE SUMMARY .....	i
1. INTRODUCTION .....	1
1.1 Pipeline Safety Requirements .....	1
1.2 Pipeline Assessment Methods.....	1
1.3 R&D Needs for DA of Cased Pipelines at Road Crossings.....	2
1.4 Application of Long-Range Guided-Wave for Cased-Section DA and the Magnetostrictive Sensor (MsS) Technology .....	2
1.5 Objectives of the Subject Project, and Work Scope .....	3
1.6 Outline of the Report .....	3
2. TECHNICAL BACKGROUND.....	4
2.1 Long-Range Guided-Wave Inspection .....	4
2.2 MsS Technology .....	5
2.3 Defect Characterization Approach.....	7
2.4 Transmission Line Model for Defect Signal Simulation .....	7
3. TRANSMISSION LINE MODEL REFINEMENT AND EXPERIMENTAL VALIDATION	9
3.1 Refinement of Transmission Line Model .....	9
3.2 Simulation Software.....	12
3.3.1 Experimental Setup and Procedures .....	15
3.3.2 Comparison of Experimental and Simulated Defect Signals.....	18
3.3.3 Discussion and Other Findings .....	25
4. DEFECT CHARACTERIZATION ALGORITHM.....	29
4.1 Signal Feature Analyses for Relevance to Defect Characteristics.....	29
4.2 Defect Characterization Algorithm Development .....	33
5. PREPARATION FOR FIELD TESTING .....	37
5.1 Adhesive Bonding Material Testing .....	37
5.2 Improvement of Data Analysis Software.....	39
6. TESTING AT NYSEARCH/NGA TEST BED.....	42
6.1 Cased Line Test Pipes at NYSEARCH/NGA Test Bed Facility .....	42
6.2 Baseline Testing and Sensor Installation .....	42
6.2.1 Proceedings.....	42
6.2.2 Results and Overall Findings .....	44
6.3 Monitoring Test and Results .....	46
6.3.1 Proceedings.....	46
6.3.2 Results and Overall Findings .....	46
7. FIELD TESTING AND RESULTS.....	48
7.1 Testing on Coated Lines in Astoria Tunnel, New York, NY.....	48
7.1.1 Proceedings.....	48
7.1.2 Results and Findings .....	48
7.2 Testing on Cased-Line Mockups Subjected to an Accelerated Corrosion Treatment at RG&E Facility in Rochester, NY.....	49
7.2.1 Proceedings.....	49

7.2.2	Results and Findings from 1 <sup>st</sup> Test Mockup .....	51
7.2.3	Results and Findings from 2 <sup>nd</sup> Test Mockup .....	53
8.	INVESTIGATIONS OF GUIDED-WAVE ATTENUATION CHANGES WITH COATED PIPE TEMPERATURE AND GENERAL CORROSION .....	65
8.1	Experimental Arrangements .....	65
8.1.1	Temperature dependence of attenuation in coated pipes .....	65
8.1.2	Effects of general corrosion on attenuation .....	66
8.2	Attenuation Measurement Procedures .....	67
8.3	Experimental Results .....	70
8.3.1	Temperature dependence of wave attenuation in coated pipes.....	70
8.3.2	Effects of general corrosion on wave attenuation.....	73
9.	CONCLUSIONS AND RECOMMENDATIONS .....	79
9.1	Conclusions.....	79
9.2	Recommendations.....	79
10.	REFERENCES .....	80
	APPENDIX A.....	82
	APPENDIX B.....	91
	APPENDIX C.....	101
	APPENDIX D.....	110

## LIST OF FIGURES

	<b>PAGE</b>
Figure 1. Long-range guided wave inspection of piping .....	4
Figure 2. Photo of thin strips bonded around a pipe (left) and the MsS coil placed over the strip (right) .....	5
Figure 3. Photo of MsS coils wound over bonded strips for long-term SHM .....	6
Figure 4. MsS Instrument Model MsSR 3030 (left) and MsSR 3030R (right) .....	6
Figure 5. Defect cross-section along the pipe length and its transmission line model representation .....	7
Figure 6. Photo of 4.5-inch-OD, 0.337-inch-wall pipe sample with 6-inch-long machined-in 360-degree notch .....	9
Figure 7. Example of data from the test sample shown in Figure 6 (for 128-kHz, 50-percent-wall notch) .....	10
Figure 8. Reflection coefficients from the front end of a 360-degree notch as a function of the notch cross-sectional area relative to the total pipe-wall cross-section .....	11
Figure 9. Theoretical reflection coefficient from the front end of 360-degree notch. Black line is for longitudinal wave mode. Blue and red lines are for torsional wave modes; continuous lines for the OD side notch and dotted lines for the ID side notch. ....	12
Figure 10. Example of OD defect configurations that can be input in the simulation software... ..	13
Figure 11. Example of ID defect configurations that can be input in the simulation software ....	13
Figure 12. Computer screen display of the simulation software .....	14
Figure 13. Examples of defect signals mixed with varying degrees of noise level. The noise level is in the unit of % reflection. The simulated defect signal's reflection coefficient is 1.42%. ....	15
Figure 14. Photos of experimental setup and examples of notch defects of varying axial length and slope .....	16
Figure 15. Configuration of ellipsoidal-shaped defect (for 2.5"L/1.5"W).....	17
Figure 16. Photo of ellipsoidal defects: (a) 0.5"L/ 1.0"W with 2.6% CSA and (b) 2.5"L/ 1.5"W with 3.81% CSA .....	17
Figure 17. Experimental (left and center) and simulated (right) waveforms for 32-kHz T-wave and 50%-deep circumferential notches with axial length from 3 to 4 inches with 3.2% CSA....	18
Figure 18. Relationship between the reflection coefficient and the normalized notch length: (a) 50-percent-wall-deep notch with 3.2% CSA and (b) 80-percent-wall-deep notch with 6.44% CSA.....	19
Figure 19. 128-kHz defect signal waveforms from 50%-wall-deep circumferential notch at various angled slopes on one end of the notch. The axial length of the notch is 1.5 inches, and the slope angle is from the radial direction of pipe (a) with the wave incident on the sloped end and (b) with the wave incident from the opposite end of the sloped end. ....	21
Figure 20. Normalized amplitude of the signal reflected from the sloped end of notch (from the signals measured off the 80%-wall-deep and 4-inch-long circumferential notch with the wave incident on the sloped end); (a) as a function of slope angle and (b) as a function of slope axial length/wavelength .....	22
Figure 21. Experimental and simulated signals from ellipsoidal defects at 32 kHz; CSA of defects was 1.32% for W=0.5", 2.60% for W=1.0", and 3.81% for W=1.5" .....	23

Figure 22. Experimental and simulated signals from ellipsoidal defects at 64 kHz; CSA of defects was 1.32% for W=0.5", 2.60% for W=1.0", and 3.81% for W=1.5" .....	24
Figure 23. Experimental and simulated signals from ellipsoidal defects at 128 kHz; CSA of defects was 1.32% for W=0.5", 2.60% for W=1.0", and 3.81% for W=1.5" .....	25
Figure 24. Attenuation coefficients of T-wave .....	26
Figure 25. 128-kHz signal waveforms from notches with various axial lengths. Left—from 50%-wall-deep notches; Right—from 80%-wall-deep notches. ....	27
Figure 26. Examples of trailing (T) signals. The data are from the signals measured with the 80%-wall-deep notches. L refers to the axial length of the notch. ....	28
Figure 27. Illustration of feature parameters used for defect characterization algorithms .....	30
Figure 28. Correlation between the base of envelope and defect length for ellipsoidal defects: (a) without noise, (b) distribution of SNR of defect signals versus defect length and CSA, (c) with noise added to the defect signal, and (d) after the denoising algorithm was applied to improve SNR.....	31
Figure 29. Correlation between the spectral peak amplitude of defect signal with noise and the maximum circumferential cross-sectional area of defect (left) and the defect volume (right) for the ellipsoidal defects. The color bar indicates the defect length from 0.5 inch (dark blue) to 8 inches (dark red). ....	32
Figure 30. Classification of defect type based on two feature parameters— center of spectrum and spectral peak amplitude. The black line is the discriminant line for distinguishing the defect type.....	32
Figure 31. Flow diagram of the defect classification algorithm .....	33
Figure 32. Photo of the 12-inch-OD pressure test sample (left) and the strips and MsS coils installed on the test sample (right).....	37
Figure 33. MsS sensitivity variations with line pressure change for strips bonded using Hysol U-10FL at 0 psi (top) and 2140 psi (bottom) line pressure. The hoop stress caused by 2140 psi was 36 ksi. ....	38
Figure 34. Example of correlated data from both ends of a cased section of gas transmission line (data from the previous DOT project) [5].....	40
Figure 35. Example of the baseline data and the newly acquired monitoring data (top) and the subtraction results after the two sets of data were properly aligned (bottom two).....	41
Figure 36. Photos of link joint seal at the edge of casing (left) and vaulted excavation for access to the underground test pipe (right) .....	42
Figure 37. Photos of MsS testing at the NYSEARCH/NGA test bed facility: (a) rubber strap wrapped over the magnetostrictive strips bonded around the 16-inch-OD TGF-3-coated pipeline, (b) applying epoxy on the magnetostrictive strips for bonding to the 12-inch-OD CTE steel pipeline, (c) MsS system during data acquisition from the 20-inch-OD bare steel pipeline, (d) MsS ribbon coils placed over the magnetostrictive strips for testing, (e) wax tape applied over the MsS ribbon coils for protection from environment for long-term monitoring, and (f) MsS ribbon coils installed with protective wax tape on the 12-inch-OD CTE steel pipeline; the exposed ends of the ribbon coils were later wrapped with plastic tape for protection.....	43
Figure 38. Photos from the 2 <sup>nd</sup> SHM testing: scenery of the test bed (left), installed sensors on 20-inch bare pipe (middle), and the iron-cobalt strips exposed after the wax tape and MsS ribbon coils were removed (right).....	46

Figure 39. Photos of MsS testing on 26-inch OD gas pipeline: (a) a spool of #22 gauge insulated wire, (b) wires wound over the iron cobalt strips, (c) electrical connections to MsS instrument, (d) protective tape wound over the coils, and (e) acquisition of baseline data.....	48
Figure 40. Photos of MsS testing on the 1st cased-pipeline mockup and installed probes .....	49
Figure 41. Photos taken during the testing on the 2 <sup>nd</sup> mockup: test pipe (top left), MsS probes (top right), and ends of test pipe (bottom) .....	50
Figure 42. 16-kHz (a) and 25-kHz (b) data from the 1 <sup>st</sup> RG&E cased-line mockup: top – baseline data, bottom – data taken after the accelerated corrosion treatment. Blue line is for the data taken from the east end of the pipe (EP1). Pink line is for the data taken from the west end of the pipe (EP2). C1 and C2 are the casing ends.....	51
Figure 43. Photos of defects induced in the 1 <sup>st</sup> RG&E test pipe: large defects (left two) and 2.8% CSA defect around the weld location (right).....	52
Figure 44. 32 kHz baseline data from the 2 <sup>nd</sup> RG&E test pipe.....	53
Figure 45. 16 kHz baseline data from the 2 <sup>nd</sup> RG&E test pipe.....	54
Figure 46. 1 <sup>st</sup> SHM data at 32 kHz from the 2 <sup>nd</sup> RG&E test pipe.....	55
Figure 47. 1 <sup>st</sup> SHM data at 16 kHz from the 2 <sup>nd</sup> RG&E test pipe.....	56
Figure 48. Difference between the baseline and the 1 <sup>st</sup> SHM data at 32 kHz .....	57
Figure 49. Difference between the baseline and the 1 <sup>st</sup> SHM data at 16 kHz .....	57
Figure 50. 2 <sup>nd</sup> SHM data at 32 kHz from the 2 <sup>nd</sup> RG&E test pipe.....	59
Figure 51. 2 <sup>nd</sup> SHM data at 16 kHz from the 2 <sup>nd</sup> RG&E test pipe.....	59
Figure 52. Comparison between the 1 <sup>st</sup> and 2 <sup>nd</sup> SHM data at 32 kHz .....	60
Figure 53. Comparison between the 1 <sup>st</sup> and 2 <sup>nd</sup> SHM data at 16 kHz .....	60
Figure 54. Photos of defects induced in the 2 <sup>nd</sup> RG&E Test Pipe: RG&E defect ID Nos. 1, 7, 8 (top row from left to right) and 11, 12, 15 (bottom row from left to right).....	62
Figure 55. Environmental chamber (left) and three coated pipe samples (middle and right) .....	65
Figure 56. Photos of experimental setup for investigation of corrosion effects on guided-wave attenuation; samples placed in PVC pipes (left) and with the PVC pipe filled with sand (right) .....	66
Figure 57. Photos of present experimental setup; PVC pipe filled with simulated seawater (left), power supply used to impress the electric current (middle), and fiberglass mesh wrapped around pipe sample (right) .....	67
Figure 58. Comparison between the measured center frequency and the operating frequency of the MsS .....	67
Figure 59. Example of the filter (left) and plots of original and filtered data (right) per procedure steps 2 and 3.....	69
Figure 60. Example of enveloping and exponential curve fitting to envelop peaks per step 4 ...	69
Figure 61. Example of a 3-D data plot and smoothly varying surface. ....	70
Figure 62. Experimental results from the coal tar epoxy (CTE) coated pipe sample. Left: attenuation surface as a function of frequency and temperature (data measured at the center frequencies shown as the black dots). Right: temperature dependence of attenuation at discrete frequencies. ....	71
Figure 63. Experimental results from the polyethylene (PE; PRITEC®) coated pipe sample. Left: attenuation surface as a function of frequency and temperature (data measured at the center frequencies shown as the black dots). Right: temperature dependence of attenuation at discrete frequencies, where dashed lines represent the extrapolated approximations. ....	72

Figure 64. Experimental results from the coal tar (TGF-3) coated pipe sample. Left: attenuation surface as a function of frequency and temperature (data measured at the center frequencies shown as the black dots). Right: temperature dependence of attenuation at discrete frequencies, where dashed lines represent the extrapolated approximations. .... 73

Figure 65. Photos of pipe surface on the bottom side (upper left), on sides (upper middle and right and a piece of corrosion product (lower right) ..... 74

Figure 66. Remaining wall thickness around the circumference of both pipe “A” (left) and pipe “B” (right); Black line represents the original pipe wall thickness and red line represents the remaining wall at the end of corrosion treatment ..... 74

Figure 67. Theoretically calculated wall loss level over the duration of the corrosion treatment. The “squares” indicate the days in which periodic attenuation measurements were made. The final average wall loss level from both pipes is also shown. .... 75

Figure 68. 3-D plots of the attenuation value as a function of frequency and days of corrosion treatment ((data measured at the center frequencies shown as the black dots). .... 75

Figure 69. Attenuation as a function of days of corrosion treatment at various frequencies ..... 76

Figure 70. Attenuation as a function of wall loss level (left) and attenuation caused by corrosion (right) ..... 77

Figure 71. Attenuation as a function of wall loss level (left) and attenuation caused by corrosion (right) ..... 77

## LIST OF TABLES

	<b>PAGE</b>
Table 1. Performance of the Classifier Tested with Training Data .....	35
Table 2. Performance of the Classifier Tested with Independent Data .....	35
Table 3. Defect Characterization Results for Defects Found from the Above-Ground 20-inch-OD Bare Steel Pipe in 24-inch Casing.....	44
Table 4. Defect Characterization Results for Defects Found from the Above-Ground 16-inch-OD Bare Steel Pipe in 24-inch Casing.....	44
Table 5. Defect Characterization Results for Defects Found from the Below-Ground 12-inch-OD CTA Coated Steel Pipe in 16-inch Casing.....	45
Table 6. Axial Locations and Characteristics of Defects Detected from the 1 <sup>st</sup> SHM Data.....	58
Table 7. Characteristics of Defects Detected from the 2 <sup>nd</sup> SHM Data .....	61
Table 8. Actual Locations and Sizes of Defects Induced in the Test Pipe .....	61
Table 9. Comparison between Actual Defect Length and CSA and Those Determined from the SHM Data.....	63

# 1. INTRODUCTION

## 1.1 Pipeline Safety Requirements

Per the Pipeline Safety Improvement Act in 2002 (PSIA 2002), the Office of Pipeline Safety (OPS), Department of Transportation (DOT), issued a ruling on 49 CFR Part 192, Pipeline Safety: Gas Pipeline Integrity Management in High Consequence Areas (HCAs) on December 15, 2003. According to the ruling, all operators of gas transmission lines are required to develop and implement an Integrity Management Program (IMP) to ensure the safety and integrity of the pipelines.

Key requirements of the IMP include: (1) identify HCAs on pipeline systems each operator owns, (2) conduct risk analyses of these areas, (3) perform baseline integrity assessments of each pipeline segment, and (4) inspect the entire pipeline system according to a prescribed schedule and using prescribed methods. Key timetables for the operators to follow are: (1) identify all HCAs and submit specific IMPs to OPS by December 17, 2004, and (2) inspect all pipeline segments within HCA and complete remediation plans (if required) by December 17, 2008. All segments must be reinspected every 7 years, with certain exceptions. Extensive information on this subject is available on the OPS website: <http://ops.dot.gov>.

## 1.2 Pipeline Assessment Methods

The OPS ruling identifies three primary methods for assessing pipeline integrity: in-line inspection (ILI), hydrostatic pressure testing, and direct assessment (DA).

The ILI method involves inserting sophisticated inspection tools, known as “smart pigs,” into a pipeline and inspecting the line while pushing the tools along the line. This method can be applied only to those pipelines that are designed for such an inspection. These so-called “piggable” lines comprise approximately 25 to 30 percent of the nation’s pipelines.

The hydrostatic pressure testing involves filling a line with water and testing the leak-tightness of the line at a prescribed pressure (in excess of the maximum operating pressure of the line being tested) and for a prescribed duration. This method is widely used on hazardous liquid pipelines, but is not preferred for gas pipelines.

The DA method is a continuous improvement process through successive structured applications of multiple assessment techniques and procedures. It utilizes physical characteristics and the operating history of a pipeline, together with the results of various diagnostic tests performed on the line, to determine the line’s integrity. This method is applied to “unpiggable” lines and includes indirect inspection (at grade level or aboveground) for corrosion activity and coating damage using various cathodic protection survey tools and direct examination of their physical condition by excavating the line.

Further information on assessment methods can be found on the OPS website: <http://ops.dot.gov>.

### **1.3 R&D Needs for DA of Cased Pipelines at Road Crossings**

When properly applied, the DA method is effective in finding and mitigating potential problems and, thus, ensuring the structural integrity of the line. To be effective, DA requires a combination of aboveground surveys and direct examination of physical conditions at the suspect area.

The “cased” section of unpiggable pipelines at road crossings is an HCA and thus is subjected to the OPS rule. Because of the electromagnetic interference from the casing, the various cathodic protection survey tools used for indirect inspection for corrosion activity are not applicable [1]. Furthermore, the cased section is difficult to access for direct examination. Excavating the cased section for direct examination is too costly to be practical. In addition, retrofitting unpiggable lines for ILI is cost-prohibitive and unjustifiable considering that the cased sections constitute only segments of a pipeline.

To meet the requirements of the OPS rule, a serious need exists to develop technologies that can expand the applicability of the DA method to the cased sections economically.

This project is one of developmental efforts by NYSEARCH/NGA to address the technical needs for DA of unpiggable pipelines including the cased sections at road crossings. This project is co-sponsored by the Pipeline and Hazardous Materials Safety Administration (PHMSA), Department of Transportation (DOT).

### **1.4 Application of Long-Range Guided-Wave for Cased-Section DA and the Magnetostrictive Sensor (MsS) Technology**

The long-range guided-wave inspection technique is an emerging technology widely used for surveying pipelines for corrosion damage [2-4]. This technique can inspect the inaccessible cased section of pipeline from an accessible location near the casing ends and detect and locate corrosion damage areas in the line. Particularly if the guided-wave probe is permanently installed and left on the pipeline after the baseline testing, it can be used to monitor and track condition changes any time on demand without costly preparation (excavation for testing and site restoration after the testing). With a capability to monitor corrosion damage over time and determine defect size, the technology would allow accurate tracking of the line conditions with time and could, therefore, provide operators a cost-effective DA tool for cased sections. For example, if defect indications found during the baseline testing do not change with time, the line is stable and safe to continue to operate. If any defect indications change significantly with time, it means that the line is degrading and requires more close monitoring and appropriate corrective measures. This long-term monitoring approach would improve the reliability of the DA and help to assure the line safety by eliminating unnecessary excavation of the cased section for direct examination.

The magnetostrictive sensor (MsS) technology is a long-range guided-wave inspection and monitoring technology developed at Southwest Research Institute<sup>®</sup> (SwRI<sup>®</sup>) [4]. It uses a guided-wave probe called “MsS” which is inexpensive, rugged, and suitable for long-term structural health monitoring (SHM). In view of its potential and cost-effectiveness for pipeline DA, the MsS technology was further improved under the sponsorship of PHMSA and co-funding industrial members [5]. The feasibility of long-term SHM of a cased section was also proven in

the laboratory under NYSEARCH/NGA support [6]. Further technical information on the long-range guided-wave inspection and the MsS technology is given in Section 2.

This project is a continuation of the above work and aimed at improving the effectiveness of the long-range guided-wave inspection/monitoring in DA applications by enhancing the ability to characterize and size defects and validating the field applicability of the MsS technology for cased sections.

### **1.5 Objectives of the Subject Project, and Work Scope**

The technical objectives of the subject project were to:

- (1) Develop the capability of defect characterization and sizing from guided-wave signals.
- (2) Develop the capability of long-term condition monitoring of the cased section of pipelines at road crossings.
- (3) Evaluate and validate the capabilities in the field.

To achieve the objectives, the work scope of the subject project included:

- (1) Refinement and experimental validation of the transmission line model for defect signal simulation.
- (2) Development of the defect characterization algorithm based on the simulated defect signals.
- (3) Improvement of data analysis software for inspection and monitoring.
- (4) Evaluation of the long-term stability of the MsS and the capability of inspection and monitoring and defect characterization in field conditions.

The work in this project was focused on defects with circumferential cross-sectional area (CSA) of up to 10% of the total pipewall cross-section for which the application of SHM would be valuable. Defects greater than 10% CSA would be considered a serious condition and would require immediate corrective measures.

### **1.6 Outline of the Report**

Section 2 describes the technical background on the long-range guided-wave inspection technique, the MsS technology including the sensor configuration and the instrument system, the defect characterization approach, and the transmission line model for simulating defect signals employed in this project. Section 3 describes the refinement of the transmission line model, its experimental validation, and the simulation software developed in this work. Section 4 describes the algorithm developed for defect characterization and its limitations. Section 5 describes the preparatory work for field evaluations that included identifying suitable adhesive bonding materials for installing the MsS to attain its long-term stability and improving the existing data analysis software for inspection and monitoring. Section 6 describes the results of inspection and monitoring conducted on cased pipeline mockups in the NYSEARCH/NGA test bed in Johnson City, New York. Section 7 describes the results from an operating pipeline in a tunnel in New York City and a cased line mockup at an RG&E facility in Rochester, New York, that was subjected to accelerated corrosion treatments. Finally, the overall conclusions and recommendations for follow-on work are given in Section 8.

## 2. TECHNICAL BACKGROUND

### 2.1 Long-Range Guided-Wave Inspection

Guided waves refer to mechanical (or elastic) waves in sonic and ultrasonic frequencies that propagate in a bounded medium (such as pipe, plate, rod) parallel to the plane of its boundary. They exist in many different forms (such as longitudinal, torsional, and flexural waves in pipe; shear-horizontal and Lamb waves in plate) and their properties vary with the geometry and size of the medium. For technical details on the guided waves and their properties, readers are referred to reference books [7-9].

For long-range guided-wave inspection and monitoring, a short pulse of guided waves in relatively low frequencies (up to a few hundred kHz) is launched along the structure under testing, and signals reflected from irregularities in the structure such as welds and defects are detected in the pulse-echo method as illustrated in Figure 1. From the occurrence time of the defect signal and the signal amplitude, the axial location and severity of the defects are determined.

From a given probe location, the guided-wave method can inspect a long segment of the structure (for example, more than 100 meters in above-ground bare or painted pipe in one direction) and can quickly detect and locate defective areas in the structure. The primary guided-wave mode used for the long-range inspection of piping is the torsional (T) wave in pipe. Since the wavelength of the guided waves used for long-range inspection is relatively long (for example, 10 cm for 32-kHz T-wave), detectable defects are relatively large in size compared to those detectable using MHz ultrasonic waves.

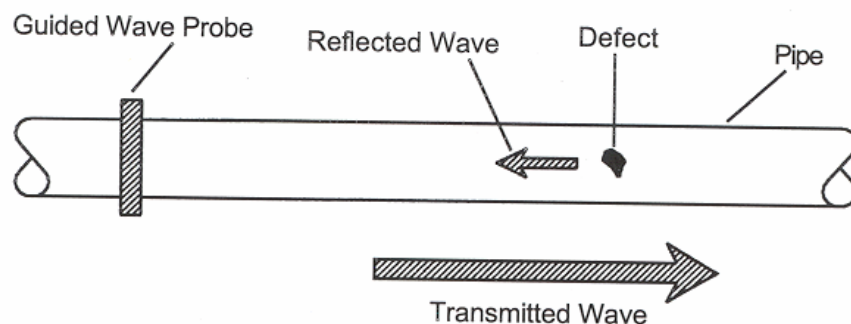


Figure 1. Long-range guided wave inspection of piping

Because of its ability to quickly examine long lengths of piping, the guided-wave technology is widely used as a screening tool for detecting and locating relatively large (for example, 2~3% or greater CSA relative to the total pipewall cross-section) corrosion defects in piping [2-4]. This technology is particularly useful for inspecting difficult-to-access segments of pipe from a remote accessible location such as the cased section of pipelines at road crossings addressed in this project.

The technique is good for detecting the presence of corrosion defects and their locations along the length of pipeline and can provide a rough estimate of the defect CSA relative to the total pipewall cross-section. To obtain details of defect characteristics (depth, shape, axial length, and circumferential extent), a follow-up inspection of the defect location with conventional inspection methods (such as ultrasonics or x-ray radiography) is performed. When the defect is found in a difficult-to-access area, the follow-up direct inspection of the defect location becomes very expensive. Therefore, to avoid unnecessary excavation of the cased section of pipeline for direct examination and, at the same time, to assure the safety of the line, a need exists to further extend the capability of the guided-wave technique. The objectives of this project are aimed at addressing this need.

## 2.2 MsS Technology

The MsS technology is a guided-wave probe and system developed at SwRI. The MsS probe generates and detects guided waves electromagnetically based on the magnetostrictive and its inverse effects in ferrous materials [10, 11].

For T-wave inspection and monitoring of piping, the MsS technology uses a thin strip of magnetostrictive material that is bonded (or mechanically coupled) around the pipe circumference and a coil placed over the strips as shown in the Figure 2 photos.



Figure 2. Photo of thin strips bonded around a pipe (left) and the MsS coil placed over the strip (right)

The transmitter in the MsS instrument applies a short pulse of electric current to the MsS coil placed over the strip. The resulting magnetic fields produced by the coil generate the T-waves in the strip that are subsequently coupled to, and propagate along, the pipe. Detection of the guided waves is achieved in reverse order where the arriving guided-waves cause magnetization changes in the strip, which in turn induce the electrical voltage in the MsS coil via Faraday effects. The receiver in the MsS instrument then detects the induced voltage signals.

For control of wave direction (namely, to the right or to the left), a pair of MsS probes are used with the system. The primary strip material used for MsS is an iron-cobalt alloy (49% Fe, 49% Co, 1.9% V, 0.05% Mg, 0.05% Si, 0.01% C, and 0.3% Cb/Nb) that is approximately 0.006 inch

(0.15 mm) thick and 1 inch (25.4 mm) wide [5]. The material requires a specific heat treatment to have proper magnetostrictive properties for MsS applications.

For long-term SHM applications, coils are manually wound over the strips and fixed in place as shown in the Figure 3 photo. An extension cable is then connected to the installed coils and terminated at a readily accessible location for future MsS operation.

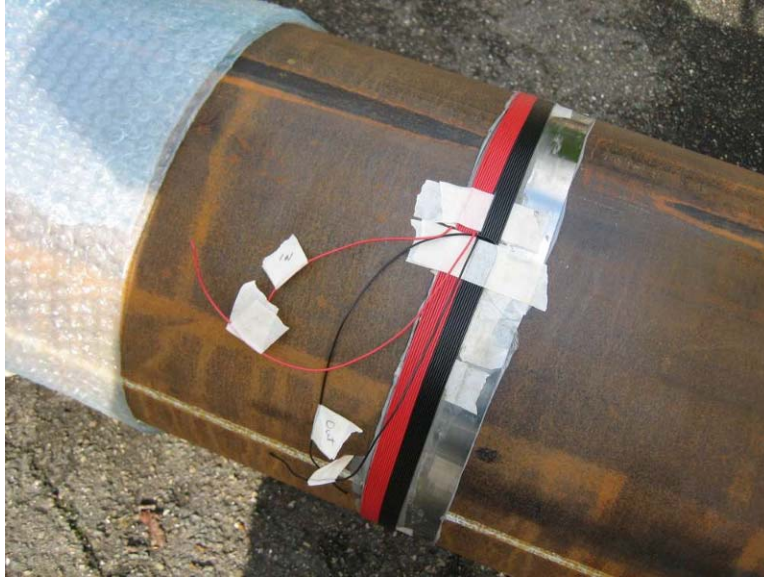


Figure 3. Photo of MsS coils wound over bonded strips for long-term SHM

Figure 4 shows photos of the MsS instrument (Model MsSR 3030 and MsSR 3030R, a battery-powered and ruggedized version). The data are displayed on a laptop computer that is also used to store and analyze the data.



Figure 4. MsS Instrument Model MsSR 3030 (left) and MsSR 3030R (right)

### 2.3 Defect Characterization Approach

The signal reflected from a defect depends on various parameters including the wave frequency, defect length (in axial direction), depth, and width (in circumferential direction), and defect shape and topology. Because the defect signal is a function of multiple parameters, the signal amplitude alone used as the defect detection criterion cannot provide defect characteristics other than a rough estimate of CSA of the defect.

To develop the capability of determining defect characteristics (depth, width, length, and shape) from guided-wave signals, detailed knowledge on how the signal (in amplitude and waveform) varies with defect characteristics and wave frequency is prerequisite. From this knowledge base, inter-relationships between defect characteristics and guided-wave signal features may be established that are useful for developing defect characterization algorithms from measured guided-wave signal features.

To establish statistically meaningful inter-relationships, an extensive defect signal database is necessary. Collecting a large number of defect signals experimentally is impractical because of the high cost involved.

Therefore, to cost-effectively generate and assemble a large database, the simulation model approach described in Section 2.4 was employed in this project. The database was utilized to identify key signal features that are useful for relating to defect characteristics. Algorithms for defect characterization were developed using these key signal features.

### 2.4 Transmission Line Model for Defect Signal Simulation

The transmission line model used in this project is a one-dimensional analytical model. In the model, a volumetric defect is treated as a region of  $n$ -layered media of different acoustic impedances, as illustrated in Figure 5 [12].

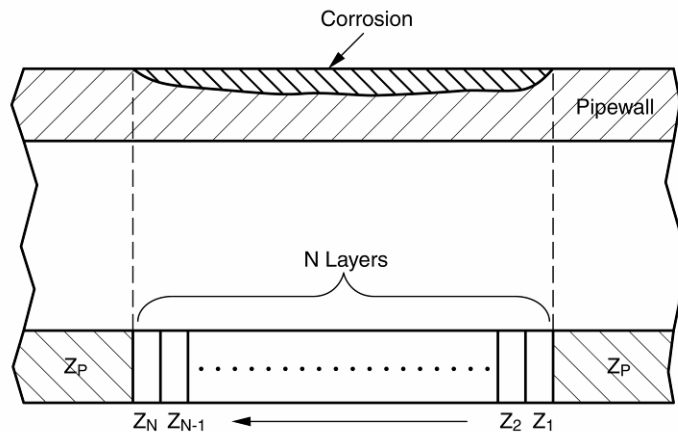


Figure 5. Defect cross-section along the pipe length and its transmission line model representation

The reflection coefficient,  $R(\omega)$ , from the defect at angular wave frequency  $\omega$  can then be expressed as:

$$R(\omega) = \frac{Z_d^{eff} - Z_p}{Z_d^{eff} + Z_p}, \quad (1)$$

where  $Z_d^{eff}$  is the effective impedance of the defect and is equal to the input impedance of the overall layer,  $Z_{n+1}^{IN}$ . According to the transmission line theory,  $Z_{n+1}^{IN}$  is obtained using the recursion relation for the input impedances of the two successive layers:

$$Z_{i+1}^{IN} = Z_i \frac{Z_i^{IN} + jZ_i \tan(k\zeta_i)}{Z_i + jZ_i^{IN} \tan(k\zeta_i)}, \quad (2)$$

where  $i = 1, \dots, n$ ,  $Z_i = \rho v A_i$  is the acoustic impedance of the  $i$ th layer whose pipewall cross-sectional area is  $A_i$ ,  $k$  is the wave number,  $\zeta_i$  is the thickness of the  $i$ th layer, and  $Z_1^{IN} = Z_p$ . The time-domain waveform of a defect signal,  $E_d(t)$ , is then given as:

$$E_d(t) = \frac{1}{2\pi} \int R(\omega) E_{in}(\omega) e^{j\omega t} d\omega, \quad (3)$$

where  $E_{in}(\omega)$  is the  $\omega$  component of the Fourier transformation of the incident pulse.

The advantages of this model are in its simplicity and short computation time (less than 1 second). Shortcomings of the model, being a one-dimensional model, are that it cannot treat mode conversions and beam spreading that occur when guided waves interact with a localized defect. Earlier experimental investigations showed that the model is very effective in simulating defect signal waveforms but somewhat lacking in quantitatively predicting the reflection coefficient [12, 13].

For defect characterization algorithm development, the transmission line model was further refined and experimentally validated in this project as described in Section 3. The refined model was subsequently used to generate a database (composed of 18,809 defect signals) for algorithm development.

### 3. TRANSMISSION LINE MODEL REFINEMENT AND EXPERIMENTAL VALIDATION

#### 3.1 Refinement of Transmission Line Model

From previous experimental investigations, it was observed that, when the guided wave interacts with an abrupt change in pipewall cross-section (such as at an end of a notch), the reflection coefficient differed depending on the direction of incident wave (from the larger cross-section area to the smaller cross-section area or vice versa) [13]. This difference (which we termed “geometric shadow effects” at that time) increased with the wave frequency and the magnitude of the abrupt change. The initial transmission line model could not produce the observed geometric effects and, thus, required a modification by introducing appropriate correction factors for the effects [13].

The refinement efforts in this project therefore were focused on finding and incorporating proper correction factors for the geometric effects in the simulation model. To determine the proper correction factors as a function of defect depth and T-wave frequency, a series of experimental measurements of the front and rear end signals from a 360-degree notch was made. The notch was machined in 4.5-inch-OD, 0.337-inch-wall pipe samples by using a lathe. To separate the front (F) and rear (R) end signals, the axial length of the notch was made 6 inches long, as shown in Figure 6. The MsS was placed approximately 11 inches from one end of the pipe sample, and the measurements were made at 32-, 64-, and 128-kHz frequencies while varying the notch depth from 10- to 100-percent wall at 10-percent increments. An example of the measured data is shown in Figure 7. To improve the measurement accuracy, the experiments were repeated on a second pipe sample. From the experimental data, the reflection coefficients from both F and R were measured.



Figure 6. Photo of 4.5-inch-OD, 0.337-inch-wall pipe sample with 6-inch-long machined-in 360-degree notch

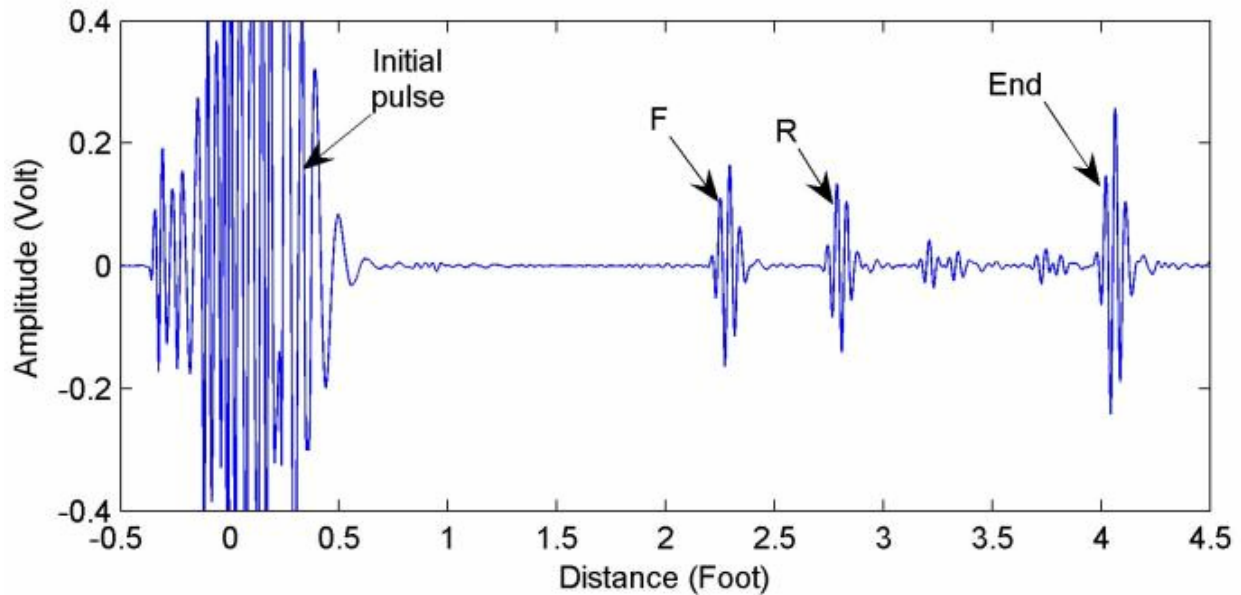


Figure 7. Example of data from the test sample shown in Figure 6 (for 128-kHz, 50-percent-wall notch)

The reflection coefficients from the front end of the 360-degree notch were plotted in Figure 8 as a function of the cross-section area (CSA) of the notch relative to the total pipewall cross section. The experimental values measured at 32, 64, and 128 kHz were all larger than the simple theoretical values (indicated with a red line) given as  $R = (Z_2 - Z_1) / (Z_2 + Z_1)$  used in the transmission line model, where  $Z_j$  is the acoustic impedance of medium  $j$  and the wave is incident from medium 1. This difference from the theoretical value is due to “the geometric effects,” which increase with increasing frequency, as shown in the figure. The reflection coefficients from the rear end of the notch were approximately the same as the theoretical values up to about 60- to 70-percent notch CSA and were not plotted in the figure for clarity. The magnitude of the geometric effects and their dependence on the notch depth/CSA and wave frequency were measured from the experimental data and were subsequently incorporated into the defect signal simulation model.

For defects of up to 10% CSA, which were the main focus of the study in this project, the geometric effects were approximately the same for frequencies of 32 to 128 kHz. Therefore, in the simulation software, the geometric effects were treated as being independent of frequency for up to 10% CSA.

In addition to the geometric effects discussed above, the separation between F and R in the experimental data (such as shown in Fig. 7) indicated the presence of a phase shift at the boundaries [14]. The phase shift between the front and rear reflected signals was proportional to the wave frequency and measured to be approximately  $36^\circ$  (or 0.62 radians) at 128 kHz. This phase shift was also incorporated into the simulation model.

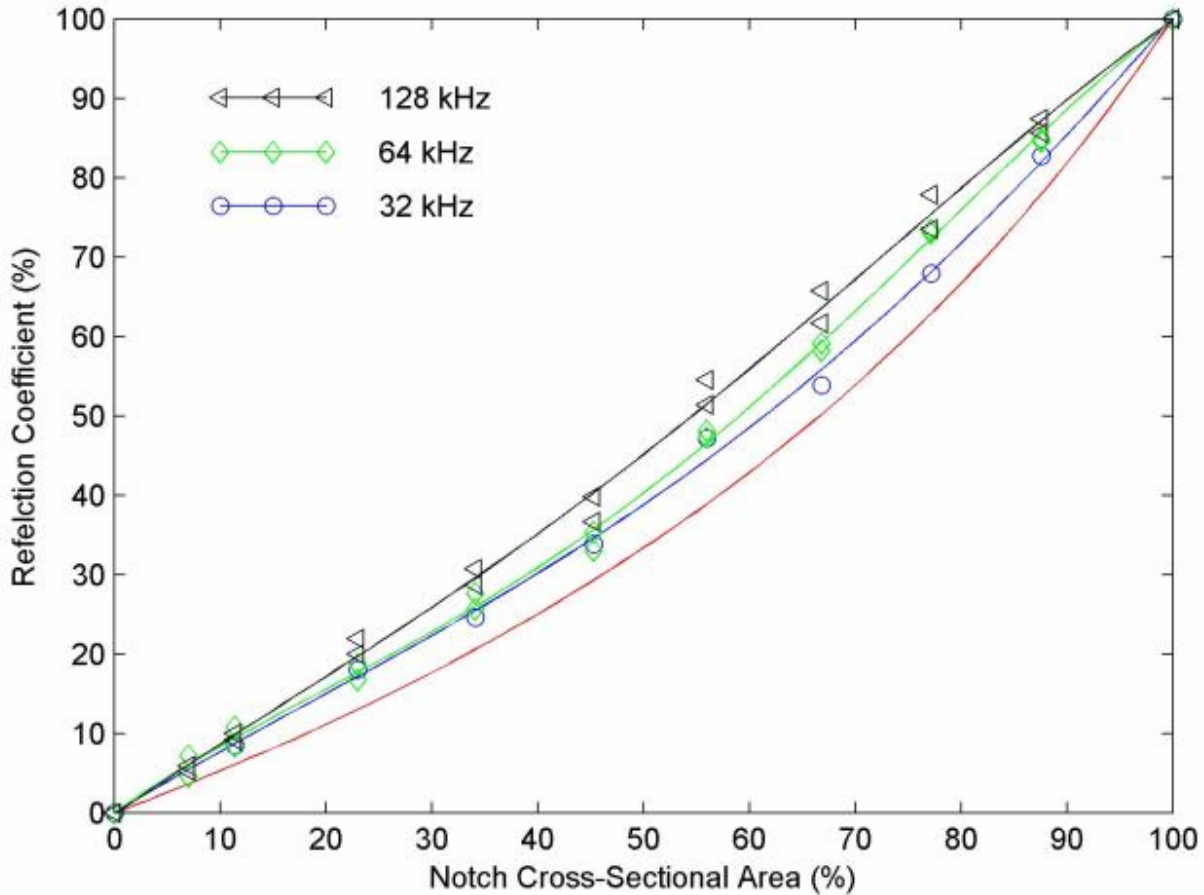


Figure 8. Reflection coefficients from the front end of a 360-degree notch as a function of the notch cross-sectional area relative to the total pipe-wall cross-section

After the geometric effects had been incorporated in the simulation software described in Section 3.2, it came to our attention that the acoustic impedance  $Z$  used in the simulation model takes a different form, depending on the guided wave mode. For longitudinal (L) wave modes,  $Z = \rho V_L A$ , where  $\rho$  is the density of the pipe material,  $V_L$  is the L-wave velocity, and  $A$  is the pipewall cross-sectional area. For torsional (T) wave modes,  $Z = \rho V_T I$ , where  $V_T$  is the T-wave velocity and  $I$  is the moment of inertia. For a pipe with OD =  $D_o$  and ID =  $D_i$ ,  $I = (\pi/32)(D_o^2 - D_i^2)(D_o^2 + D_i^2) = A(D_o^2 + D_i^2)/8$ . Because  $Z$  of the T-wave is proportional to the moment of inertia, the reflection coefficient  $R$  varies somewhat with pipe size (diameter and wall thickness) and the location of defect (for example, on the inside or outside diameter surface). To illustrate, theoretical values of  $R$  from the front end of a 360-degree notch are plotted in Figure 9 as a function of notch CSA to the pipewall cross-sectional area for two different pipe sizes: 4.5-inch OD, 0.337-inch wall and 16-inch OD, 0.5-inch wall. In the figure, the black line is for longitudinal wave mode, whose reflection coefficients are independent of the pipe size and the notch location on ID or OD. Blue and red lines are for torsional wave modes, with continuous lines for the OD side notch and dotted lines for the ID side notch. At a given notch CSA, T-wave  $R$  is larger or smaller than L-wave, depending on whether the notch is on the OD or ID side of the pipe, respectively. The difference between the T- and L-wave  $R$ s decreases with decreasing wall-thickness/OD ratio.

The simulation software uses  $Z = \rho VA$  for both L- and T-waves where  $V$  is the velocity of the wave. For up to 10-percent defect CSA in schedule 40 pipes, the error in T-wave  $R$  calculation is less than 0.5 percent. Because of the negligible impact of the above error in T-wave defect signal simulation and the budget and schedule considerations, no corrections for T-wave  $Z$  were made in the simulation software during this project. For the sake of accuracy, however, the simulation software needs to be revised at some point by using the correct  $Z$  for the T-wave (and readjusted geometric effects).

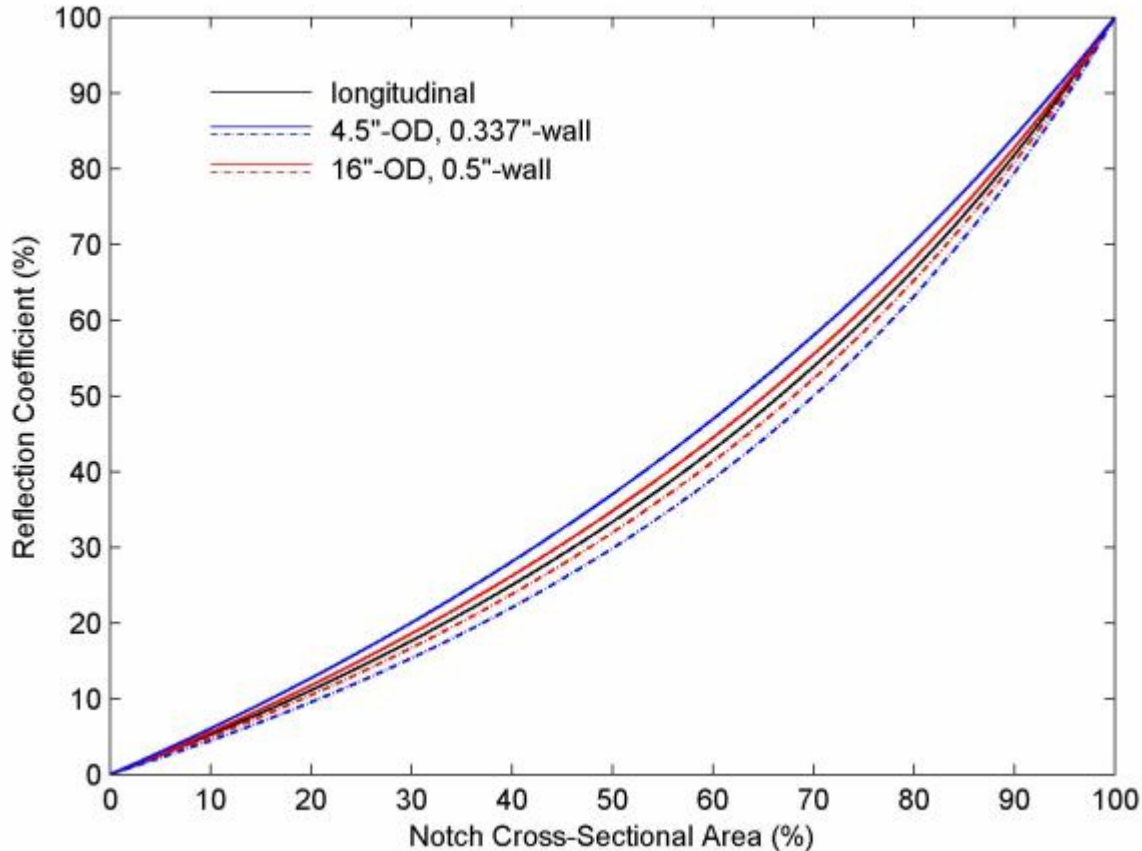


Figure 9. Theoretical reflection coefficient from the front end of 360-degree notch. Black line is for longitudinal wave mode. Blue and red lines are for torsional wave modes; continuous lines for the OD side notch and dotted lines for the ID side notch.

### 3.2 Simulation Software

A GUI (graphical user interface) version of simulation software was developed for this project. The software can handle both OD and ID defects in either rounded or trapezoidal shapes with various axial length, width (in circumferential direction of pipe), and depth. Examples of defect configurations that can be input are shown in Figure 10 for OD defects and in Figure 11 for ID defects.

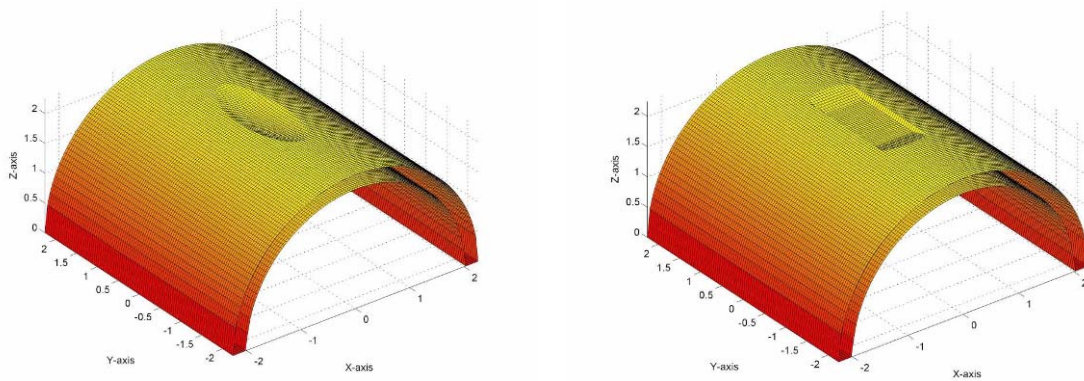


Figure 10. Example of OD defect configurations that can be input in the simulation software

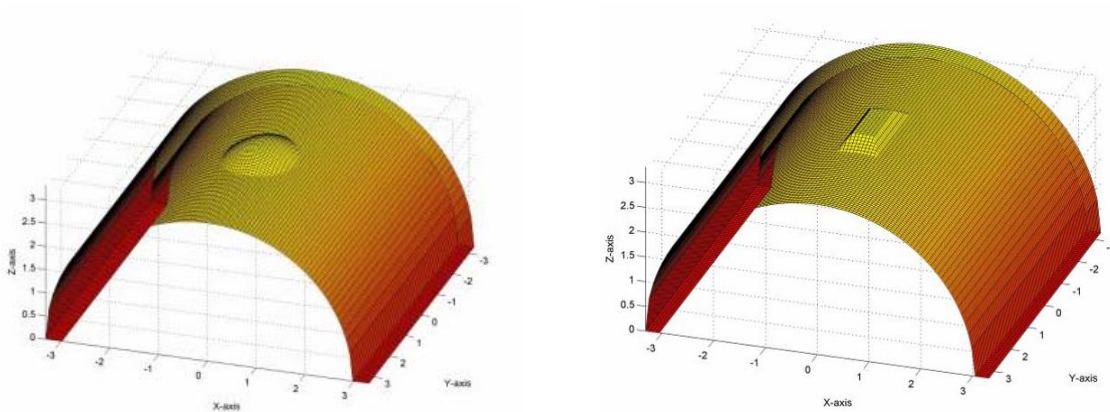


Figure 11. Example of ID defect configurations that can be input in the simulation software

A computer screen display of the simulation software is shown in Figure 12. The defect configuration is displayed in the lower left of the screen. Controls for specifying defect shape/type and their length, width, and depth, pipe OD and wall thickness, and wave frequency are in rectangular boxes on the top and right side of the screen. The defect cross-sections in the axial and circumferential directions at the center of the defect are illustrated next to the defect configuration together with defect CSA relative to the total pipewall cross-section (in this example, 1.67%). The waveforms of both the transmitted (in blue) and defect (in red) signals are displayed above the defect configuration along with the reflection coefficient of the defect (in this example, 0.24%). The spectral content of the transmitted and defect signals are also displayed next to the waveforms.



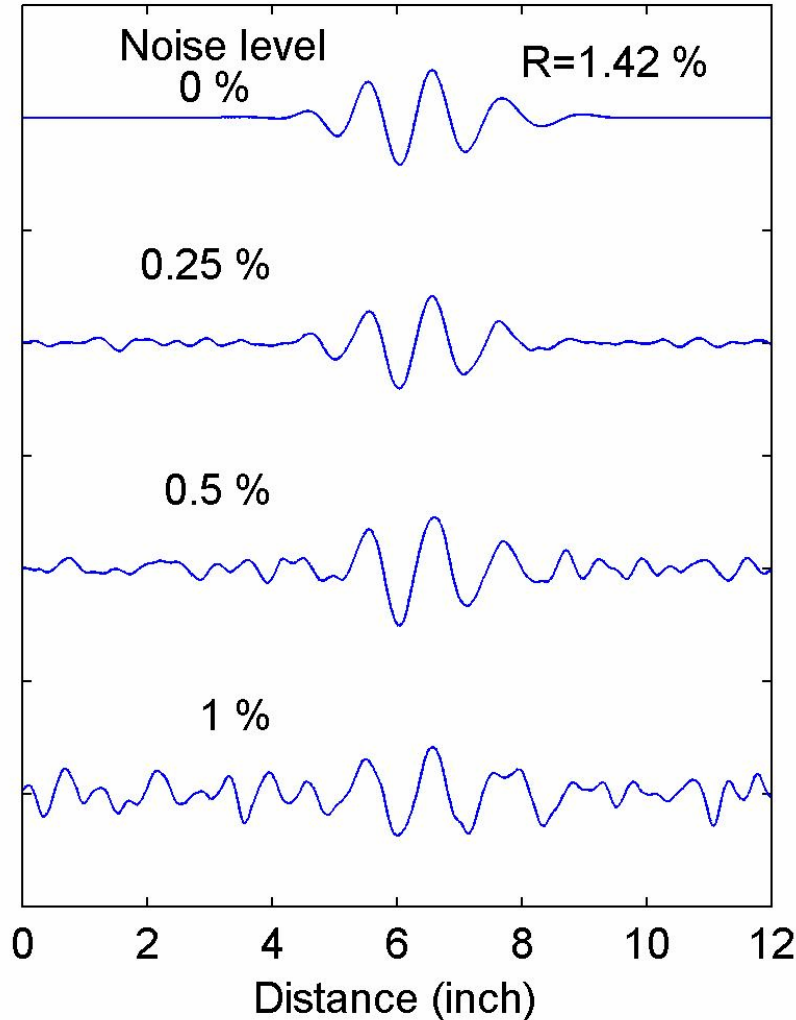


Figure 13. Examples of defect signals mixed with varying degrees of noise level. The noise level is in the unit of % reflection. The simulated defect signal's reflection coefficient is 1.42%.

### 3.3 Experimental Validation

#### 3.3.1 Experimental Setup and Procedures

A series of experimental measurements of defect signals was performed on bare, 20-foot-long, 6-inch-OD, 0.28-inch-wall pipe samples for validation of the simulation results. Defects used for experimental measurements were: circumferential notches with fixed depth (50 and 80% wall) and varying axial length (up to 4 inches), circumferential notches with fixed depth and axial length but varying slope at one of the edges (30-, 45-, and 60-degree slope from the vertical axis), ellipsoidal defects with fixed maximum depth (75% wall) and varying width (up to 1.5 inches) and axial length (up to 2.5 inches). Defect signals were measured at three frequencies (32, 64, and 128 kHz) using the MsS system.

The notch defects were machined in the sample as shown in the photos in Figure 14. Defect signals were collected while increasing the axial length of the notch (from 0.25 inch up to 4 inches at every 0.25-inch increment). In limited cases, measurements were also made after machining one edge of the notch to a slope (in the order of 30-, 45-, and 60-degree slope from the vertical axis). The CSA of the notch relative to the pipewall cross-section area was 3.20% for the 50%-wall-deep notch and 6.44% for the 80%-wall-deep notch.



Figure 14. Photos of experimental setup and examples of notch defects of varying axial length and slope

The ellipsoidal defects were manually placed in a sample by using a grinder. The maximum depth of the defects was fixed at 75-percent wall, and the axial length (L) and circumferential width (W) of the defects were varied per the following order: 0.5"L/0.5"W; 0.5"L/1.0"W; 1.0"L/1.0"W; 1.0"L/1.5"W; 1.5"L/1.5"W; 2.0"L/1.5"W; and 2.5"L/1.5"W. An example of defect configuration used in the measurements is illustrated in Figure 15. Examples of the defects are shown in the Figure 16 photos. The maximum CSA of these defects relative to the pipewall cross-section area was 1.32 percent for W=0.5", 2.60 percent for W=1.0", and 3.81 percent for W=1.5".

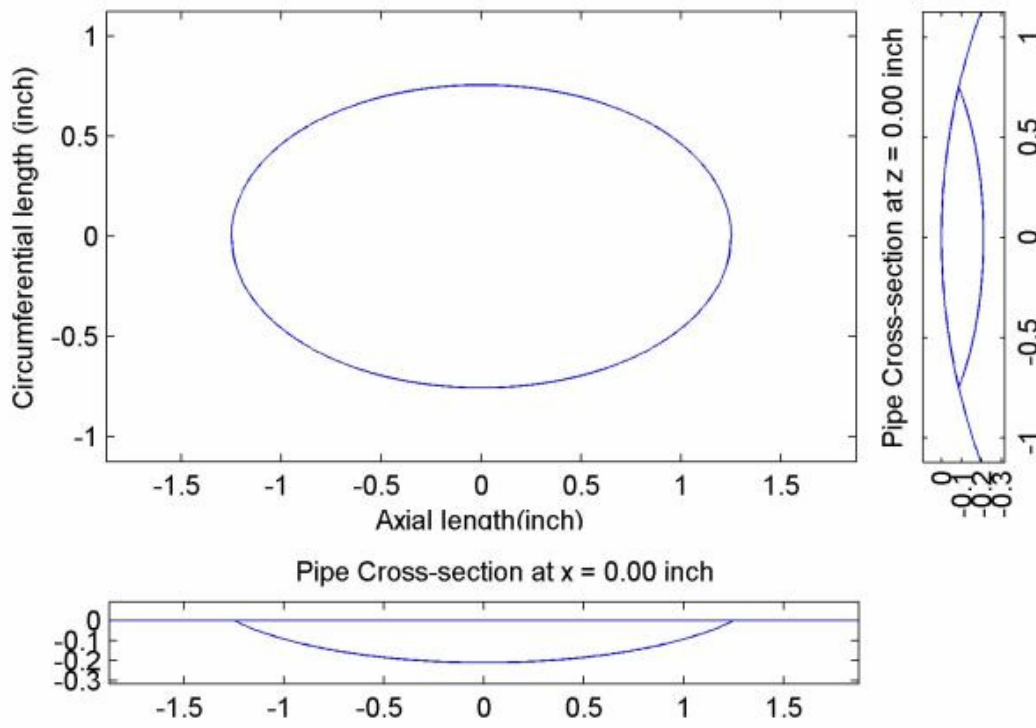
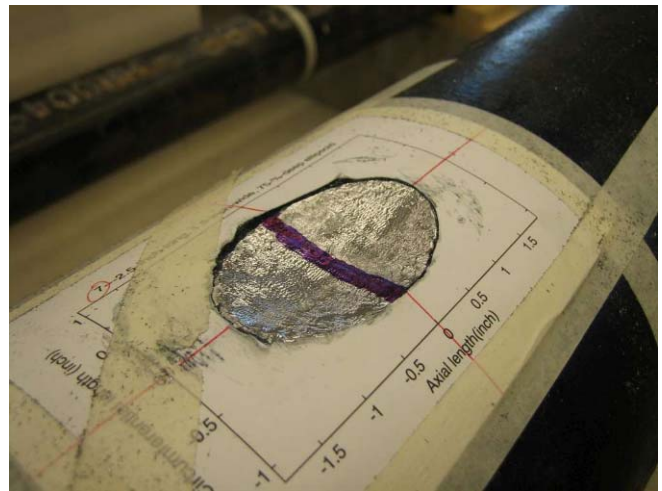


Figure 15. Configuration of ellipsoidal-shaped defect (for 2.5"L/1.5"W)



(a)



(b)

Figure 16. Photo of ellipsoidal defects: (a) 0.5"L/ 1.0"W with 2.6% CSA and (b) 2.5"L/ 1.5"W with 3.81% CSA

### 3.3.2 Comparison of Experimental and Simulated Defect Signals

(i) Circumferential Notch

Figure 17 shows an example of experimentally measured and simulated notch-signal waveforms for comparison. The data were for 32-kHz T-wave signals from 50%-deep circumferential notches with the axial length (L) from 3 to 4 inches. These experimental data were chosen for their subtle changes in waveforms with L. As can be seen, the simulated and experimentally measured signal waveforms agreed well, including the details of subtle changes in the waveforms with L. The slight difference between the two experimental results was caused by variations in the MsS probes and background noise.

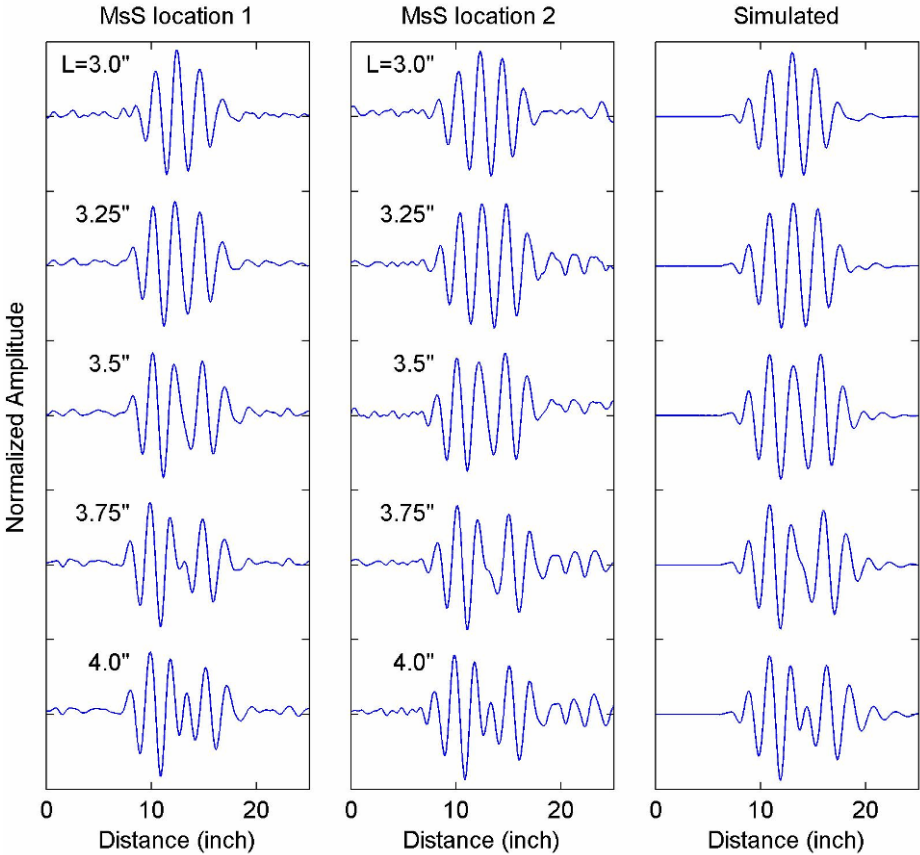
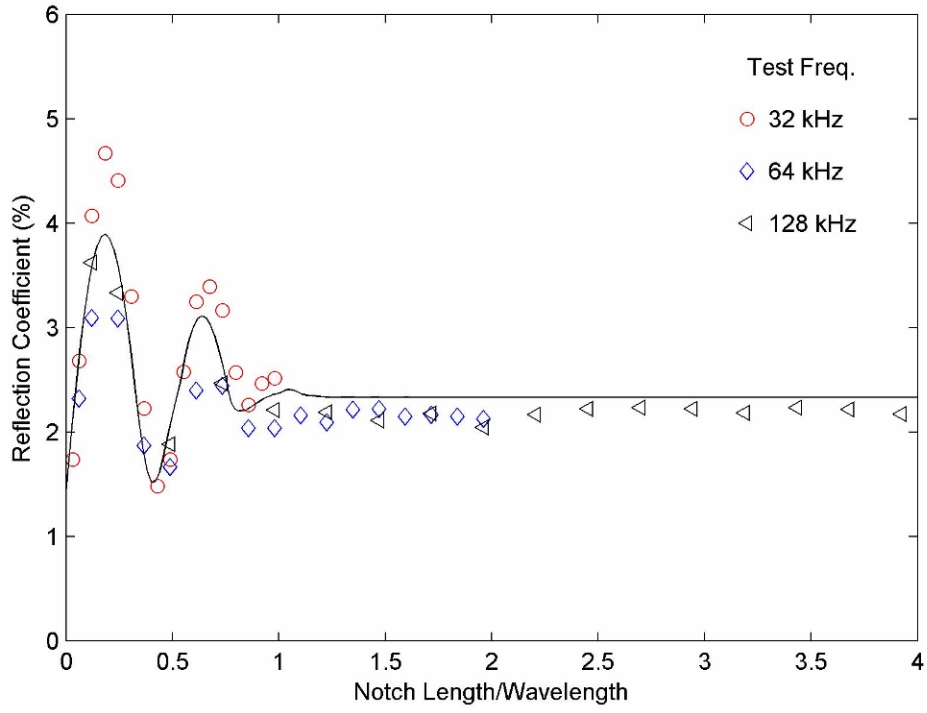
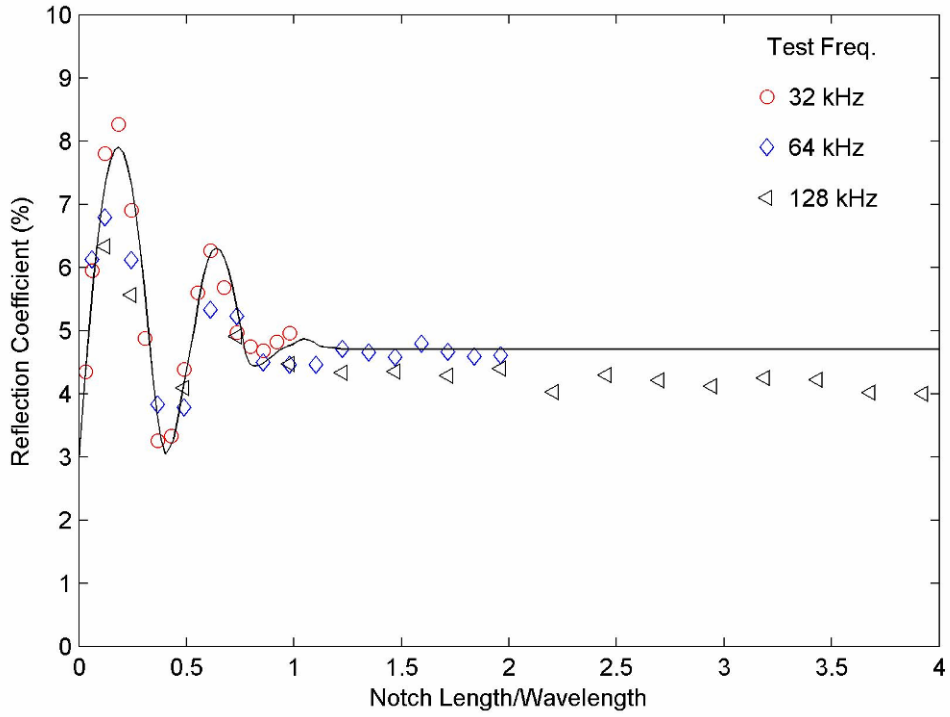


Figure 17. Experimental (left and center) and simulated (right) waveforms for 32-kHz T-wave and 50%-deep circumferential notches with axial length from 3 to 4 inches with 3.2% CSA

Figure 18 shows the relationship between the reflection coefficients of the circumferential notch and the axial length of the notch normalized with respect to the wavelength of T-wave. Figure 18(a) is for the 50%-wall-deep notch and Figure 18(b) is for the 80%-wall-deep notch. In the figures, experimentally measured values are indicated with symbols (circles—32 kHz, diamonds—64 kHz, triangles—128 kHz) and calculated values using the simulation model. The experimental error in the reflection coefficient measurements was approximately  $\pm 0.5\%$ . Within the measurement error, the calculated and the experimental values of the reflection coefficient agreed.



(a)



(b)

Figure 18. Relationship between the reflection coefficient and the normalized notch length: (a) 50-percent-wall-deep notch with 3.2% CSA and (b) 80-percent-wall-deep notch with 6.44% CSA

The notch signal is composed of the waves reflected from both the front and rear ends of the notch mixed together. They interfere constructively and destructively depending on  $L$ , until they are spatially separated when  $2L$  is longer than the signal length (here, the factor 2 is to account for the round trip over the notch length). Consequently, the reflection coefficient exhibits a damped oscillation behavior as a function of  $L$  shown in Figure 18.

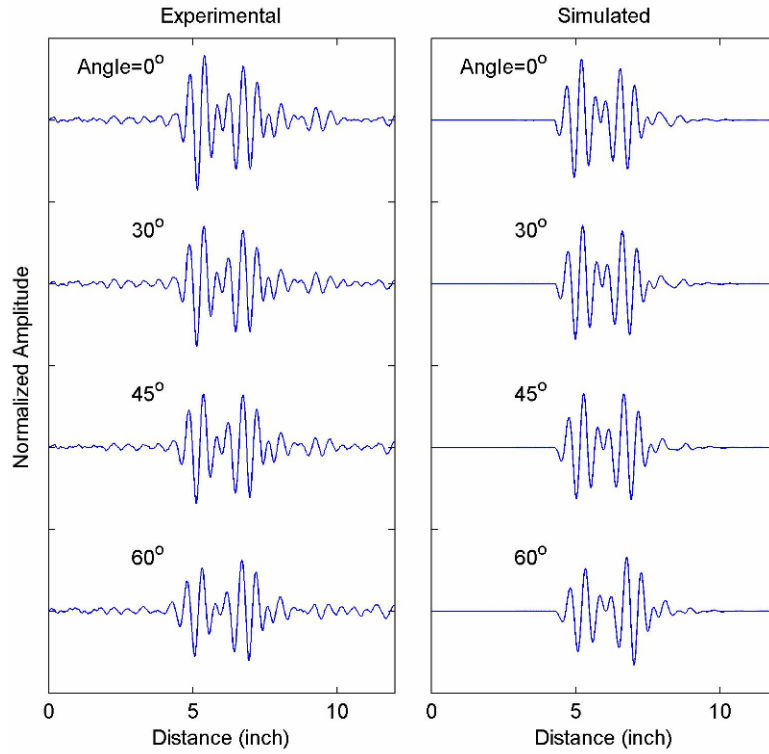
The results of the above comparison indicated that the simulation software is valid in producing quantitatively accurate notch signal waveform and amplitude for  $L \leq \lambda$ , where  $\lambda$  is the wavelength. For  $L > \lambda$ , the software was valid only for simulating the signal reflected from the front end but not for the rear end. This was because, when the notch was long, the experimental data exhibited the presence of additional effects that led to a substantially smaller rear-end reflected signal which could not be accounted for in the transmission line model (further discussed in Section 3.3.3).

(ii) *Circumferential Notch with Sloped End*

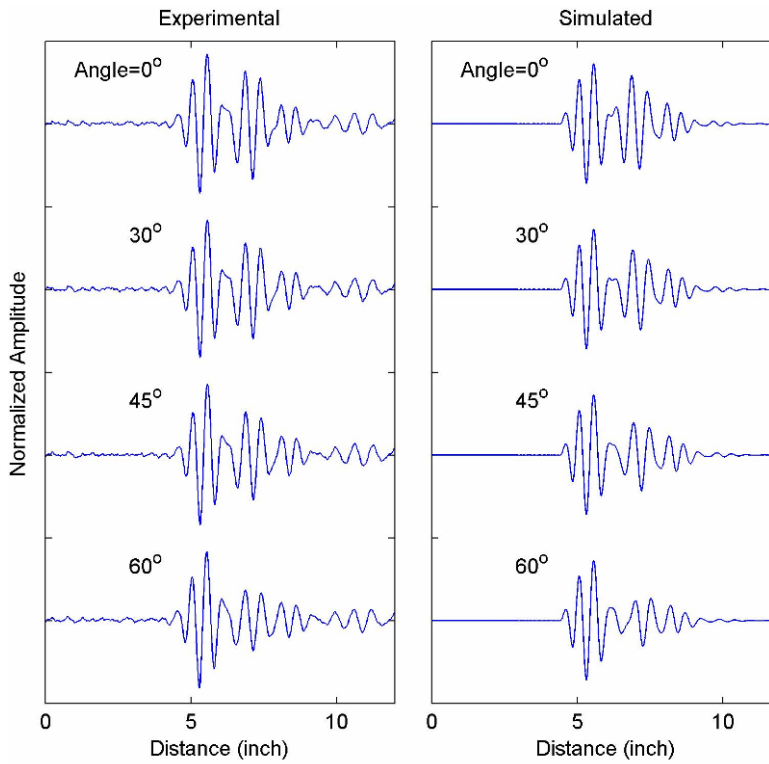
Figure 19 shows variations of the 128-kHz defect signal waveform with the angle of slope on one end of the 50%-wall-deep circumferential notch. The axial length of the notch was 1.5 inches, and the angle was measured from the radial direction of the pipe. Figure 19(a) shows the waveforms measured with the transmitted wave incident on the sloped end of the notch. Figure 19(b) shows those measured with the transmitted wave incident from the opposite side of the sloped end. Simulated waveforms are also shown for comparison. In the figures, the signals reflected from the front and rear ends of the notch (from the direction of incident wave) are indicated as F and R, respectively.

As shown in the experimentally detected signals, the amplitude of signals reflected from the sloped end of the notch [Fs in Figure 19(a) and Rs in Figure 19(b)] decreased with the increasing slope angle, indicating that a gradual change in wall thickness reduces the wave reflection and thus is harder to detect. The simulation software produced the same slope effects and, within the experimental error, the simulated signals agreed well with the experimentally measured signals (in both the waveform and the amplitude). The agreement indicated that the simulation software could also reliably simulate signals from a defect with sloped edges.

It was observed that, for a given slope, the effects of the slope on the signal amplitude were greater the higher the wave frequency, as shown in the example plotted in Figure 20(a). The data in Figure 20 were determined from the experimentally measured signals from the 80%-wall-deep notch. When the same data were plotted as a function of the axial length of the notch relative to the wavelength, they followed approximately a linear line as shown in Figure 20(b). This means that the effects of a slope are relative to the wavelength of the guided wave and that a given slope looks steeper (or appears as a more abrupt change) to a lower frequency wave while it looks gentle (or appears as a gradual change) to a higher frequency wave.

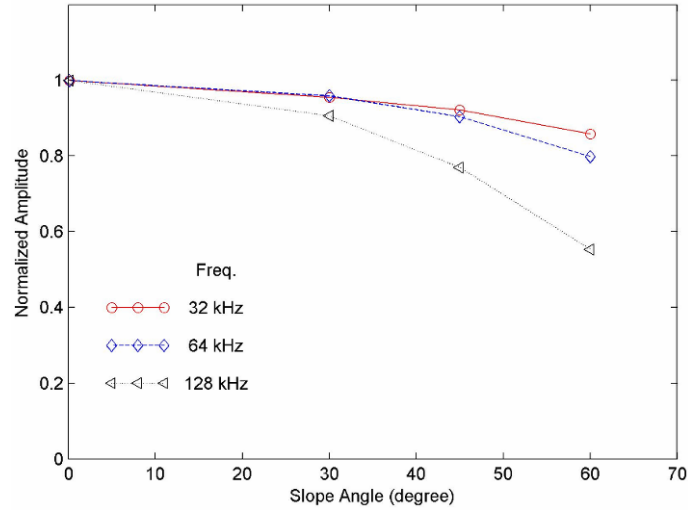


(a)

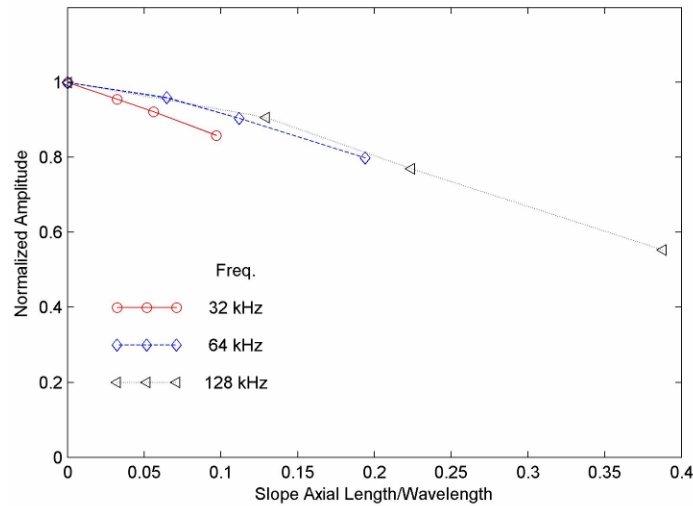


(b)

Figure 19. 128-kHz defect signal waveforms from 50%-wall-deep circumferential notch at various angled slopes on one end of the notch. The axial length of the notch is 1.5 inches, and the slope angle is from the radial direction of pipe (a) with the wave incident on the sloped end and (b) with the wave incident from the opposite end of the sloped end.



(a)



(b)

Figure 20. Normalized amplitude of the signal reflected from the sloped end of notch (from the signals measured off the 80%-wall-deep and 4-inch-long circumferential notch with the wave incident on the sloped end); (a) as a function of slope angle and (b) as a function of slope axial length/wavelength

(iii) *Ellipsoidal Defects*

Figures 21, 22, and 23 show the experimentally measured and simulated signals from ellipsoid-shaped defects at 32, 64, and 128 kHz, respectively. As can be seen, the experimentally measured and simulated signals in these figures agreed well in both signal waveforms and reflection coefficients (in most cases, within 1 percent of each other). The good agreement for these ellipsoidal defects with varying slopes and configurations (which are harder to treat than notch-type defects) indicated and confirmed the reliability of the simulation model and software (within, of course, the limitations of the transmission line model used for simulation that includes inability to handle mode conversions and other physical phenomena observed and discussed in Section 3.3.3).

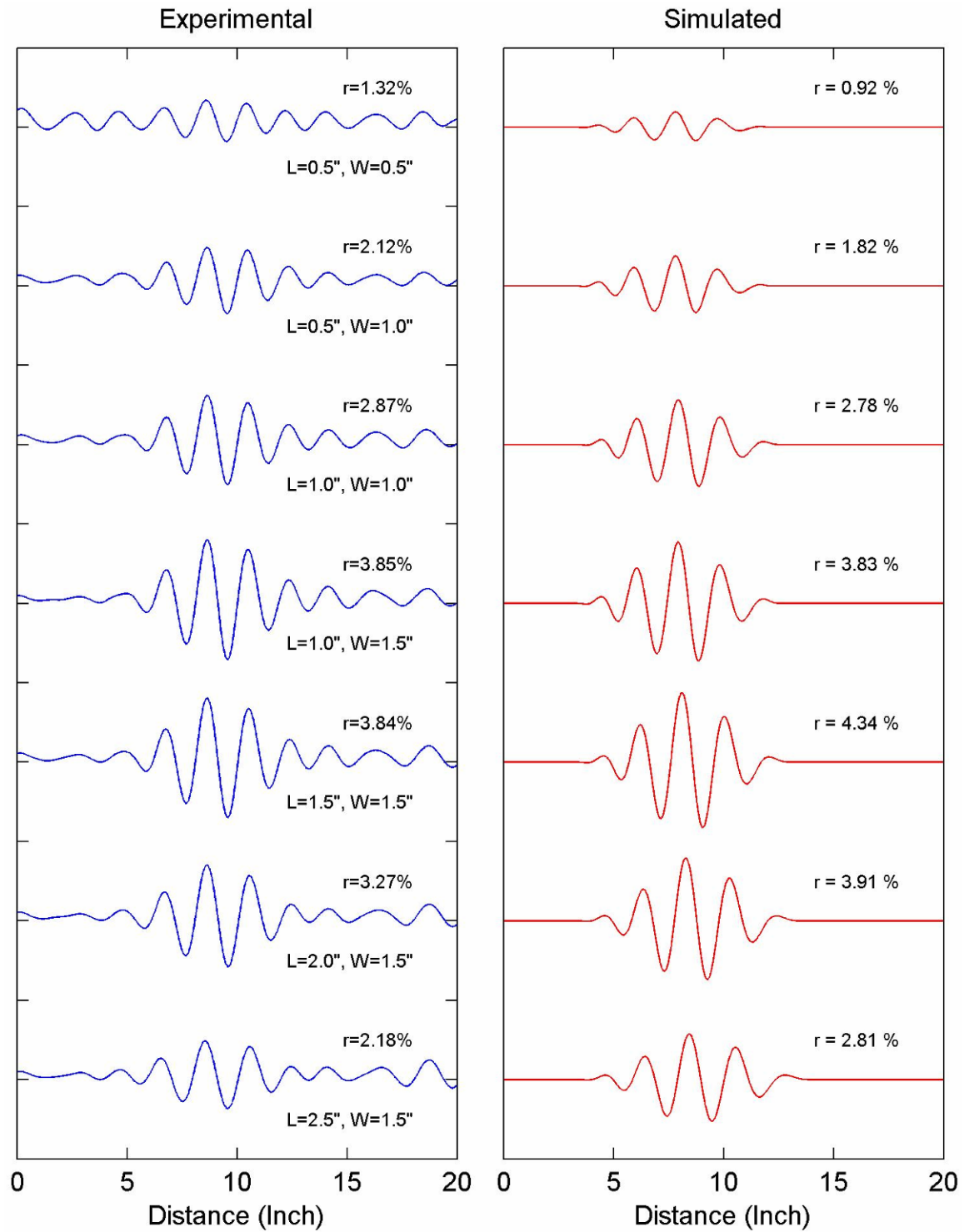


Figure 21. Experimental and simulated signals from ellipsoidal defects at 32 kHz; CSA of defects was 1.32% for W=0.5", 2.60% for W=1.0", and 3.81% for W=1.5"

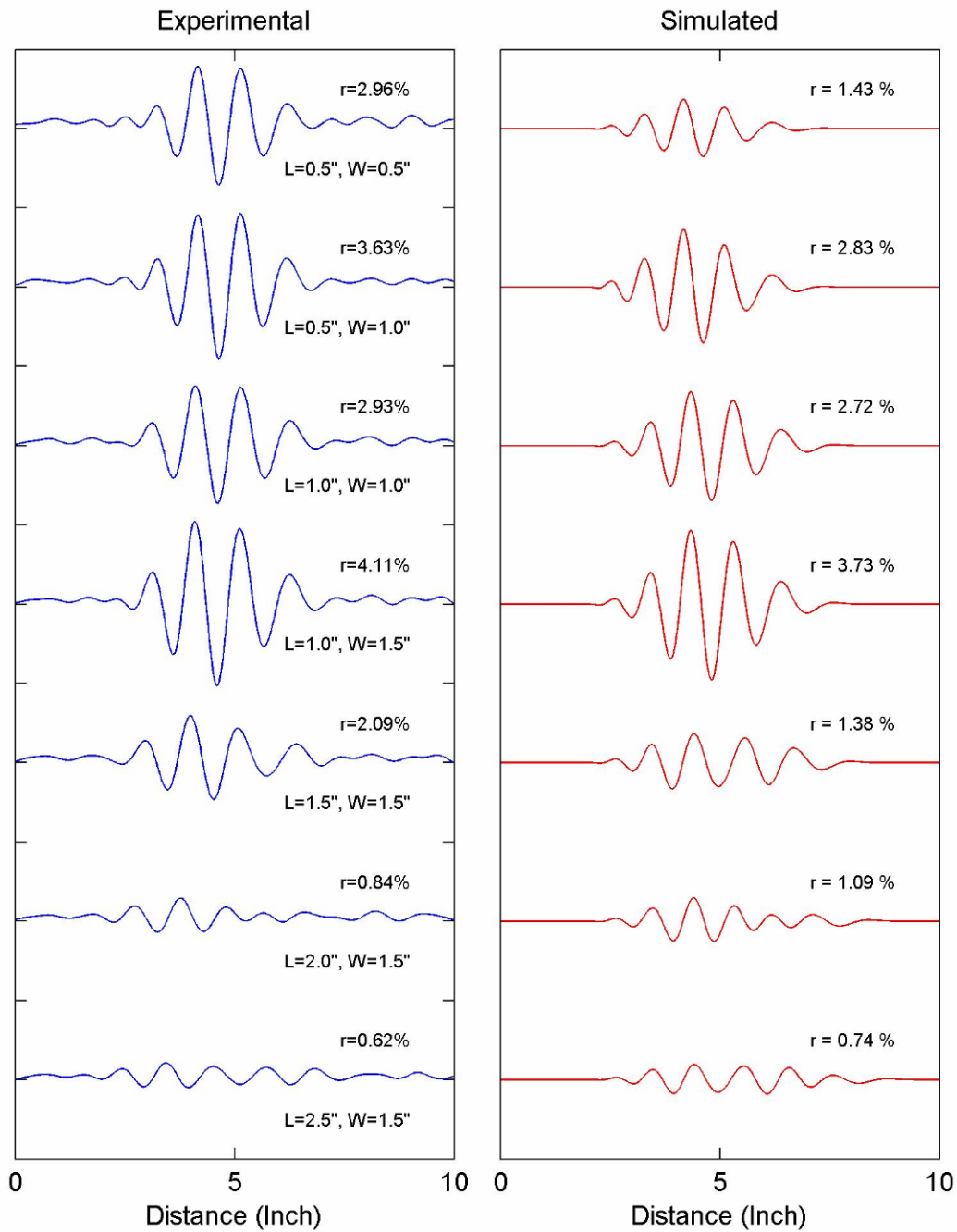


Figure 22. Experimental and simulated signals from ellipsoidal defects at 64 kHz; CSA of defects was 1.32% for W=0.5", 2.60% for W=1.0", and 3.81% for W=1.5"

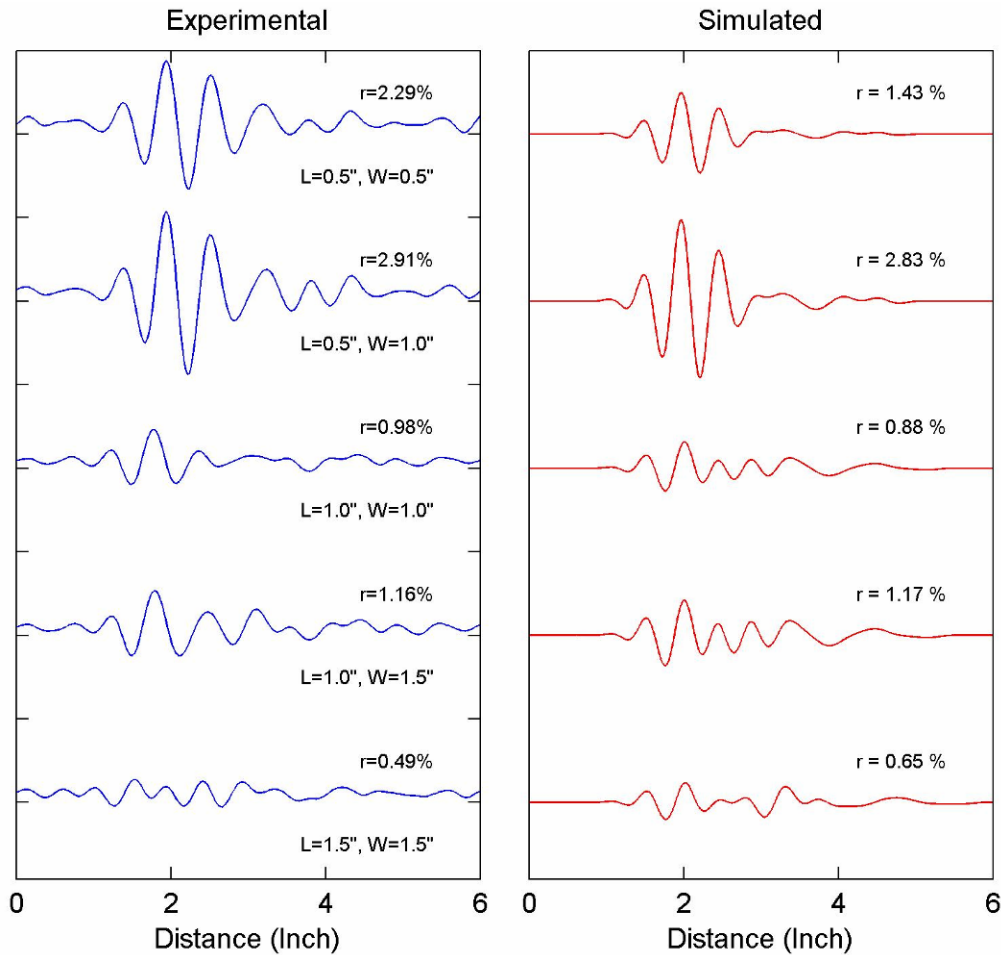


Figure 23. Experimental and simulated signals from ellipsoidal defects at 128 kHz; CSA of defects was 1.32% for  $W=0.5''$ , 2.60% for  $W=1.0''$ , and 3.81% for  $W=1.5''$

The signal amplitude (or equivalently the reflection coefficient) decreased with increasing  $L$ . This was expected because the change in wall thickness (or slope) becomes more gradual with increasing  $L$ . Since the effects of slope are greater at a higher frequency (discussed in Section 3.3.2(ii)), the elliptical defect with  $L=1.5''$  was hardly detectable at 128 kHz while it was readily detectable at 32 kHz.

### 3.3.3 Discussion and Other Findings

#### (i) Overall Assessment of Simulation Accuracy

Within the test range investigated (32 to 128 kHz and up to 10% CSA defects) and experimental measurement error ( $\pm 0.5\%$  in reflection coefficient), the simulation software was accurate and reliable in simulating defect waveforms.

Since the simulation software is based on a one-dimensional model, it cannot handle the mode conversions and beam spreading that occur when guided waves interact with a localized defect. Also, the software is limited to simulating the signal from a single defect. It could be extended to handle multiple defects.

(ii) *Wave Attenuation Coefficients in Bare Pipe*

To determine the reflection coefficient from a defect placed in the test pipe, the attenuation effects on the signal amplitude must be corrected for. The measured values of the attenuation coefficients of T-wave from pipe samples with different coatings (bare, fusion-bonded epoxy (FBE), and coal-tar) are plotted in Figure 24.

The attenuation in the coal-tar-(TGF-3)-coated pipe is much higher than in bare or FBE-coated pipe. In low frequencies (up to approximately 40 kHz), the attenuation coefficients are similar in both bare and FBE-coated pipes. The difference between the two becomes significant in higher frequencies.

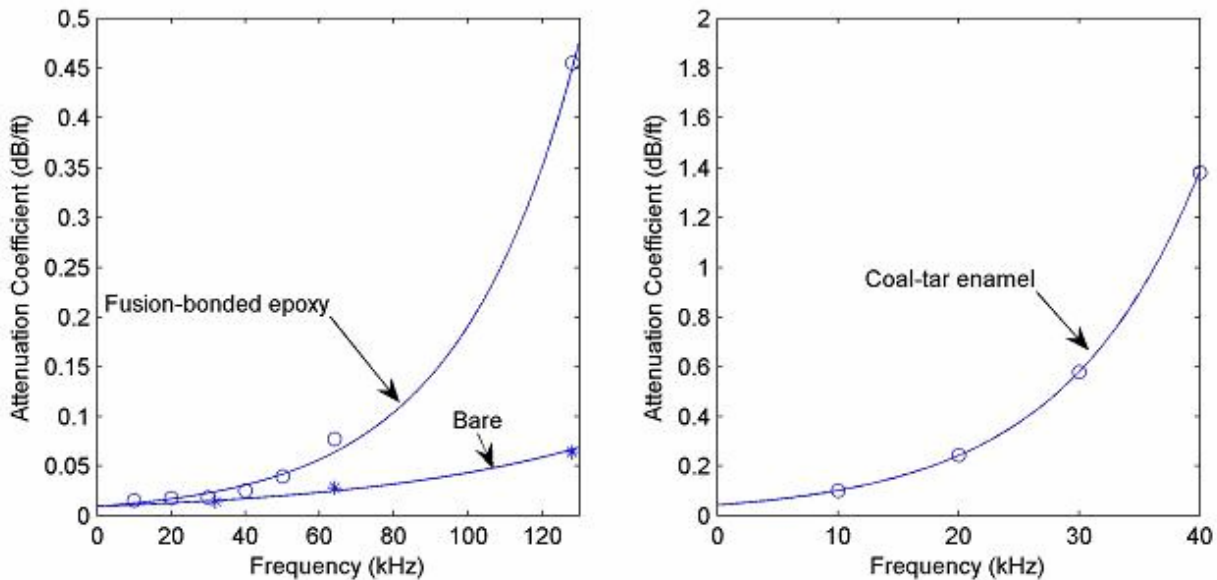


Figure 24. Attenuation coefficients of T-wave

(iii) *Behavior of Notch Rear-end Signal with Notch Length*

Notch signal waveforms obtained at various axial notch lengths,  $L$ , at 128 kHz are plotted in Figure 25. In the plots,  $F$  refers to the signal reflected from the notch front end and  $R$  from the notch rear-end. As  $L$  increased from 1 to 4 inches,  $R$  was gradually separated and moved away from  $F$  and its amplitude decreased while the amplitude of  $F$  remained the same. The rate of amplitude decrease for 80%-deep notches was about a factor of 2 greater than that for the 50%-deep notches.

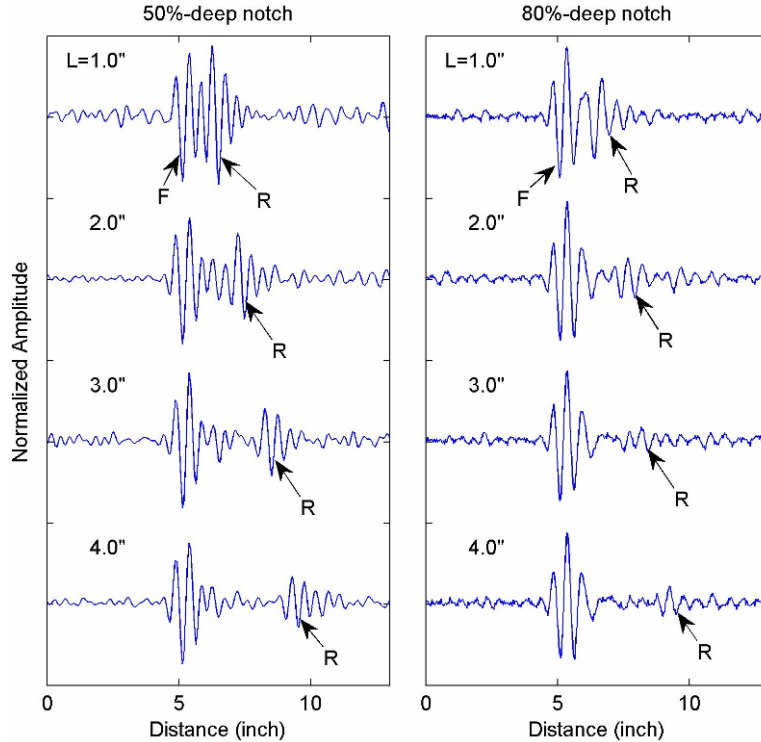


Figure 25. 128-kHz signal waveforms from notches with various axial lengths. Left—from 50%-wall-deep notches; Right—from 80%-wall-deep notches.

In the notched region between the two ends of a notch, the pipewall cross-sectional area does not change and, thus, there is no wave reflection. Over the short notch length (up to 4 inches) used in these experiments, the normal attenuation effects on the signal amplitude were negligibly small. Consequently, the amplitude of R was expected to remain constant, irrespective of L. The large decrease in the amplitude of R with increasing L shown in Figure 24 was therefore unexpected and indicated the presence of a significant energy-loss mechanism in the notched region. Presently, we do not understand how this energy loss occurs. The simulation model of course cannot account for this phenomenon.

(iv) *Trailing Signals*

In addition to the signals normally expected from the notch, we have observed other signals appear after the notch signal. These trailing signals were more noticeable for the 80%-wall-deep notches than for the 50%-wall-deep notches. Examples of trailing (T) signals are plotted in Figure 26 that were observed with the 80%-deep notches. The level of trailing signals was higher at lower frequency. The occurrence of the trailing signals and their level varied with the axial length of the notch in no orderly manner. It seems that these trailing signals are caused by waves that are reflected and perhaps mode-converted and spread around the pipe and propagated. Presently, we do not have a clear picture of what happens. We recognize that these trailing signals will increase the background noise level and could also be mistaken as defect signals. The simulation model also cannot handle these trailing signals.

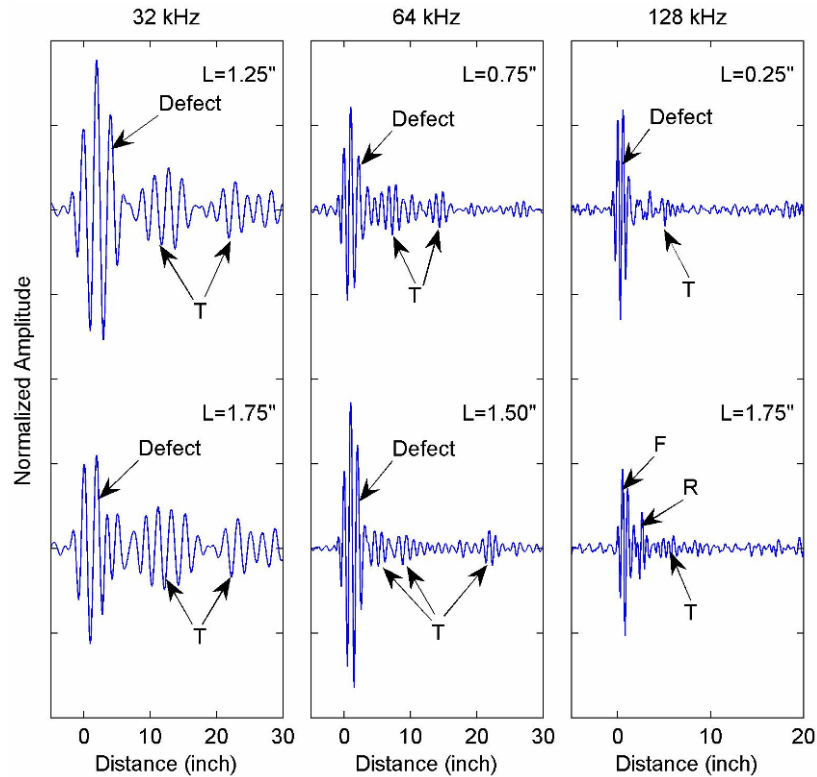


Figure 26. Examples of trailing (T) signals. The data are from the signals measured with the 80%-wall-deep notches. L refers to the axial length of the notch.

(v) *Variations in Transmitted Signals*

From the detailed analysis of the experimental data, we also have recognized that the transmitted signal waveform varied from sensor to sensor. The degree of variation was greater the higher the wave frequency. Fortunately the variations at 32 kHz, the frequency typically used for long-range pipe inspection, appeared to be relatively small. However, since the defect waveform is directly related to the transmitted signal waveform, any variations in the transmitted signal waveform will affect the defect signal waveform and, thus, contribute to the error in defect characterization.

## 4. DEFECT CHARACTERIZATION ALGORITHM

### 4.1 Signal Feature Analyses for Relevance to Defect Characteristics

The first step toward developing defect characterization algorithms is identifying the features of defect signals that are most useful to correlate to defect size (depth, width, and length) and shape. To identify the most relevant features, a total of 37 feature parameters were defined and their correlation to any of the defect characteristics was evaluated.

For the feature evaluation, a total of 19,809 defect signals were simulated, including both elliptical and trapezoidal-shaped defects with various lengths, widths, depths, and slopes and for different transmitter signal waveforms. The wave frequency was fixed at 32 kHz and the range of defect size was limited to:

Length - Up to 8 inches (equivalent to  $2\lambda$  at 32 kHz)  
CSA - Up to 8% of the total pipewall cross-sectional area

From the linear correlation analyses, the following six feature parameters illustrated in Figure 27 were the most relevant for defect characterization:

- (1) Base of Envelope – the width of the signal envelope at 10% of its peak amplitude points
- (2) Center of Envelope – a quantity defined per the following formula:

$$C = \frac{A1 \cdot T1 + A2 \cdot T2 + \dots + An \cdot Tn}{A1 + A2 + \dots + An}$$

where  $A1, A2, \dots, An$  are the amplitudes at points  $T1, T2, \dots, Tn$  along the x-axis

- (3) Center of Spectrum – a quantity defined in the same manner as (2) but applied to the signal spectrum
- (4) Spectral Peak Amplitude – peak amplitude of the signal spectrum
- (5) Peak Amplitude of Envelope – peak amplitude of the signal envelope
- (6) Max-Fall-Slope of Envelope – the maximum slope of the signal envelope on the right-hand side of the envelope

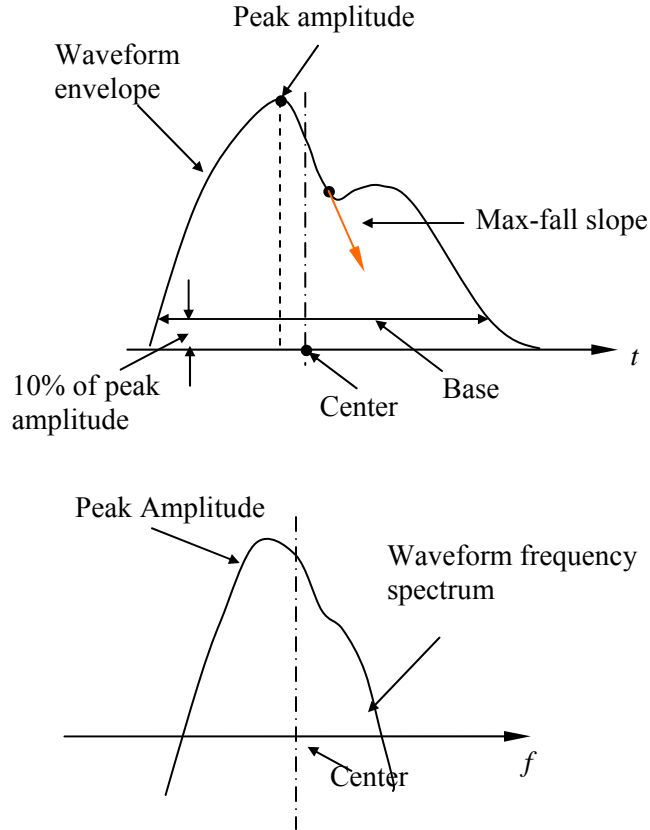


Figure 27. Illustration of feature parameters used for defect characterization algorithms

Base of envelope, center of envelope, and center of spectrum are correlated primarily to defect length. Spectral peak amplitude and peak amplitude of envelope are correlated primarily to defect CSA. Center of spectrum and spectral peak amplitude are correlated to defect shape (ellipsoidal or trapezoidal). Max-fall-slope of envelope is correlated to both defect length and CSA and was included in the algorithm development to enhance the characterization accuracy.

As an example, Figure 28 illustrates the correlation between the base of envelope and the defect length: (a) without noise, (c) with random noise on a level equivalent to 0.1% of reflection coefficient added to defect signals, and (d) after a wavelet-based denoising algorithm is applied to improve SNR ratio. The plot in Figure 28(b) is the distribution of SNR of the defect signals used in this study as a function of both defect length and cross-sectional area. The 6-dB SNR level, the criterion used for detection, is marked with a red dotted square. The signals that fell below the 6-dB SNR level would be undetectable.

When there was no noise, the base of envelope and the defect length showed a good linear correlation. The addition of noise to defect signals removed the correlation as shown in Figure 28(c), indicating the high degree of difficulty in determining the defect length. The denoising helped to partly restore the correlation. To improve the length determination, a combination of three feature parameters (base of envelope, center of envelope, and center of spectrum) was used in the defect characterization (or classification) algorithms.

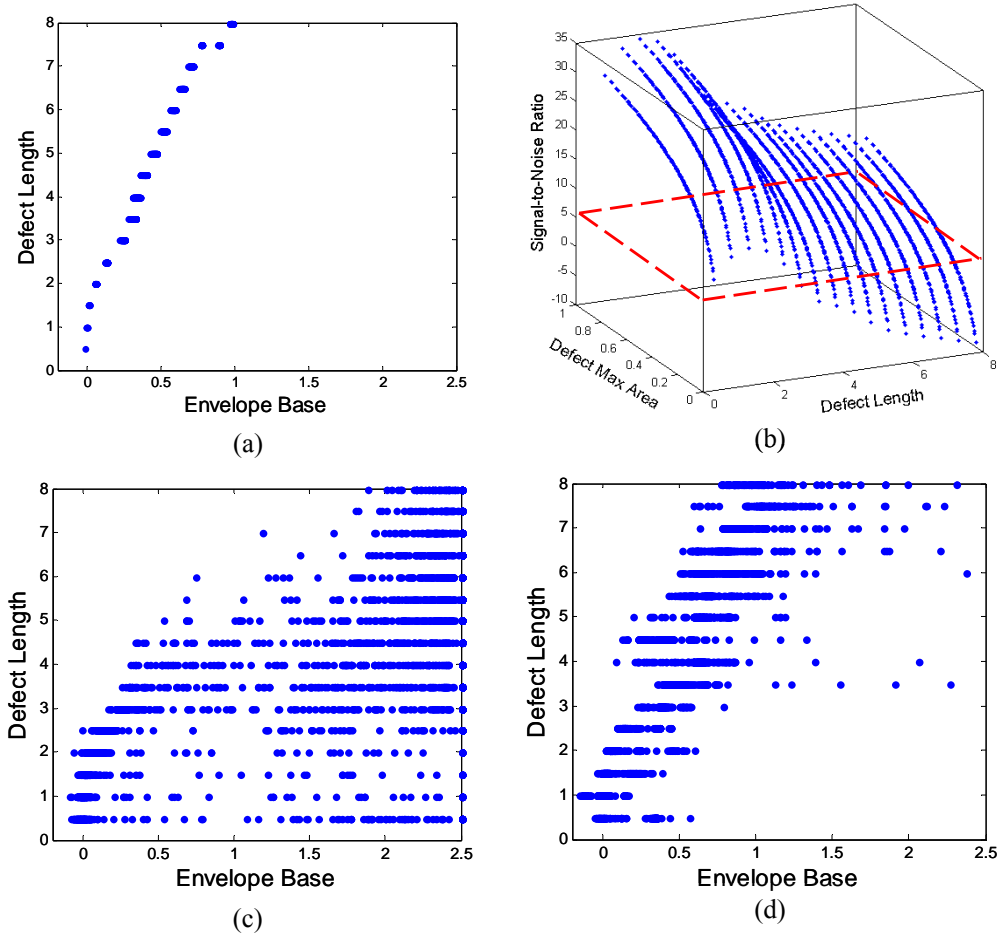


Figure 28. Correlation between the base of envelope and defect length for ellipsoidal defects: (a) without noise, (b) distribution of SNR of defect signals versus defect length and CSA, (c) with noise added to the defect signal, and (d) after the denoising algorithm was applied to improve SNR

Figure 29 illustrates the correlation between the spectral peak amplitude and defects CSA or volume in the presence of noise (on a level equivalent to 0.1% reflection coefficient). For a fixed defect length, there is an excellent linear relationship between the spectral peak amplitude and CSA or volume even in the presence of noise. Similarly, the peak amplitude of envelope also has an excellent linear relationship with CSA or volume. If the defect length is unknown, the correlation is not good. Therefore, to get an accurate measure of defect CSA, accurate determination of the defect length is prerequisite.

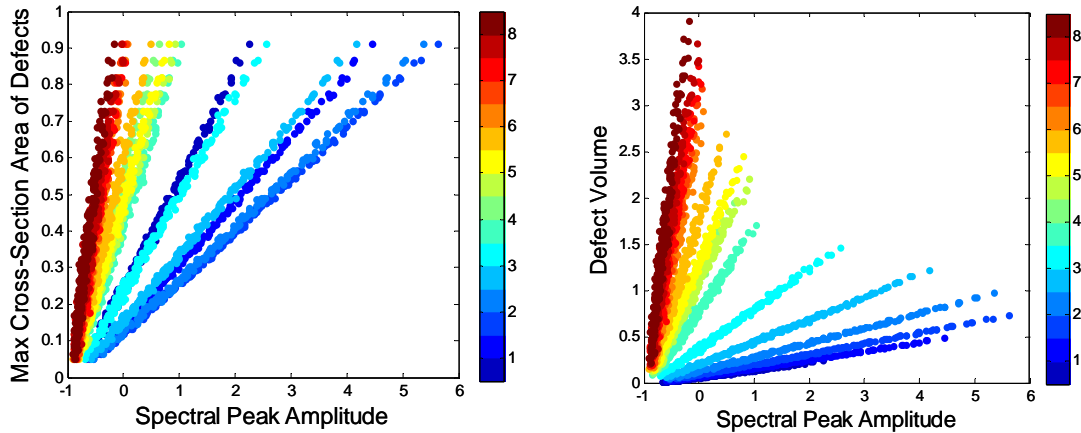


Figure 29. Correlation between the spectral peak amplitude of defect signal with noise and the maximum circumferential cross-sectional area of defect (left) and the defect volume (right) for the ellipsoidal defects. The color bar indicates the defect length from 0.5 inch (dark blue) to 8 inches (dark red).

No feature parameters were found to correlate well with either defect depth or defect width. Therefore, although CSA of the defect could be determined from the guided-wave feature parameters, separate determination of both depth and width is not feasible. This was expected because the guided wave examines the entire cross-section of the pipe and the reflection coefficient of defect is dependent on the defect CSA and is insensitive to the individual width or depth.

For distinguishing defect type (namely ellipsoidal or trapezoidal), the center of spectrum and the spectral peak amplitude were most useful. Figure 30 shows a plot of both parameters along with the discriminant line for distinguishing the defect type.

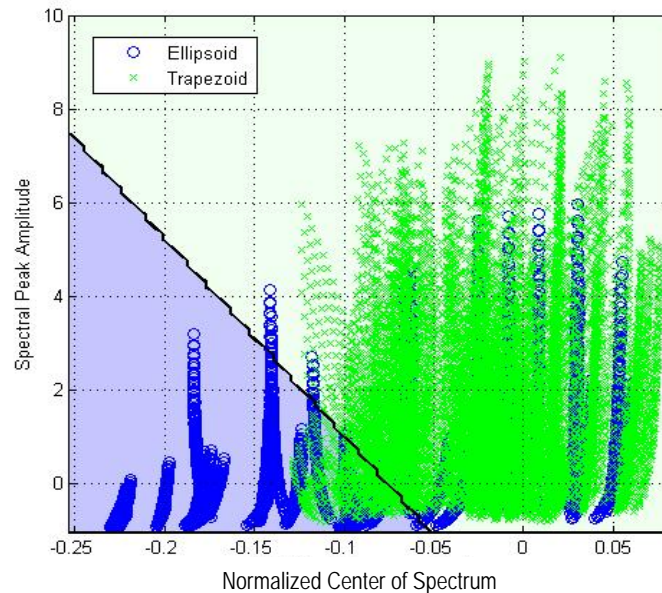


Figure 30. Classification of defect type based on two feature parameters—center of spectrum and spectral peak amplitude. The black line is the discriminant line for distinguishing the defect type.

A linear discriminant function (LDF),  $g(\bar{x})$ , which is the black line drawn in Figure 1 for distinguishing defect type, is given as:

$$g(\bar{x}) = 2.883 \cdot x_1 + 0.067x_2 + 0.714$$

if  $g(\bar{x}) < 0.5$  then *Ellipsoid Defect*  
if  $g(\bar{x}) \geq 0.5$  then *Trapezoid Defect*

where  $x_1$  is the center of spectrum and  $x_2$  is the spectral peak amplitude. The above classifier correctly determines the defect type for 95 percent of the trapezoid defects and 61 percent of the ellipsoid defects.

#### 4.2 Defect Characterization Algorithm Development

Using the six feature parameters described in Section 4.1, classification algorithms (i.e., classifiers) were developed to estimate defect length, shape, and CSA. Figure 31 illustrates the flow diagram of the defect classification algorithm. The defect signals containing noise were denoised by a wavelet-based filter. Then from the defect signal, the six feature parameters were extracted and normalized (to the corresponding features extracted from the transmit signal to minimize the effect of probe variations). The normalized values of the six feature parameters are then input to the classifier, which outputs the classification of defect length, shape, and max-cross-section area. The classification of max-cross-section area requires the determination of the defect length and shape.

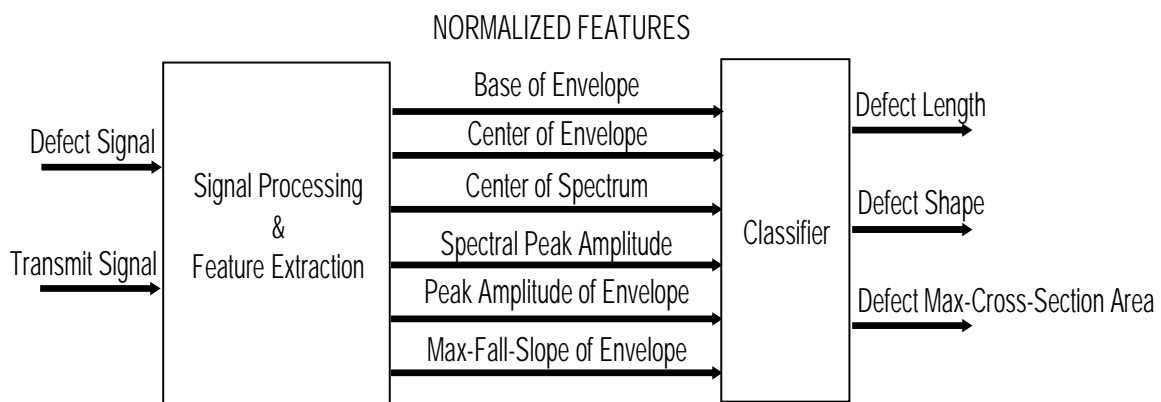


Figure 31. Flow diagram of the defect classification algorithm

The defect length output from the classifier is an integer between 1 and 8, which indicates that the defect length is between 0–1, 1–2, 2–3, 3–4, 4–5, 5–6, 6–7, and 7–8 inches, respectively.

The defect shape output from the classifier is 0 or 1, which indicates the ellipsoid and trapezoid shapes, respectively.

The defect CSA output from the classifier is an integer between 1 and 5, which indicates that the CSA is between 0–2, 2–4, 4–6, and 6–8 percent of the pipe cross-section area.

The classifier was developed by training a total of 18,809 sets of simulation data at 32 kHz that have been generated from different defect shapes, lengths, widths, and depths. All the data sets have  $\text{SNR} \geq 6$  dB.

Different classifiers—including Bayesian, maximum-likelihood, least-square error,  $k$ -nearest-neighbor, and linear-discriminant classifiers—were investigated in this study. Different feature combination algorithms, such as principal component analysis (PCA) and Fisher linear discriminant analysis, were also investigated. The results show that the use of  $k$ -nearest-neighbor classifier with all six features yielded the highest percentage of correct classifications.

Using a three-feature input [f1, f2, f3] as an example, a  $k$ -nearest-neighbor classifier searches  $k$ -neighborhood of [f1, f2, f3] in the three-dimensional space by comparing the Euclidean distance between the input feature and the features in training data [15]. The output of the classifier will assign the input feature to the class most frequently represented among the  $k$ -nearest training data; in other words, a decision is made by examining the classes on the  $k$ -nearest-neighbors and taking a vote.

The  $k$ -nearest-neighbor classifier was developed through the training of all 18,809 simulated data. After training, the performance of the classifier was evaluated using a subset of the 18,809 simulated data in three different SNR situations; namely,  $\text{SNR} \geq 6$  dB,  $\geq 12$  dB, or  $\geq 20$  dB. The results are listed in Table 1 in terms of the percentage of correct classifications and the standard deviation of the differences between the classifier outputs and the actual values.

The results in Table 1 showed that, on average, the classifier was able to correctly determine the defect length class for approximately 75% of the training data, the defect shape class for approximately 85% of the data, and the defect max-cross-section-area for approximately 84% of the data. It was noted that the higher SNR ratio improved the accuracy of the classification only slightly, a somewhat unexpected result which may be attributable to the use of the same data employed for training the classifier.

Table 1. Performance of the Classifier Tested with Training Data

Noise Condition	Defect Classification	Percent of Correct Classification	Standard Deviation
SNR $\geq$ 6 dB	Defect Length	71.6%	1.3 in.
	Defect Shape	84.8%	0.4
	Defect Max-Cross-Area	83.2%	1.0%
SNR $\geq$ 12 dB	Defect Length	74.6%	1.2 in.
	Defect Shape	85.6%	0.4
	Defect Max-Cross-Area	84.3%	1.0%
SNR $\geq$ 20 dB	Defect Length	79.8%	1.1 in.
	Defect Shape	87.6%	0.3
	Defect Max-Cross-Area	86.3%	0.8%

The performance of the classifier was further tested using an additional 1,000 simulated data that were generated independently (from the data used for training the classifier). The results are listed in Table 2.

Table 2. Performance of the Classifier Tested with Independent Data

Noise Condition	Defect Classification	Percent of Correct Classification	Mean Difference	Standard Deviation
SNR = 6 dB	Defect Length	37.3%	0.2 in	2.4 in
	Defect Shape	54.1%	0.3	0.6
	Defect Max-Cross-Area	55.3%	-0.1%	1.5%
SNR = 12 dB	Defect Length	41.7%	0.0 in	2.0 in
	Defect Shape	57.3%	0.4	0.5
	Defect Max-Cross-Area	59.9%	0.0%	1.4%
SNR = 20 dB	Defect Length	57.3%	-0.1 in	1.4 in
	Defect Shape	58.2%	0.4	0.5
	Defect Max-Cross-Area	70.3%	0.0%	1.3%

In this case, the performance of the classifier improved with the increase of SNR, an expected behavior. When SNR = 20 dB, the classifier correctly determined the defect length class for approximately 57% of the data and the defect max-cross-section area for approximately 70% of the data. When SNR = 6 dB, the accuracy decreased to approximately 37% for the defect length and 55% for the defect max-cross-section area.

The standard deviation,  $\sigma$ , represents a degree of scatter from the true value. For Gaussian distribution of data, approximately 68% of the measured data are within  $1\sigma$  from the true value, and approximately 95% of the measured data are within  $2\sigma$  from the true value. Therefore, the results in Table 2 suggest that 95% of the time, the classifier can determine the defect length within  $\pm 4.8$  inches (in reference, the wavelength of T-mode at 32 kHz is 4 inches) and the defect max-cross-section area within approximately  $\pm 3\%$  when SNR = 6 dB; when SNR = 20 dB, it improves to within  $\pm 2.8$  inches for length and  $\pm 2.6\%$  for the max-cross-section area.

The probability of correctly determining the defect shape (either ellipsoidal or trapezoidal) was approximately 50-50, which means that the defect shape could not be determined with any accuracy using the classifier. This is because the difference in the shape of an elliptical defect and a trapezoidal defect of given length and CSA lies only in whether the defect surface is curved or planar, which is a minor variation for low-frequency guided-waves (such as 32-kHz considered here).

### **4.3 Capabilities and Limitations**

The defect classification (or characterization) algorithm is capable of determining length, CSA, and shape of defect (albeit the accuracy in determining shape is not high).

The algorithm is used for 32-kHz signals. It can be used for signals at other frequencies by treating them as if they were 32-kHz signals through an appropriate normalization process.

Application of the algorithm is limited to the following range:

CSA – up to 8 %

Length – up to 8 inches at 32 kHz (or  $2\lambda$  at other frequencies)

The algorithm assumes that the transmitted signal waveform does not change with traveling distance. This assumption is satisfactory in low-attenuation pipelines. In high-attenuation pipelines (such as coal-tar-coated or polyethylene-coated lines), however, this assumption is no longer valid. Therefore, proper correction of the attenuation effects on the signal (waveform, amplitude, and spectral content) is necessary to apply the algorithm.

## 5. PREPARATION FOR FIELD TESTING

### 5.1 Adhesive Bonding Material Testing

In previous work conducted for NYSEARCH/NGA [6], it was found that the cured epoxy layer (3M's Scotch-Weld epoxy DP 125, Gray) is rigid and transmits stress changes in pipe to the MsS strip, which in turn affects the MsS sensitivity (because the stress influences the magnetostrictive properties of the strip material). When strips are bonded to a pipe with a high internal pressure and the pipe is depressurized later, the resulting pressure change induces a compressive stress in the strip and degrades the sensitivity (approximately 8 dB for 36-ksi compressive stress). When strips are bonded on a pipe with zero pressure and the pipe is pressurized later, a tensile stress is induced in the strip. The effects of tensile stress on the MsS sensitivity were found not only to be relatively small but also to improve the sensitivity (about 2 dB or so for 36-ksi tensile stress).

To operate the MsS in the T-mode, the strip is magnetically conditioned at the time of sensor installation. It involves moving a permanent magnet over the strip at a relatively constant speed (about 1 ft/sec) and inducing a residual magnetization in the strip along the circumferential direction around the pipe. The stress caused by line pressure changes alters the strip's residual magnetization condition and affects the MsS sensitivity.

The degrading effect under compressive stress is of concern because, in field applications of the long-term guided-wave SHM, it is likely that the line would have high internal pressure at the time of sensor installation. Any subsequent depressurization of the line would cause the sensor degradation and, thus, negatively impact the SHM ability in proportion to the magnitude of pressure change. To minimize the effects of line pressure change on the MsS sensitivity, therefore, it is desirable to find alternate adhesive materials that are (1) able to transmit the guided waves from the MsS strips to the pipe and vice versa, (2) flexible enough to create a discontinuity in static stress across the adhesive layer so that the stress caused by line pressure changes would not be transmitted to the strip, and (3) suitable for long-term use in pipeline environments.

Various materials were evaluated for their suitability on the 12-inch-OD pressure test sample used in the previous project [6]. Photos of the test sample and the MsS setup are shown in Figure 32.



Figure 32. Photo of the 12-inch-OD pressure test sample (left) and the strips and MsS coils installed on the test sample (right)

Materials evaluated included several construction sealant materials (such as silicone, rubberized asphaltic compound, polyurethane, and rubber cement) and adhesives based on polyurethane. Among the materials tested, Hysol U-10FL, a polyurethane-based adhesive, was found to be suitable for bonding MsS strips and to exhibit the least pressure effects. Figure 33 shows the pressure test data obtained using the Hysol U-10FL for bonding made at zero (top) and 2140 psi (bottom) line pressures.

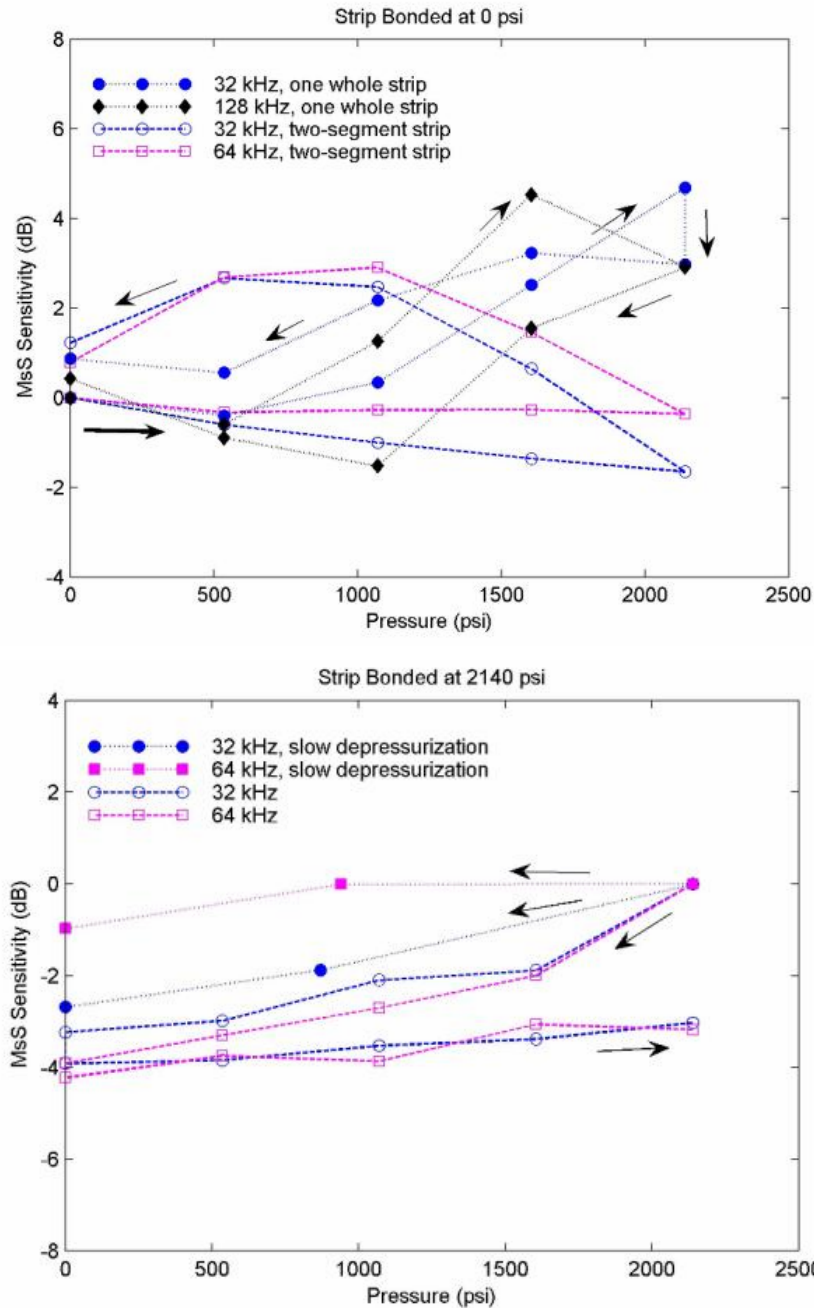


Figure 33. MsS sensitivity variations with line pressure change for strips bonded using Hysol U-10FL at 0 psi (top) and 2140 psi (bottom) line pressure. The hoop stress caused by 2140 psi was 36 ksi.

The effects on the strips bonded at zero line pressure were similar to the effects observed previously with the 3M Scotch-Weld epoxy bonding. The degradation on strips bonded at 2140 psi was approximately 4 dB, about ½ of the previous observed effects with the 3M Scotch-Weld epoxy. It was also observed that the effects were less when the strips were segmented and the rate of the pressure change was lowered (for 535-psi increment, from about 0.5 to 1 minute to 10 to 15 minutes).

Based on the limited test results, it appeared that Hysol U-10FL would be better than Scotch-Weld epoxy for MsS installation on high-pressure lines, but until an ideal bonding material is found, some degradation in the sensor sensitivity would be unavoidable.

If the sensor sensitivity is degraded, it can be restored to the original level by reconditioning the strips magnetically. Therefore, if the strips can be reconditioned, the effect of line pressure change on sensor sensitivity becomes a non-issue. Presently, reconditioning requires a direct access to the installed sensors and thus, if buried, the line needs to be excavated for reconditioning. To eliminate the costly excavation, development of a method and device that can maintain the MsS sensitivity under large line pressure changes is recommended.

## **5.2 Improvement of Data Analysis Software**

Various data analysis functions were added to the existing software used at SwRI for pipeline inspection and monitoring to improve its performance. Added functions included:

- (1) Correlating data from both ends of cased section of carrier line for cross-confirmation.
- (2) Fine adjustment of wave properties along the pipeline to properly align known signals (such as weld signals) for data subtraction so that changes occurring over time could be determined accurately. When data are taken periodically, the signals from known features do not line up exactly. The primary reason is that the variations in line temperature between the measurement times and along the pipeline cause the wave velocity to vary and thus cause the signals from known features in the line to occur at different positions in the data. Without this fine adjustment, the data subtraction (or the data correlation mentioned above) yields poor results.
- (3) Variable (instead of constant) detection threshold and attenuation correction on the signal amplitude.
- (4) Defect characterization that involves gating defect signals, normalizing the gated signal (with respect to the transmitted signal and wave frequency), extracting feature parameters, and applying the defect classifier (discussed in Section 4.2).

Figure 34 shows an example of correlated data from both ends of an approximately 250-ft-long cased section of gas transmission line in the field [5]. The correlation function has been useful in identifying signals from spacers and minimizing false calls.

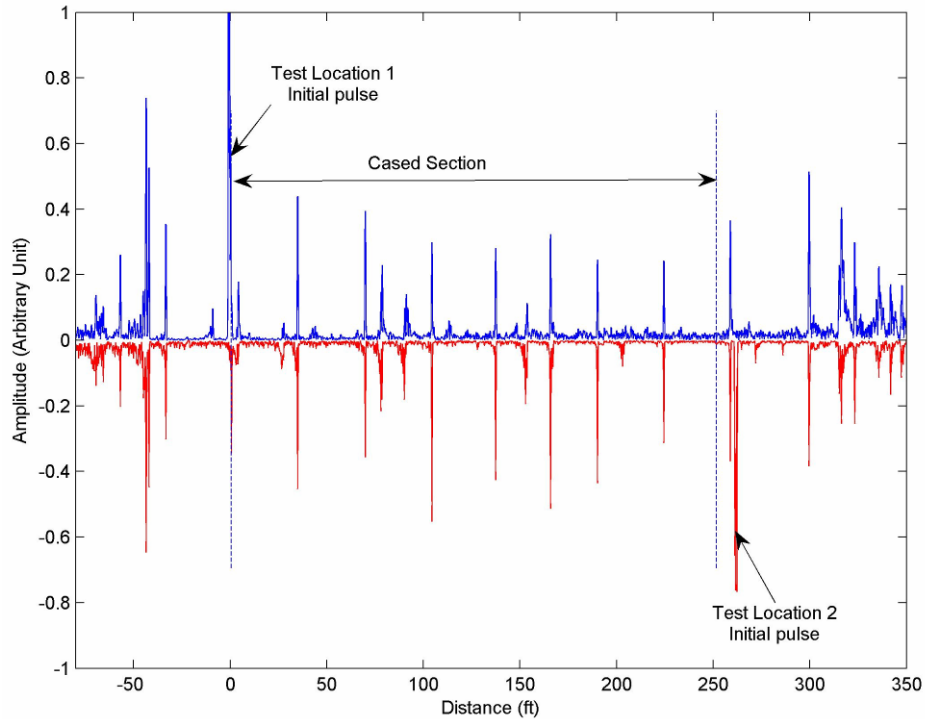


Figure 34. Example of correlated data from both ends of a cased section of gas transmission line (data from the previous DOT project) [5].

Figure 35 shows an example of baseline and monitoring data and the results of data subtraction achieved after fine adjustments of feature signals. Note that the prominent signals in the baseline data occurred further away in the monitoring data (due to a slower wave velocity when the monitoring data were acquired). The fine adjustment of wave properties allowed a proper alignment of signals in both data sets for accurate detection of changes—in the example, a new signal and a change in the previously existing signal were detected.

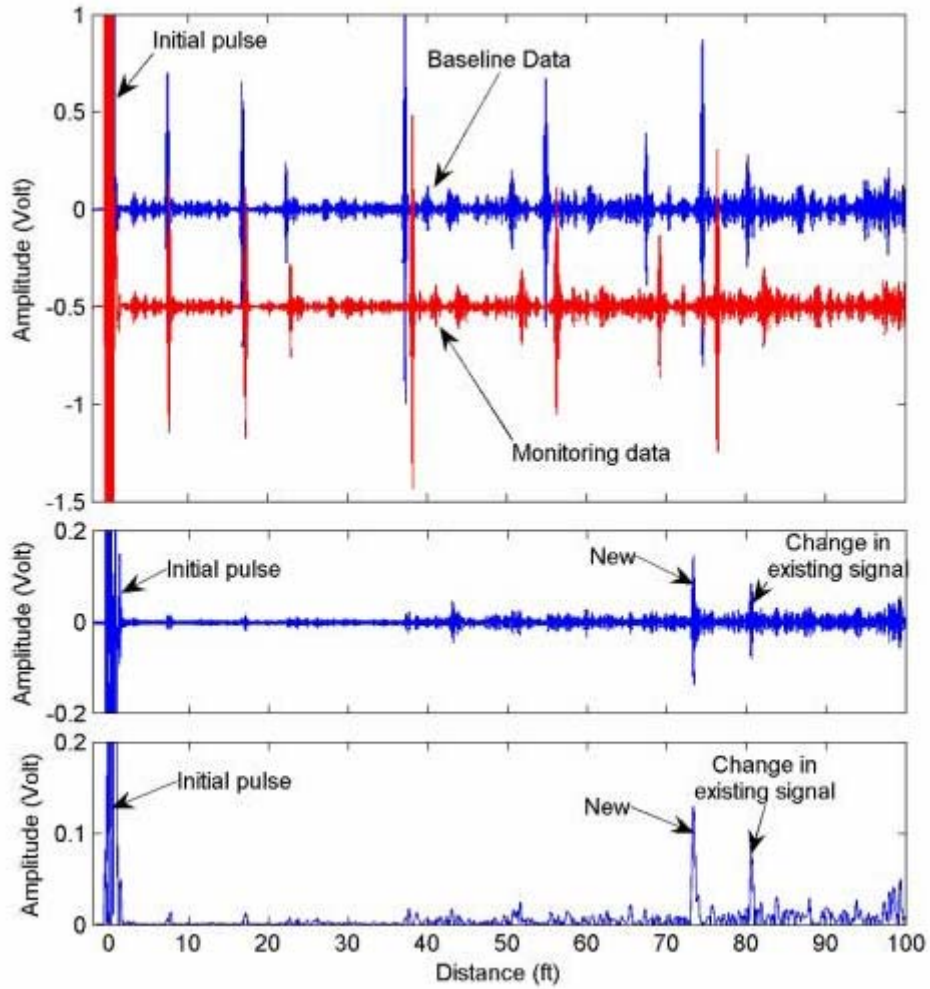


Figure 35. Example of the baseline data and the newly acquired monitoring data (top) and the subtraction results after the two sets of data were properly aligned (bottom two)

## 6. TESTING AT NYSEARCH/NGA TEST BED

### 6.1 Cased Line Test Pipes at NYSEARCH/NGA Test Bed Facility

The NYSEARCH/NGA test bed facility is located in Johnson City, NY. The facility has the following three, approximately 80 ft. long, cased-line test pipes:

- (1) Aboveground, 20-inch-OD bare steel pipe in 24-inch casing
- (2) Aboveground, 16-inch-OD steel pipe with 0.154-inch-thick coal tar TGF-3 coating in 20-inch casing
- (3) Underground, 12-inch-OD steel pipe with 20-mil-thick coal tar epoxy (CTE) coating in 16-inch casing

All test pipes were seam-welded and were 0.375-inch in wall thickness. All test pipes contained machined defects at various points around the circumference and axially along the pipe. In the cased section, casing spacers were placed along the pipe at various locations and the edge of the casing was sealed with a link joint shown in the Figure 36 photos. The underground test pipe was accessible for guided-wave testing from the two vaulted excavations shown in the Figure 36 photos.



Figure 36. Photos of link joint seal at the edge of casing (left) and vaulted excavation for access to the underground test pipe (right)

### 6.2 Baseline Testing and Sensor Installation

#### 6.2.1 Proceedings

Baseline MsS testing of three cased-line test pipes was conducted during the week of April 23<sup>rd</sup>, 2007. MsS coils were permanently installed for long-term condition monitoring (SHM). Photos taken during the testing are shown in Figure 37.



Figure 37. Photos of MsS testing at the NYSEARCH/NGA test bed facility: (a) rubber strap wrapped over the magnetostrictive strips bonded around the 16-inch-OD TGF-3-coated pipeline, (b) applying epoxy on the magnetostrictive strips for bonding to the 12-inch-OD CTE steel pipeline, (c) MsS system during data acquisition from the 20-inch-OD bare steel pipeline, (d) MsS ribbon coils placed over the magnetostrictive strips for testing, (e) wax tape applied over the MsS ribbon coils for protection from environment for long-term monitoring, and (f) MsS ribbon coils installed with protective wax tape on the 12-inch-OD CTE steel pipeline; the exposed ends of the ribbon coils were later wrapped with plastic tape for protection.

## 6.2.2 Results and Overall Findings

Details of the baseline test data and results are given in Appendix A.

The results of defect characterization algorithm (axial length, defect shape, and circumferential cross-sectional area (CSA)) are listed in Tables 3 through 5. The defect numbers refer to those in the test results given in Appendix A.

For comparison, the %-Reflection determined based on the signal amplitude (given in test results in Appendix A) and the actual CSA per the information from NGA/NYSEARCH are also listed in the tables. The results in the tables are from the lower-frequency data (i.e., 32 kHz for bare pipe sample and 16 kHz for the coated pipe samples). The results from the higher-frequency data (particularly the data acquired from the coated pipe samples) were unreliable due to the uncertainty in compensating the attenuation effects on the waveform. The CSA determined using the classifier was about the same as the %-Reflection determined previously based on the signal amplitude.

**Table 3. Defect characterization results for defects found from the above-ground 20-inch-OD bare steel pipe in 24-inch casing**

Defect No.	Axial Length	Shape	CSA (%)	% Reflection	Actual CSA (%)
D2	0 ~ 1"	Trapezoid	0 ~ 2	2.2	$2 < x < 3$
D3	0 ~ 1"	Trapezoid	0 ~ 2	3.0	$2 < x < 3$
D4	5 ~ 6"	Trapezoid	0 ~ 2	1.7	$1 < x < 2$

**Table 4. Defect characterization results for defects found from the above-ground 16-inch-OD TGF-3coated steel pipe in 20-inch casing.**

Defect No.	Axial Length	Shape	CSA (%)	% Reflection	Actual CSA (%)
D2	0 ~ 1"	Trapezoid	0 ~ 2	2.4	$1 < x < 2$
D3	0 ~ 1"	Ellipsoid	2 ~ 4	3.1	$3 < x < 4$
D4	2 ~ 3"	Trapezoid	2 ~ 4	2.4	$3 < x < 4$
D5	4 ~ 5"	Trapezoid	6 ~ 8	4.4	$4 < x < 5$
D6	5 ~ 6"	Trapezoid	4 ~ 6	3.7	$3 < x < 4$

**Table 5. Defect characterization results for defects found from the below-ground 12-inch-OD CTE-coated steel pipe in 16-inch casing**

Defect No.	Axial Length	Shape	CSA (%)	% Reflection	Actual CSA (%)
D2	6 ~ 7"	Ellipsoid	4 ~ 6	6.4	$6 < x < 7$
D3	0 ~ 1"	Ellipsoid	2 ~ 4	2.3	$x < 1$
D4	3 ~ 4"	Trapezoid	2 ~ 4	3.0	$1 < x < 2$
D5	0 ~ 1"	Trapezoid	4 ~ 6	4.0	$1 < x < 2$
D6	0 ~ 1"	Trapezoid	4 ~ 6	10.1	$3 < x < 4$
D7	2 ~ 3"	Trapezoid	2 ~ 4	2.6	$1 < x < 2$
D8	5 ~ 6"	Ellipsoid	4 ~ 6	3.8	$1 < x < 2$

The baseline test results given in Appendix A were evaluated by NGA/NYSEARCH and the overall findings are as follows:

- (1) Welds – All welds in the three test pipes were detected and correctly identified.
- (2) Casing Spacers
  - a. Casing spacers on bare pipe did not produce detectable signals and thus were not detected.
  - b. Casing spacers (and link seal) on TGF-3 and CTE-coated pipe produced detectable signals. Out of a total 17 spacers (9 on the aboveground 16-inch and 8 on the underground 12-inch pipes), 16 (9 on the aboveground 16-inch and 7 on the underground 12-inch pipes) were detected and correctly identified.
- (3) Defects
  - a. In 20-inch aboveground bare pipe
    - i. Detected – 4 ea ( $1\% \leq 3ea \leq 2\%$ ,  $2\% \leq 1ea \leq 3\%$  CSA)
    - ii. Missed – None
  - b. In 16-inch aboveground pipe with 0.154-inch TGF-3 coating
    - i. Detected – 6 ea ( $3ea \leq 2\%$ ,  $3\% \leq 3ea \leq 5\%$  CSA)
    - ii. Missed – 12 ea ( $11ea \leq 2\%$ ,  $2\% \leq 1ea \leq 3.5\%$ )
  - c. In 12-inch underground pipe with 20-mil CTE coating
    - i. Detected – 8 ea ( $1ea \leq 1\%$ ,  $1\% \leq 5ea \leq 2\%$ ,  $1ea \approx 4\%$ ,  $1ea \approx 6\%$  CSA)
    - ii. Missed – 13 ea ( $7ea \leq 1\%$ ,  $1\% \leq 3ea \leq 2\%$ ,  $3\% \leq 3ea \leq 5\%$ )

No false calls.

Other observations include:

- (1) Locations were within 12 inches of the actual features (welds, casing spacers, and defects) 92% of the time.
- (2) Shapes of defect were correctly predicted 87% of the time.
- (3) Axial lengths of defect were correctly predicted less than 30% of the time. Noise renders the measurements of axial length of small defects a challenge.

## 6.3 Monitoring Test and Results

### 6.3.1 Proceedings

Two monitoring tests were conducted – 1<sup>st</sup> on November 6, 2007 and 2<sup>nd</sup> on February 20, 2008. The temperature during the 1<sup>st</sup> SHM measurements was in the low 40s in F. During the 2<sup>nd</sup> SHM measurements, the temperature ranged from about 15 to 25° in F. After the 2<sup>nd</sup> SHM measurements, the installed sensors on the test pipes were removed. Photos taken during the 2<sup>nd</sup> SHM testing are shown in Figure 38.



Figure 38. Photos from the 2<sup>nd</sup> SHM testing: scenery of the test bed (left), installed sensors on 20-inch bare pipe (middle), and the iron-cobalt strips exposed after the wax tape and MsS ribbon coils were removed (right)

### 6.3.2 Results and Overall Findings

Details of the SHM test data and the comparison results with the baseline data are given in Appendix B for the 1<sup>st</sup> test and Appendix C for the 2<sup>nd</sup> test. Overall findings from the SHM measurements are:

- (1) All MsS probes installed on the test pipes performed well over the 10-month duration, indicating that the probes are suitable for long-term SHM applications.
- (2) Data from the bare pipe were reproducible within 0.2% reflection, indicating that a 0.4% CSA change could be reliably detected from SHM measurements.
- (3) In the TGF-3 and CTE-coated test pipes, existing signals from actual features on the pipe (welds, spacers, and defects) were reproducible within approximately 1 to 2% reflection – which is about 5 to 10 times worse than the reproducibility in the bare pipe. This means that the growth of the existing defects or formation of new defects at weld or spacer locations would not be detectable until the changes exceed 2 to 4% reflection level.

The primary cause of the above poor reproducibility is the temperature variations that cause a change in wave attenuation (which leads to alteration of waveforms and resulting changes in feature signals). The temperature variations also alter the mechanical coupling state of the casing spacers to the pipe and contribute to changes in the spacer signals. The velocity change with temperature alters the interference pattern between the adjacent signals and also contributes to signal changes.

- (4) When the existing feature signals in the TGF-3 and CTE-coated test pipes were excluded, the SHM data were reproducible within 0.5% reflection, indicating that the formation of approximately 1% CSA new defects would be reliably detectable from SHM measurements.
- (5) The data reproducibility described in (2) to (4) above was similar in all cases; namely between the baseline and the 1<sup>st</sup> SHM data, between the baseline and the 2<sup>nd</sup> SHM data, and between the 1<sup>st</sup> and 2<sup>nd</sup> SHM data.

To achieve the detection sensitivity of 1% CSA (or better) changes in defect size in coated pipes, the effect of attenuation change with temperature on signal waveforms needs to be minimized by developing suitable data processing techniques for correcting the attenuation effects.

During the removal of the installed sensors, the iron-cobalt strips were generally found to be in pristine condition, indicating that the wax tape protected them well over the 10-month period. In some sensor installation locations, however, water was found at the bottom side of the pipe along with corrosion discolored iron-cobalt strips in that area, indicating that the wax tape did not completely repel the water, perhaps due to imperfect placement of the wax tape during the installation. Appropriate measures need to be taken to eliminate the observed water intrusion problem, either procedurally or using a better protective tape material or both.

## 7. FIELD TESTING AND RESULTS

### 7.1 Testing on Coated Lines in Astoria Tunnel, New York, NY

#### 7.1.1 Proceedings

Testing on a 26-inch-OD gas pipeline in the Astoria tunnel in Queens, NY, was conducted during the week of May 28<sup>th</sup>, 2007. The pipeline was coated with wax tape wrap. Two short sections where the wax tape wrap was removed for sensor installation showed generalized corrosion around the pipe circumference. After the iron cobalt strips were bonded around the pipe (using 3M Scotch-Weld epoxy DP 125, Gray, chosen since the line pressure was relatively low) and bonding was cured, MsS coils were installed by manually winding #22 gauge insulated wire over the iron cobalt strips as shown in the photos in Figure 39. Baseline data were then acquired using the installed sensors.



Figure 39. Photos of MsS testing on 26-inch OD gas pipeline: (a) a spool of #22 gauge insulated wire, (b) wires wound over the iron cobalt strips, (c) electrical connections to MsS instrument, (d) protective tape wound over the coils, and (e) acquisition of baseline data

#### 7.1.2 Results and Findings

Detailed test data and results are given in Appendix D.

Because of the wax tape wrap coating and the general corrosion, the wave attenuation was high (about 0.5 dB/ft at 16 kHz and 1.0 dB/ft at 32 kHz, greater than the typical attenuation in TGF-3-coated pipe plotted in Figure 24) and varied along the length of pipe (understandable due to different degrees of generalized corrosion). On average, the achievable test range at 16 kHz was about 40 to 45 ft.

From the baseline test data, four defect indications were found which were estimated to be 10 to 15% CSA. Afterward, staff members of Con Ed (owner of the pipeline) removed the wax tape

wrap at the defect indication locations and visually inspected the locations. They found the generalized corrosion around the circumference (similar to the condition at the sensor installation locations shown in photos in Figure 39) and the degree of wall loss benign.

The installed sensors remain in place for potential future SHM measurements.

## **7.2 Testing on Cased-Line Mockups Subjected to an Accelerated Corrosion Treatment at RG&E Facility in Rochester, NY**

### **7.2.1 Proceedings**

Two separate tests were conducted at the RG&E facility in Rochester, NY, to evaluate and validate the capability of detecting changes in the pipe using the MsS SHM approach.

The 1<sup>st</sup> test was conducted on a cased-line mockup composed of an approximately 66-ft-long, 4.5-inch-OD and 0.237-inch-wall pipeline inside an approximately 43-ft-long, 6-5/8-inch-OD casing. The test pipeline was made by welding two 33-ft-long pipe joints; one with a two-layer polyethylene (PE) coating (called PRITEC<sup>®</sup>) and the other with a field-applied coal tar tape wrap (called Tapecoat<sup>®</sup> 20).

The MsS probes were installed at both sides of the casing and the baseline data were measured on September 20, 2007. Figure 40 shows photos of the testing and installed probes at one end (the probes were wrapped with a protective tape).



Figure 40. Photos of MsS testing on the 1st cased-pipeline mockup and installed probes

After the baseline measurements, RG&E staff members applied reverse cathodic protection current to the test pipe and induced accelerated corrosion defects in the pipe at various locations along the pipe. After several weeks of accelerated corrosion treatments, SHM measurements were conducted on November 6, 2007. Then RG&E staff members removed the casing and measured the actual corrosion defects induced in the test pipe for comparison with the SHM results.

The 2<sup>nd</sup> test was conducted on a cased-line mockup composed of an approximately 62-ft-long, 4.5-inch-OD and 0.237-inch-wall pipeline in an approximately 44.5-ft-long, 6-5/8-inch-OD casing. The test pipe was made of approximately 44-ft-long, fusion-bonded-epoxy (FBE) coated pipe, to each end of which was welded an end section that was cut out of the 1<sup>st</sup> test pipe and instrumented with the MsS probes. The FBE-coated pipe section was cased in the mockup.

The baseline measurements on the 2<sup>nd</sup> mockup were conducted on January 8, 2008. Then the test pipe was subjected to accelerated corrosion treatments and the 1<sup>st</sup> SHM measurements were made on February 5, 2008, followed by additional accelerated corrosion treatments and the 2<sup>nd</sup> SHM measurements on February 19, 2008.

Figure 41 shows photos taken during the testing on the 2<sup>nd</sup> mockup.



Figure 41. Photos taken during the testing on the 2<sup>nd</sup> mockup: test pipe (top left), MsS probes (top right), and ends of test pipe (bottom)

## 7.2.2 Results and Findings from 1<sup>st</sup> Test Mockup

Figures 42(a) and (b) show the data acquired at 16 and 25 kHz.

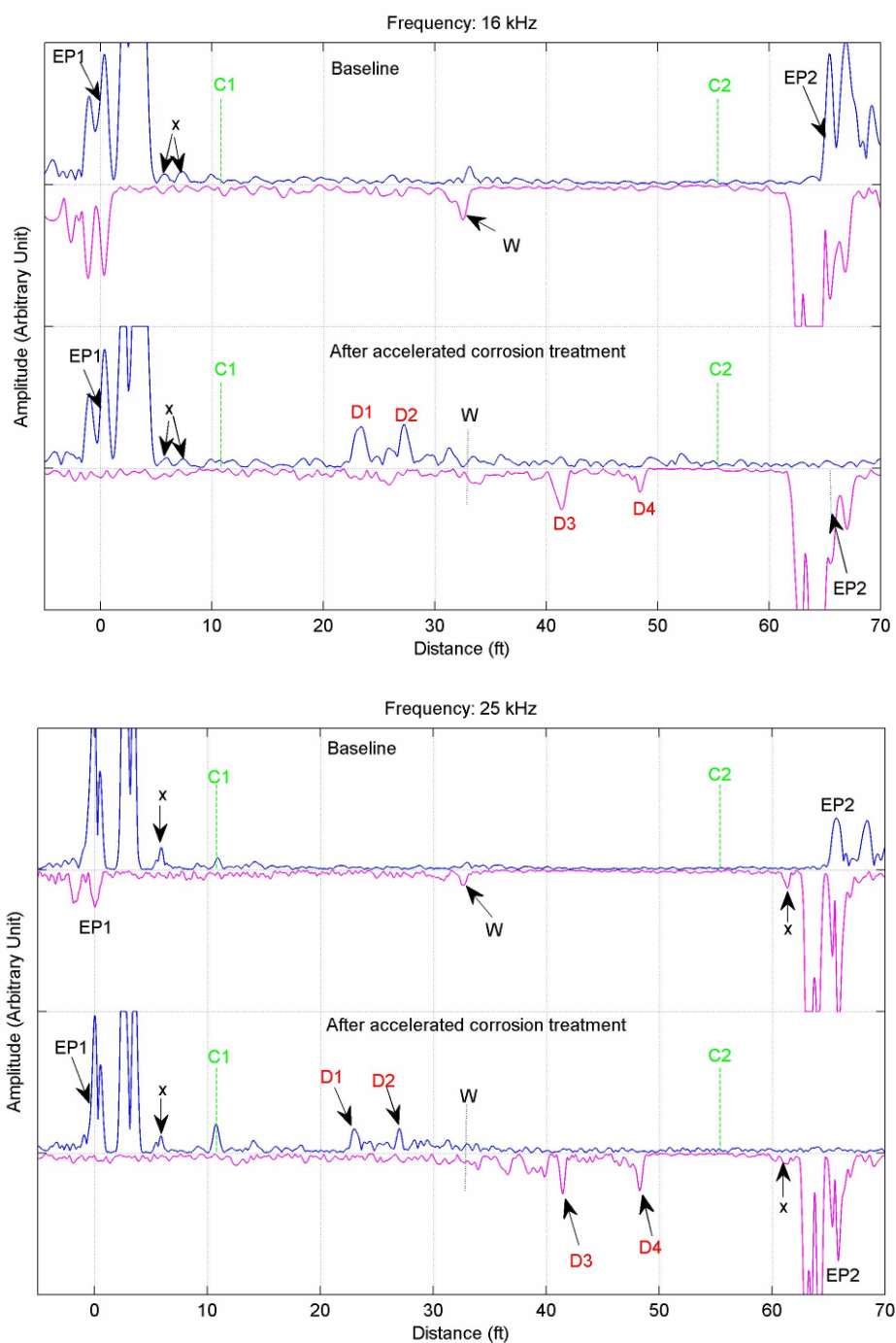


Figure 42. 16-kHz (a) and 25-kHz (b) data from the 1<sup>st</sup> RG&E cased-line mockup: top – baseline data, bottom – data taken after the accelerated corrosion treatment. Blue line is for the data taken from the east end of the pipe (EP1). Pink line is for the data taken from the west end of the pipe (EP2). C1 and C2 are the casing ends.

Because of the high wave attenuation in the test pipe, relatively low wave frequencies (25 kHz and lower) were used for baseline measurements so that the signal from the far end (from the sensor location) could be detected as shown in the Figure 42 baseline data. The wave attenuation was measured to be about 0.2dB/ft at 16 kHz and 0.36 dB/ft at 25 kHz, approximately the same as the attenuation in TGF-3-coated pipe plotted in Figure 24. The signal from the weld was detectable in the baseline data, but its signal-to-noise (S/N) ratio was low (about 2 to 3) due to high-level background noise (caused by non-uniform field-applied wrap coating).

The SHM data taken after the accelerated corrosion treatments were drastically different from the baseline data. In spite of the cold temperature on that day, which lowers the wave attenuation in a coated pipe, the wave attenuation was much higher than before. As a result, neither the far end signal nor the weld signal was detectable, indicating that a severe general corrosion had occurred along the pipe (several local corrosion pits would not lead to the loss of signal from the far end). In addition, there were large, local defect indications (D1 through D4) that were absent in the baseline data. Judging from the defect signal amplitudes and the lack of weld signal (which corresponds to about a 5% defect in these low frequencies), all defects were large – greater than 10 to 20%. Because of the large defect size and difficulty in determining wave attenuation, no attempts were made to characterize the defects.

After the SHM measurements, RG&E staff members pulled the test pipe out of the casing and observed the defects induced in the test pipe. The four defects were large rectangular-shaped through-holes with circumferential CSA ranging from 21 to 42% of the total pipe-wall cross-section and about 3 to 6 inches in axial length. Photos of these large defects are shown in Figure 43 along with a photo of 2.8% CSA defect induced around the weld location; the latter defect was not clearly detectable from the SHM data because of the poor S/N ratio.



Figure 43. Photos of defects induced in the 1<sup>st</sup> RG&E test pipe: large defects (left two) and 2.8% CSA defect around the weld location (right)

Overall findings from the 1<sup>st</sup> test include:

- (1) The large changes induced in the pipe were readily detectable. However, the defects were too large for evaluating SHM capability (this prompted the 2<sup>nd</sup> mockup testing).
- (2) The wave attenuation in the PE and the field-wrapped coal-tar-tape-coated pipe was similar to the wave attenuation in TGF-3-coated pipe.
- (3) The field-wrapped coal-tar-tape coating is uneven and, thus, produces relatively large background noise (about 2% reflection level).

- (4) General corrosion increases the wave attenuation significantly. This means that the attenuation level can be used to determine the degree of general corrosion (and not the detection of localized corrosion wall loss areas). The

### 7.2.3 Results and Findings from 2<sup>nd</sup> Test Mockup

#### (i) Baseline test results

Figures 44 and 45 show the baseline data acquired from the 2<sup>nd</sup> test pipe at 32 and 16 kHz, respectively. Because the test pipe in the cased section was FBE-coated, the wave attenuation was low (approximately 0.09 dB/ft at 32 kHz and 0.07 dB/ft at 16 kHz; this was higher than the FBE-coated pipe plotted in Figure 24 because the instrumented sections of the test pipe that were cut from the 1<sup>st</sup> test pipe were more attenuative) and, consequently, the data were clean with low background noise level (equivalent to approximately 0.4% reflection or 0.4% CSA relative to the total pipewall cross-section). In the 32-kHz data, there were seven (7) defect indications (designated as d1 through d7) and their distances from the east end of the pipe were respectively 11.3, 14.4, 20.4, 27.4, 32.2, 37, and 40 ft. The defect indications were equivalent to approximately 0.8% CSA. Since the indications were small, they were harder to find in the 16-kHz data (wavelength at this frequency, 8-inch, was too long to detect small defects). Signals labeled as X in the figures are those caused by imperfections in direction control or multiple reflections.

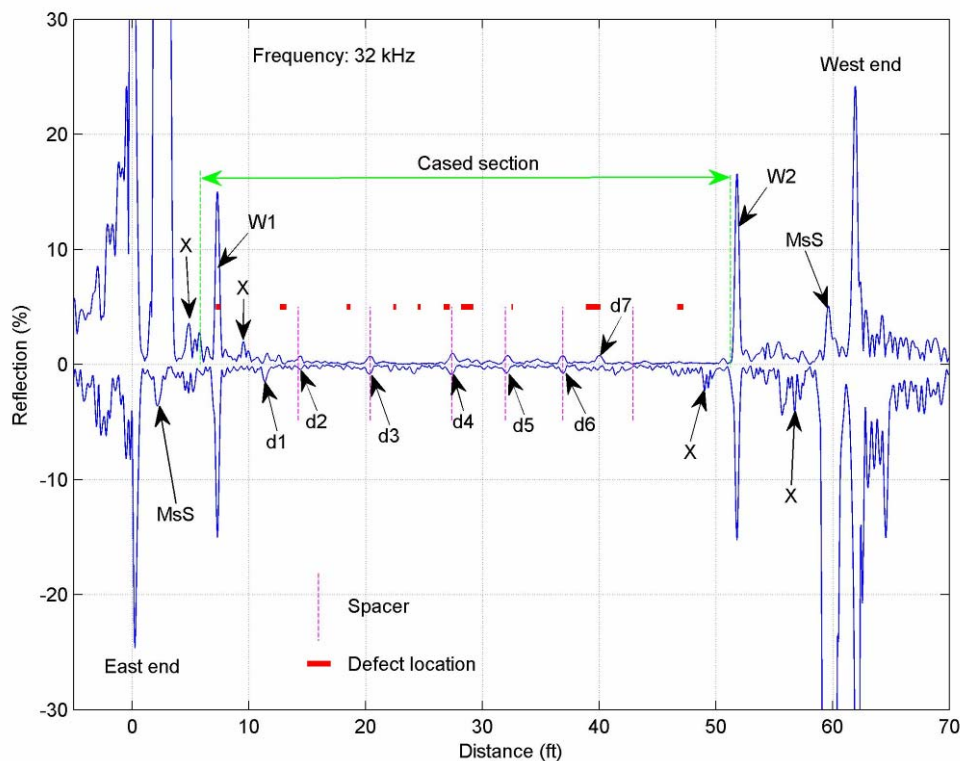


Figure 44. 32 kHz baseline data from the 2<sup>nd</sup> RG&E test pipe

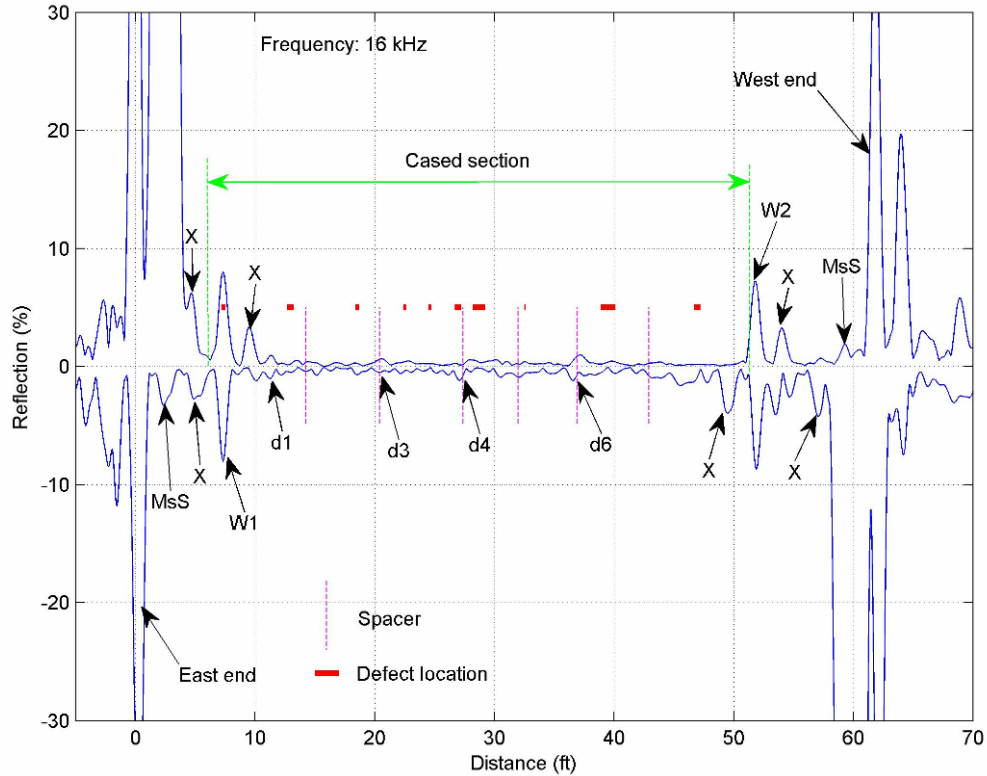


Figure 45. 16 kHz baseline data from the 2<sup>nd</sup> RG&E test pipe

Casing spacers are several inches wide. Therefore, if they produce detectable signals, the signals at 32 kHz are generally double-peaked due to the separation of the signals reflected from the front and rear ends of the spacer. All indications found in the 32-kHz data were single-peaked and thus were thought to be from locations where the coating was removed to produce corrosion defects. However, based on the detailed technical information provided by RG&E after the completion of SHM testing and data analyses, 5 out of 7 indications turned out to be from the casing spacers. For reference, casing spacer locations are indicated as dotted vertical lines and the locations of coating removal area for defect placements as bold red dots in Figures 44 and 45 (here, the length of the red dots corresponds to the length of the coating removal areas). It was noted that all spacers, except the one closest to the west end, produced detectable signals. The coating removal areas did not produce detectable signals, except perhaps at d4 and d7 locations and between d1 and d2. It is also unclear what caused the d1 signal.

(ii) 1<sup>st</sup> SHM test results

Figures 46 and 47 show the 1<sup>st</sup> SHM data acquired from the 2<sup>nd</sup> test pipe at 32 and 16 kHz, respectively. Because of the general corrosion induced in the test pipe, the wave attenuation was higher than before. Using the two weld signals as reference, it was determined that the attenuation was increased to about 0.24 dB/ft from 0.09 dB/ft at 32 kHz and to about 0.19 dB/ft from 0.07 dB/ft at 16 kHz. In addition, there were 8 defect signals. The majority of the 32-kHz defect signals (for example, d1, d4, d5, d7, and d8) were double-peaked, indicating that the defect length was sufficiently long to separate the signals reflected from the front and the rear end of the defect, as discussed in Section 3.3.2. For comparison, the actual defect locations are also indicated as bold red dots in these figures.

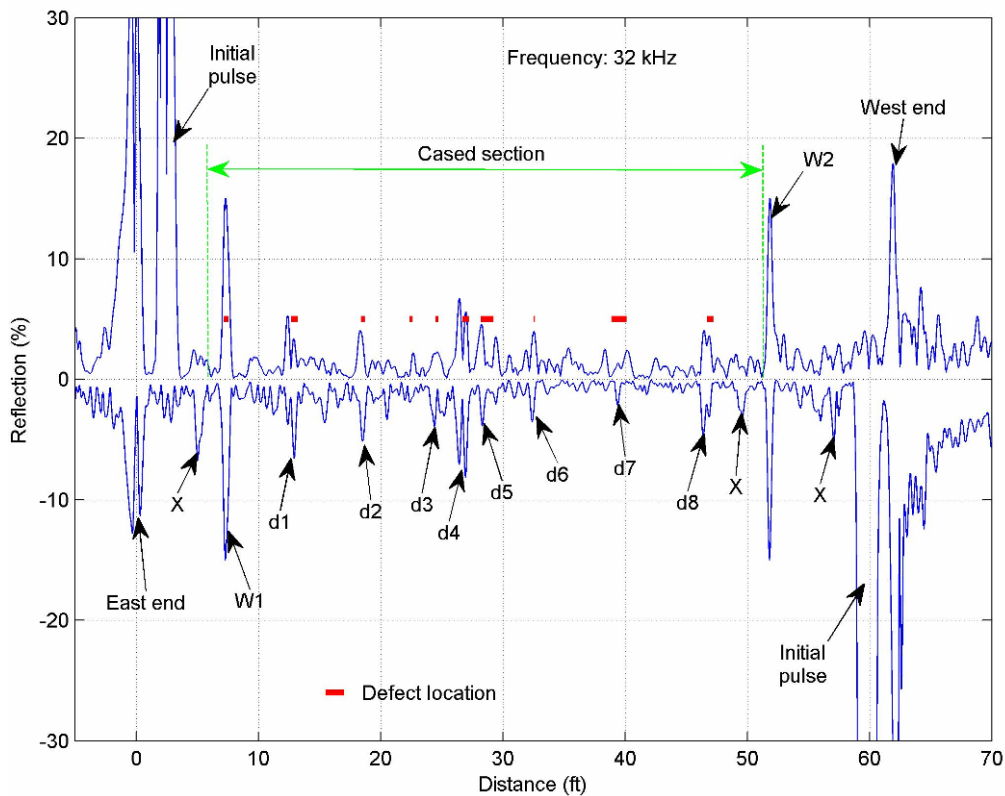


Figure 46. 1<sup>st</sup> SHM data at 32 kHz from the 2<sup>nd</sup> RG&E test pipe

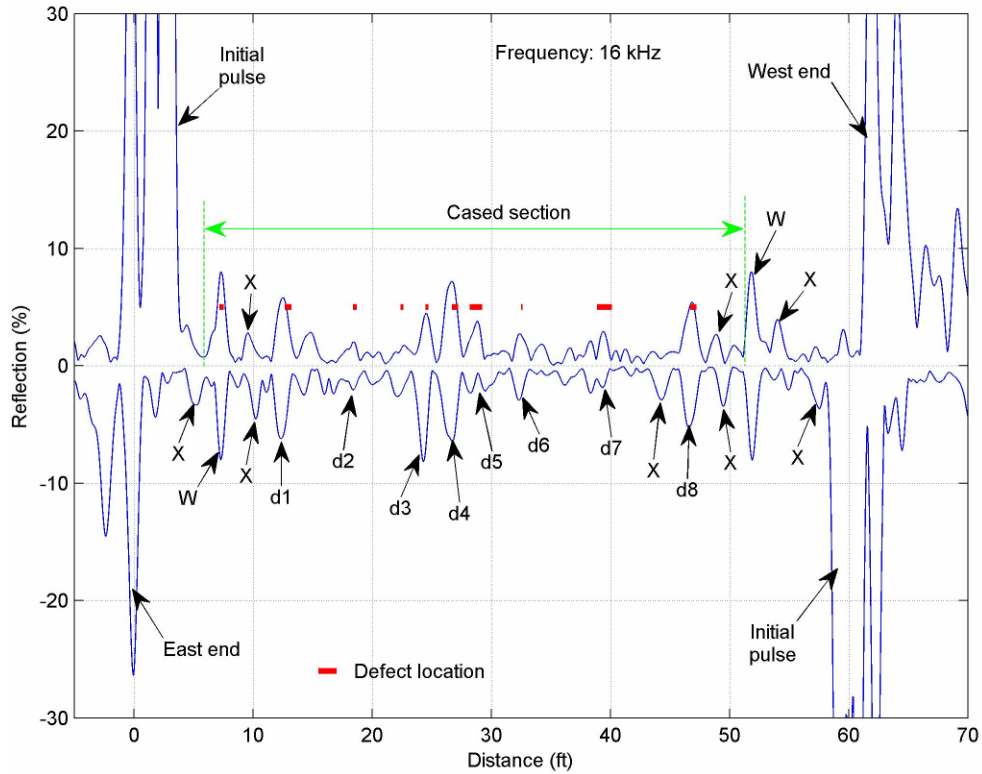


Figure 47. 1<sup>st</sup> SHM data at 16 kHz from the 2<sup>nd</sup> RG&E test pipe

The difference between the baseline and the 1<sup>st</sup> SHM data is plotted in Figure 48 for 32 kHz and Figure 49 for 16 kHz. Because the changes were large, the defect signals in Figures 48 and 49 were about the same as those in Figures 46 and 47. In the difference data, there were substantial weld and end signals. Reasons why the weld and end signals changed include the waveform change due to attenuation increase, energy loss at the induced defects, interference from multiple reflected signals, and condition changes at the end (with and without the end cap shown in the photos at the bottom of Figure 41). Therefore, it was difficult to positively determine whether a defect was formed at or near the weld, particularly because the results of the 32- and 16-kHz test data were inconsistent with each other. In the subsequent data analyses, the welds were assumed to be defect-free and their signals were used as the calibration reference.

Table 6 lists the defect axial locations, axial length, shape, and CSA determined from the 1<sup>st</sup> SHM data. As will be discussed later in subsection (iv), the east-side weld area (W1) in fact contained a large defect (with approximately 31% CSA). The assumption employed in the analysis therefore underestimates the defect CSA.

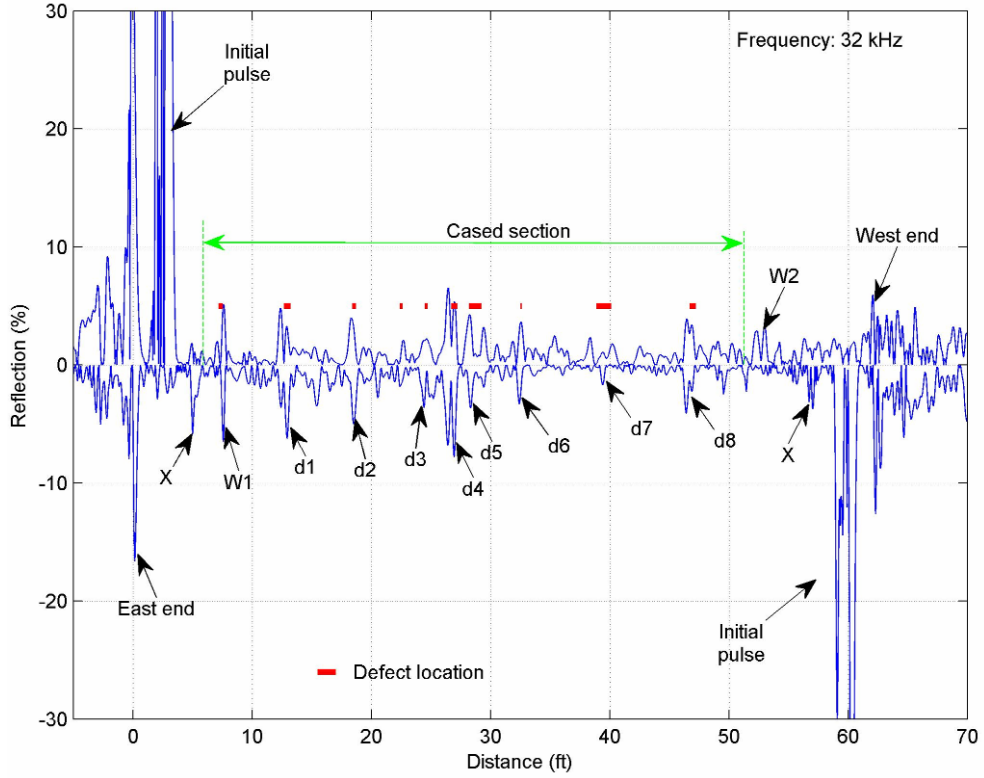


Figure 48. Difference between the baseline and the 1<sup>st</sup> SHM data at 32 kHz

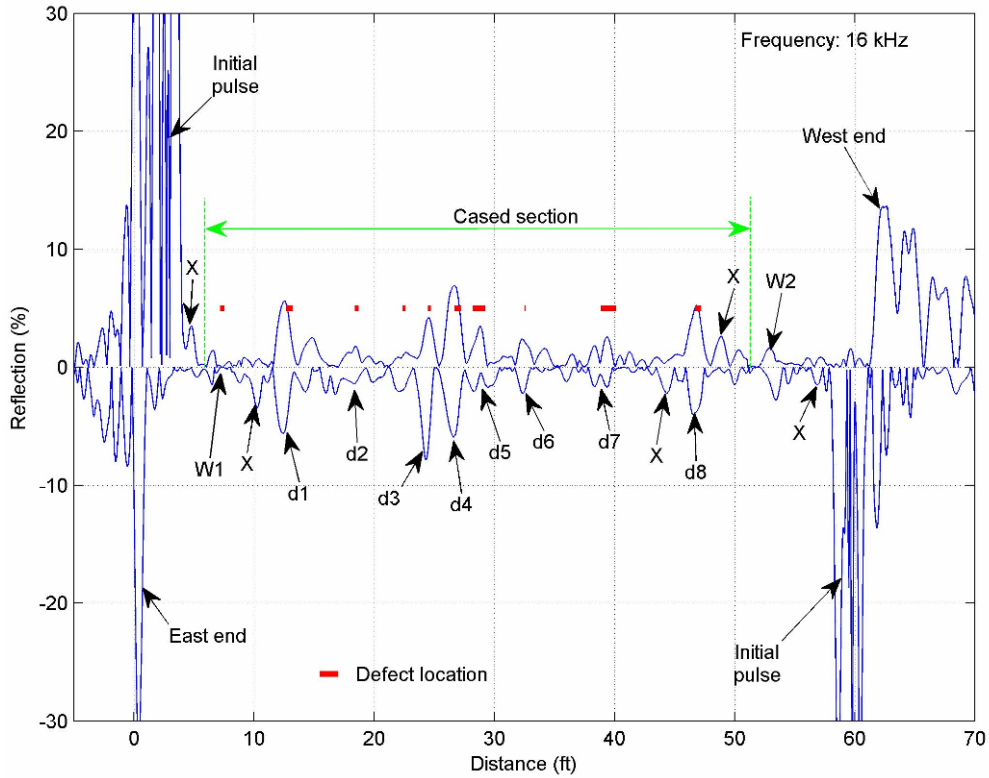


Figure 49. Difference between the baseline and the 1<sup>st</sup> SHM data at 16 kHz

**Table 6. Axial Locations and Characteristics of Defects Detected from the 1<sup>st</sup> SHM Data**

Defect		d1	d2	d3	d4	d5	d6	d7	d8
Location* (ft)		12.6	18.5	25.5	26.6	28.5	32.4	39.1	46.6
Length (inch)	A	7	N/A	7	6	13	7	12.5	5
	B	8-10	2-3	4-6	6-8	6-8	4-6	12-14	4-6
Shape	B	Trap.							
CSA (%)	C	6	4.5	4.5	7	3.5	3	2	4
	B	6-8	4-6	6-8	6-8	4-6	2-4	4-6	6-8

- \* – Measured from the east end of the test pipe to the center of the defect  
A – Determined from the separation between the two peaks in the 32-kHz signal  
B – Results of defect classifier algorithms (primarily based on the 16-kHz signal)  
C – Based on the average signal % reflection

*(iii) 2<sup>nd</sup> SHM test results*

Figures 50 and 51 show the 2<sup>nd</sup> SHM data acquired from the 2<sup>nd</sup> test pipe at 32 and 16 kHz, respectively. Compared to the 1<sup>st</sup> SHM data, the 2<sup>nd</sup> SHM data exhibited two different properties. The first difference was that the overall wave attenuation was significantly higher, evidenced by the fact that the far-end signal was not detectable at 32 kHz and may be barely noticeable at 16 kHz. The high attenuation indicated that the degree of general corrosion induced in the test pipe was substantially higher than at the time of the 1<sup>st</sup> SHM measurements. The second difference was that the test range of the east-side MsS was about 4 times shorter than that of the west-side MsS, indicating that the section of the pipe between the locations of d1 and d4 was more heavily corroded (and thus more attenuative) than the other sections of the pipe.

To determine the amount of the changes in defect size that occurred since the time of the 1<sup>st</sup> SHM measurements requires knowledge of attenuation values and how they vary along the pipe so that the attenuation effects on the signal amplitude could be corrected for. Since the required knowledge was lacking, the correction was made approximately by (1) dividing the pipe into two sections – section 1 from W1 to d4 and section 2 from d4 to W2, and (2) assuming that the attenuation change in section 2 is negligible and that the overall increase in wave attenuation in the 2<sup>nd</sup> SHM data is due to the attenuation in section 1. With the above approximation, the attenuation in section 1 was determined to be about 0.64 dB/ft (increased from 0.24 dB/ft at the time of the 1<sup>st</sup> SHM measurements) at 32 kHz and about 0.54 dB/ft (increased from 0.19 dB/ft at the time of the 1<sup>st</sup> SHM measurements) at 16 kHz.

The corrected 2<sup>nd</sup> SHM data (in blue) are plotted along with the 1<sup>st</sup> SHM data (in red) in Figure 52 for 32 kHz and in Figure 53 for 16 kHz. Defect 2 was not detectable in the 2<sup>nd</sup> SHM data. In general, the CSA of all other defects appeared to be doubled since the 1<sup>st</sup> SHM measurements. The defect characteristics determined from the 2<sup>nd</sup> SHM measurements are listed in Table 7. In the analyses, the weld signals were used again as calibration references. Since the W1 area contained a large defect (at this time, approximately 51% CSA), the CSA of d1 was significantly underestimated as discussed in the next subsection.

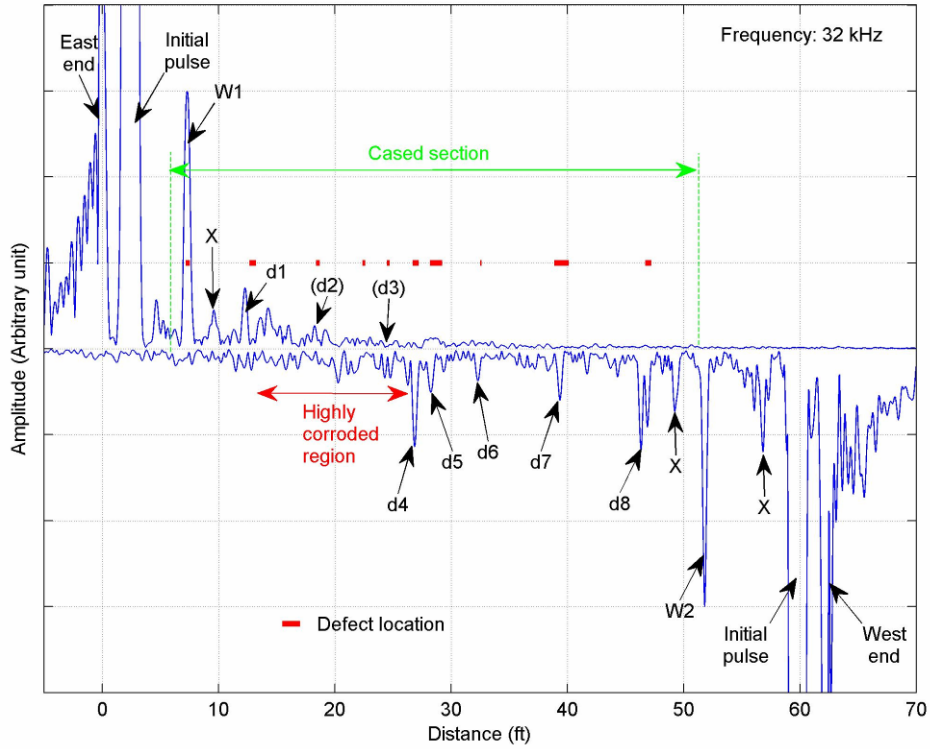


Figure 50. 2<sup>nd</sup> SHM data at 32 kHz from the 2<sup>nd</sup> RG&E test pipe

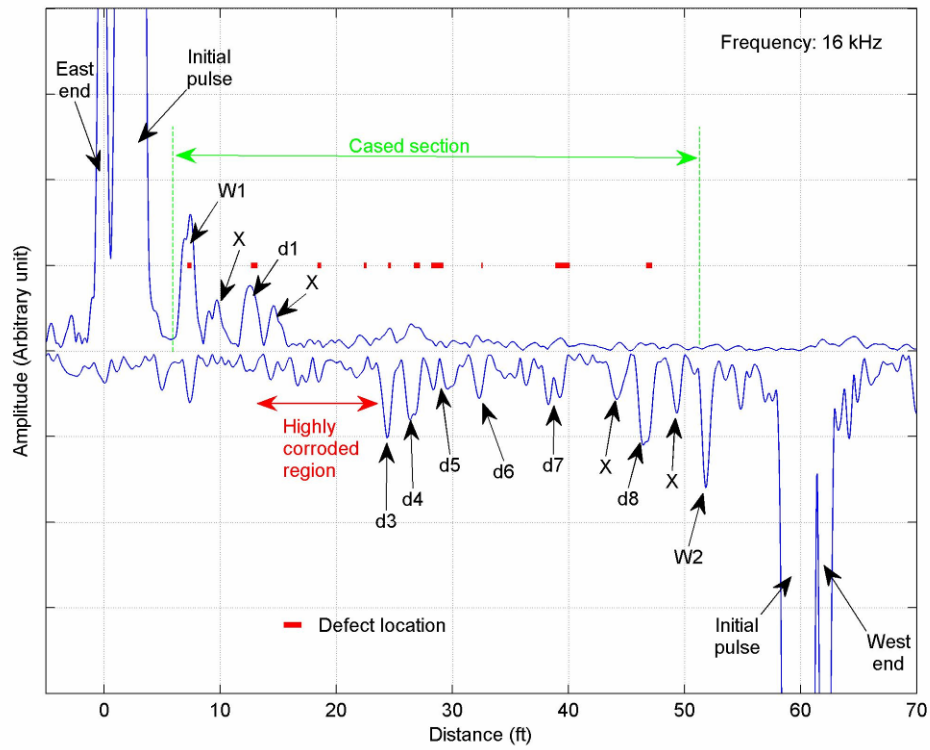


Figure 51. 2<sup>nd</sup> SHM data at 16 kHz from the 2<sup>nd</sup> RG&E test pipe

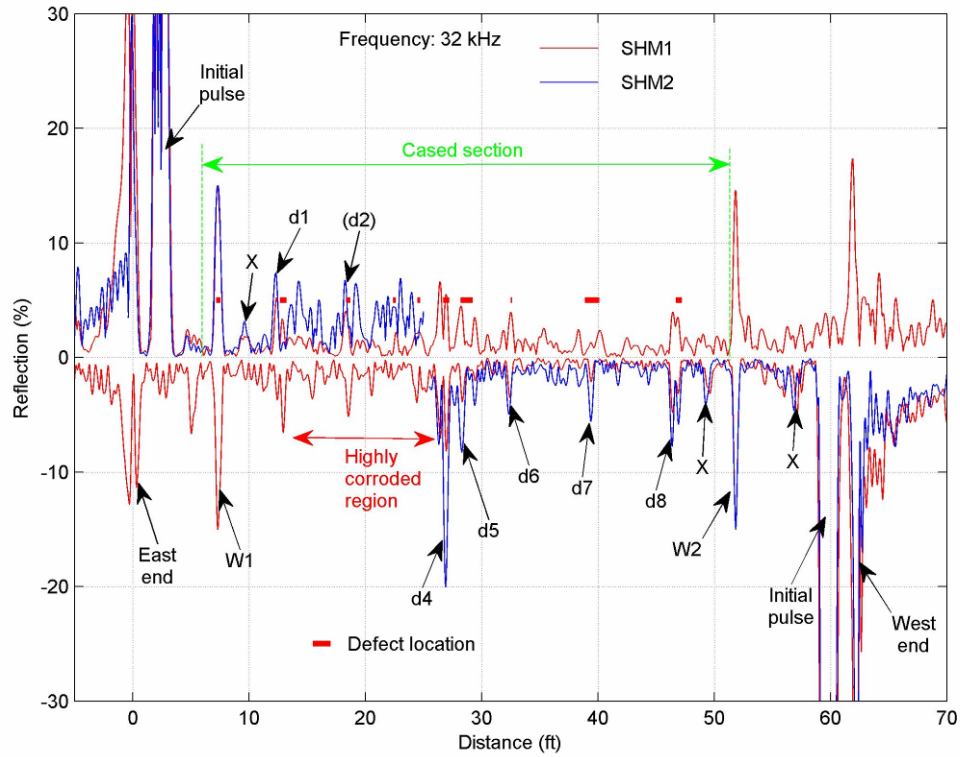


Figure 52. Comparison between the 1<sup>st</sup> and 2<sup>nd</sup> SHM data at 32 kHz

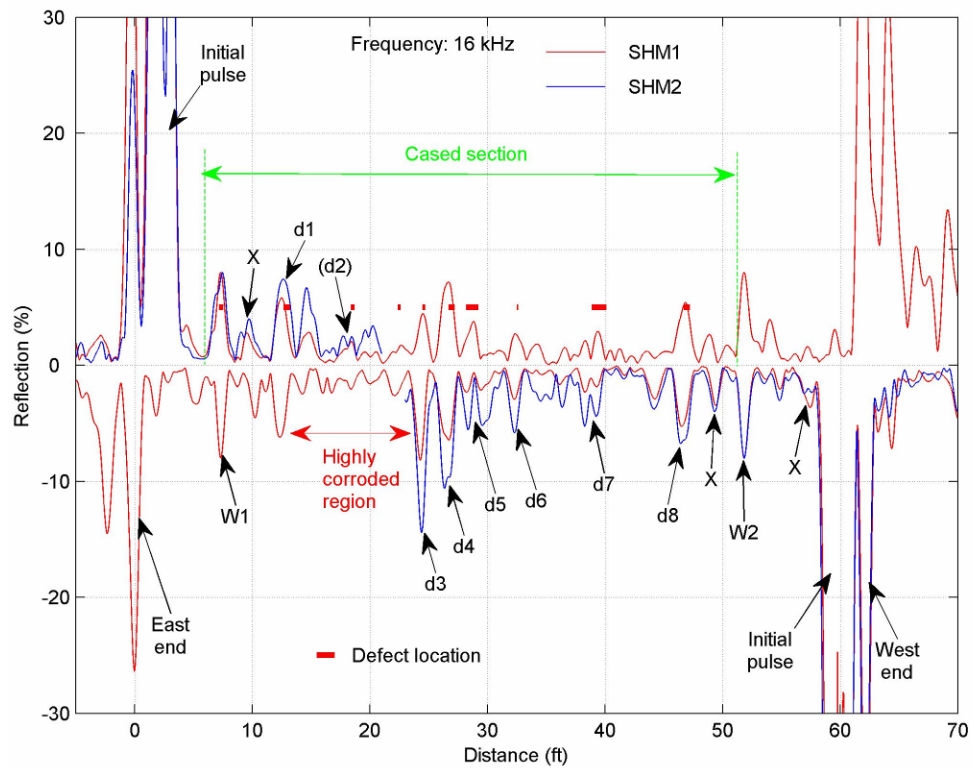


Figure 53. Comparison between the 1<sup>st</sup> and 2<sup>nd</sup> SHM data at 16 kHz

**Table 7. Characteristics of Defects Detected from the 2<sup>nd</sup> SHM Data**

Defect		d1	d2	d3	d4	d5	d6	d7	d8
Location* (ft)		12.5	N/A	24.4	26.6	28.5	32.3	39.1	46.4
Length (inch)	A	N/A	N/A	N/A	8	N/A	N/A	N/A	8
	B	8-10	N/A	6-8	6-8	6-8	6-8	14-16	6-8
Shape	B	Trap.	N/A	Trap.	Trap.	Trap.	Trap.	Trap.	Trap.
CSA (%)	C	8	N/A	15	15	6.5	6	5	7.5
	B	6-8	N/A	O/R	O/R	6-8	6-8	6-8	6-8

\* – Measured from the east end of the test pipe to the center of the defect

A – Determined from the separation between the two peaks in the 32-kHz signal

B – Results of defect classifier algorithms (primarily based on the 16-kHz signal); O/R –over the range of the classifier algorithm (this means CSA  $\geq$  10%)

C – Based on the average signal % reflection

Note – The W1 (east-side weld) signal at 16 kHz showed a change, suggesting a possible defect in the vicinity.

It should be stressed here that, *without the 1<sup>st</sup> SHM data, the interpretation of the 2<sup>nd</sup> SHM data would have been very difficult and, thus, subject to a much greater error.* The data from the 2<sup>nd</sup> RG&E test pipe, therefore, are a good example that shows the advantages of SHM over one-time inspection.

(iv) *Comparison with the actual defects induced in the test pipe*

Based on the information provided by RG&E, actual locations and sizes of defects induced in the test pipe are listed in Table 8. Except for the full-circumferential defect in the east-side weld (W1) area (RG&E defect ID No.1), all other defects were square or rectangular in shape. Photos of some defects that were taken after the 2<sup>nd</sup> SHM test are shown in Figure 54.

**Table 8. Actual Locations and Sizes of Defects Induced in the Test Pipe**

SHM defect No.	RG&E defect ID No.	Axial Location (a)	Clock position (b)	Circ. width	Axial length	At the time of 1 <sup>st</sup> SHM test		At the time of 2 <sup>nd</sup> SHM test	
						depth	CSA	depth	CSA
N.C (c)	1	7.3 ft	—	14” (full)	4”	0.071”	31.3%	0.116”	51.2%
d1	12	12.7	9:00	6	6	0.080	15.1	0.134	25.4
d2	11	18.4	6:00	3	3	0.087	8.2	0.177	16.7
N.C (c)	10	22.4	6:00	1	1	0.101	3.2	0.213	6.7
	13	22.6	9:00	2	2	0.108	6.8	0.176	11.1
d3	14	24.5	9:00	2	2	0.117	7.3	0.170	10.7
d4	5	26.7	3:00	6	6	0.083	15.7	0.101	19.1
d5	6	28.3	3:00	1	1	0.126	4.0	0.186	5.9
	15	28.9	9:00	1	12	0.090	2.8	0.151	4.8

d6	7	32.5	3:00	1	1	0.093	2.9	0.166	5.2
d7	3	38.9	12:00	1	12	0.065	2.0	0.102	3.2
	9	38.9	6:00	1	12	0.074	2.3	0.127	4.0
d8	2	46.7	12:00	1	6	0.049	1.6	0.094	3.0
	8	46.7	3:00	1	6	0.098	3.1	0.098	3.1
	16	46.7	9:00	1	6	0.098	3.1	0.144	4.5

- (a) Measured from the east end of the test pipe to the center of the defect
- (b) Position around the pipe circumference
- (c) Not called during the data analyses



Figure 54. Photos of defects induced in the 2nd RG&E Test Pipe: RG&E defect ID Nos. 1, 7, 8 (top row from left to right) and 11, 12, 15 (bottom row from left to right)

A total of 15 defects were induced in the test pipe. In guided-wave testing, multiple defects at approximately the same axial location produce one signal. Therefore, defects at approximately the same axial location are grouped together in Table 8 (for example, the d5 signal in the SHM data was produced by RG&E defects 6 and 15; the d8 signal by RG&E defects 2, 8 and 16). This made a total of 10 defects along the length of the cased section of the test pipe.

Out of 10 defects, 8 were positively identified from the SHM data. Indications for the two other defects (RG&E defect 1 in the east-side weld area and RG&E defects 10 and 13 at approximately 22.5-ft location) were present in the SHM data; but because of the uncertainty, they were not called during the data analyses. Importantly, there were no false calls made from the data analyses.

Table 9 shows a comparison between the actual defect length and CSA and those determined from the SHM data.

**Table 9. Comparison between Actual Defect Length and CSA and Those Determined from the SHM Data**

SHM defect No.	At the time of 1 <sup>st</sup> SHM Test						At the time of 2 <sup>nd</sup> SHM Test					
	Axial Length (inch)			CSA(%)			Axial Length (inch)			CSA (%)		
	Act. <sup>(a)</sup>	A	B	Act. <sup>(b)</sup>	C	B	Act. <sup>(a)</sup>	A	B	Act. <sup>(b)</sup>	C	B
d1	6	7	8-10	15.1	6	6-8	6	--	8-10	25.4	8	6-8
d2	3	--	2-3	8.2	4.5	4-6	3	--	--	16.7	--	--
d3	2	7	4-6	7.3	4.5	6-8	2	--	6-8	10.7	15	≥10
d4	6	6	6-8	15.7	7	6-8	6	8	6-8	19.1	15	≥10
d5	12	13	6-8	6.8	3.5	4-6	12	--	6-8	10.7	6.5	6-8
d6	1	7	4-6	2.9	3	2-4	1	--	6-8	5.2	6	6-8
d7	12	12.5	12-14	4.3	2	4-6	12	--	14-16	7.2	5	6-8
d8	6	5	4-6	7.8	4	6-8	6	8	6-8	10.6	7.5	6-8

- (a) For multiple defects in the same location, it represents the longest length  
(b) For multiple defects in the same location, it represents the sum of all defects  
A Determined from the separation between the two peaks in the 32-kHz signal  
B Results of defect classifier algorithms (primarily based on the 16-kHz signal)  
C Based on the average signal % reflection

As mentioned in the previous subsections, W1 and W2 signals in the data were used as calibration reference for data analyses. Since a large defect (RG&E defect 1 in Table 8) was present in the W1 area, the above data analysis procedure led to an underestimation of defect CSA – particularly for the defect closest to W1 (namely, d1) and for the defects that were detected from the east-side MsS. Otherwise, defect CSAs determined using the classifier algorithm (column B in table 9) was in fair agreement with the actual CSAs. It is now clear that the cause for the short test range of the east-side MsS in the 2<sup>nd</sup> SHM data was the presence of the large defect in the W1 area (51% CSA) and d1 (25% CSA) and not the high corrosion area between d1 and d4 (a misinterpretation of the data that resulted from the use of the W1 signal as a reference).

Regarding the axial length of defects, the values determined using the classifier algorithm (column B in table 9) were in good agreement with the actual lengths except for the short defects (d3 and d6). The axial length of a short defect is harder to determine because the base of the envelope (see Section 4), the primary parameter related to the defect length, changes little until the length becomes comparable to the wavelength (8 inches at 16 kHz).

(v) *Overall findings and lessons learned*

Overall findings from the 2<sup>nd</sup> test include:

- (1) The accelerated corrosion defects were readily detectable from the 1<sup>st</sup> SHM data, indicating that the defect growth could be accurately tracked using the SHM approach during the early stages of degradation (for defects up to 10% CSA and until the attenuation caused by the general corrosion limits the detection accuracy).
- (2) Within the known limitations, the classifier algorithms worked reasonably well.

- (3) The test results further confirmed the existence of good correlation between the wave attenuation and the degree of general corrosion. Establishing quantitative correlation between the two would be very useful for DA applications. To relate the attenuation with the degree of corrosion in coated lines, the portion of attenuation that was caused by the coating itself needs to be separately accounted for. Therefore, collecting attenuation data on various types of coated pipe and their dependence on temperature would be very useful.
- (4) Since the weld signals are used as references in the data analyses, the presence of a large defect in the weld area led to substantial error in data interpretation. To minimize the error and to be able to positively detect a defect formation and growth in the weld area, more reliable calibration methods and procedures are necessary.
- (5) The MsS probes performed well throughout the whole testing process (that involved mechanical handling when the test pipe was pulled out of the casing for visual confirmation of induced defects, cutting from the 1<sup>st</sup> test pipe, and welding to the 2<sup>nd</sup> test pipe) and the incrementally cold winter weather at Rochester, indicating the probe's long-term durability and reliability in field conditions.

## 8. INVESTIGATIONS OF GUIDED-WAVE ATTENUATION CHANGES WITH COATED PIPE TEMPERATURE AND GENERAL CORROSION

From the results of field testing and the testing at the NYSEARCH/NGA test bed facility, it was observed that (a) the general corrosion significantly increases the guided-wave attenuation, (b) the attenuation in coated pipes increases with pipe temperature, and (c) if the attenuation caused by coating is properly accounted for, attenuation measurements may be used to assess the general corrosion state of pipeline and presence of corrosion activity for DA use.

To evaluate the capability of assessing corrosion state from attenuation measurements, the extent of attenuation changes with temperature in coated pipes and general corrosion was investigated experimentally. This section describes the experimental arrangements used for the investigation, procedures used to determine wave attenuation, and the results.

### 8.1 Experimental Arrangements

#### 8.1.1 Temperature dependence of attenuation in coated pipes

For use in the investigation of the dependence on the coating type and temperature, the following three coating type were selected – coal tar (more specifically TGF-3), coal tar epoxy, and polyethylene (more specifically PRITEC®). All three coating types are widely used in the industries. The test pipes at the NYSEARCH/NGA test bed facility had TGF-3 and coal tar epoxy coating as well as bare steel. The first cased line mockup at the RG&E facility in Rochester, NY, had PRITEC® coating.

For each coating type, a 10-ft-long, 6-5/8-inch OD and 0.28-inch wall pipe sample was acquired. On each sample, MsS probes were installed near one end. All three samples were then placed in a large environmental chamber as shown in Figure 55 photos.



Figure 55. Environmental chamber (left) and three coated pipe samples (middle and right)

The temperature was cycled over a range from 0 to 120° F and MsS data (that showed several end reflected signals for attenuation measurements) was acquired at every 10° F increment at six different frequencies (10 to 60 kHz at every 10 kHz interval).

### 8.1.2 Effects of general corrosion on attenuation

For the investigation of general corrosion effects on the wave attenuation, two 10.3-ft-long, 6-5/8-inch OD and 0.28-inch wall, bare carbon steel (CS) pipe samples were acquired. Each sample was placed in a 10.5-inch OD PVP pipe with approximately 4-inch section of one end exposed for MsS as shown in Figure 56 (left photo). To encourage uniform corrosion, the pipe sample was sandblasted before placing it in the PVC pipe.



Figure 56. Photos of experimental setup for investigation of corrosion effects on guided-wave attenuation; samples placed in PVC pipes (left) and with the PVC pipe filled with sand (right)

The initial plan for inducing general corrosion on the pipe OD surface involved embedding the pipe samples in sand by filling the PVC pipe with fine sand and then keeping the sand saturated with simulated seawater. Baseline MsS measurements on the pipe samples embedded in sand (right photo in Figure 56) showed that the surrounding sand causes a large increase in wave attenuation (from approximately 0.02 dB/ft at 10-kHz to 0.05 dB/ft at 140-kHz in air to 0.24 to 0.27 dB/ft with dry sand, and then to 0.80 to 0.83 dB/ft with saturated sand). Because accurate measurements of additional attenuation caused by general corrosion (which is expected to be small in the early stages of corrosion) in the presence of the large attenuation caused by the saturated sand are very difficult, the initial plan was abandoned.

Subsequently, a revised plan was developed that involved inducing general corrosion in simulated seawater solution with impressed electric current to accelerate corrosion. To implement the above, the sand was removed and three stainless steel tubes (1.25-inch OD) were attached to the inside surface of the PVC pipe, spaced at 120° apart around the pipe along the entire length of the PVC pipe. The PVC pipe was then filled with simulated seawater and anodic potentials were applied between the pipe sample and the stainless steel rods surrounding the sample. To help the resulting corrosion oxides remain attached to the pipe sample surface and the sample was wrapped with a fiberglass mesh. Figure 57 shows photos of the final experimental setup used for the investigation.

Baseline MsS measurements (made on November 17, 2008), confirmed that the water surrounding the pipe sample has no effects on the wave attenuation. While subjecting the pipe samples to impressed electric current, MsS data were acquired periodically (from 10- to 140-kHz at every 10-kHz interval). Final periodic measurements were made on February 9, 2009. Further details on the measurements are given in section 8.3.2.



Figure 57. Photos of present experimental setup; PVC pipe filled with simulated seawater (left), power supply used to impress the electric current (middle), and fiberglass mesh wrapped around pipe sample (right)

## 8.2 Attenuation Measurement Procedures

When a wave (either ultrasonic wave or guided wave) propagates in an attenuative medium, its amplitude changes as a function of distance,  $x$ , per the following equation:

$$A(x) = A_0 e^{-\alpha x}$$

where  $A_0$  is the amplitude at  $x = 0$  and  $\alpha$  is the attenuation coefficient of the medium.

Therefore, when the amplitude of the wave is measured at various distances, they follow an exponentially decaying curve. The attenuation of the medium can then be experimentally determined by measuring the signal amplitude at various travelling distances and fitting the amplitudes to an exponentially decaying curve [16]. The multiple end-reflected signals acquired from the pipe samples therefore generally follow an exponentially decaying curve.

When the center frequency of the end-reflected signals was examined, it was found to be substantially different from the operating frequency of the MsS. When the attenuation is low, the center frequency was either higher or lower than the operating frequency. This is due to the fixed MsS position and interference between the incoming and outgoing waves reflecting from the sensor-end of pipe. Figure 58 illustrates the difference between the operating and measured center frequencies from the baseline data acquired from pipe samples shown in Figure 56 photo.

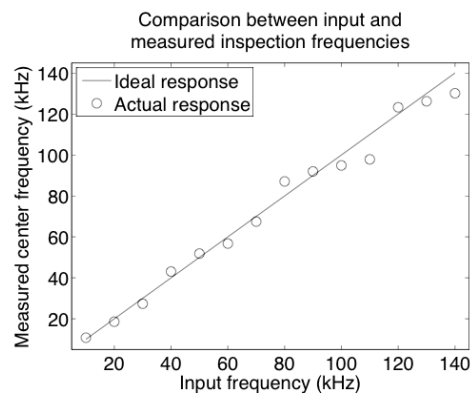


Figure 58. Comparison between the measured center frequency and the operating frequency of the MsS

Additionally, when the attenuation becomes high, the center frequency was generally lower than the operating frequency. The reason is that the wave pulse transmitted into the pipe contains a

range of frequencies (around its operating frequency) and, because attenuation is higher for higher frequency, the higher frequency components in the pulse decreases faster than the lower frequency components and, thus, lowering the center frequency of the end-reflected signals with travelling distance (frequency content shifts toward lower frequencies was also mentioned in comments 3 in Appendix B).

At first, the attenuation values were determined by band-pass filtering (centered on the operating frequency) the end-reflected signals and fitting the resulting signal amplitudes to an exponentially decaying curve. When the results were plotted as a function of corrosion level or temperature, the data showed a large variation particularly in high attenuation values indicating substantial errors in attenuation calculation. The primary reason for the error stems from the center frequency being substantially different from the operating frequency. For example, approximately 30% of the 207 MsS data taken periodically from corrosion investigations had greater than 5 kHz difference between the measured center frequency and the operating frequency. Band-pass filtering these signals near the operating frequencies led to very low signal amplitude and, thus, to substantial errors in attenuation calculation.

To reduce the attenuation measurement error, modified procedures were used in this investigation that involved:

1. Determine the center frequency,  $f_c$ , of the first end-reflected signal in each MsS data acquired
2. Design a minimum-order, narrow band-pass Butterworth filter centered on  $f_c$  with the following specifications:
  - a. No more than 3dB ripple in the pass-band.
  - b. At least 20 dB attenuation in stop-bands.
  - c. Pass-band region defined as  $f_{pass} \in \left(\frac{7}{8}f_c, \frac{9}{8}f_c\right)$ .
  - d. The two stop-band regions are defined as  $f_{stop}^1 \in \left(-\infty, \frac{3}{4}f_c\right)$  and  $f_{stop}^2 \in \left(\frac{5}{4}f_c, \infty\right)$ .
3. Zero-phase filter the MsS data
4. Create an envelope of the filtered end-reflected signals and least-square fit envelop peaks to an exponentially decaying curve and determine the attenuation value
5. Process all MsS data sets acquired (as a function of temperature or corrosion level) per the steps 1 through 4 and determine attenuation values
6. Plot the attenuation data in a 3-D (the 3 axes are attenuation, center frequency, and condition parameter which is either temperature or corrosion level) and create a smoothly varying surface that best fits all data points
7. Determine the attenuation values at discrete frequencies (e.g., 10, 20, 30, ... kHz) from the smoothed surface

Figure 59 shows an example of filter designed in step 2 and the filtered data in step 3. In this example, the original data were acquired by operating the MsS at 50 kHz and  $f_c$  of the first end-reflected signal in the original data was 45 kHz. The filtering process reduces the peak amplitudes of the end-reflected signals.

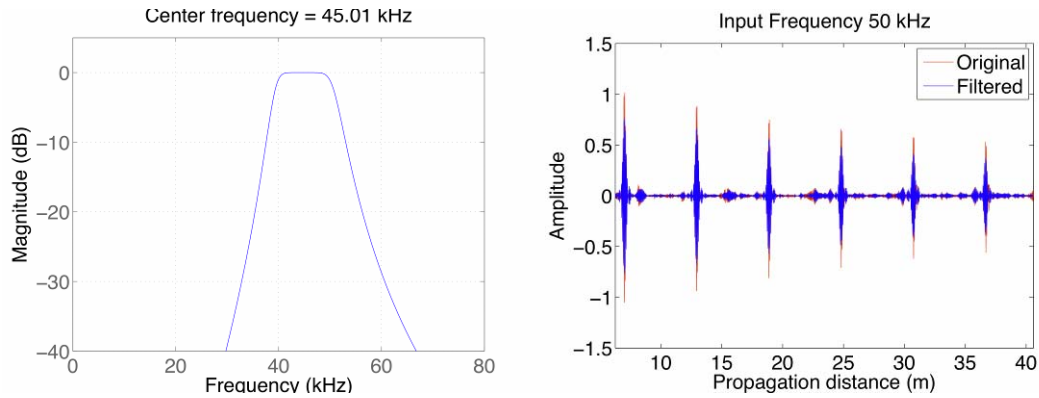


Figure 59. Example of the filter (left) and plots of original and filtered data (right) per procedure steps 2 and 3

Figure 60 shows an example of enveloping and least-square fitting of the envelop peaks to an exponentially decaying curve in step 4. In this example, the attenuation value was determined to be 0.065 dB/ft (0.214 dB/m).

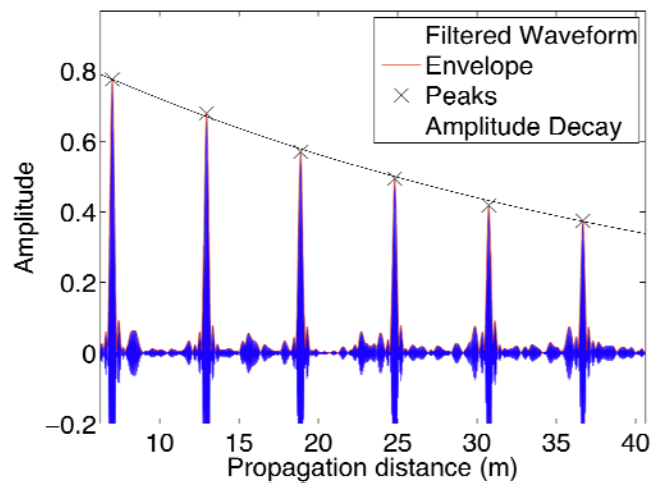


Figure 60. Example of enveloping and exponential curve fitting to envelop peaks per step 4

Figure 61 shows an example of a 3-D data plot and the smoothly varying surface that best fits all data points. The data points in this example were from periodic measurements made on one of the pipe samples subjected to accelerated corrosion treatments. The surface in this 3-D plot shows increasing attenuation with increasing frequency and corrosion treatment days.

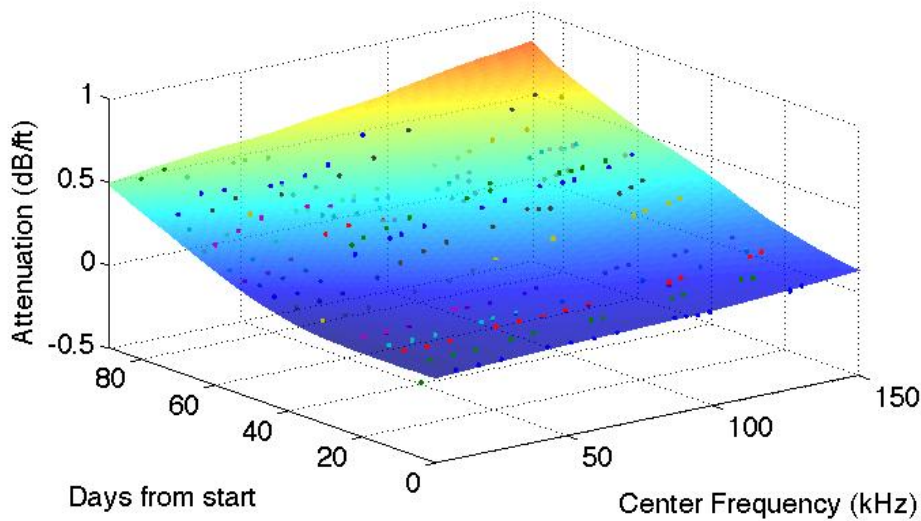


Figure 61. Example of a 3-D data plot and smoothly varying surface.

The approach used for determining the smoothly varying surface is to assume that the surface is piece-wise planar. In other words, a plane can approximate small rectangular regions of the frequency/condition (temperature or corrosion level) plane). The frequency / condition parameter plane is then divided into a large number of overlapping rectangular regions and least square regression is used to find the best plane to fit the data points. These planes are then averaged together and smoothed using a 3rd order moving average filter. Using the approximation given by the 3-D surface, the attenuation as a function of corrosion or temperature can be given for discrete inspection frequencies.

The attenuation values determined per the above procedures assume a uniform attenuation along the entire length of the pipe sample. For the sensor installation however, a small length (6 inch or so) of the pipe samples was uncoated at an end. Similarly, a small length of an end of bare pipe samples was on the outside of the corrosion environment. Since the changes in the attenuation were caused in the coated section or the section subjected to the corrosion environment (and not across the whole sample length), a correction was made to the attenuation values to account for the length difference.

### 8.3 Experimental Results

#### 8.3.1 Temperature dependence of wave attenuation in coated pipes

##### (i) Coal Tar Epoxy (CTE) Coating

The experimental results from the CTE coated pipe samples are plotted in Figure 62. The left plots show the surface that best fit the attenuation data measured at center frequencies. The right plots show the temperature dependence of attenuation at discrete frequencies (10 to 50 kHz) that was determined from the 3-D surface in the left plots. As shown, the attenuation increased with increasing frequency and temperature which is the typical behavior of wave attenuation.

The attenuation in the CTE coated pipe was low, only slightly higher than in bare pipes and almost identical to the attenuation in painted pipelines. Apparently the CTE coating, which is thin, acts like a thin paint coating on pipes. Further at a given frequency, the effect of temperature also produced a very small ( $<0.05$  dB/ft) attenuation change.

The low attenuation values and slight temperature effects indicates that pipelines with CTE coating would be benign to long-range guided-wave inspection and easiest to detect corrosion state from attenuation measurements.

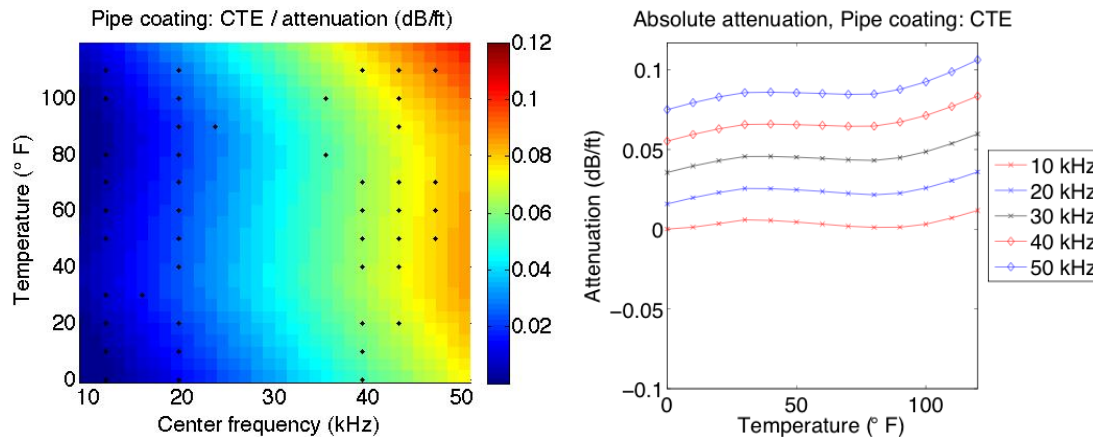


Figure 62. Experimental results from the coal tar epoxy (CTE) coated pipe sample. Left: attenuation surface as a function of frequency and temperature (data measured at the center frequencies shown as the black dots). Right: temperature dependence of attenuation at discrete frequencies.

### (ii) Polyethylene (PE) Coating

The experimental results from the PE (PRITEC®) coated pipe samples are plotted in Figure 63. The left plots show the surface that best fit the attenuation data measured at center frequencies. The right plots show the temperature dependence of attenuation at discrete frequencies (10 to 50 kHz) that was determined from the 3-D surface in the left plots. Unlike with the CTE coating, there were limited measurements for the high frequency / temperature cases ( $>90^{\circ}\text{F}$  for 40 kHz and  $>60^{\circ}\text{F}$  for 50 kHz). This implies that the absolute attenuation values in the left plot for this frequency / temperature region are extrapolated assuming the attenuation has the same growth trend. The absolute attenuation values are shown for this region as “dashed” lines to imply a lower degree of confidence.

The PE coated pipe also showed the typical behavior of attenuation; namely increase with increasing frequency and temperature. The attenuation values at room temperature (e.g.,  $70^{\circ}\text{F}$ ) ranged from 0.024 dB/ft at 10-kHz to 0.749 dB/ft at 50-kHz which are significantly higher than those in the CTE coated pipe. Also, the temperature has a large influence on the attenuation and the temperature effects were greater at higher frequencies.

Because of the large increase in attenuation with temperature, results of guided-wave inspection of PE coated pipelines would become increasingly poorer with increasing temperature. This means that significantly better results would be obtained if the inspection is conducted in cool

weather than in hot weather. Therefore, if practical, the guided wave inspection of PE coated pipelines should be conducted at the lowest temperatures possible.

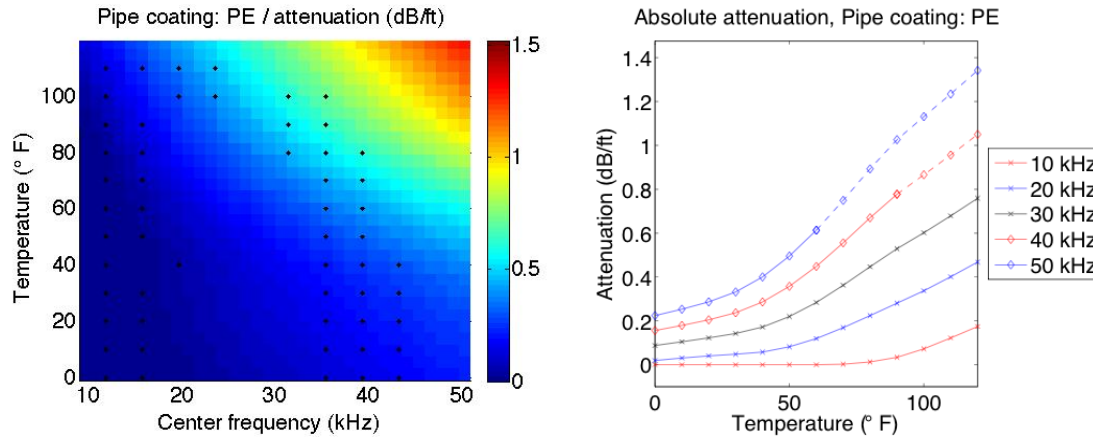


Figure 63. Experimental results from the polyethylene (PE; PRITEC®) coated pipe sample. Left: attenuation surface as a function of frequency and temperature (data measured at the center frequencies shown as the black dots). Right: temperature dependence of attenuation at discrete frequencies, where dashed lines represent the extrapolated approximations.

(iii) Coal Tar (TGF-3) Coating

The experimental results from the TGF-3 coated pipe samples are plotted in Figure 64. The left plots show the surface that best fit the attenuation data measured at center frequencies. The right plots show the temperature dependence of attenuation at discrete frequencies (10 to 50 kHz) that was determined from the 3-D surface in the left plots. As with the polyethylene coated pipe, there was limited information for the high frequency/temperature combinations, shown by the “dashed” lines.

The attenuation in the TGF-3 coated pipe also increased with increasing frequency and temperature. Of the three coating types investigated in this project, the TGF-3 coating was the most attenuative. Similarly to the PE coated pipe, the temperature has a large influence on the attenuation and the temperature effects were greater at higher frequencies. The degree of temperature effects in the TFG-3 coated pipe was about twice as much as that in the PE coated pipe. Thus, the consideration of temperature is doubly important for guided-wave inspection of TGF-3 coated pipelines.

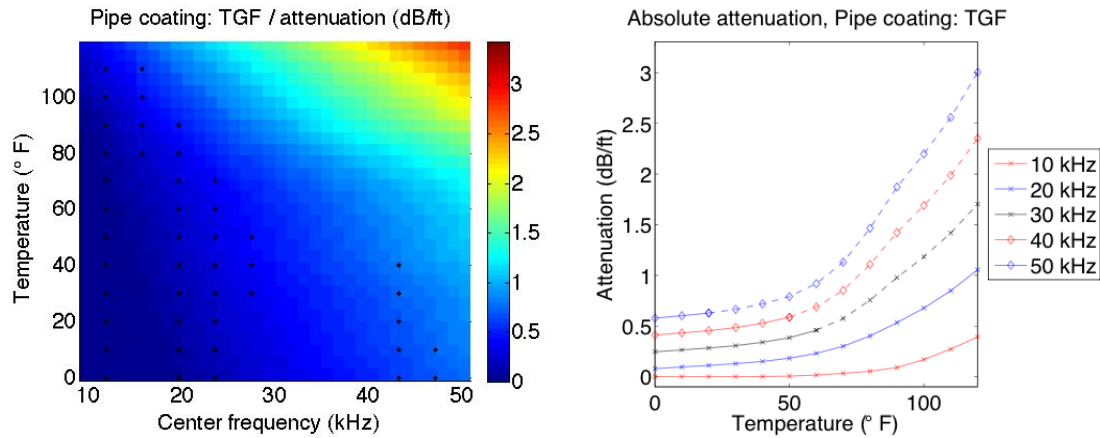


Figure 64. Experimental results from the coal tar (TGF-3) coated pipe sample. Left: attenuation surface as a function of frequency and temperature (data measured at the center frequencies shown as the black dots). Right: temperature dependence of attenuation at discrete frequencies, where dashed lines represent the extrapolated approximations.

### 8.3.2 Effects of general corrosion on wave attenuation

#### (i) Determination of Corrosion Wall Loss Level

The investigation of the corrosion effects on the wave attenuation began on November 21, 2008 and ended on February 10, 2009, over a total of 82-days. Over this span, a total of 15 periodic MsS measurements were conducted. Also during the span, the impressed electric current level was increased to increase the corrosion level. When the corrosion treatment began, the impressed current level was approximately 0.4 amperes. On December 4, 2008, the current level was increased to approximately 1.1 amperes and then it was further increased to approximately 10 amperes on January 7, 2009. Excluding 5 days at the end of January during which the power supply used to impress the electric current was accidentally turned off, the total number of corrosion treatment days was 77.

To determine the corrosion wall loss level during the corrosion treatment, ultrasonic wall thickness measurements were performed periodically together with MsS measurements. Because of large error in ultrasonic thickness measurements ( $\pm 0.003$  inches or so) however, the wall loss level induced in the pipe samples could not be determined reliably.

Therefore, to more accurately track the wall loss level over the duration of the corrosion treatment, the corrosion level was estimated from the impressed current level first and then the overall estimated corrosion level at the end of treatment was calibrated using the actual wall thickness measured from the pipe samples. To actually observe the corrosion state induced and measure the remaining wall thickness, pipe samples were removed from PVC cylinders.

Figure 65 shows photos of pipe surface and a piece of corrosion products. Except for about the top  $\frac{1}{4}$  of the pipe circumference, the pipe surface was covered with a thick layer of corrosion products that were somewhat loosely attached to the pipe.



Figure 65. Photos of pipe surface on the bottom side (upper left), on sides (upper middle and right) and a piece of corrosion product (lower right)

After observing the corrosion scales induced on pipe surfaces, both samples were cut into three sections and the remaining wall thickness was measured around the circumference using a caliper at both cuts. Figure 66 shows plots of remaining wall (red line) and its distribution around the pipe. The original wall thickness (black line) was measured at the sensor end of the pipe. As can be seen, the wall loss was not uniform around the pipe. On average, the final wall loss was approximately 0.023 inch for pipe sample A and 0.021 inch for pipe sample B.

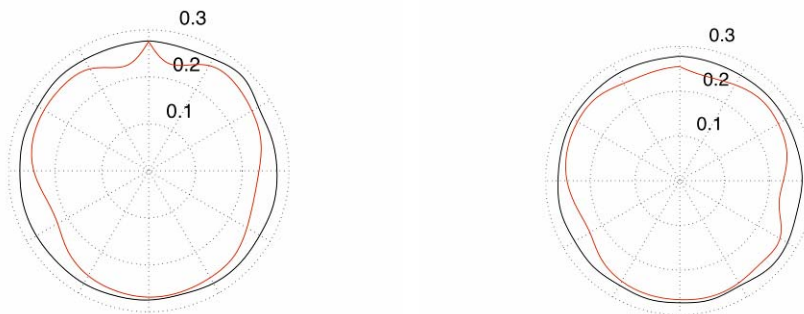


Figure 66. Remaining wall thickness around the circumference of both pipe "A" (left) and pipe "B" (right); Black line represents the original pipe wall thickness and red line represents the remaining wall at the end of corrosion treatment

Figure 67 shows the theoretical wall loss level over the duration of the corrosion treatment. The three different slopes represent the different impressed current level. The constant wall loss over 74-79 days in the plot reflects the accidental turn-off of the impressed current. The total wall loss level at the end of the corrosion treatment was calculated to be approximately 0.025-inch which was in good agreement the final average wall loss level measured.

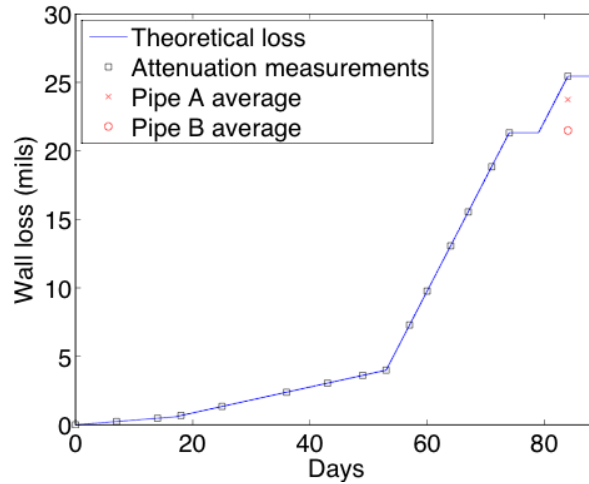


Figure 67. Theoretically calculated wall loss level over the duration of the corrosion treatment. The “squares” indicate the days in which periodic attenuation measurements were made. The final average wall loss level from both pipes is also shown.

The days in which periodic attenuation measurements were made also indicated with “square” symbols in Figure 67. Since the final average wall loss levels measured experimentally were in good agreement with the theoretically calculated values, the theoretical wall loss levels at the time of MsS measurements are used to correlate with the attenuation measurement data.

(ii) *Dependence of Wave Attenuation on Corrosion Wall Loss Level*

Figure 68 shows the 3-D plots of attenuation data as a function of frequency and days of corrosion treatment.

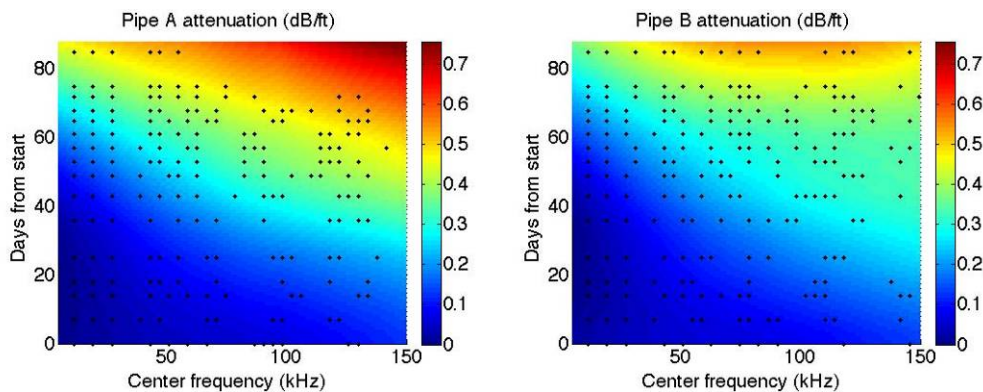


Figure 68. 3-D plots of the attenuation value as a function of frequency and days of corrosion treatment ((data measured at the center frequencies shown as the black dots).

The attenuation values at discrete frequencies (10, 20, etc.) determined from the 3-D surface are plotted in Figure 69.

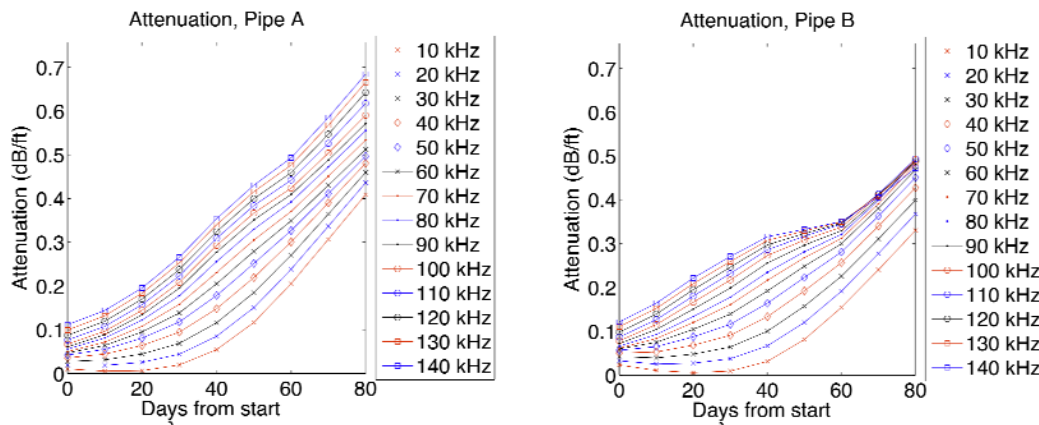


Figure 69. Attenuation as a function of days of corrosion treatment at various frequencies

As expected, the attenuation increased continuously with the days of corrosion treatment. In the early days of corrosion treatment, the attenuation increased at a faster rate at higher frequencies. After 30 days or so, the rate of attenuation increase became almost the same for all frequencies within the range investigated (10 to 140 kHz). The attenuation change was greater for pipe sample A than sample B which also exhibited a stunted attenuation increase for 70 kHz or higher frequencies over a period from 40 to 70 days of corrosion treatment. It is believed that corrosion products on sample B got detached during that period of time and caused the stunted attenuation increase and lower attenuation than sample A. During that period of time however, the attenuation in lower frequencies (<70 kHz) increased at approximately the same rate. The difference between the high and low frequencies suggests that the thickness of corrosion layer that affects the attenuation is inversely proportional to wave frequency.

Using the estimated corrosion wall loss level from the theoretically calculated plotted in Figure 67, the attenuation measured from sample A was re-plotted as a function of corrosion wall loss level in Figure 70 as well as the attenuation caused by the corrosion by subtracting the attenuation value at zero corrosion level. To show the effects in early stages of corrosion more clearly, the data are also plotted as a function of corrosion wall loss level in logarithmic scale in Figure 71.

From the plots in Figures 70 and 71, it was observed that, each time the impressed current level increased, it lowered the rate of attenuation increase. The impact of sudden change in the impressed current level was particularly severe when it was changed from 1.1 Amperes to 10 Amperes. It appears that the sudden increase of the impressed current level alters surface conditions (maybe through the generation of hydrogen gas bubbles) that diminish the corrosion effects.

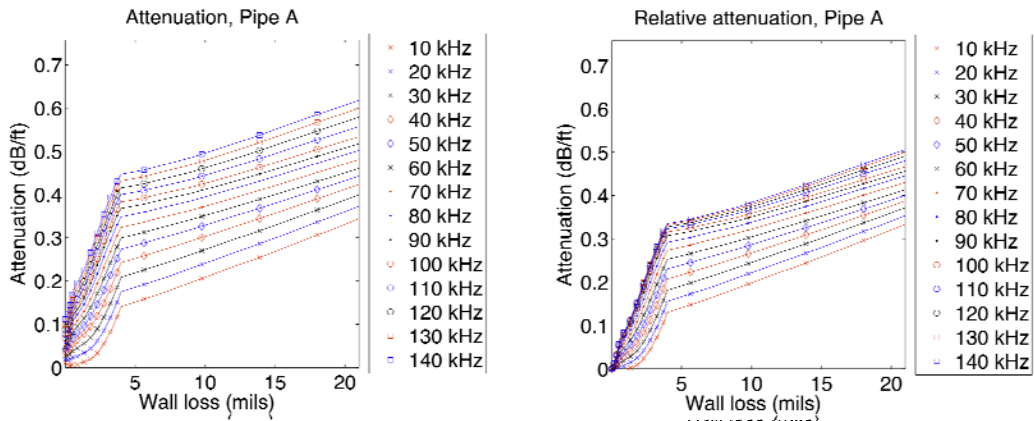


Figure 70. Attenuation as a function of wall loss level (left) and attenuation caused by corrosion (right)

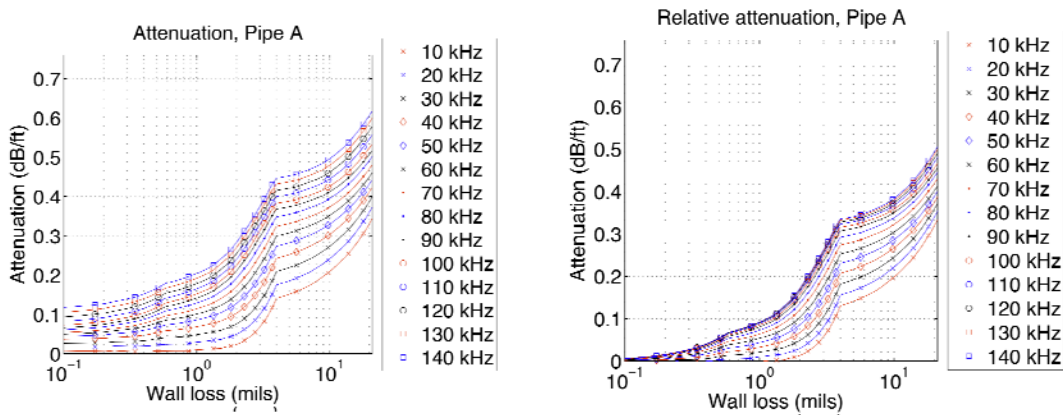


Figure 71. Attenuation as a function of wall loss level (left) and attenuation caused by corrosion (right)

At a given impressed current level, the attenuation for a given frequency increased linearly with the wall loss level. Since the higher impressed current level lowered the rate of attenuation increase, it is logical to conclude that, if the impressed current level were kept at a low value, the resulting attenuation caused by the corrosion would have been significantly greater than what was observed from the experiments. In addition, the corrosion products were found to be loosed attached to the surface of pipe samples (because the samples were kept in aqueous solution). Naturally caused corrosion products would be more firmly attached to pipe surface and, thus, would cause a higher degree of attenuation. We believe, therefore, that the effects of naturally occurring corrosion on the wave attenuation would be significantly greater than what is described in this report.

The attenuation caused by corrosion (right plots in Figures 70 and 71) increased in proportion to the wave frequency up to 90 kHz. When the frequency exceeded 100 kHz, the corrosion effects on the attenuation were the same.

In early stages of corrosion (less than 0.002 inch wall loss), the rate of attenuation increase with corrosion level was approximately linearly proportional to the wave frequency; namely the rate at 100 kHz was about 10 times higher than the rate at 10 kHz. When the corrosion wall loss exceeded 0.002 inch, the rate of attenuation increase became approximately the same for all frequencies.

It is understandable that the corrosion product adhering to the surface of the pipe during the early stage of corrosion would affect higher frequency waves first, thus resulting in larger attenuation increase. The experimental results show that, once the layer of corrosion product is beyond a certain thickness, adding more products to the pipe surface has the same effects on all frequencies.

### *(iii) Discussion on the Capability of Assessing Corrosion State from Attenuation*

The magnitude of corrosion-caused-attenuation ranged from approximately 0.13 dB/ft at 10 kHz to 0.23 dB/ft at 50 kHz for 0.004 inch wall loss. The ability to assess corrosion state from attenuation measurements would depend on the relative magnitude of corrosion-caused-attenuation to coating-caused-attenuation.

In pipelines with low attenuation (such as CTE coated pipeline whose attenuation values at room temperature ranged from less than 0.005 dB/ft at 10 kHz to 0.08 dB/ft at 50 kHz; see Figure 62), the corrosion has a high impact on the apparent attenuation particularly in low frequencies (for example, at 10 kHz, the attenuation in pipes with 0.004 inch wall loss would be more than 20 times greater than its initial value with no corrosion). Therefore it would be relatively easy to recognize the presence of corrosion and determine the corrosion wall loss level from attenuation measurements.

In pipelines with high attenuation (such as PE coated or coal tar TGF-3 coated), the attenuation varies significantly with wave frequency. Therefore the impact of corrosion on the apparent attenuation and consequently capability for assessing the corrosion state would be highly dependent on wave frequency. For example at room temperature (70° F), the attenuation in the PE coated sample ranged from about 0.01 dB/ft at 10 kHz, 0.2 dB/ft at 20 kHz, to 0.8 dB/ft at 50 kHz (Figure 63); in the coal tar (TGF-3) coated sample ranged from about 0.01 dB/ft at 10 kHz, 0.3 dB/ft at 20 kHz, to 1.1 dB/ft at 50 kHz (Figure 64). At 50 kHz, the corrosion-caused-attenuation (for 0.004 inch wall loss) was only a fraction of the coating-caused-attenuation and therefore assessing corrosion from attenuation measurements would be quite difficult. Whereas at 10 kHz, the corrosion-caused-attenuation was 13 times greater than the coating-caused-attenuation and corrosion assessment could be achieved more readily.

The experimental results obtained from coated pipe samples and samples subjected to accelerated corrosion treatment confirm that wave attenuation is a good indicator of general corrosion level. The results also indicate that, even in PE or TGF-3 coated pipelines, the assessment of corrosion state from attenuation measurements is achievable using low frequency waves (such as 10 kHz).

## 9. CONCLUSIONS AND RECOMMENDATIONS

### 9.1 Conclusions

- (1) The long-term guided-wave SHM approach, which involves periodic measurements with permanently installed guided-wave probes and comparison of measurement data, can detect the presence (or lack) of corrosion activity and its locations in the cased sections of pipelines and, therefore, is suitable for DA purposes.
- (2) The MsS is applicable in the field for long-term guided-wave SHM of cased sections.
- (3) Small CSA changes (1 to 2% in bare pipe and 2 to 4% in coal-tar-TGF-3-coated pipe) in pipewall cross-sectional area could be detectable. To improve detection sensitivity in coal-tar-TGF-3-coated pipes, further development of data processing techniques is needed to correct for the effects of wave attenuation on the defect signal waveform.
- (4) Defect characterization (within 1 to 2 inches in axial length and 2 to 4% in CSA) is achievable.
- (5) The wave attenuation significantly increases with general corrosion wall loss level as the corrosion products adhere to the pipe surface (from approximately 0.13 dB/ft at 10 kHz to 0.23 dB/ft at 50 kHz for 0.004 inch wall loss). The wave attenuation is therefore a good indicator of the degree of general corrosion and is particularly useful for assessing the early stages of corrosion. Because of the large corrosion effects on wave attenuation, the assessment of corrosion state from attenuation measurements is achievable even in highly attenuative polyethylene or coal tar TGF-3 coated pipelines using low frequency waves (such as 10 kHz).

### 9.2 Recommendations

- (1) Implement the guided-wave survey and long-term SHM approach in the field.
- (2) In parallel with the field implementation, further improve the detection accuracy of CSA change in coated pipelines by developing signal processing methods for correcting attenuation effects on waveforms (including investigations of the attenuation characteristics of different coating materials/types and the temperature effects).
- (3) Investigate the corrosion effects on wave attenuation under a low corrosion rate over a long duration of time (such as 1 year or more). Because the attenuation values were measured under a high rate of corrosion over a short duration (less than 3 months), the magnitude of the corrosion-caused-attenuation reported here was significantly undervalued. To utilize the attenuation measurements for corrosion assessment in the fields, the magnitude of attenuation increase that would be caused by natural corrosion process needs to be determined accurately under realistic conditions.
- (4) Develop an improved calibration methodology. If a defect is formed and grows in a weld area, the current method which is based on the weld signals can lead to a significant error in data analysis and may fail to detect the defect in the weld area.
- (5) Develop a method and device for maintaining the MsS sensitivity under large (1,000 psi or greater) line pressure changes.
- (6) Take steps for technology transfer that include development of a GUI (graphical user interface) program for data analysis that can be used by inspectors, for preparing training material, and for establishing industry-accepted procedures for probe installation and testing.

## 10. REFERENCES

1. “Pipeline External Corrosion Direct Assessment Methodology,” ANSI/NACE Standard RP0502-2002, p.12, NACE International, Houston, Texas (2002).
2. P. J. Mudge, “Field Application of the Teletest Long-Range Ultrasonic Testing Technique,” *Insight*, **43**, pp. 74-77 (2001).
3. P. Cawley, M. J. S. Lowe, D. N. Alleyene, B. Pavlakovic and P. Wilcox, “Practical Long-Range Guided-Wave Testing: Applications to Pipes and Rail,” *Mat. Eval.* **61**, pp. 66–74 (2003).
4. Kwun, S. Y. Kim, and G. M. Light, “The Magnetostrictive Sensor Technology for Long-Range Guided-Wave Testing and Monitoring of Structures,” *Mat. Eval.* **61**, pp. 80–84 (2003).
5. H. Kwun and S. Y. Kim, “High-Power Long-Range Guided-Wave Inspection of Pipelines,” Final Report on Other Transaction Agreement DTRS56-03-T-0013, SwRI Project 14.10062, prepared for PHMSA, DOT (August 2005).
6. H. Kwun, “Long-Range Guided-Wave Survey and Monitoring of Cased Pipelines at Crossing,” Final Report on SwRI Project 14.11277 for NYSEARCH/NGA (October 2005).
7. M. Redwood, *Mechanical Waveguides: The Propagation of Acoustic and Ultrasonic Waves in Fluids and Solids with Boundaries*, Pergamon Press, New York, 1960.
8. J. D. Achenbach, *Wave Propagation in Elastic Solids*, Elsevier, New York, 1975.
9. J. L. Rose, *Ultrasonic Waves in Solid Media*, Cambridge, Cambridge University Press, 1999.
10. J. P. Joule, “On the Effects of Magnetism upon the Dimensions of Iron and Steel Bars,” *Philosophical Magazine*, Vol. III, No. 30, p.76 (1847).
11. E. Villari, “Change of Magnetization by Tension and by Electric Current,” *Annalen der Physik und Chemie/Leipzig*, **126**, pp. 87-122 (1865).
12. M. S. Choi, S. Y. Kim, and H. Kwun, “Transmission Line Model for Simulation of Guided-Wave Defect Signals in Piping,” *IEEE Trans. on Ultrasonics, Ferroelectrics, and Frequency Control*, **51**, pp. 640-643 (2004).
13. H. Kwun, S. Y. Kim, and M. S. Choi, “Experimental Comparison of Analytical Modeling of a Guided-Wave Interaction with a Notch in a Pipe,” *J. Korean Physical Society*, **45**, pp. 380-385 (2004).
14. A. Demma, P. Cawley, and M. Lowe, “Scattering of the fundamental shear horizontal mode from steps and notches in plates,” *J. Acoustic. Soc. Am.*, **113**, pp. 1880-1891 (2003).
15. R. O. Duda, P. E. Hart, and D. G. Stork, “Nonparametric Techniques,” in *Pattern Classification*, 2nd Edition, John Wiley & Sons, 2001: pp. 161–215.

16. R. Truell, C. Elbaum, and B. B. Chick, *Ultrasonic Methods in Solid State Physics*, Academic Press, New York, 1969, Chap. 2.

## **APPENDIX A**

# NGA/NYSEARCH TEST BED BASELINE TESTING RESULTS

Prepared by Hegeon Kwun and Sang Y. Kim

## I. Above ground 20-inch-OD bare pipe with 24-inch casing

### (a) Test Conditions

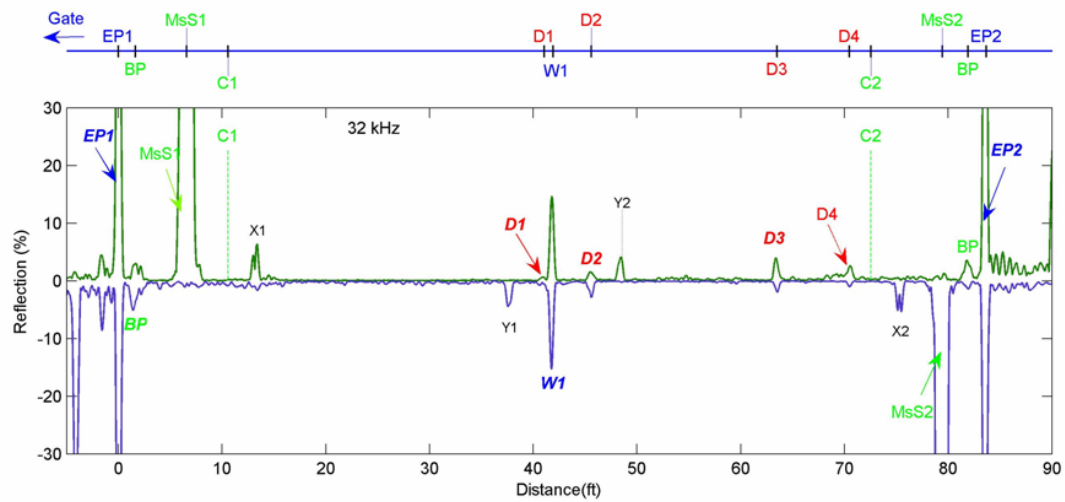
Test Frequencies – 32-kHz and 64-kHz

Guided-Wave Mode – Torsional

Test Locations – From both sides of the casing

### (b) Test Results

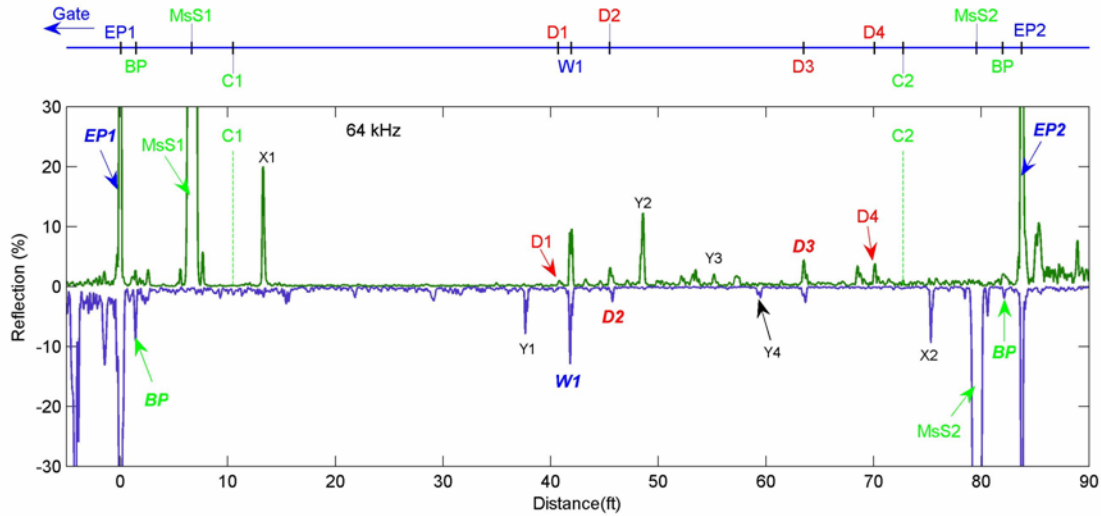
#### 1. 32-kHz Results



Location 1:p1af32k2cmop.dat & p1af32k2cmom.dat; Location 2:p1bf32k2cmop.dat & p1bf32k2cmom.dat			
Sym.	Dist.(ft)	% Refl.	Comment
EP1	0.0	100.0	End of Pipe
BP	1.6	4.0	Branch Pipe and weld attachments
MsS1	6.6	--	Initial Pulse
C1	10.6	--	Casing End
X1	13.5	--	EP1
Y1	37.5	--	W1-EP2
D1	41.0	0.7	-
W1	41.9	15.0	-
D2	45.6	2.2	-
Y2	48.6	--	W1-EP1
D3	63.5	3.0	-
D4	70.5	1.7	-
C2	72.5	--	Casing End
X2	75.5	--	EP2
MsS2	79.4	--	Initial Pulse
BP	81.9	3.6	Branch Pipe and weld attachments
EP2	83.7	100.0	End of Pipe

Legend: D/d - defect; W/w - weld; X/x - imperfect direction control; Y/y - multiple reflection

## 2. 64-kHz Results



Location 1:p1af64k2cinp.dat & p1af64k2cinm.dat;				Location 2:p1bf64k2cinp.dat & p1bf64k2cinm.dat			
Sym.	Dist.(ft)	% Refl.	Comment	Sym.	Dist.(ft)	% Refl.	Comment
EP1	0.0	100.0	End of Pipe	Y3	55.2	--	EP1-W1-EP1
BP	1.5	6.3	Branch pipe and weld attachments	Y4	59.5	--	D3-EP2
MsS1	6.7	--	Initial Pulse	D3	63.5	4.0	-
C1	10.6	--	Casing end	D4	70.1	3.9	-
X1	13.3	--	EP1	C2	72.5	--	Casing end
Y1	37.7	--	W1-EP2	X2	75.4	--	EP2
D1	40.7	1.1	-	MsS2	79.5	--	Initial Pulse
W1	41.9	12.2		BP	82.0	2.2	Branch Pipe
D2	45.5	3.1	-	EP2	83.7	100.0	End of Pipe
Y2	48.5	13.9	; W1-EP1				

Legend: D/d - defect; W/w - weld; X/x - imperfect direction control; Y/y - multiple reflection

### (c) Comments

- The distance in the test results was referenced to the end of the 20-inch pipe from the north side (gate side) end.
- The data required from the north end are plotted on the top and the data acquired from the south end are plotted on the bottom. To aid the comparison between the two sets of data, the data acquired from the south end are plotted in the mirror-image-fashion.
- The four defect indications detected were all relatively small.

- The seal at the casing end shown in the photo or any spacers placed on the pipe did not produce detectable signals.



- The branch piping for pressure gauge and the weld attachments (indicated as BP in the test results) are shown in the photo below.



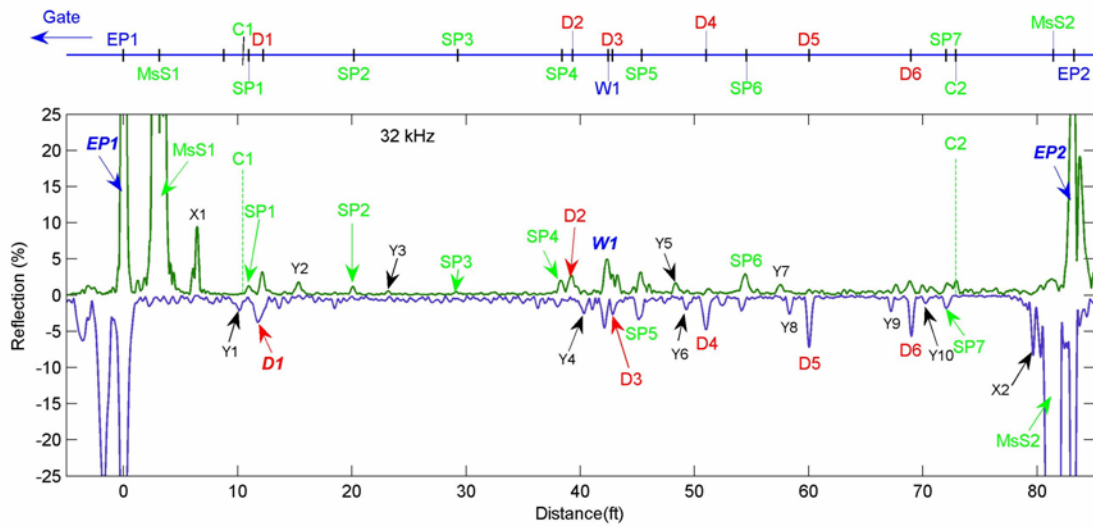
II. Above ground 16-inch-OD coal tar TGF-3 coated pipe with 20-inch casing

(a) Test Conditions

Test Frequencies – 32-kHz and 16-kHz  
 Guided-Wave Mode – Torsional  
 Test Locations – From both sides of the casing

(b) Test Results

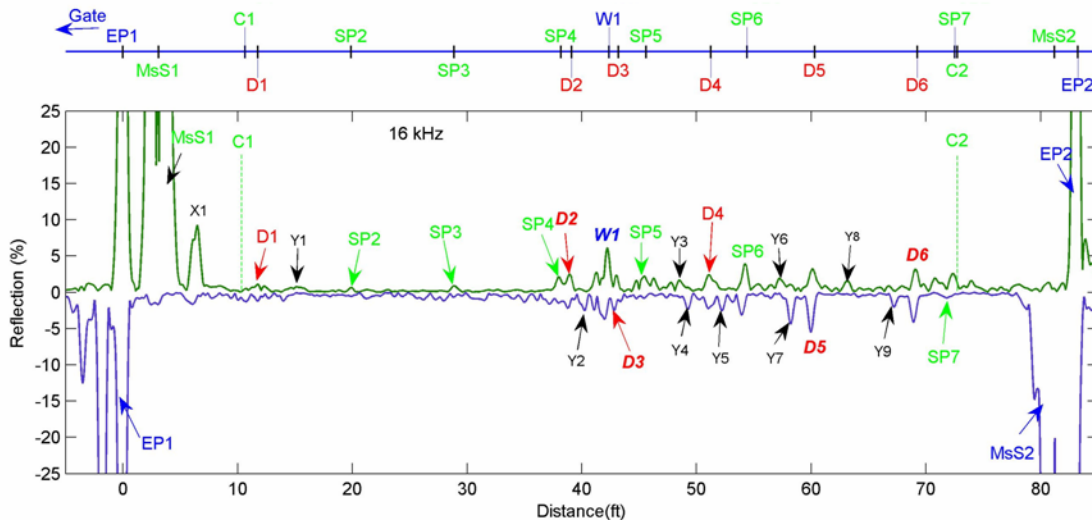
1. 32-kHz Results



Location 1:p2af32k2cin2p.dat & p2af32k2cin2m.dat;				Location 2:p2bf32k2cinp.dat & p2bf32k2cinm.dat			
Sym.	Dist.(ft)	% Refl.	Comment	Sym.	Dist.(ft)	% Refl.	Comment
EP1	0.0	100.0	End of Pipe	SP5	45.4	3.2	Spacer?
MsS1	3.1	--	Initial Pulse	Y5	48.4	--	SP5-EP1
X1	6.5	--	EP1	Y6	49.3	--	D4-EP2
Y1	10.1	--	D1-EP2	D4	51.0	4.7	-
C1	10.5	--	Casing End	SP6	54.6	2.5	Spacer?
SP1	11.0	1.3	Spacer	Y7	57.6	--	SP6-EP1
D1	12.3	3.4	-	Y8	58.3	--	D5-EP2
Y2	15.4	--	D1-EP1	D5	60.0	7.1	
SP2	20.2	1.2	Spacer?	Y9	67.2	--	D6-EP2
Y3	23.3	--	SP2-EP1	D6	69.0	5.7	-
SP3	29.3	0.4	Spacer?	Y10	70.2	--	SP7-EP2
SP4	38.4	2.0	Spacer?	SP7	72.0	1.8	Spacer
D2	39.3	2.6	-	C2	72.6	--	Casing End
Y4	40.3	--	W1-EP2	X2	79.6	--	EP2
W1	42.4	4.6		MsS2	81.4	--	Initial Pulse
D3	42.8	2.6	-	EP2	83.2	100.0	End of Pipe

Legend: D/d - defect; W/w - weld; X/x - imperfect direction control; Y/y - multiple reflection

## 2. 16-kHz Results



Location 1:p2af16k1cinp.dat & p2af16k1cinm.dat;				Location 2:p2bf16k1cinp.dat & p2bf16k1cinm.dat			
Sym.	Dist.(ft)	% Refl.	Comment	Sym.	Dist.(ft)	% Refl.	Comment
EP1	0.0	100.0	End of Pipe	Y4	49.2	--	D4-EP2
MsS1	3.1	--	Initial Pulse	D4	51.3	2.4	-
X1	6.6	--	EP1	Y5	52.2	--	SP6-EP2
C1	10.5	--	Casing End	SP6	54.4	3.5	Spacer
D1	11.7	1.1	-	Y6	57.1	--	SP6-EP1
Y1	15.1	--	D1-EP1	Y7	58.2	--	D5-EP2
SP2	19.9	0.6	Spacer	D5	60.3	4.4	-
SP3	28.9	0.9	Spacer	Y8	63.1	--	D5-EP1
SP4	38.2	2.2	Spacer	Y9	67.2	--	D6-EP2
D2	39.1	2.4	-	D6	69.3	3.7	-
Y2	40.2	--	W1-EP2	SP7	72.5	1.0	Spacer
W1	42.4	4.9		C2	72.6	--	Casing End
D3	43.2	3.1	-	MsS2	81.2	--	Initial Pulse
SP5	45.6	2.2	Spacer	EP2	83.3	100.0	End of Pipe
Y3	48.5	--	SP5-EP1				

Legend: D/d - defect; W/w - weld; X/x - imperfect direction control; Y/y - multiple reflection

### (c) Comments

- The distance in the test results was referenced to the north end of the pipe.
- The data are plotted in the same manner as the data for the 20-inch-OD bare pipe.
- The seal at the casing end and spacers produced detectable signals.
- Some of signals interpreted as from spacers may be from defects.
- The test results at both frequencies were approximately the same except the quantitative values of reflection coefficients of indications and spatial resolutions – expected due to wavelength difference
- The six defect indications detected were small to medium size.

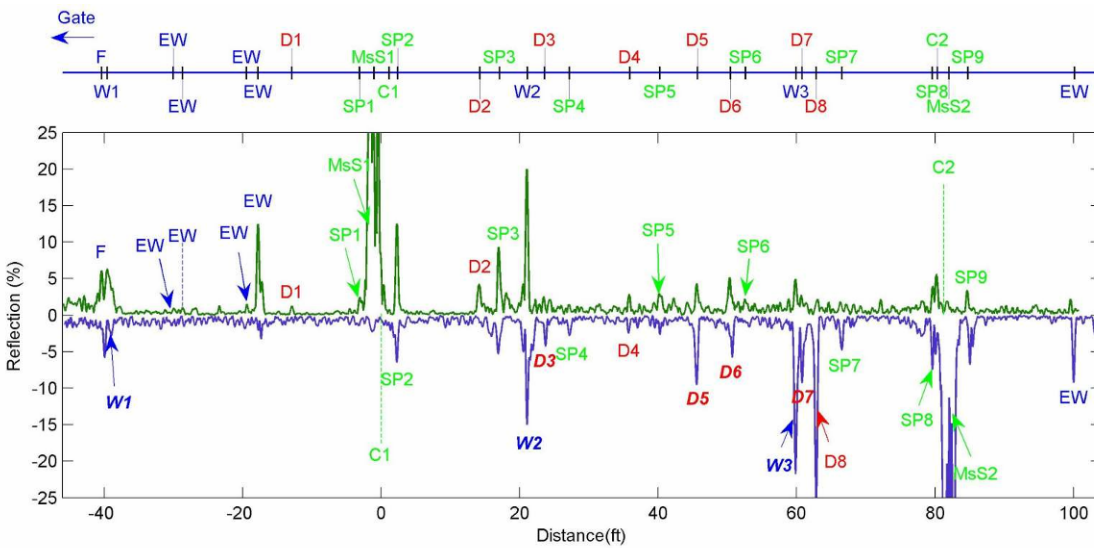
### III. Underground 12-inch-OD coal tar epoxy (CTE) coated pipe with 16-inch casing

#### (a) Test Conditions

Test Frequencies – 32-kHz and 16-kHz  
 Guided-Wave Mode – Torsional  
 Test Locations – From both sides of the casing

#### (b) Test Results

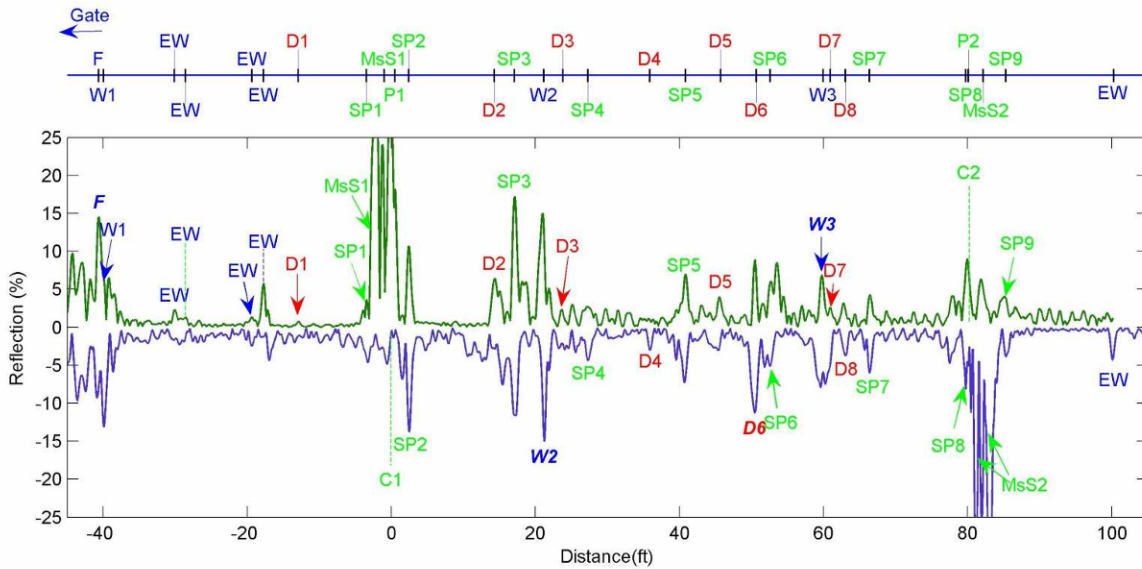
##### 1. 32-kHz Results



Location 1:p3af32k2cmop.dat & p3af32k2cmom.dat;				Location 2:p3bf32k2cmop.dat & p3bf32k2cmom.dat			
Sym.	Dist.(ft)	% Refl.	Comment	Sym.	Dist.(ft)	% Refl.	Comment
F	-40.4	6.1	Flange	SP4	27.2	2.8	Spacer
W1	-39.3	2.9	Flange Weld	D4	35.9	3.1	--
EW	-30.0	0.9	Elbow Weld	SP5	40.3	3.2	Spacer
EW	-28.7	1.0	Elbow Weld	D5	45.7	7.1	--
EW	-19.4	1.5	Elbow Weld	D6	50.4	5.7	--
EW	-17.8	13.6	Elbow Weld	SP6	52.6	2.4	Spacer
D1	-12.9	1.2	--	W3	59.9	4.9	
SP1	-3.1	2.7	Spacer	D7	60.8	9.3	--
MsS	-1.0	--	Initial Pulse	D8	62.8	25.8	--
C1	0.0	--	Casing end	SP7	66.5	4.8	Spacer
SP2	2.4	10.1	Spacer	SP8	79.6	7.5	Spacer
D2	14.3	4.7	--	C2	80.3	--	Casing end
SP3	17.1	9.3	Spacer	MsS	82.0	--	Initial Pulse
W2	21.2	18.4		SP9	84.7	5.2	Spacer
D3	23.6	4.2	--	EW	100.1	9.2	Elbow Weld

Legend: D/d - defect; W/w - weld; X/x - imperfect direction control; Y/y - multiple reflection

## 2. 16-kHz Results



Location 1:p3af16k1cmop.dat & p3af16k1cmom.dat;				Location 2:p3bf16k1cmop.dat & p3bf16k1cmom.dat			
Sym.	Dist.(ft)	% Refl.	Comment	Sym.	Dist.(ft)	% Refl.	Comment
F	-40.6	13.8	Flange	SP4	27.3	4.4	Spacer
W1	-39.9	5.9	Flange Weld	D4	35.9	3.0	--
EW	-30.1	2.3	Elbow Weld	SP5	40.8	7.0	Spacer
EW	-28.6	1.2	Elbow Weld; Not detected	D5	45.7	4.0	--
EW	-19.4	2.3	Elbow Weld	D6	50.6	10.1	--
EW	-17.7	5.8	Elbow Weld	SP6	52.6	5.2	Spacer
D1	-12.9	0.7	--	W3	59.9	7.4	
SP1	-3.5	4.6	Spacer	D7	60.9	2.6	--
MsS1	-1.0	--	Initial Pulse	D8	63.1	3.7	--
C1	0.0	--	Casing end	SP7	66.4	6.0	Spacer
SP2	2.4	12.2	Spacer	SP8	79.7	9.0	Spacer
D2	14.3	6.4	--	C2	81.25	--	Casing end
SP3	17.1	14.4	Spacer	MsS2	83.5	--	Initial Pulse
W2	21.2	15.0		SP9	85.3	3.7	Spacer
D3	23.8	2.3	--	EW	100.3	4.3	Elbow Weld

Legend: D/d - defect; W/w - weld; X/x - imperfect direction control; Y/y - multiple reflection

(c) Comments

- The distance in the test results was referenced to the casing end of the 12-inch pipe (shown in the photo) in the north side vault.



- The data are plotted in the same manner as the data for the 20-inch-OD bare pipe.
- The seal at the casing end and spacers produced large signals.
- The test results at both frequencies were approximately the same except the quantitative values of reflection coefficients of indications and spatial resolutions – expected due to wavelength difference.
- The seven defect indications detected were small to large size.
- The large difference in response (for example D7) with wave frequency suggests that multiple frequency testing is necessary to improve the defect detection accuracy.
- The signal from the flanged end of the 12-inch line shown in the photo was detectable. The guided waves were propagated through two 45-degree elbows to reach the flange some sections of which were buried underground and some aboveground.



## **APPENDIX B**

# NGA/NYSEARCH TEST BED STRUCTURAL HEALTH MONITORING (SHM) TEST RESULTS

Prepared by  
Hegeon Kwun, Southwest Research Institute  
Sang Y. Kim, Guided Wave Analysis LLC

December 12, 2007

## (a) Background Information

### 1.1 Test Dates

Baseline Measurements – April 25, 2007  
SHM Measurements – November 6, 2007

### 1.2 Legends in the Data Plot

MsS – location of MsS probe  
EP – End of Pipe  
C – End of Casing  
W – Weld  
SP – Spacer  
BP – Branch Pipe  
F – Flange  
D – Defect Indication  
x – Signal caused by imperfect wave direction control  
y – Signal caused by multiple reflections involving 2 or more reflectors

Distance is from the North End of pipe.

### 1.3 Other Relevant Information

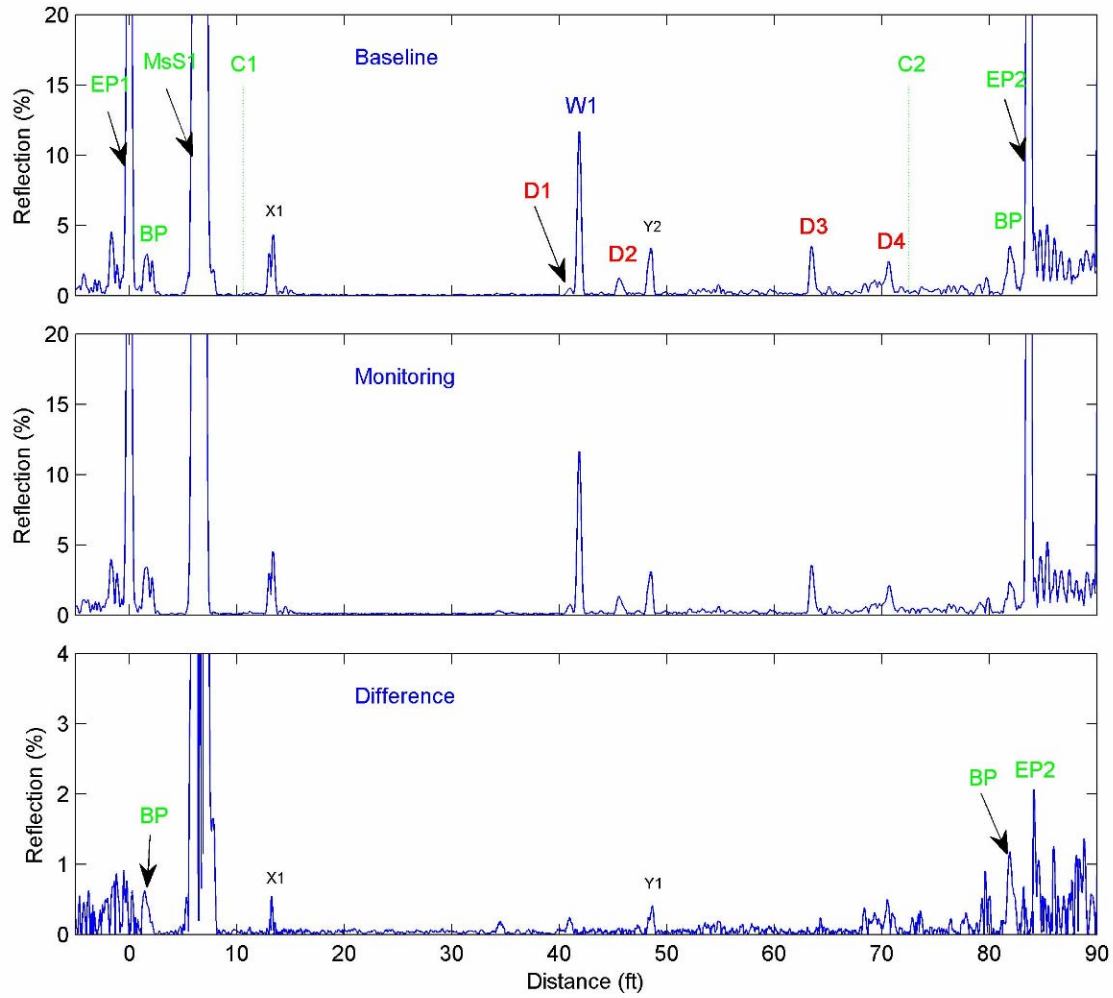
- (1) NGA/NYSEARCH did not modify or add any defects in the samples. Ideally therefore, the baseline data and the monitoring data should match.
- (2) All MsS probes installed on the three test bed samples were found to operate properly.
- (3) November 6 was a cold day (in low 40s degree F)

2. Aboveground 20-inch-OD bare pipe with 24-inch casing

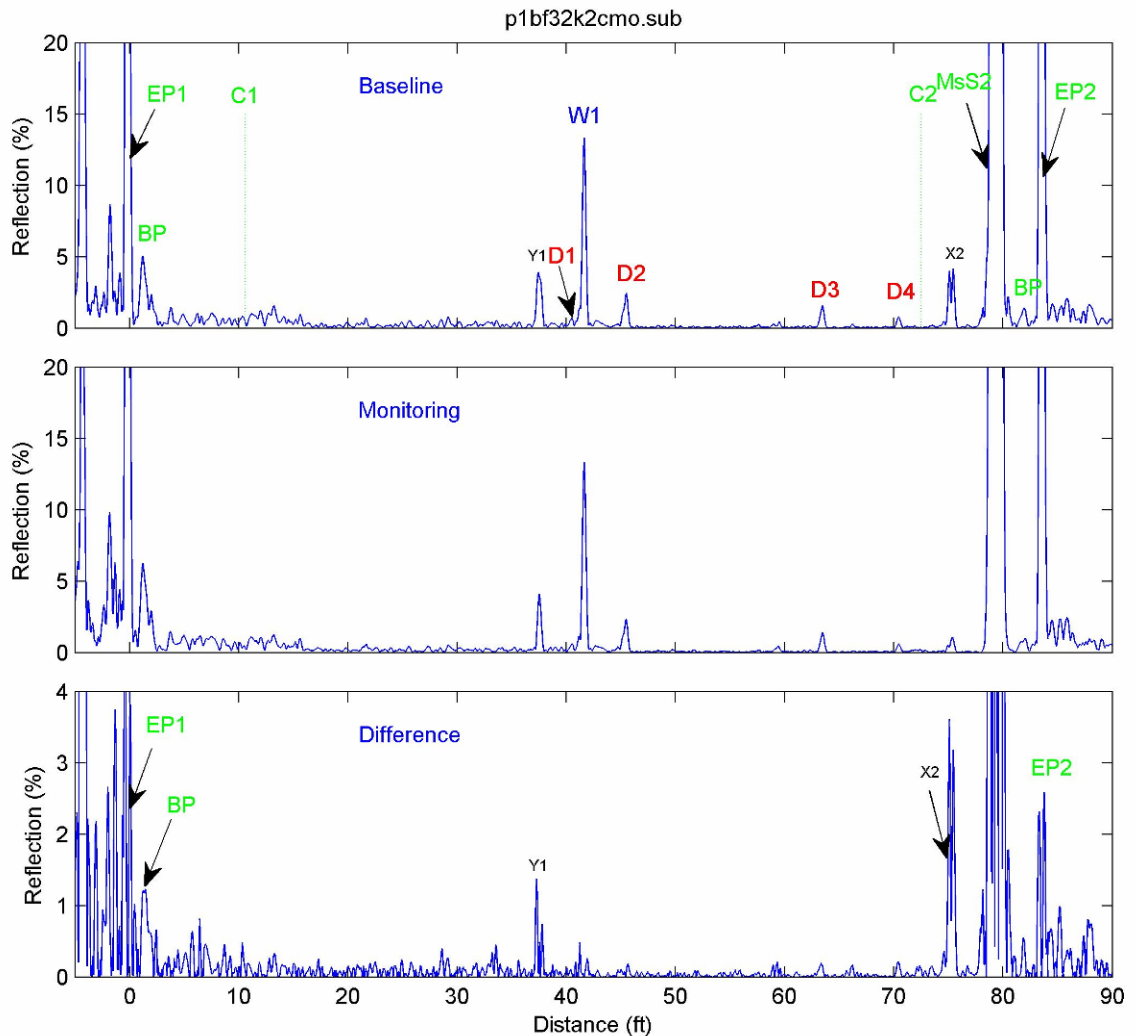
(1) Test Frequency – 32 kHz

(2) Data (Baseline, Monitoring, and Difference between the Two)

(a) Data from the North End



(b) Data from the South End



2.3 Comments

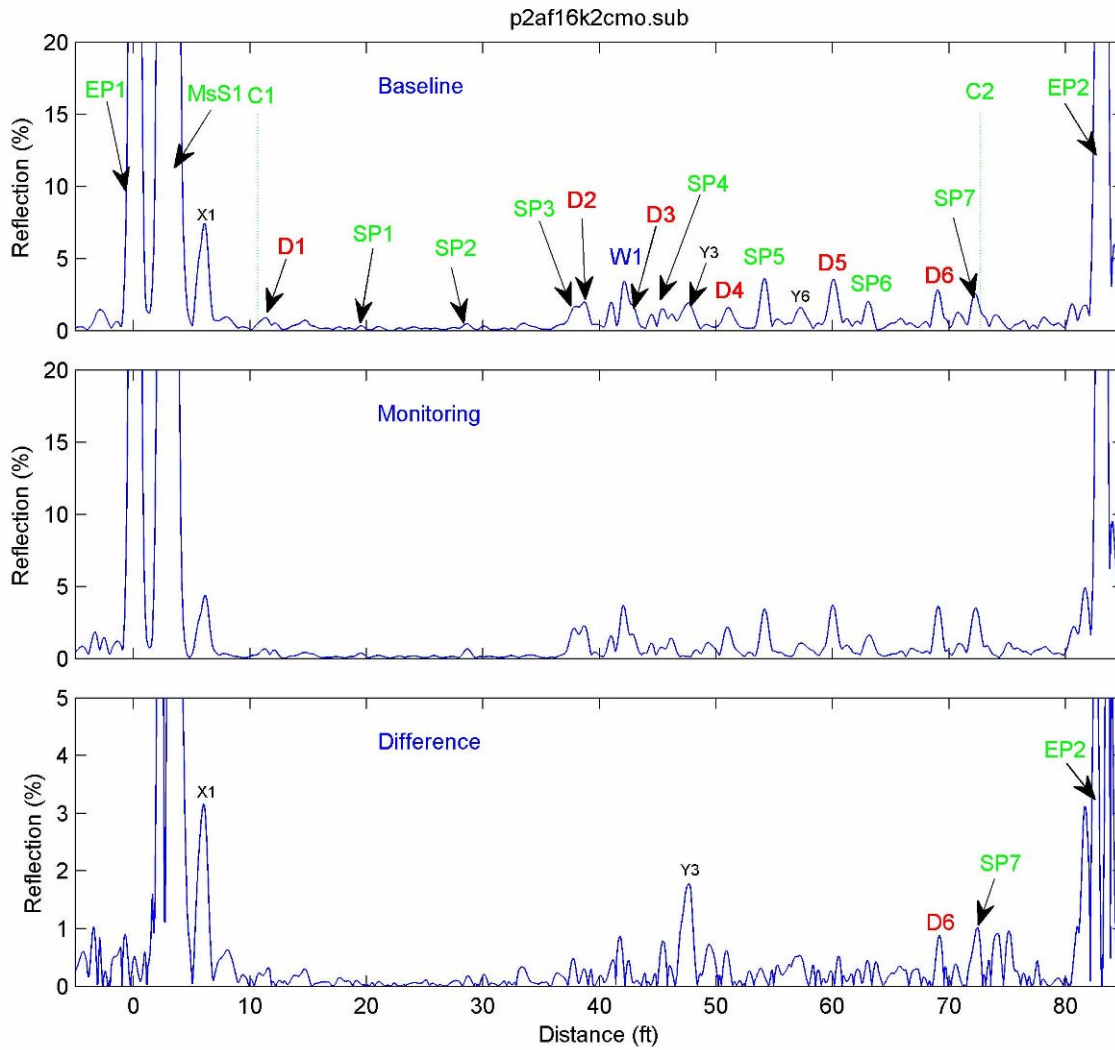
- (1) The monitoring data matched very well with the baseline data. Therefore, difference between the two sets of data was small – generally less than 0.2% reflection.
- (2) The relatively large x and y signals in the difference data indicate a change in the condition of the end caps placed on the pipe (namely, the mechanical contact condition of the end cap to the test pipe).
- (3) In both the baseline and monitoring data, the background noise level start increasing at about 60-ft distance from the MsS location. Consequently beyond the 60-ft distance point, the background noise level was also higher in the difference data (this makes sense since noise is not repeatable) and the sensitivity of detecting changes is also reduced.
- (4) The test results indicate that the MsS probes have good long-term stability.

3. Aboveground 16-inch-OD coal tar TGF-3 coated pipe with 20-inch casing

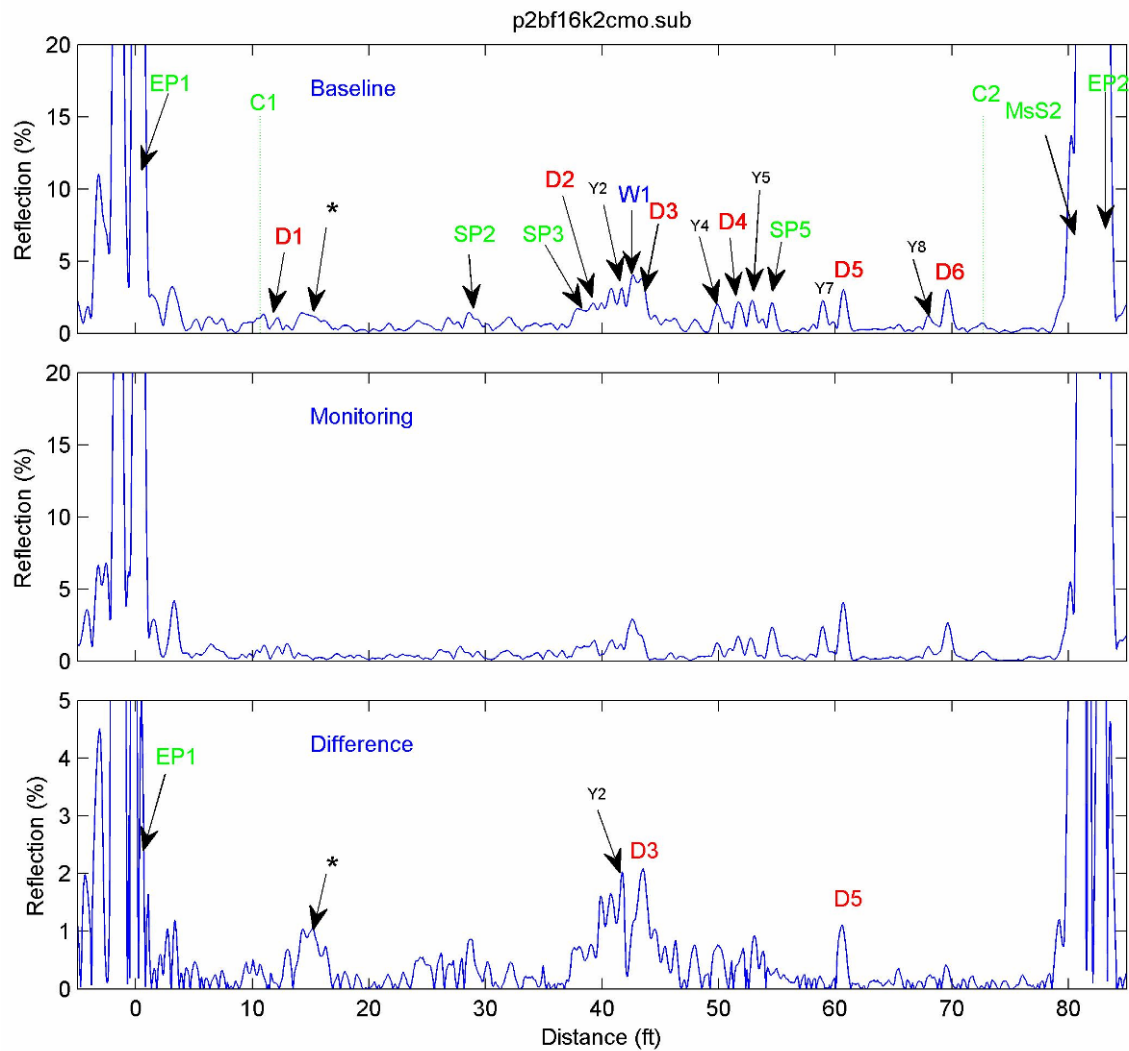
3.1 Test Frequency – 16 kHz

3.2 Data (Baseline, Monitoring, and Difference between the Two)

(a) Data from the North End



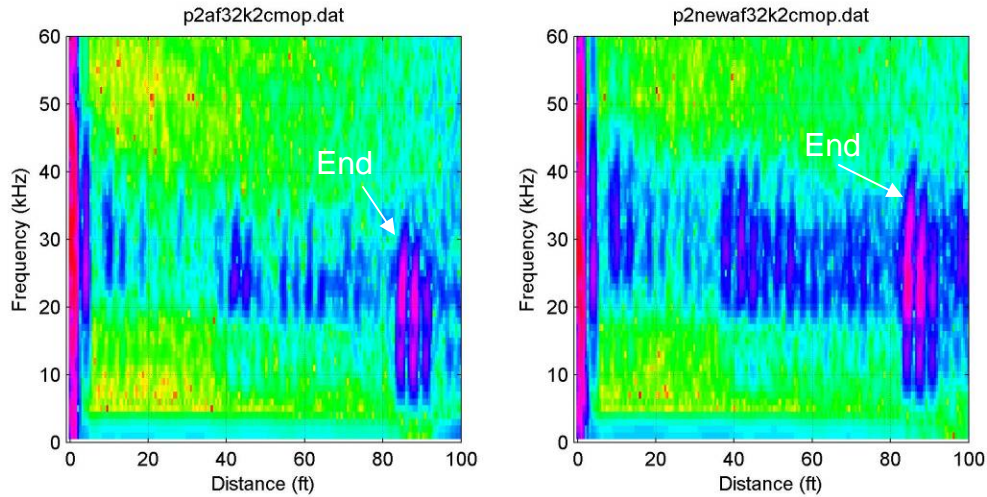
(b) Data from the South End



3.3 Comments

- (1) The agreement between the two sets of data was somewhat less than what was observed in the aboveground bare pipe described in Section 2, with the general difference being about 1% reflection (instead of 0.2%). The difference level at 32-kHz was about two times greater (to about 2%).
- (2) The primary reason for the relatively large difference between the monitoring and baseline data was the temperature related attenuation change. In coated pipes, the wave attenuation increases significantly with the increasing temperature. Because the day the monitoring data were acquired was cold, the test pipe exhibited significantly lower wave attenuation than before as shown in the spectrograms given below. In the plots, the left one is the spectrogram of the 32-kHz baseline data and the right one is the spectrogram of

the 32-kHz monitoring data from this test sample. The end signal in the baseline data spectrogram contained frequency components ranging from about 6 to 30-kHz, whereas the end signal in the monitoring data spectrogram contained components ranging from about 6 to 40-kHz. In the baseline data spectrogram, the 30 to 40-kHz components were absent due to high wave attenuation at that time. Because of the significant difference in spectral contents, the shape and length of signal waveforms from defects and pipeline features (weld and spacers) changed substantially that lead to the relatively large signals in the difference data. To improve the accuracy of SHM and the detection of structural condition changes, more sophisticated data processing techniques need to be developed to correct the effects of temperature-related attenuation changes on the signal waveforms.



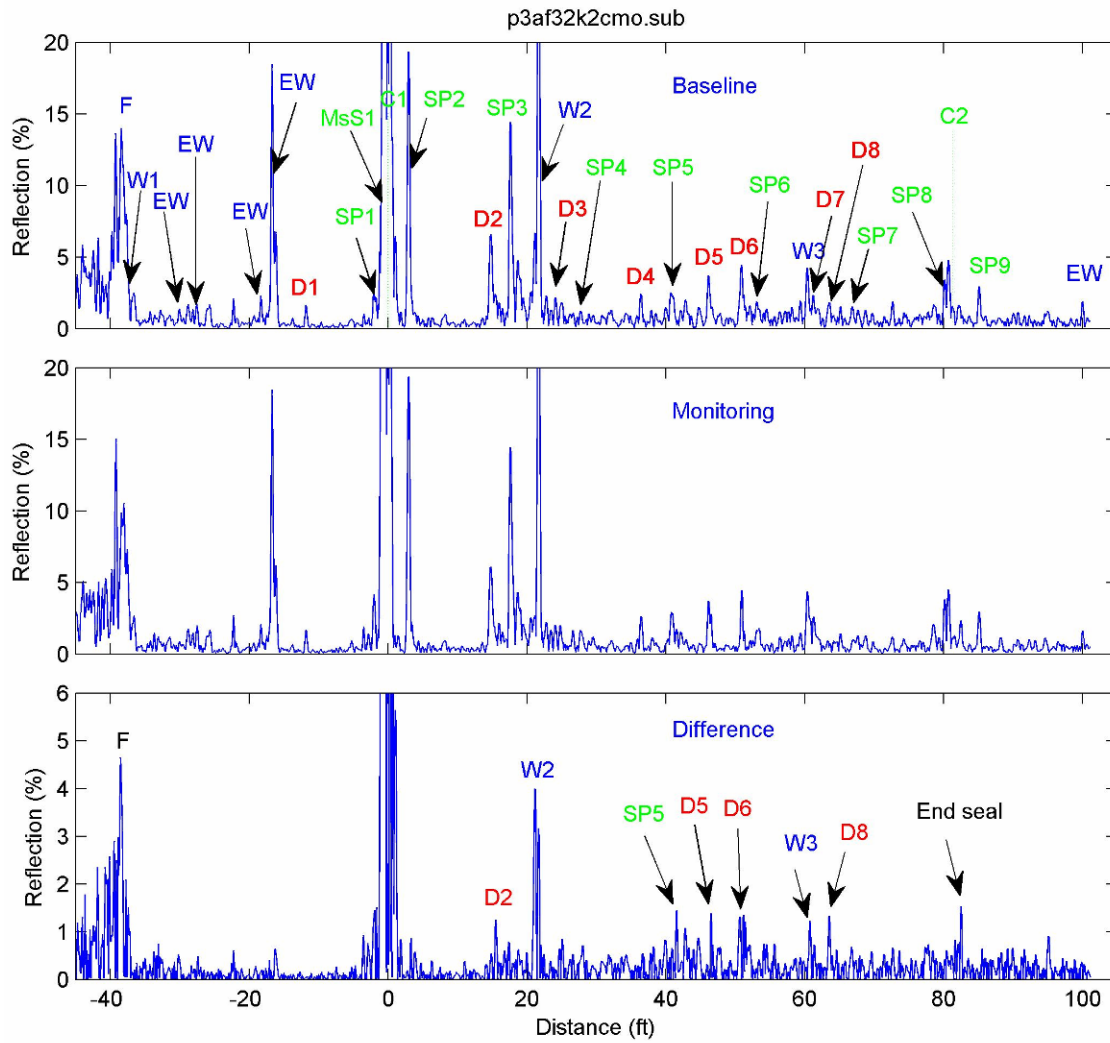
- (3) In addition to the temperature-related-attenuation effects discussed above, the relatively large x and y signals in the difference data indicate a change in the condition of the end caps placed on the pipe (namely, the mechanical contact condition of the end cap to the test pipe).
- (4) In the data from the South End of the sample, the background noise level in the monitoring data was generally lower than that in the baseline data. In addition to the signals from defect and pipeline features (weld and spacers), the differing background noise also contributed significantly to the difference data: for example, the noise signal indicated with \* in the baseline data was absent in the monitoring data and resulted in a prominent signal in the difference data.
- (5) The change in the signal waveforms caused by the temperature-related attenuation effects will alter interference patterns and is believed to be partly responsible to the large signals at around 40-45 ft in the difference data.

4. Underground 12-inch-OD coal tar epoxy (CTE) coated pipe with 16-inch casing

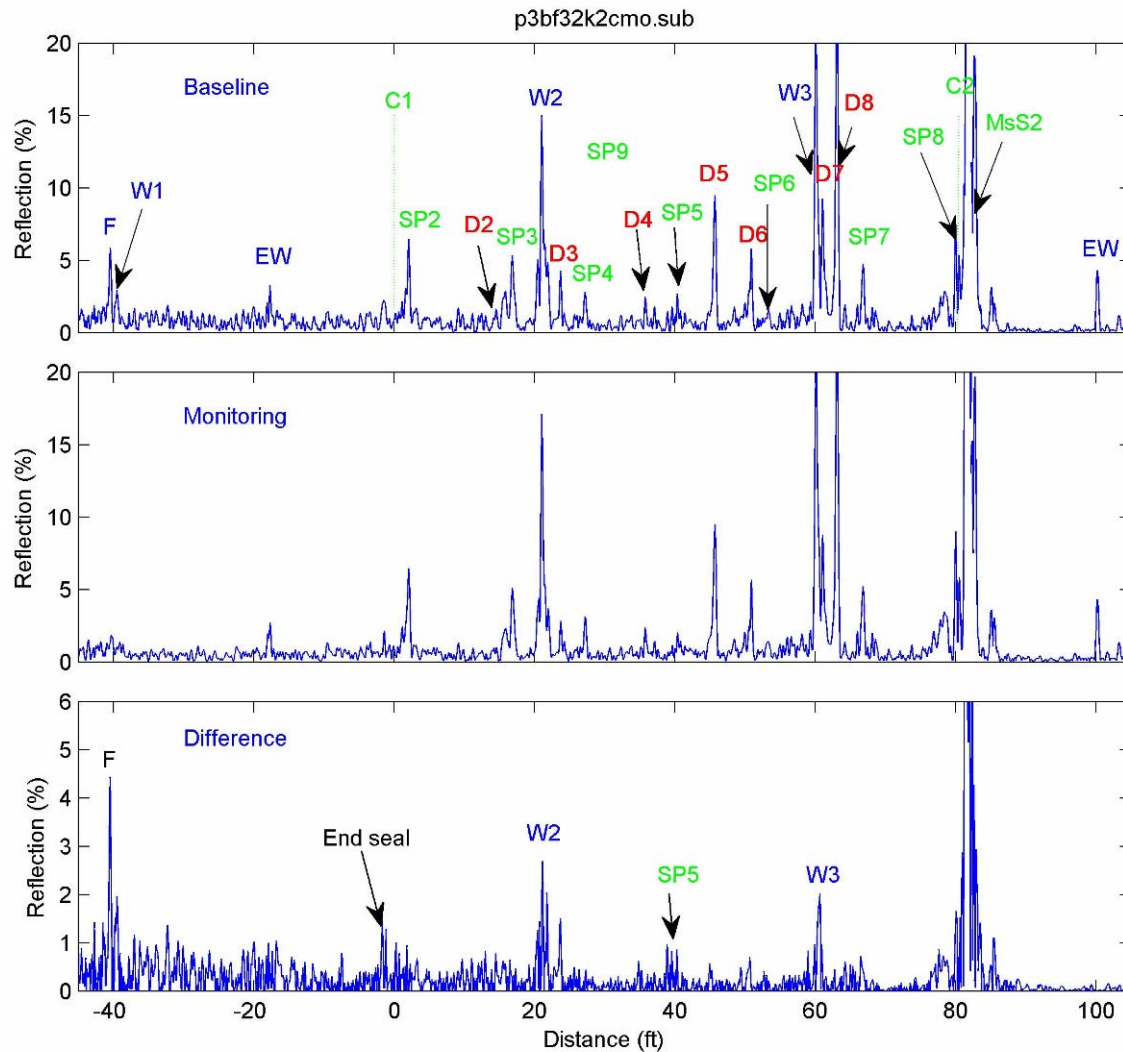
4.1 Test Frequency – 32 kHz

4.2 Data (Baseline, Monitoring, and Difference between the Two)

(a) Data from the North End Excavation Vault



(b) Data from the South End Excavation Vault



4.3 Comments

- (1) The difference level between the baseline and monitoring data in this test sample was similar to what was observed from the aboveground coal tar TGF-3 coated test sample discussed in Section 3.
- (2) Due to the change in the shape of signal waveforms from defects and pipeline features (welds and spacers) that was caused by the temperature-related-attenuation effects discussed in Section 3, these signals generally did not match well and thus produced large signals in the difference data -- for example, the difference level in W2 signal ranged from 3 to 4% reflection.
- (3) Excluding the defect and feature signals, the background noise level in the difference data was only about 0.5% reflection for over 80-ft distance. This suggests that, if the

temperature-related attenuation effects on the large feature signals could be corrected, detection of 1%-size defect growth or newly formed defects could be achievable.

## 5. Summary of Findings and Conclusions

- (1) All MsS probes installed in April were found to operate properly in November (over a span of about 6-month), indicating the long-term stability of the probes.
- (2) The SHM data from the aboveground bare test pipe agreed very well with the baseline data, showing a high degree of reproducibility. The background noise level in the difference data between the two was less than 0.2% reflection level, indicating the ability to detect a 0.4% change (based on the 2:1 signal-to-noise ratio for detection).
- (3) The SHM results from both the aboveground TGF-3 and underground CTE coated test pipes were several times worse than the results from the bare test pipe. The primary cause of the poorer performance on the coated test pipes was the signal waveform change induced by a large change in wave attenuation characteristics in the coated pipes with the ambient temperature fluctuations and the limitations of data subtraction software presently available. To improve the SHM performance on the coated pipelines, data processing techniques need to be developed that can correct the attenuation effects on the waveform.

## **APPENDIX C**

# NGA/NYSEARCH TEST BED 2<sup>nd</sup> STRUCTURAL HEALTH MONITORING (SHM) TEST RESULTS

Prepared by  
Hegeon Kwun, Southwest Research Institute  
Sang Y. Kim, Guided Wave Analysis LLC

March 5, 2008

## 1. Background Information

### 1.1 Test Dates

Baseline Measurements – April 25, 2007  
1<sup>st</sup> SHM Measurements – November 6, 2007  
2<sup>nd</sup> SHM Measurements – February 20, 2008

### 1.2 Legends in the Data Plot

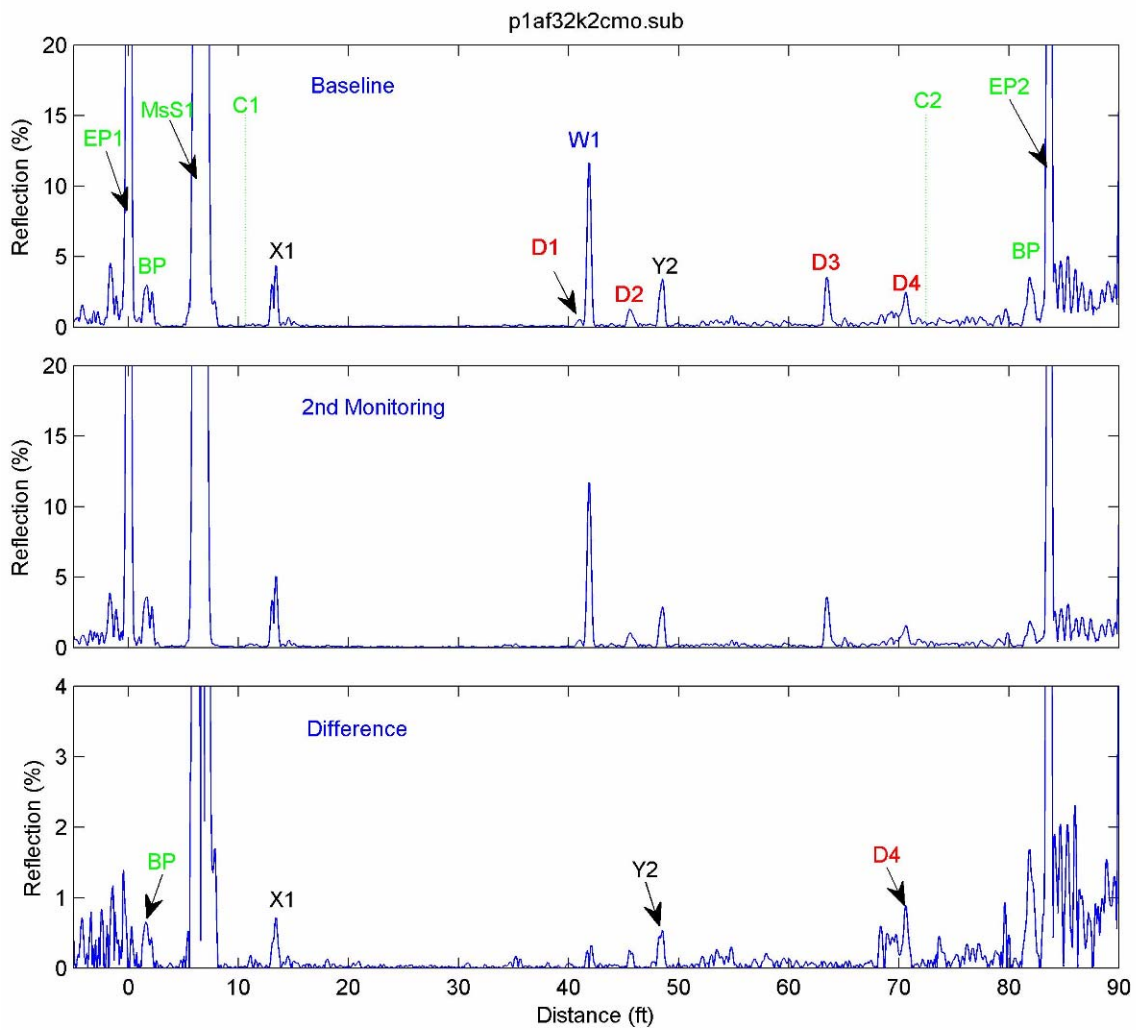
MsS – location of MsS probe  
EP – End of Pipe  
C – End of Casing  
W – Weld  
SP – Spacer  
BP – Branch Pipe  
F – Flange  
D – Defect Indication  
x – Signal caused by imperfect wave direction control  
y – Signal caused by multiple reflections involving 2 or more reflectors

Distance is from the North End of pipe.

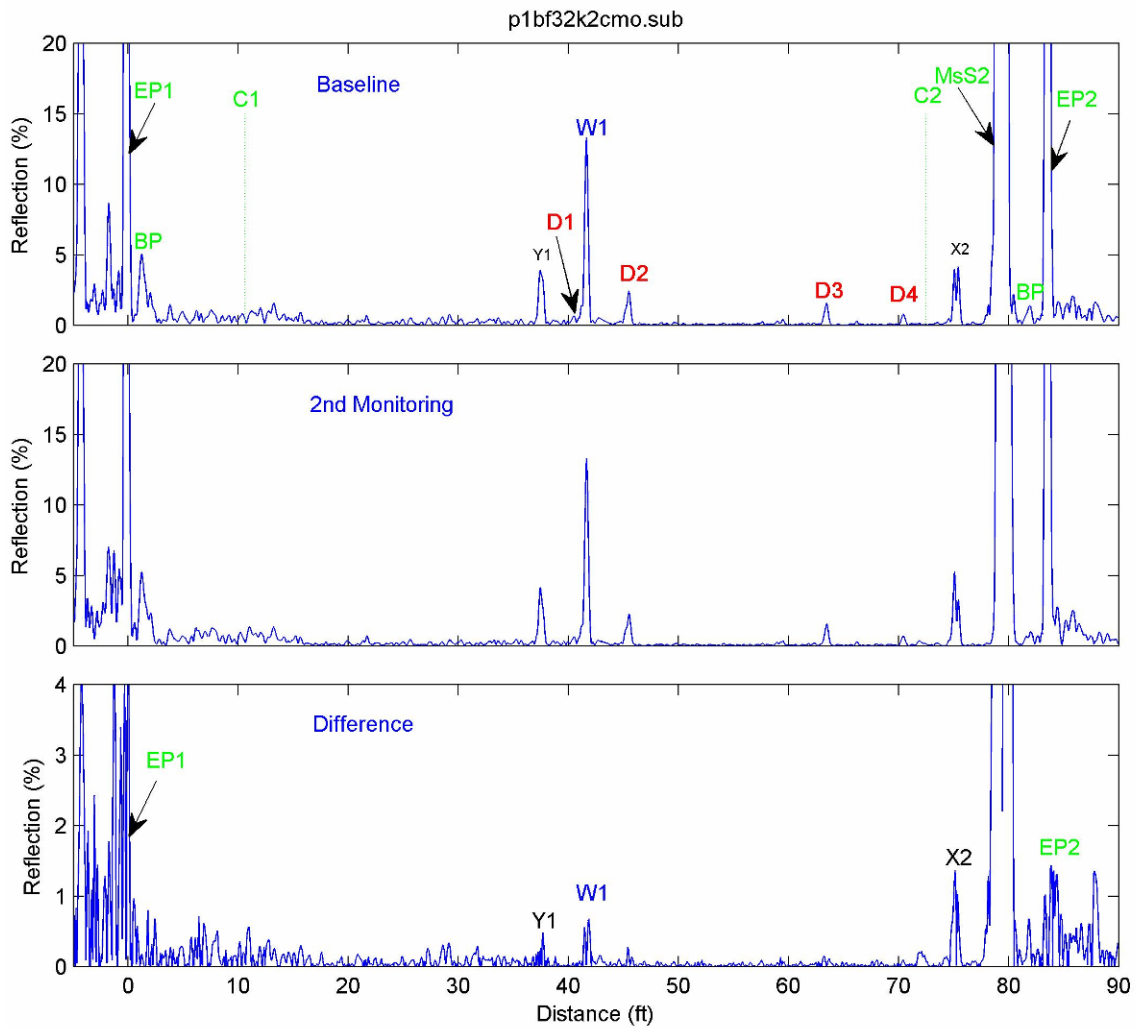
### 1.3 Other Relevant Information

- (1) NGA/NYSEARCH did not modify or add any defects in the samples. Ideally therefore, the baseline data and the monitoring data should match.
- (2) All MsS probes installed on the three test bed samples were found to operate properly.
- (3) Temperature on February 20<sup>th</sup> ranged from about 15 to 25 degree F.

- 2. Aboveground 20-inch-OD bare pipe with 24-inch casing
- 2.1 Test Frequency – 32 kHz
- 2.2 Data (Baseline, 2<sup>nd</sup> Monitoring, and Difference between the Two)
- (a) Data from the North End



(b) Data from the South End



2.3 Comments

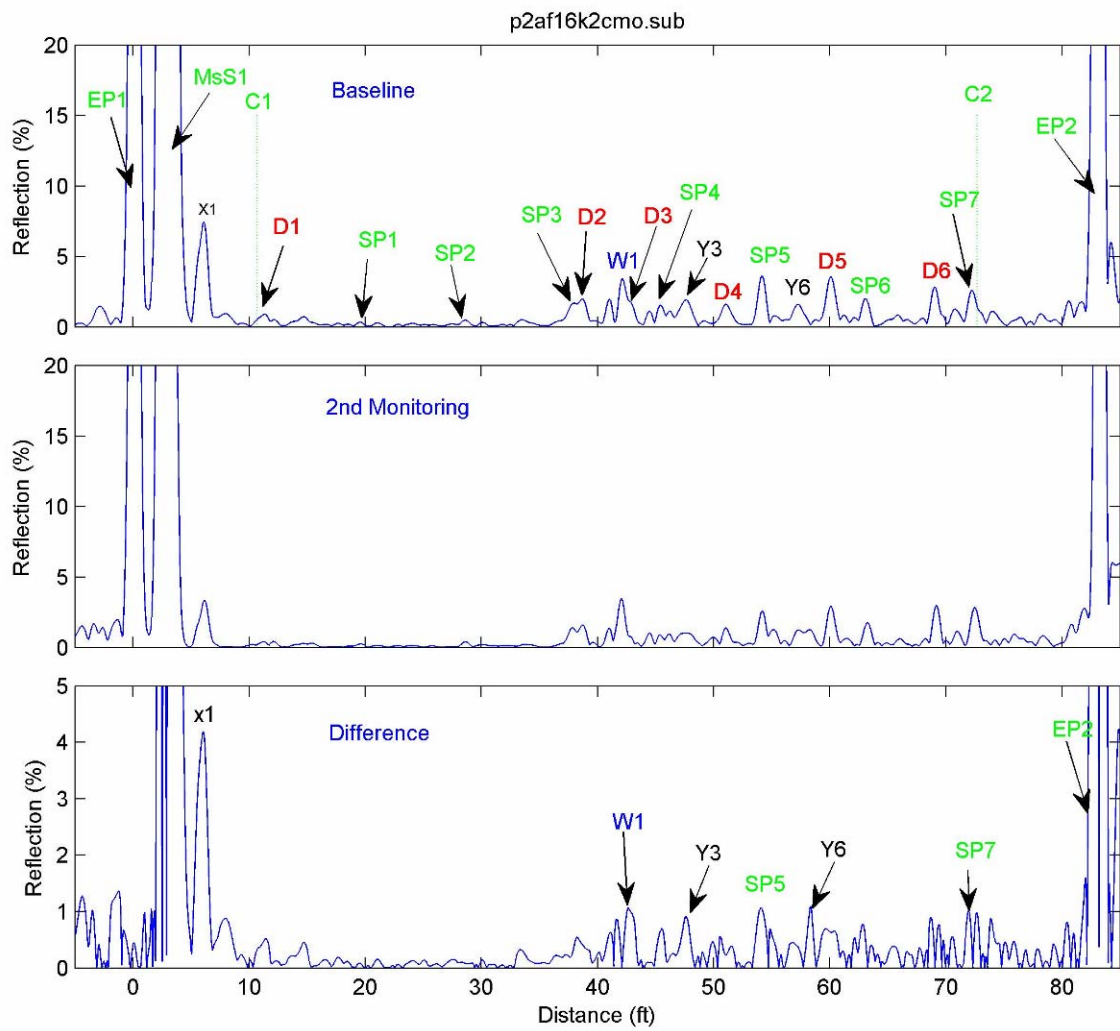
- (1) The 2<sup>nd</sup> monitoring data matched very well with the baseline data. Therefore, difference between the two sets of data was small – generally less than 0.2% reflection as found from the 1<sup>st</sup> SHM test results given in Appendix B.
- (2) The good reproducibility of data indicates again that the MsS probes are suitable for long-term SHM.
- (3) Comparison results between the 1<sup>st</sup> and 2<sup>nd</sup> SHM data were similar to the shown above.

3. Aboveground 16-inch-OD coal tar TGF-3 coated pipe with 20-inch casing

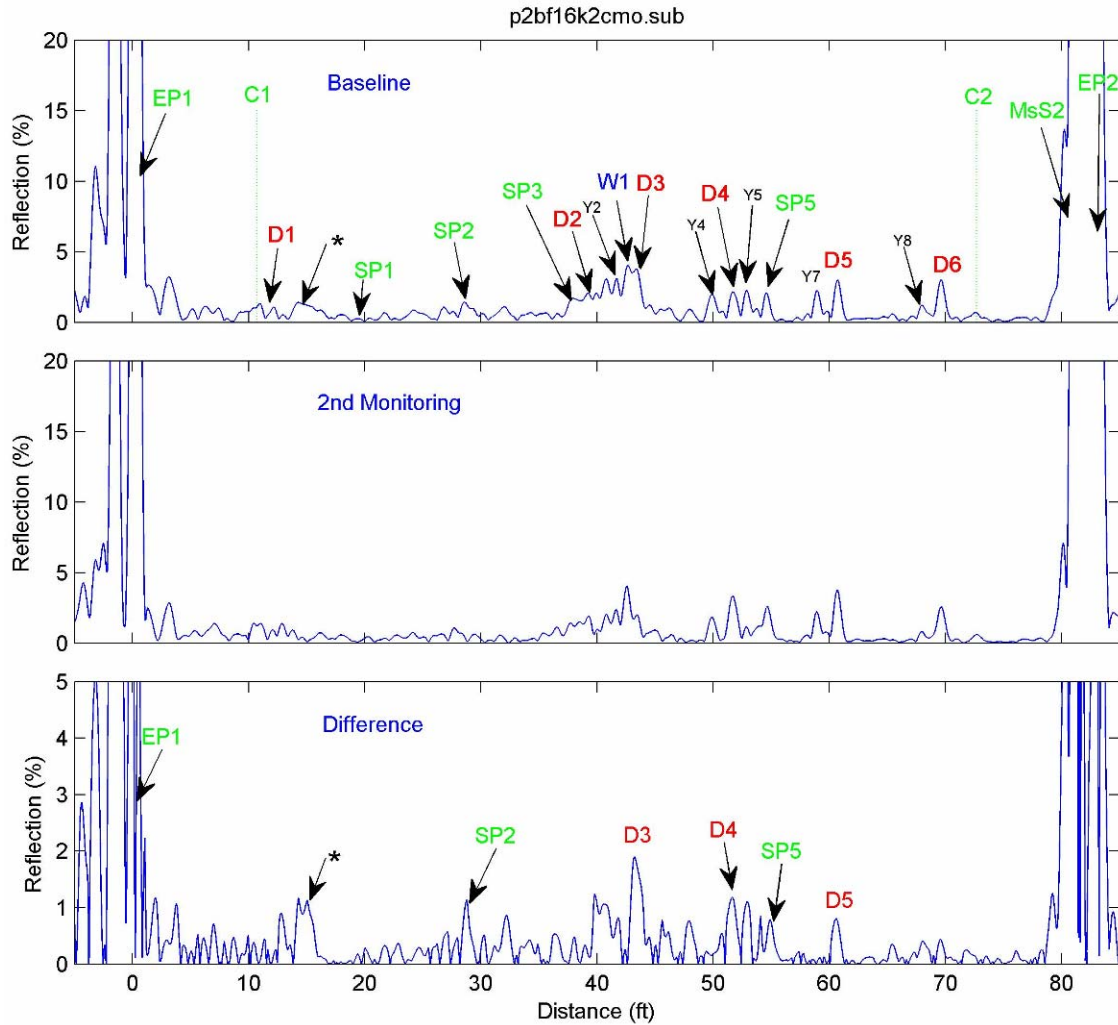
3.1 Test Frequency – 16 kHz

3.2 Data (Baseline, 2<sup>nd</sup> Monitoring, and Difference between the Two)

(a) Data from the North End



(b) Data from the South End



3.3 Comments

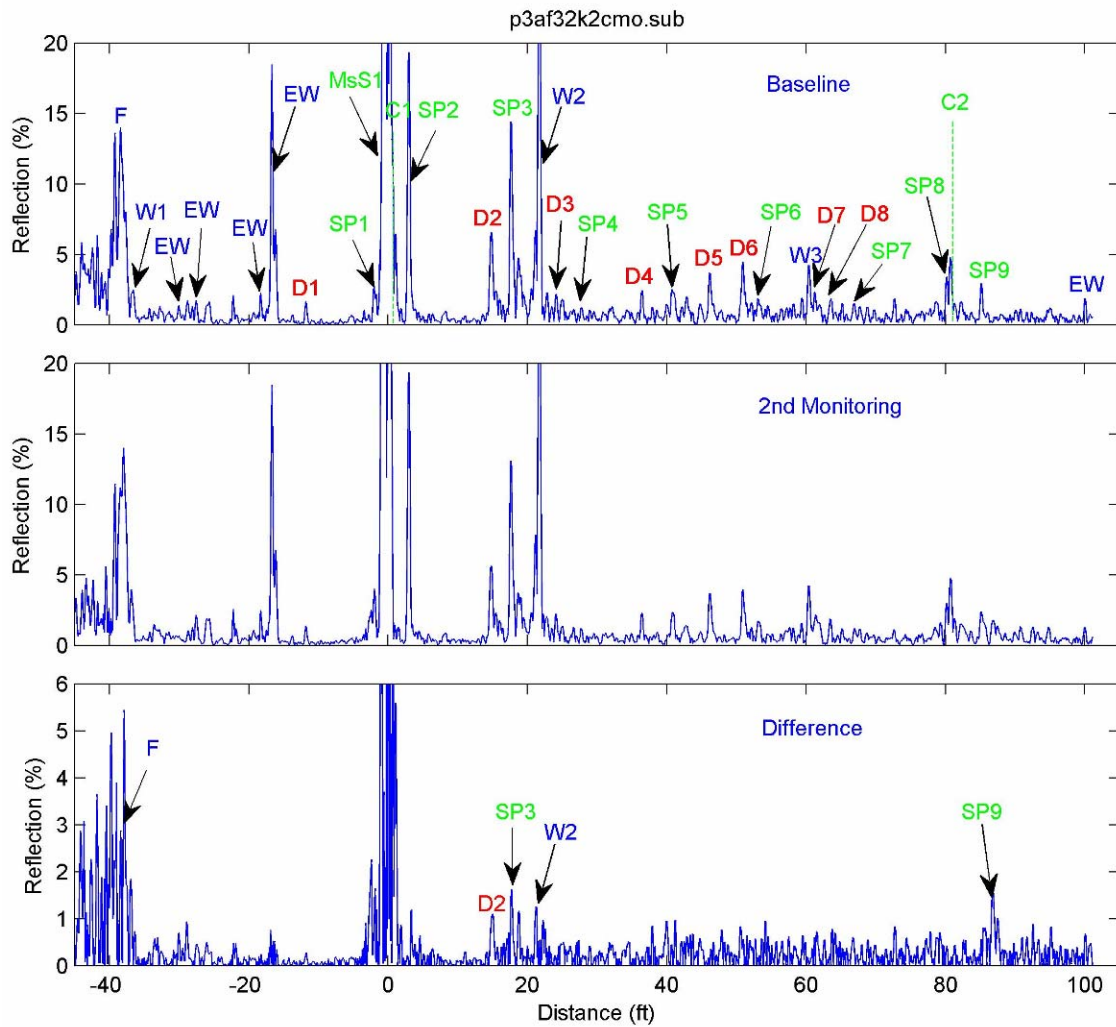
- (1) The comparison results between the baseline and the 2<sup>nd</sup> SHM data were approximately the same with the 1<sup>st</sup> SHM results described in Appendix B. Therefore the same comments in Appendix B also apply here and, thus, are not repeated. The general difference (or reproducibility) in the existing feature signals was about 1% reflection.
- (2) The comparison results between the two SHM data were similar to those with baseline (except for the details; for example, the signal indicated with \* in the baseline data was absent in both SHM data and, thus, that signal was absent in the difference of the two SHM data).

4. Underground 12-inch-OD coal tar epoxy (CTE) coated pipe with 16-inch casing

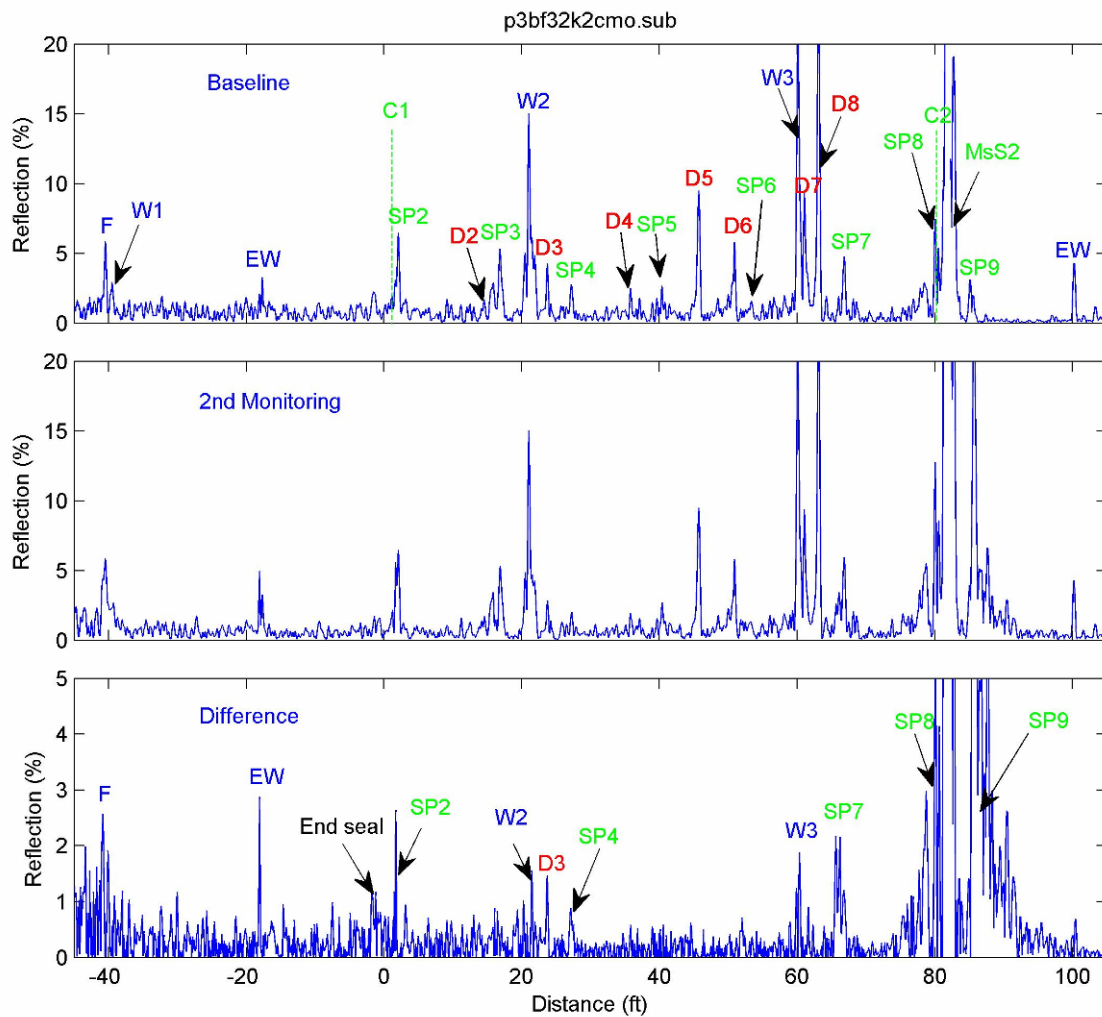
4.1 Test Frequency – 32 kHz

4.2 Data (Baseline, 2<sup>nd</sup> Monitoring, and Difference between the Two)

(a) Data from the North End Excavation Vault



(b) Data from the South End Excavation Vault



4.3 Comments

- (1) The comparison results between the baseline and the 2<sup>nd</sup> SHM data were approximately the same with the 1<sup>st</sup> SHM results described in Appendix B. Therefore the same comments in Appendix B also apply here and, thus, are not repeated.
- (2) The comparison results between the two SHM data were also similar to those with baseline.

- (3) The 2<sup>nd</sup> SHM data from the south end vault showed a large signal from SP9. It appeared that the cold temperature on that day increased the tightness of the spacer (shown in the following picture), leading to a large wave reflection.



A photo of Spacer 9 in the South Excavation Vault

## 5. Summary of Findings and Conclusions

- (1) All MsS probes installed in April, 2007 were found to operate properly in February, 2008 (over a span of about 10-month), indicating the long-term stability of the probes.
- (2) The SHM data from the aboveground bare test pipe agreed very well with the baseline data, showing a high degree of reproducibility. The background noise level in the difference data between the two was less than 0.2% reflection level, indicating the ability to detect a 0.4% change (based on the 2:1 signal-to-noise ratio for detection).
- (3) The SHM results from both the aboveground TGF-3 and underground CTE coated test pipes were several times worse than the results from the bare test pipe. The primary cause of the poorer performance on the coated test pipes was the signal waveform change induced by a wave attenuation change with the ambient temperature fluctuations and the limitations of data subtraction software presently available. To improve the SHM performance on the coated pipelines, data processing techniques need to be developed that can correct the attenuation effects on the waveform.

Another contributing factor to the poor reproducibility that was not mentioned in the 1<sup>st</sup> SHM results is the velocity change with temperature that alters the interference pattern between the adjacent signals and changes the signals in the data. The many feature signals in the CTE coated test pipes increased the contribution of this factor to the overall data variation.

## **APPENDIX D**

# ASTORIA TUNNEL 26-INCH PIPELINE BASELINE TESTING RESULTS

Prepared by Hegeon Kwun and Sang Y. Kim

## A. Test Conditions

Test Frequencies – 16-kHz and 32-kHz

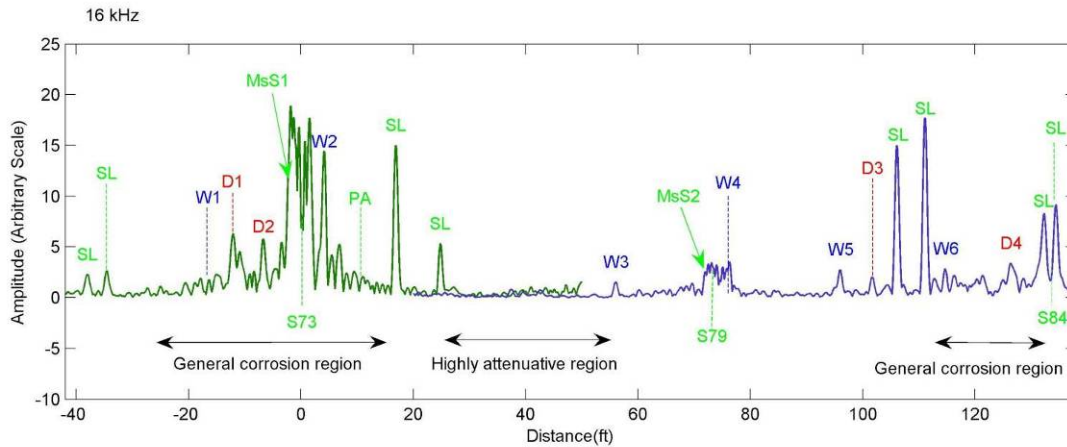
Guided-Wave Mode – Torsional

Test Locations – 1<sup>st</sup> location: 6-inches from Section 73 marker toward Bronx

2<sup>nd</sup> location: 23-inches from Section 79 marker toward Queens

## B. Test Results

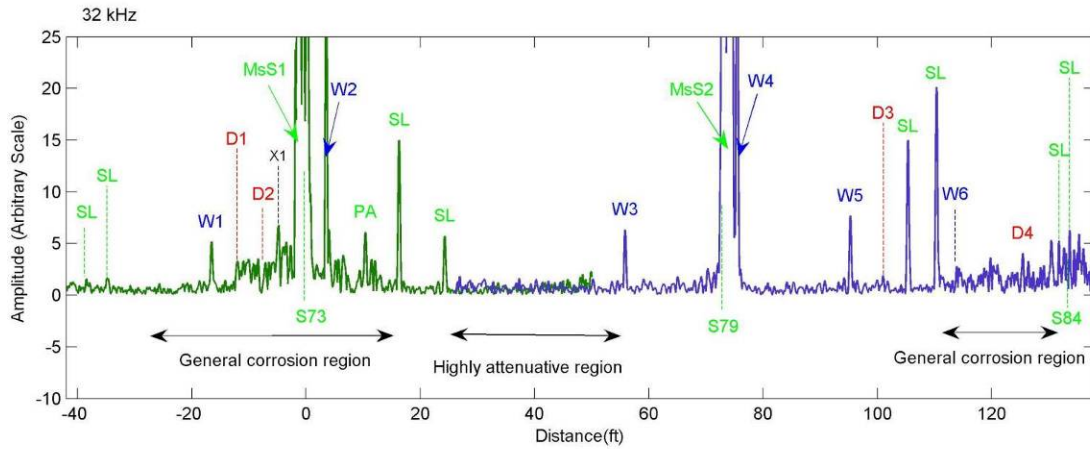
### (1) 16-kHz Results



Location 1:S73f16k2cmop.dat & S73f16k2cmon.dat;			Location 2:S79f16k2cmop.dat & S79f16k2cmon.dat		
Sym.	Dist.(ft)	Comment	Sym.	Dist.(ft)	Comment
SL	-38.5	Sleeve end	S79	72.0	Section 79
SL	-35.1	Sleeve end	MsS2	73.9	Initial Pulse
W1	-16.6	Weld	W4	75.8	Weld
D1	-12.6	Defect	W5	95.6	Weld
D2	-8.5	Defect	D3	101.3	Defect
MsS1	-0.5	Initial Pulse	SL	105.7	Sleeve end
S73	0	Section 73; Distance reference	SL	110.7	Sleeve end
W2	3.6	Weld	W6	114.3	Weld
PA	10.4	Patch	D4	126.0	Defect
SL	16.4	Sleeve end	SL	132.0	Sleeve end
SL	24.3	Sleeve end	S84	132.0	Section 84
W3	55.7	Weld	SL	134.0	Sleeve end

Legend: D/d - defect; W/w - weld; X/x - imperfect direction control; Y/y - multiple reflection

(2) 32-kHz Results



Location 1:S73f32k2cmo2p.dat & S73f32k2cmo2n.dat;			Location 2:S79f32k2cmo1p.dat & S79f32k2cmo1n.dat		
Sym.	Dist.(ft)	Comment	Sym.	Dist.(ft)	Comment
SL	-38.5	Sleeve end	S79	72.0	Section 79
SL	-34.9	Sleeve end	MsS2	73.9	Initial Pulse
W1	-16.6	Weld	W4	75.5	Weld
D1	-12.0	Defect	W5	95.3	Weld
D2	-8.4	Defect	D3	101.1	Defect
X1	-4.8	(W2), Imperfect direction control	SL	105.4	Sleeve end
MsS1	-0.5	Initial Pulse	SL	110.4	Sleeve end
S73	0	Section 73; Distance reference	W6	114.3	Weld
W2	3.5	Weld	D4	125.5	Defect
PA	10.4	Patch	SL	131.8	Sleeve end
SL	16.3	Sleeve end	S84	132.0	Section 84
SL	24.3	Sleeve end	SL	133.9	Sleeve end
W3	55.8	Weld			

Legend: D/d - defect; W/w - weld; X/x - imperfect direction control; Y/y - multiple reflection

C. Comments

- (1) Both test locations had general corrosion and the pipe surface was rough as shown in Figure 1.



Figure 1. photo of pipe surface at the 1<sup>st</sup> test location

- (2) Due to the wax tape wrap and the general surface corrosion (corrosion oxide layers are good attenuators), the wave attenuation was high: average-wise about 0.5-dB/ft at 16-kHz and 1.0-dB/ft at 32-kHz.

Because of the different degree of surface corrosion, the attenuation varied along the pipeline. Within the range of testing (please see the data plots in B):

Highest attenuation – between Sections 73 and 79

Lowest attenuation – between Sections 79 and 84

Achievable test range at 16-kHz was:

Region before section 73 – approximately 40-ft

Region between sections 73 and 79 – approximately 30-ft

Regions past section 79 – approximately 60-ft

Figure 2 shows the 16-kHz data acquired by transmitting the guided-wave pulse from the 1<sup>st</sup> test location and receiving it at the 2<sup>nd</sup> test location. Because of the high attenuation, 32-kHz signals were not detectable.

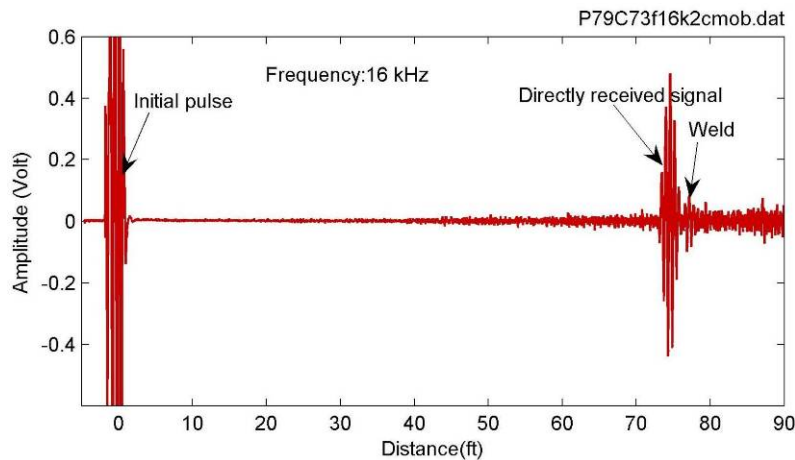


Figure 2. 16-kHz signals detected by the pitch-catch method. The weld signal after the directly received signal is W4 in the test data in B.

- (3) Conditions and Defects
- (a) The high wave attenuation and high level of background noise level observed in the data indicate that the pipeline has general corrosion such as those seen at the 1<sup>st</sup> test location (Figure 1).

- (b) Defect indications D1 through D4 in the test results in B are believed to be 10 to 15% defects and a separate examination of these locations using conventional local inspection technique is recommended.
- (c) The highly attenuative region between SL and W3 in the test results B (about 30-ft-long section) may contain significant defects. Additional guided-testing of this region is recommended.